

Catalytic Applications and Mechanistic Investigations of Iron Bis (oxazolinyphenyl)amino Pincer Complexes in Kumada Cross Coupling and Hydrosilylation Reactions

THÈSE N° 6658 (2015)

PRÉSENTÉE LE 12 JUIN 2015

À LA FACULTÉ DES SCIENCES DE BASE

LABORATOIRE DE SYNTHÈSE ET DE CATALYSE INORGANIQUE

PROGRAMME DOCTORAL EN CHIMIE ET GÉNIE CHIMIQUE

ÉCOLE POLYTECHNIQUE FÉDÉRALE DE LAUSANNE

POUR L'OBTENTION DU GRADE DE DOCTEUR ÈS SCIENCES

PAR

Gerald BAUER

acceptée sur proposition du jury:

Dr A.-S. Chauvin, présidente du jury
Prof. X. Hu, directeur de thèse
Prof. K. A. Kirchner, rapporteur
Prof. W. Zhang, rapporteur
Prof. K. Severin, rapporteur



ÉCOLE POLYTECHNIQUE
FÉDÉRALE DE LAUSANNE

Suisse
2015

*“Gold is for the mistress – Silver for the maid –
Copper for the craftsman cunning at his trade.”*
“Good!” said the Baron, sitting in his hall,
“But Iron – Cold Iron – is master of them all.”

(Rudyard Kipling, “*Cold Iron*”)

Acknowledgements

I want to thank everyone who supported and helped me finish my dissertation in the last four years. It would be too much to name everyone, but in fact, there are some people whom I really want to thank:

First and foremost my scientific advisor, Professor Xile Hu, for accepting me as a Ph.D. candidate. I am grateful for the interesting and promising topic he gave me to work on in the last four years. Furthermore, I want to thank him for the fruitful discussions and his guidance throughout the thesis. His optimistic point of view and his helpful advice always seemed like a light at the end of a tunnel that encouraged me to continue working even when projects did not proceed according to plan.

I want to thank my thesis jury: Dr. MER Anne-Sophie Chauvin, Prof. Wei Zhang, Prof. Karl A. Kirchner and Prof. Kay Severin, who took their time to evaluate and accept my thesis.

Many thanks to Dr. Katherine Schultz-Gomez, Dr. Shoubik Das and Prof. Xile Hu for the proof reading of my manuscript.

In addition I want to thank past and present colleagues from the LSCI. All of you made every day special and unforgettable. I really appreciated the group outings, such as the numerous BBQ's in front of the BCH or at the lake side and – unfortunately not that frequent but still as funny – the group skiing trips. I namely wanted to emphasise Daniel and Jan, two congenial members of the German speaking LSCI mafia. Both of them made every minute in the office so enjoyable that it was hard to leave work at the end of the day. I definitely will miss those moments! Also the (en)chanting people in our lab – Chi Wai, Ivan and Xu Tao – were the proof that lab work does not have to be dull and boring. Additionally, I wanted to thank the colleagues from the LCS. Over the years they grew like a second family to me. I will miss the coffee breaks on your balcony; in fact, the view is slightly better than on our side.

Although, Dr. Matthew D. Wodrich and Dr Chi Wai Cheung are not named directly in the thesis they contributed an important chunk of my projects, for which I am eternally grateful. Matthew did the dreadful work of elucidating and underpinning the catalytic cycle in Chapter 3 with DFT calculations. Regarding the time he spent on all the calculations I really do not envy his work. Without his contribution this chapter would lose half of its significance. I also have to thank Chi Wai for synthesising and providing all the substrates that are depicted in Table 2.2. He also was a huge help in isolating and characterising the obtained products. In this spirit, I also have to send my regards to my two master students, Gaëlle Lapicorey and Céline Monnard, who were a great help for most of the results depicted in Chapter 2.

I am really grateful for the aid of the supporting staff: Dr. Euro Solari and Dr. Rosario Scopelliti for their assistance in elemental and/or X-ray analysis; Annelise Carrupt, Gladys Pache and Benjamin Kronenberg for their help and support in the ordering of various chemical and non-chemical products and their endless kindness; Dr. Pascal Miéville for his help in NMR; Patrick Favre and Donald Zbinden for their helpful advice in electronic and IT questions; Anne-Lene Odegaard and Christina for their administrative work.

For the leisure activities I want to thank Justus, Matt, Cornel and Jésus with whom I had many chances to discover the “outback Vaudois” on two wheels. Together we also enjoyed several marvellous skiing adventures in the Lausanne area. I am further grateful for the numerous journeys and day trips with Ivan and Natasha. I hope we continue this habit.

Last but not least, a big THANK YOU to my family for their moral and financial support throughout my life. I would not be here today without their love and understanding.

“So long and thanks for all the fish!”

(Douglas Adams)

Abstract

The aim of the project was to investigate iron bis(oxazolinyphenyl)amino (bopa) pincer complexes as pre-catalysts in the enantioselective Kumada cross coupling of non-activated alkyl halides with aryl Grignard reagents. From this preliminary cross coupling studies we were able to isolate potential intermediate iron species that were then investigated for their catalytic activity. Further reactivity studies, kinetic studies and DFT computations revealed the feasible catalytic cycles. Some intermediate species also proved to be relevant in the enantioselective hydrosilylation reaction of ketones.

In the first chapter, a short overview is given of state-of-the-art iron pincer complexes and their catalytic application. The focus was put on symmetric pincer systems which are rigidified with aromatic rings in the ligand backbone. They proved themselves as highly active catalysts for the hydrogenation and hydrosilylation reaction of olefins, acetylenes and carbonyls. There are also some examples given for trapping and releasing of hydrogen as potential applications for the storage of hydrogen on a molecular level. Examples for C-C bond formations are given to a lesser extent.

In chapter two, the enantioselective Kumada cross coupling of alkyl halides with aryl Grignard reagents was investigated. Iron(III) bopa pincer complexes are efficient pre-catalysts for the cross coupling of non-activated primary and secondary alkyl halides with aryl Grignard reagents. The reactions proceed at room temperature in moderate to excellent yields. A variety of functional groups can be tolerated. The enantioselectivity of the coupling of secondary alkyl halides is low. The cross coupling with secondary benzylic bromides solely yielded the homo-coupling products, 2,3-diphenylbutane and biphenyl. Modifications on the oxazoline and diphenylamino moiety showed similar reactivity but did not improve the enantiomeric excess (ee).

In chapter three, we isolated and characterised well-defined iron complexes and probed and supported their catalytic roles. Reactivity studies identified an Fe(II) "ate" complex, $[\text{Fe}(\text{Bopa-Ph})(\text{Ph})_2]^-$, as the active species for the oxidative addition of alkyl halide. Experiments using radical-probe substrates and DFT computations reveal a bimetallic and radical mechanism for the oxidative addition. The kinetics of the coupling of an alkyl iodide with PhMgCl indicates

that formation of the "ate" complex, rather than oxidative addition, is the turnover determining step.

In chapter four, the preliminary results on a possible mechanism in the enantioselective hydrosilylation of 4-acetylbiphenyl is presented. We could show that $[(\text{Fe}(\text{bopa})\text{OAc})_2]$, a 5-coordinated dimeric iron complex, is formed as the catalytic active species from the reaction of bopa ligands with $\text{Fe}(\text{OAc})_2$. The gathered results are consistent with an inner sphere reaction pathway, including the formulation of an iron-hydride species. For the reactions with zinc, no mechanism could yet be proposed.

Keywords:

Kumada Cross coupling, Iron Pincer Complex, Bimetallic Oxidative Addition Mechanism, Inner Sphere Hydrosilylation Mechanism, Enantioselectivity

Zusammenfassung

Das Ziel des Projektes war es, Bis(oxazolinyphenyl)aminoeisenpincerkomplexe ($[\text{Fe}(\text{bopa})\text{X}_n]$) als Präkatalysatoren für die enantioselektive Kumada-Kreuzkupplung von nichtaktivierten Alkylhalogeniden mit Arylgrignardreagenzien zu untersuchen. Es konnten potenzielle Intermediärspezies isoliert werden, die im Anschluss auf ihre katalytische Aktivität untersucht wurden. Weiterführende Reaktivitätsstudien, kinetische Untersuchungen und DFT Berechnungen ermöglichte es einen Katalysezyklus zu formulieren. Einige, der zuvor isolierten, Intermediärspezies erwiesen sich bei der enantioselektiven Hydrosilylierung von Ketonen als relevant.

Im ersten Kapitel wird ein kurzer Überblick über aktuelle Eisenpincerkomplexe und ihre katalytische Anwendung gegeben. Der Fokus lag hierbei auf symmetrischen, durch aromatische Ringe verstärkte Ligandensysteme. Diese Komplexe erwiesen sich im Allgemeinen als hochreaktiv und fanden eine breite Anwendung für die Hydrierung und Hydrosilylierung von Olefinen, Acetylenen und Carbonylen. Sie wurden auch zur Fixierung und Freigabe von Wasserstoff angewendet. Beispiele, die Eisenpincerkomplexe in der Bildung von Kohlenstoff-Kohlenstoff Bindung einsetzen, werden auch diskutiert.

Im zweiten Kapitel wurde die enantioselektive Kumada-Kreuzkupplung von Alkylhalogeniden mit Arylgrignardreagenzien untersucht. $[\text{Fe}(\text{III})(\text{bopa})\text{Cl}_2]$ erwies sich hierfür als effizienter Präkatalysator. Die Reaktionen fanden bei Raumtemperatur statt und gaben mäßige bis gute Ausbeuten. Eine gute Toleranz gegenüber funktionellen Gruppen konnte gezeigt werden. Trotz guter Ausbeuten blieben die Enantiomerenüberschüsse gering. Versuche den Enantiomerenüberschuss durch den Einsatz von sekundären Benzylbromiden zu erhöhen war nicht erfolgreich. Weiterführende Veränderungen am Ligandensystem zeigten zwar ähnliche Reaktivität aber keine Verbesserungen im Enantiomerenüberschuss.

Das dritte Kapitel beschreibt die Isolierung und Charakterisierung von wohldefinierten Eisenkomplexen. Diese wurden auf ihre katalytische Relevanz hin untersucht. Reaktionsstudien zeigten einen „Eisen(II)-at“-Komplex, $[\text{Fe}(\text{bopa-Ph})(\text{Ph})_2]^+$, als katalytisch aktive Spezies für die oxidative Addition von Alkylhalogeniden. Experimente zur Sondierung von Radikalen und DFT-Berechnungen ergaben, dass die oxidative Addition über einen bimetallichen,

radikalischen Mechanismus verläuft. Kinetische Studien zeigten, dass die Bildung des "at"-Komplexes der geschwindigkeitsbestimmende Schritt der Reaktion war.

Im vierten Kapitel wurden die vorläufigen Ergebnisse für einen möglichen Katalysezyklus der enantioselektiven Hydrosilylierung von 4-Acetylbiphenyl diskutiert. Es konnte gezeigt werden, dass sich $[(\text{Fe}(\text{bopa})\text{OAc})_2]$ als katalytisch aktiver Präkatalysator, bildete. Die gewonnenen Erkenntnisse sind konsistent mit einer Reaktion an der inneren Koordinationssphäre. Zusätzlich ist die Bildung einer Eisenhydridspezies denkbar. Das System, dass einer Präaktivierung mit Zink bedarf, konnte noch kein Mechanismus vorgeschlagen werden.

Schlüsselwörter:

Kumada-Kreuzkupplung, Eisenpincerkomplexe, Bimetallisch Oxidative Addition, Hydrosilylierungsmechanismus an der inneren Koordinationssphäre, Enantioselektivität

Résumé

Le but de ce projet est d'étudier les "pincer complexes", appelés bis(oxazolinyphenyl)amino (bopa), comme pré-catalyseurs pour le couplage de Kumada énantioselectif entre des halogénures d'alkyles non-activés et des organomagnésiens. Grâce à des résultats préliminaires, nous avons été capables d'isoler l'intermédiaire potentiel des complexes de fer dont l'activité catalytique a par la suite été étudiée. Des études approfondies de leur réactivité, de leur cinétique et des calculs DFT ont montré la faisabilité du cycle catalytique. Des espèces intermédiaires ont également montré des résultats prometteurs dans la réaction d'hydrosilylation énantiosélective de cétones.

Dans le premier chapitre, une brève vue d'ensemble de la recherche sur les complexes pinces à base de fer est donnée, ainsi que leurs utilités catalytiques. Les systèmes avec pinces symétriques sont explorés plus en détails. Ces derniers sont rigidifiés grâce aux cycles aromatiques présents sur les ligands. Ils ont montré une grande réactivité pour l'hydrogénation et l'hydrosilylation des oléfines, des acétylènes et des carbonyles. Quelques exemples sont aussi donnés pour le stockage et la libération contrôlés d'hydrogène comme application potentielle du stockage d'hydrogène au niveau moléculaire. Des exemples de couplage C-C sont ensuite décrits.

Dans le deuxième chapitre, le couplage Kumada énantiosélectif des halogénures d'alkyles avec des réactifs de Grignard a été étudié. Les "pincer complexes" - bopa - de fer(III) sont des pré-catalyseurs efficaces pour ce couplage d'halogénure d'alkyles, primaires ou secondaires, avec des organomagnésiens de type aryle. La réaction se déroule à température ambiante avec un rendement oscillant de moyen à excellent. Une grande variété de groupements fonctionnels est tolérée. L'énantiosélectivité du couplage avec les alkyles secondaires est faible. Le couplage de Kumada avec des bromures de benzyle donne accès seulement aux produits 2,3-diphénylbutane et biphenyle provenant de la réaction d'homo-couplage. Des modifications sur l'oxazoline et le groupement diphénylamino montrent une réactivité similaire, mais n'améliorent pas l'excès énantiomérique (ee) pour les catalyseurs obtenus.

Dans le troisième chapitre, nous avons isolé, caractérisé et étudié des complexes de fer. Les études de réactivité ont permis d'identifier un complexe de Fer(II) "ate", $[\text{Fe}(\text{Bopa-Ph})(\text{Ph})_2]^-$,

comme étant l'espèce active lors de l'addition oxydante d'halogénure d'alkyle. Certaines expériences utilisant des sondes radicales et des calculs DFT ont révélé un mécanisme bimétallique et radicalaire pour l'addition oxydante. La cinétique du couplage d'un iodure d'alkyle avec PhMgCl indique que la formation du complexe "ate" est l'étape déterminante du cycle catalytique, et non l'addition oxydante.

Dans le quatrième chapitre, les résultats préliminaires sur le mécanisme probable de l'hydrosilylation du 4-acétylbiphényle sont présentés. Nous avons pu montrer que $[(\text{Fe}(\text{bopa})\text{OAc})_2]$, qui est un complexe dimérique de fer pentacoordiné, est la forme active de la réaction des ligands bopa avec $\text{Fe}(\text{OAc})_2$. Les résultats obtenus sont consistants avec un mécanisme de réaction de sphère interne, incluant la formation d'un hydrure ferrique. Pour les réactions avec le zinc, aucun mécanisme n'est pour le moment avancé.

Mots clefs:

Couplage de Kumada, "Pincer Complex" de Fer, Mécanisme d'Addition Oxydante Bimétallique, Mécanisme d'Hydrosilylation en Sphère Interne, Enantiosélectivité.

List of Abbreviations

°C	degree Celcius
Å	Ångström
acac	acetylacetonate
a.m.u.	atomic mass unit
APCI	atmospheric pressure chemical ionisation
Ar	aryl
Bn	benzyl
Boc	tertiary butyloxycarbonyl
bopa	bis(oxazolinylphenyl)amine
cp	cyclopentadienyl (C ₅ H ₅ ⁻)
d	doublet
dd	doublet doublet
DCC	<i>N,N'</i> -dicyclohexylcarbodiimide
DCM	dichloromethane (methylene chloride)
DFT	density functional theory
DMA	dimethylacetamide
dmpe	1,2-bis(dimethylphospino)ethane
DMSO	dimethylsulfoxide
dpm	diphenylmethyl
ee	enantiomeric excess
EPR	electron paramagnetic resonance
ESI	electrospray ionisation
Et ₂ O	diethylether
EtOAc	ethyl acetate

equiv	equivalent(s)
FI-detector	flame ionisation detector
GC	gas chromatography
GC/MS	gas chromatography coupled with mass detector
hex	hextet
HPLC	high pressure liquid chromatography
HRMS	high resolution mass spectrometry
Hz	hertz (s^{-1})
<i>i</i> Pr	isopropyl
LC	liquid chromatography
m	milli / multiplet
M	molar / molecule / mega (10^6)
μ	micro
μ_B	Bohr magneton
mesityl	2,4,6-trimethylphenyl
mg	milligram
μ g	microgram
MHz	megahertz ($10^6 s^{-1}$)
mL	millilitre
μ L	microliter
mM	millimolar
mmol	millimole
MsCl	mesylchloride (methanesulfonyl chloride)
mp	melting point
m/z	mass-to-charge ratio
N	normal

NMP	<i>N</i> -methylpyrrolidone
NMR	nuclear magnetic resonance
<i>n</i> Bu	neobutyl
<i>o</i>	ortho
O-tmeda	bis[2-(<i>N,N</i> -dimethylamino)ethyl]ether
<i>p</i>	para
Ph	phenyl
PPh ₃	triphenylphosphine
pybox	pyridinebisoxazoline
quint	quintet
r.t.	room temperature
sec	second
t	triplet
t _{1/2}	“half-life” (time until 50% conversion were reached)
td	triplet doublet
<i>t</i> Bu	tertiary butyl
TEA	triethylamine
temp	temperature
THF	tetrahydrofuran
TLC	thin layer chromatography
tmeda	<i>N,N,N',N'</i> -tetramethylethane-1,2-diamine
TMS	tetramethylsilane
TOF	turn over frequency
TON	turn over number
TS	transition state
UV-Vis	ultraviolet-visible

Table of Contents

Acknowledgements	I
Abstract	III
Zusammenfassung	V
Résumé	VII
List of Abbreviations	IX
Table of Contents	XII
Chapter 1 Introduction	1
1.1 General.....	2
1.2 Neutral Pyridine Based $R^L P^L N^L P$ -type Ligand Systems and Their Application in Iron Catalyses	5
1.3 Monoanionic Benzene-Based $R^L C^L P$ Ligand Systems and Their Application in Iron Catalysis	15
1.4 Pyridine Di(imino) Pincer Systems and Their Application in Iron Catalysis.....	19
1.5 Pyridine- and Phenyl Bis(oxazoliny) Pincer Systems and Their Application in Iron Catalysis	36
1.6 Pyridine Bis(<i>N</i> -Heterocyclic Carbene) Pincer Systems and Their Application in Iron Catalysis	39
1.7 <i>N,N</i> -Diphenylamino-Based Pincer Systems and Their Application in Iron Catalysis	41
1.8 Concluding Remarks and Outlook	45
1.9 References.....	47
Chapter 2 Cross Coupling of Non-Activated Primary and Secondary Alkyl Halides with Aryl Grignard Reagents Catalysed by Chiral Iron Pincer Complexes	53
2.1 Introduction.....	54
2.2 Optimisation of the Reaction Conditions	55

2.3	Scope of Kumada Cross Coupling of Primary and Secondary Alkyl Halides with Phenyl Grignard Reagents.....	57
2.4	Screening for Applicability in the Enantioselective Kumada Cross coupling of Secondary Alkyl Halides with Aryl Grignard Reagents	59
2.5	Measures to Improve the Existing Enantioselectivities	61
2.6	Experimental.....	70
2.7	References.....	88
Chapter 3	Iron Pincer Complexes as Catalysts and Intermediates in Alkyl-Aryl Kumada Coupling Reactions	91
3.1	Introduction.....	92
3.2	Results	93
3.3	Discussion.....	108
3.4	Concluding Remarks	112
3.5	Experimental.....	113
3.6	Appendix.....	150
3.7	References.....	154
Chapter 4	Investigation of Active Species in Enantioselective Hydrosilylation of Substituted Acetophenones Catalysed by Bis(oxazolonyl-diphenyl)amino Iron(II) Pincer Complexes	159
4.1	Introduction.....	160
4.2	Acetate Route.....	164
4.3	Zinc Route	171
4.4	Concluding Remarks	174
4.5	Experimental.....	174
4.6	References.....	181
	Curriculum Vitae	183

Chapter 1

Introduction

1.1 General

Sustainability is one of the driving forces in nowadays synthetic chemistry. Therefore the development of new and efficient catalysts is very important. On the one hand to keep the production costs low, by reducing the energy required for the reactions and also by reducing the amount of by-products and waste and on the other hand to facilitate the synthesis of more complex organic structures. Since the beginning of homogeneous catalysis the focus was put on precious metals, especially those from the platinum group. The problem that goes along with those elements is not only the high cost and their unpredictable market prices it is also their toxicity. It was not that long ago that the focus in catalysis was turned on the more abundant and benign first row d-block elements, such as iron, copper, nickel, *etc.* It is ironic that those elements find their way into chemistry that late because nature exclusively relies on them. Famous examples are the iron containing haemoglobin and cytochrome P-450 in the human body. Even though the research and the application of earth abundant elements in catalysis is still fledgling further development in this field proves to be promising.

1.1.1 Metal Centre

Iron became an important metal in catalytic processes at the beginning of the last century, when Fritz Haber and Carl Bosch invented a process to synthesise ammonia from its elements. With an annual output of 168 Mt of NH_3 in 2005 this process is still one of the most common processes in the fixation of nitrogen.¹ Iron is also employed in the water-gas shift reaction to produce hydrogen from carbon monoxide and water. Another example is the Fischer-Tropsch synthesis of hydrocarbons. These large-scale industrial processes use iron as a heterogeneous catalyst - iron has not been widely used as a homogeneous catalyst for the better part of the last century. Meanwhile, more noble and precious metals like platinum, palladium, ruthenium, rhodium, *etc.* took their place in the catalytic arena. Their catalytic potential and reactivity was investigated and became well-established over decades. Although efficient and broadly applicable, their toxicity and high price do not make them the elements of choice for industrial scale syntheses. Paired with the recent trend to put the world on track for a “greener” and more sustainable future, the quest for more benign alternatives has begun.

Amongst other late first row transition metals, iron has proved to be an interesting choice. It is one of the most abundant elements in the earth's crust, easy to mine and incredibly cheap. Iron itself is also non-toxic. On the contrary, it is an essential metal co-factor in the human body. Apart from economic and ecologic factors, iron is also interesting due to its higher potential to undergo spin state changes caused by the lower ligand field splitting of first row transition metals. They are more prone to undergo spin state changes between HOMO and LUMO.² This electronic variation may open up new possibilities for the catalytic application of iron. Although interesting findings have been reported over the last decades,³⁻⁵ iron catalysis is still a novel process and compared to the other noble metals, relatively unexplored.

1.1.2 Ligand

The choice and design of the ligand surrounding the catalytic active centre is almost as important as the choice of the metal itself. To sustain the concept of benign iron catalysis, the ligand design should be simple, versatile and effective. Other factors in ligand choice are low production cost and reduction of the environmental food print of its synthesis. The purpose of the ligand is to keep the catalyst in solution, stabilise the metal throughout the catalysis and direct or induce selectivity.

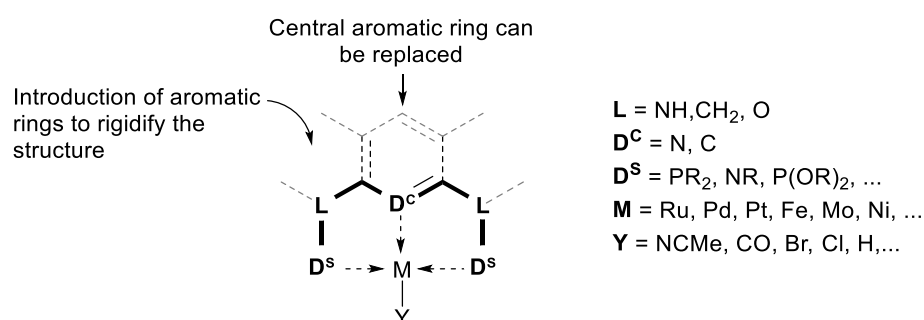


Figure 1.1: Generalised structure of pincer complexes.^{6,7}

The first pincer-type ligands were described in the early 1970's.^{8,9} Van Koten coined the name "pincer" for this kind of ligand in 1989.¹⁰ Pincer ligands in general are tridentate, 6-electron donor ligands and are isoelectronic to cp-ligands. However, there is no strict definition of the structure of "pincer" class ligands. Following Moulton's and Shaw's work, a pincer ligand traditionally consists

of a central benzene ring, which is 1,3-disubstituted with two chelating side arms (Figure 1.1). The central atom ($\mathbf{D}^{\mathbf{C}}$) binds to the metal centre. The two donor groups on the side ($\mathbf{D}^{\mathbf{S}}$) provide a strong chelating effect and give both structural and thermal stability.¹¹⁻¹⁷ The two flanking side arms are linked to the central aromatic ring with a linker (\mathbf{L}).^{6,7} All parameters ($\mathbf{D}^{\mathbf{C}}$, $\mathbf{D}^{\mathbf{S}}$ and \mathbf{L}) can be freely changed according to the nature of the desired complex. Additionally, the whole ligand backbone can be modified. In fact every tridentate ligand that binds the metal centre on three coplanar sides, like a “pincer”, can be considered as pincer ligand. This opens up an even larger opportunity to vary the ligand scaffold and its properties. The advantage of pincer ligands is their modular composition. The combination of the different building blocks makes it possible to synthesise an almost endless amount of different ligands.⁷

In the following sections is a short review on the existing iron-pincer complexes and their catalytic relevance. A focus was put on neutral and anionic systems containing a central aromatic ring, 2,6-disubstituted pyridine and 1,3-disubstituted benzene pincer ligands. The discussion was then extended to ligand systems which are rigidified by aromatic rings in the ligand backbone, specifically *N,N*-diarylamino pincer ligands. Unsymmetric substituted pincer ligands, meaning ligands without a C_2 or C_{2v} symmetry, are not included in the discussion. Also excluded are iron pincer complexes based on terpyridine ligands.

1.2 Neutral Pyridine Based $R^L P^L N^L P$ -type Ligand Systems and Their Application in Iron Catalyses

The first iron $R^L P^L N^L P$ complex was synthesised by Dahlhoff and Nelson in 1971. They coordinated 2,6-bis(diphenylphosphinomethyl)pyridine to FeX_2 ($X = Cl, Br, I, NCS^-$). The resulting complexes were in a high spin configuration and exhibited a 5-coordinate geometry with a slightly distorted square pyramidal structure.⁸ The linker (L) that connects the side donor substituents to the central pyridine ring can be either CH_2 ,^{8,18-27} NR ($R = H, \text{organic residue}$),^{7,28-35} or O .³⁶

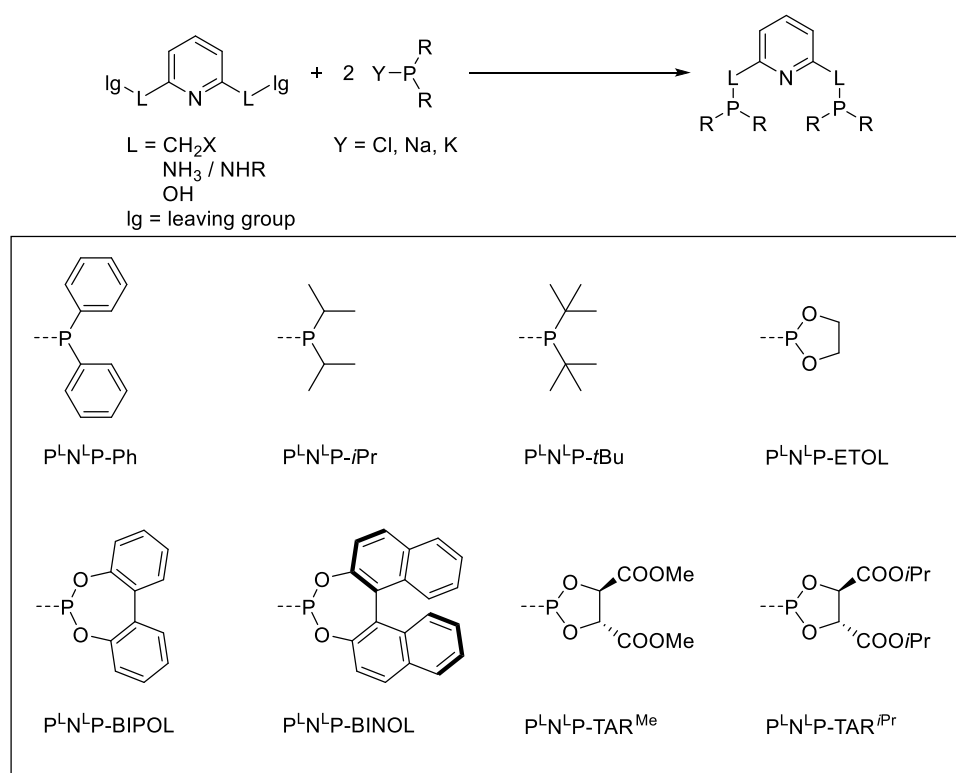


Figure 1.2: Examples of chiral and achiral phosphines and phosphides groups as potential flanking substituents of $R^L P^L N^L P$ ligands.⁷

The syntheses of $R^L P^L N^L P$ ligands are usually straightforward and consist of facile one-pot reactions. No precious metals are needed for the bond formation. $R^L P^L N^L P$ ligands are typically synthesised by coupling lithium or potassium phosphides to 2,6-bis(bromomethyl)pyridine. The phosphides are formed *in situ* from the corresponding phosphine chloride. $R^L P^L N^L P$ ligands are synthesised by a condensation reaction of chlorophosphines with a primary or secondary amine in the presence of a base. $R^L P^L N^L P$ pincer ligands are typically prepared from 2,6-dihoxypyridine

hydrochloride with chlorophosphines, analogue to ${}^R\text{P}^{\text{N}}\text{N}^{\text{N}}\text{P}$ ligands. It is interesting to note that the starting 2,6-dihydroxypyridine is in a tautomeric equilibrium with 6-hydroxypyridine-2-one, which could be problematic in the ligand synthesis. The phosphines and phosphides can be freely chosen depending on the electronic properties of the metal centre. They can be chiral or achiral (Figure 1.2).⁷

DeRieux and co-workers were able to show the influence of phosphine, phosphinite and phosphite ligands on the electronic density of the metal centre. In their study they synthesised, amongst others, $[(i\text{Pr}^{\text{O}}\text{P}^{\text{O}}\text{N}^{\text{O}}\text{P})\text{FeCl}_2\text{CO}]$ (**1.1**), $[(i\text{Pr}^{\text{O}}\text{P}^{\text{O}}\text{N}^{\text{O}}\text{P})\text{Fe}(\text{CO})_2]$ (**1.2**) and $[(\text{Et}^{\text{O}}\text{P}^{\text{O}}\text{N}^{\text{O}}\text{P})\text{Fe}(\text{CO})_2]$ (**1.3**). The CO stretching frequencies were analysed by IR and compared to literature values (Figure 1.3 and 1.4).³⁶

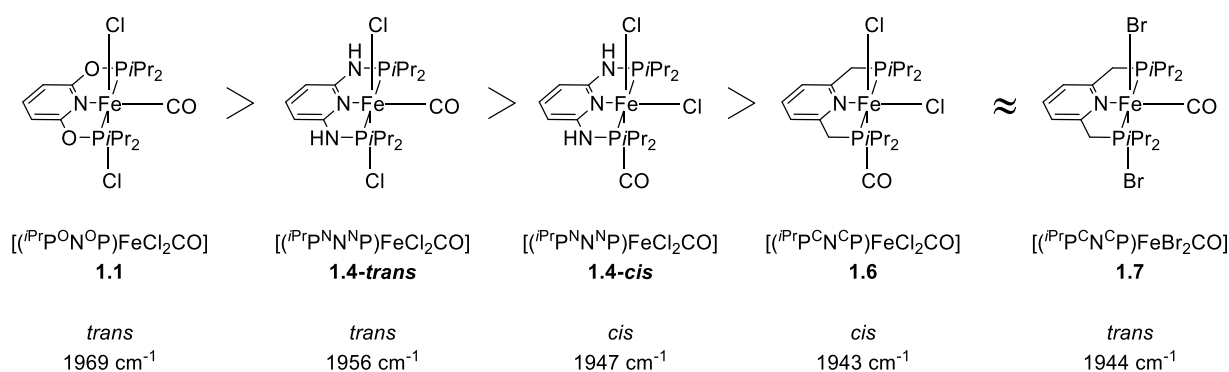


Figure 1.3: CO stretching frequencies for **1.1**, **1.4-cis**, **1.4-trans**, **1.6** and **1.7**.

The IR spectrum for **1.1** was measured in ATR mode. The obtained stretching frequency was found to be 1969 cm^{-1} . Benito-Garagorri was able to isolate $[(i\text{Pr}^{\text{P}}\text{N}^{\text{N}}\text{N}^{\text{P}})\text{FeCl}_2\text{CO}]$ as a *cis*- (**1.4-cis**) and *trans*-chloro isomer (**1.4-trans**). The red *cis*-isomer is synthesised by reacting CO gas with $[(i\text{Pr}^{\text{P}}\text{N}^{\text{N}}\text{N}^{\text{P}})\text{FeCl}_2]$ (**1.5**) in the solid state. The *trans*-isomer forms in solution. The obtained CO stretching frequencies were 1947 cm^{-1} (**1.4-cis**) and 1956 cm^{-1} (**1.4-trans**). Both values were obtained in the ATR mode.³⁰ For $[(i\text{Pr}^{\text{P}}\text{C}^{\text{N}}\text{C}^{\text{P}})\text{FeCl}_2\text{CO}]$ (**1.6**) Benito-Gargorri was only able to synthesise the *cis*-isomer, regardless of the reaction conditions. The obtained wavenumber was 1943 cm^{-1} (ATR).³⁰ Langer and co-workers synthesised the *trans*- $[(i\text{Pr}^{\text{P}}\text{C}^{\text{N}}\text{C}^{\text{P}})\text{FeBr}_2\text{CO}]$ (**1.7**) which showed 1944 cm^{-1} , which was slightly higher than for the *cis*-chloro compound.²² The ligation of FeCl_2 with $\text{Et}^{\text{O}}\text{P}^{\text{O}}\text{N}^{\text{O}}\text{P}$ was not successful, only impure iron complexes were isolated. The comparison of the wavenumbers for the CO stretching of compounds **1.4-cis**, **1.4-trans**, **1.6** and **1.7** to **1.1** (Figure 1.3) clearly shows that the frequencies are increasing from $i\text{Pr}^{\text{P}}\text{C}^{\text{N}}\text{C}^{\text{P}}$ - over $i\text{Pr}^{\text{P}}\text{N}^{\text{N}}\text{N}^{\text{P}}$ - to the $i\text{Pr}^{\text{O}}\text{P}^{\text{O}}\text{N}^{\text{O}}\text{P}$ ligand system. This suggests that the iron with phosphinito ligand system has the lowest electron density on the metal centre and therefore a reduced π -backbonding to the carbonyl.

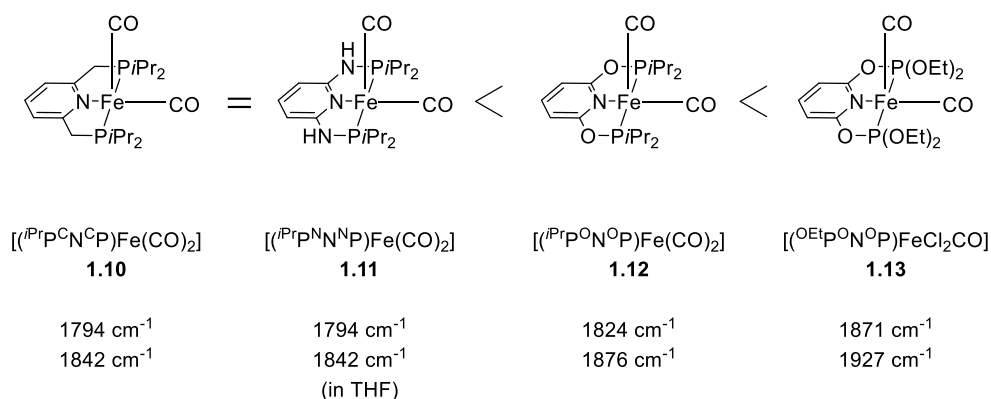


Figure 1.4: CO stretching frequencies for iPr^CN^CP , iPr^NN^NP , iPr^ON^OP , Et^ON^OP iron (0) dicarbonyl complexes.

The iron(0) dicarbonyl complexes were synthesised by stirring $[(iPr^CN^CP)FeCl_2]$ (**1.8**), $[(iPr^ON^OP)FeCl_2]$ (**1.9**) and **1.5** in presence of 0.5% sodium amalgam in a CO atmosphere.^{20,32,36} DeRieux was able to isolate a clean iron(0) bis-carbonyl complex from the reaction of ferrous dichloride and Et^ON^OP with 0.5% sodium amalgam in a CO atmosphere. $[(iPr^CN^CP)Fe(CO)_2]$ (**1.10**) was measured in a KBr pellet and showed two bands at a frequency of 1794 cm^{-1} and 1842 cm^{-1} .²⁰ Bichler isolated $[(iPr^NN^NP)Fe(CO)_2]$ (**1.11**) as an orange/red powder. The IR stretching frequencies show the same results as for **1.10**.³² $[(iPr^ON^OP)Fe(CO)_2]$ (**1.12**) and $[(Et^ON^OP)Fe(CO)_2]$ (**1.13**) show an increase in wave number to 1824 cm^{-1} /1876 cm^{-1} and 1871 cm^{-1} /1927 cm^{-1} . The results are summarised in Figure 1.4. DeRieux was able to show that by increasing the acidity of the phosphines the electron density on the metal centre is decreased. The electron density can be therefore exactly tuned by the choice of the right linker and the substituents on the phosphine.

1.2.1 Application of Iron(II) $R^NP^NN^NP$ Pincer Complexes in the Selective Formation of 3-Hydroxyacrylates from Benzaldehyde Derivatives and Ethyl Diazoacetates

Aldehydes react with ethyl diazoacetates (EDA) in the presence of Lewis acids (e.g. BF_3 , $ZnCl_2$, $AlCl_3$, $SnCl_2$, $GeCl_2$) to β -keto esters.³⁷ Previously, Mossain was able to show that the Lewis acid

$[(\eta^5\text{-cp})\text{Fe}(\text{CO})_2\text{THF}](\text{BF}_4)$ catalysed the reaction of benzaldehyde derivatives with EDA to give mainly β -hydroxy-2-aryl acrylates.^{38,39} Also Brønsted acids like $\text{HBF}_4 \cdot \text{Et}_2\text{O}$ gave similar results.⁴⁰

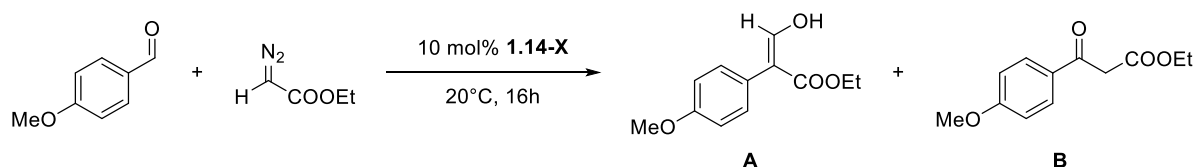


Figure 1.5: Formation of ethyl 3-hydroxy-2-(4-methoxyphenyl)acrylate from *p*-anisaldehyde and EDA catalysed by **1.14-X**.

More recently Benito-Garagorri and co-workers employed *cis*- $[(i^{\text{Pr}}\text{P}^{\text{N}}\text{N}^{\text{P}})\text{Fe}(\text{CO})(\text{CH}_3\text{CN})_2](\text{X})_2$ ($\text{X} = \text{BF}_4^-$, BArF^-) (**1.14-X**) in the coupling of *p*-anisaldehyde with EDA (Figure 1.5).²⁹ **1.14-BF₄** gave 84% of **A** after 16 hours at room temperature. Only trace amounts of the β -keto ester (**B**) could be observed. Changing the counter ion to a more loosely bound BArF^- , **1.14-BArF**, gave the coupling product, **A**, in 80% yield, with <3% of product **B**. This showed that the counter ion did not affect the reactivity of **1.14-X**. A tentative mechanistic proposal could be given (Figure 1.6), which was similar to the suggested mechanism by Mahmood.³⁸ The acetonitrile ligand *trans* to the CO ligand is more labile than the one *trans* to the pyridine N. This is due to the stronger *trans* effect of CO. The dissociation of the acetonitrile generates a free coordination site, which is then occupied by the aldehyde. Nucleophilic attack of EDA *via* an $\text{S}_{\text{N}}2$ -type mechanism formed the transition state **1.15** which gave complex **1.16** upon elimination of N_2 . A preferential migration of the aryl substituent over a hydride migration then gave intermediate **1.17** featuring a κ^1 (O)-coordinated aldehyde ester. A *p*-anisaldehyde then replaced the newly formed aldehyde. Immediate tautomerisation yielded the thermodynamically more stable ethyl 3-hydroxy-2-(4-methoxyphenyl)acrylate.²⁹

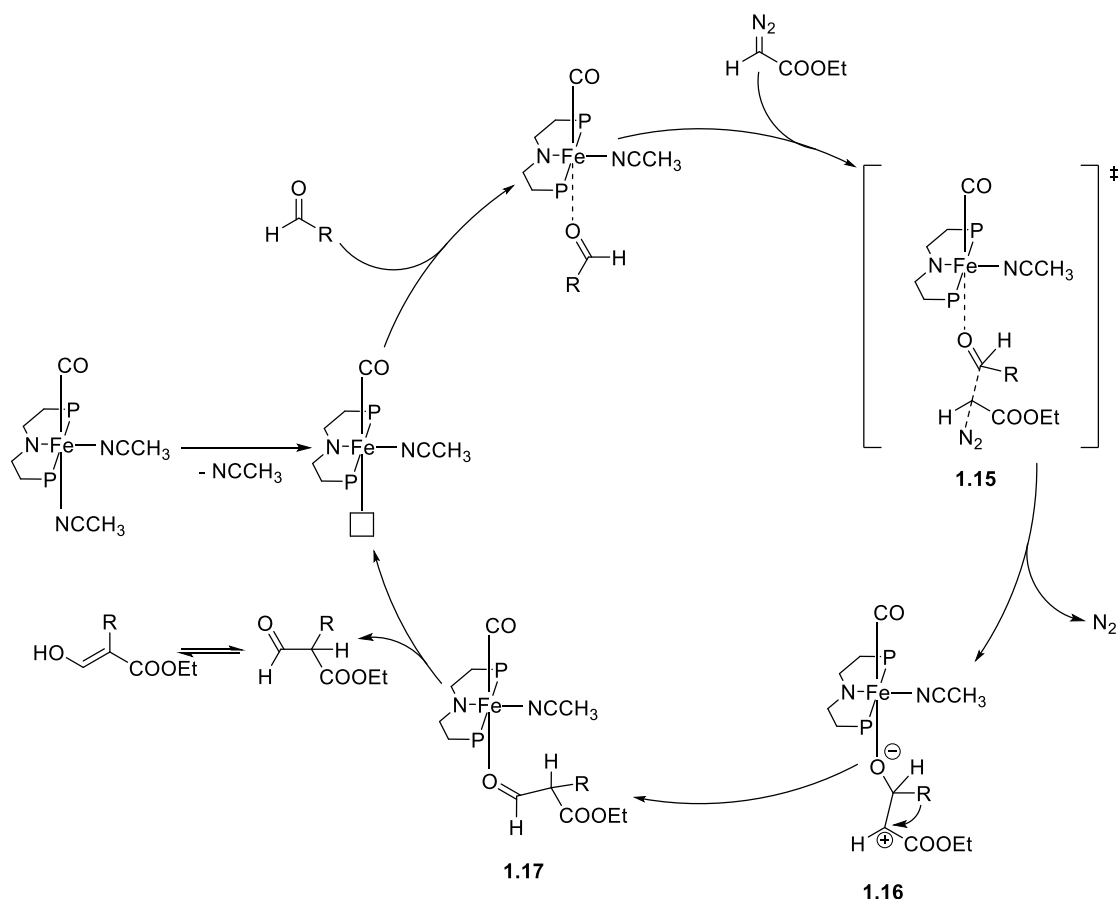


Figure 1.6: Mechanistic proposal for the formation of ethyl 3-hydroxy-2-(4-methoxyphenyl)acrylate from *p*-anisaldehyde and EDA catalysed by **1.14-X**.

Alves *et al.* extended the catalyst scope to *trans*-[(ⁱPrP^NN^NP)Fe(CO)₂Cl](X) (**1.18-X**) with X = NO₃⁻, CF₃COO⁻, CF₃SO₃⁻, BF₄⁻, PF₆⁻, SbF₆⁻ and BArF⁻.⁴¹ They were synthesised by treating **1.5** with the corresponding silver or sodium salt of X in the presence of CO. Interestingly the corresponding *cis*-isomer, [(ⁱPrP^NN^NP)Fe(CO)₂Cl](BPh₄) is catalytically inactive.²⁹ The substrate scope was then tested on various substituted benzaldehydes using **1.18-BF₄** as a catalyst. The yields of the ethyl 3-hydroxy-2-arylacrylates ranged between 34 – 90%, whereas the yields for the β-keto esters were below 3%. The influence of the counter ions on the reaction was then tested. Complex **1.18-X** (X = NO₃⁻, CF₃COO⁻, CF₃SO₃⁻, PF₆⁻, SbF₆⁻, BArF⁻) was used as the catalyst precursor and *p*-anisaldehyde as a model substrate. Interestingly **1.18-X** (X = NO₃⁻, CF₃COO⁻, CF₃SO₃⁻, SbF₆⁻, BArF⁻), showed no activity. Complex **1.18-PF₆** showed reduced activity and gave 20% yield (compared to 88% using **1.18-BF₄**). These results are in strong contrast to the previous results using **1.14-BF₄** and **1.14-BArF** as catalyst, where no counter ion influence was observed.²⁹ To gain insight into this phenomenon, the probable mechanism was investigated by means of DFT/B3LYP calculations, elucidating the chemoselectivity and the role of the counter ions in the reaction.

The reaction to form the desired ethyl 3-hydroxy-2-arylacrylates as the main product follows a lower energy barrier compared to the β -keto ester side product. More favourable is the pathway which is stabilised by hydrogen bonds between the acidic N-H of the ligand, the BF_4 anion and the EDA forming $(\text{N-H}\cdots\text{F-BF}_2\text{-F}\cdots\text{EDA})$.⁴¹

1.2.2 Application of Iron(II) $\text{R}^{\text{P}}\text{L}^{\text{N}}\text{L}^{\text{P}}$ Pincer Complexes in Molecular Hydrogen Reactivity

Trovitch *et al.* described the synthesis of the dinitrogen dihydride complex $[(^i\text{PrP}^{\text{C}}\text{N}^{\text{C}}\text{P})\text{Fe}(\text{H})_2(\text{N}_2)]$ (**1.19**). It showed to be unstable, undergoing decomposition to the free $^i\text{PrP}^{\text{C}}\text{N}^{\text{C}}\text{P}$ ligand and insoluble iron products over the course of hours in a benzene- d_6 solution at room temperature. Despite the decomposition, it readily hydrogenates simple acyclic and cyclic alkenes. The hydrogenation of 1-hexene took place in three hours with 0.3% catalyst loading and 4 bar of H_2 . The conversion was higher than 98%. Attempts to hydrogenate cyclohexene under same conditions were less successful. Only 10% conversion were observed after 6 and 24 hours, owing the fact that **1.19** decomposes over the course of the reaction.²⁰

Langer *et al.* described the synthesis of a new iron pincer complex $[(^i\text{PrP}^{\text{C}}\text{N}^{\text{C}}\text{P})\text{FeH}(\text{CO})\text{Br}]$ (**1.20**). It was active towards hydrogenation of ketones under very mild conditions. The reaction proceeded in ethanolic solution with 0.05 mol% of **1.20** and 0.1% of base. 4.1 bar of hydrogen pressure. Slightly elevated temperatures of 26 – 28°C were employed. It reached turnover numbers of up to 1880. A wide range of different aromatic ketones could be hydrogenated, with yields ranging from 54 to 94%. Aliphatic ketones like cyclohexanone could be reduced with 64% yield. This protocol showed to be less selective when it was applied to enone systems, like *E*-4-phenylbut-3-en-2-one and cyclohex-2-enone, where the double bond was preferably hydrogenated. From benzaldehyde only 36% benzylic alcohol could be isolated.²² This low yield could be due catalyst poisoning by benzoic acid, which was formed in small quantities *via* a Cannizzaro reaction. Zell *et al.* were able to show that, by lowering the catalyst loading to 0.025 mol% and increasing the loading of $\text{KO}t\text{Bu}$ to 0.625% in an ethanol/ NEt_3 (2:1) solution at 40°C and 30 bar H_2 , the yield could be increased to 99%, with TON's of up to 4000. This protocol is applicable to different aromatic and aliphatic aldehydes.²⁷

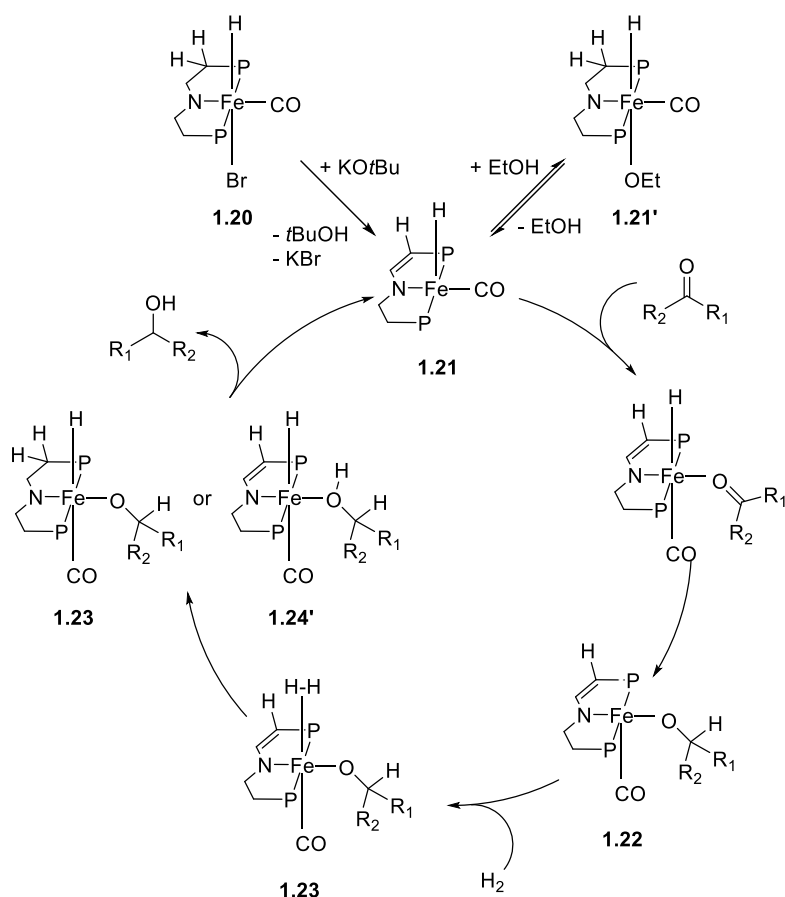


Figure 1.7: Proposed catalytic cycle for the hydrogenation reactions of ketones using $[(iPr)PCNCP]FeH(CO)Br$ (**1.20**) as a pre-catalyst.

However, to gain some mechanistic insight in the hydrogenation reaction of **1.20** with ketones, stoichiometric reactions were undertaken. Preliminarily it was shown that the reaction which gave the best results was in ethanol; in THF and neat acetophenone no reaction was observed. These experiments revealed that the bridging methyl group of **1.20** gets deprotonated in the presence of $KOtBu$ to form a dearomatized pyridine ring (Figure 1.7, Species **1.21**). The 5-coordinated 16 VE species $[(iPr)PCNCP-H]FeH(CO)$ (**1.21**) might be stabilised by reversible addition of ethanol to afford the 6-coordinate species **1.21'**. The ketone then coordinates to **1.21** and inserts into the iron-hydride bond to give the alkoxide complex **1.22**. This intermediate then readily adds hydrogen to give intermediate **1.23**. Heterolytic cleavage of the hydrogen may afford the re-aromatized hydrido alkoxide complex **1.24**. Alternatively, the adjacent alkoxy could act as base for the heterolytic cleavage of the hydrogen to give complex **1.24'**. The formation of **1.24'** would not require the protonation of $iPrPCNCP-H$. The catalytic cycle is closed by elimination of the alcohol, which thereby regenerates **1.21**.^{22,42}

Based on the $[(iPr^CNCP)FeH(CO)Br]$ complex system Langer *et al.* then developed a catalytic protocol that enabled the hydrogenation of ketones without the use of an additional base. Therefore they synthesised $[(iPr^CNCP)FeH(CO)(\eta^1BH_4)]$ (**1.25**) and $[(iPr^CNCP)FeH(\eta^2BH_4)]$ (**1.26**). Both borohydride complexes (**1.25** and **1.26**) were then employed in the hydrogenation reaction of acetophenone with 4.1 bar hydrogen pressure at ambient temperatures. 0.05 mol% catalyst was used in ethanolic solution. While **1.25** showed a poor conversion of 12%, increasing the temperature to 40°C also increased the catalytic activity to a similar level as compared with **1.20** at ambient temperatures. **1.26** showed no conversion at either temperature. Extending the substrate scope showed a similar behaviour as for the $[(iPr^CNCP)FeH(CO)Br]$ system. Aromatic and aliphatic ketones could be readily reduced to the corresponding alcohol with yields ranging from 53% to 99%. **1.25** also has a low selectivity. The reaction of *E*-4-phenylbut-3-en-2-one as substrate gave 4-phenyl-2-butanol as major product with a yield of 65%. In aprotic solvents, like benzene-*d*₆ and toluene-*d*₈, $[(iPr^CNCP)FeH(CO)(\eta^1BH_4)]$ reacts under loss of BH₃ to *trans*- $[(iPr^CNCP)Fe(H)_2(CO)]$, which is in equilibrium with *cis*- $[(iPr^CNCP)Fe(H)_2(CO)]$. Neither complex reacts with acetophenone, which excludes their participation in the catalytic reaction. The mechanism was then investigated using DFT calculations, but the results were too inconsistent to be further discussed.²⁴

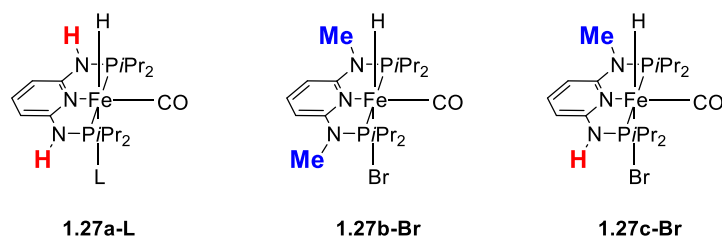


Figure 1.8: Structures of complexes **1.27a-L**, **1.27b-Br** and **1.27c-Br**.

Gorgas recently synthesised a series of $[(iPr^PN^NCP)FeH(CO)L]^n$ (**1.27-L**) with $L = Br^-$, CH_3CN , pyridine, PMe_3 , SCN^- , CO and BH_4^- and n ranging from 0 to +1. The spacers between the phosphines and pyridine were either NH and/or NMe. The complex **1.27a-Br** (Figure 1.8) was employed in the hydrogenation reaction of acetophenones with 5 bar hydrogen pressure and 25°C. 1.0 mol% catalyst and 2.0 mol% $KOtBu$ were used. Preliminary various solvents were tested. Interestingly the reaction proceeded only in alcoholic solutions, with ethanol giving the best results (99% yield). This was consistent with the results observed in Langer's system $[(iPr^CNCP)FeH(CO)Br]$ (**1.20**). Therein ethanol is proposed to stabilise the catalytic active **1.21**.²² Complex **1.27b-Br** was completely unreactive towards ketones, while **1.27c-Br** showed a reduced activity giving 28% of

1-phenylethanol. Changing the Br substituent of **1.27a-Br** to CH₃CN and BH₄⁻ showed a similar activity with 94% yield. Using [(ⁱPrP^CN^CP)FeH(CO)(η¹BH₄)] (**1.25**),²⁴ the reaction proceeded even without the addition of a strong base, although the elevated temperature of 50°C was necessary. The complexes with less labile ligands, **1.27-L** (L = pyridine, PMe₃, SCN⁻, CO), were catalytically inactive. The scope and limitations of **1.27a-Br** were comparable to **1.20** with yields ranging from 34% to 99%. Interestingly, the TOF's were higher than those obtained in Langer's system. In the case of **1.20** and **1.25** TOF's up to 90 h⁻¹ and 330 h⁻¹ were reached, Gorgas reached TOF's up to 770 h⁻¹. A huge difference could be observed in the hydrogenation of aldehydes. Langer reported yields of 36% and 15% in the hydrogenation of benzaldehyde using **1.20** and **1.25**, respectively. Gorgas obtained 23% with the standard conditions (0.5 mol% **1.27a-Br** and **1.27b-Br**, 1.0 mol% KO^tBu, 5 bar H₂, r.t., 2h), although increasing the catalyst and base loading to 5 and 10 mol%, respectively, gave conversions of 99%. Both aromatic and aliphatic aldehydes could be successfully reduced.³⁵

To gain further insight into the operating mechanism, stoichiometric reactions of **1.27a-Br** were investigated and later confirmed by DFT calculations. **1.27a-Br** reacts with one equivalent of base to afford the deprotonated 5-coordinated complex [(ⁱPrP^NN^NP^H)FeH(CO)] (**1.28**). An incoming ketone coordinates to the vacant coordination site on the complex and successively inserts into the iron-hydride bond to give the 5-coordinated alkoxide complex [(ⁱPrP^NN^NP^H)Fe(OCHRR')(CO)] (**1.29**; OCHRR' = alkoxide). Hydrogen coordinates to **1.29** to give [(ⁱPrP^NN^NP^H)Fe(H₂)(OCHRR')(CO)] (**1.30**). The hydrogen is then further activated by the oxygen of the alkoxide with formation of the alcohol and regeneration of the hydride species [(ⁱPrP^NN^NP^H)FeH(HOCHRR')(CO)] (**1.31**). Replacing the alcohol product with an incoming ketone closes the catalytic cycle. Gorgas could show that the amine stays deprotonated throughout the whole cycle. The energy barrier for the protonation of the alkoxide molecule is 16.0 kcal/mol, which is lower than the 34.1 kcal/mol for the protonation of the imine in the ligand. Further calculations with ethanol included showed that the alcohol acts as a proton shuttle to transfer the proton from the dihydride in species **1.29** to the alkoxide.³⁵ The results obtained are in accordance with the proposed mechanism by Milstein and Langer.²²

The *trans*-[(ⁱPrP^CN^CP)Fe(H)₂(CO)], which is in equilibrium with *cis*-[(ⁱPrP^CN^CP)Fe(H)₂(CO)] and their counterparts with a ⁱPrP^NN^NP ligand proved to be inefficient in the stoichiometric reaction with acetophenone.^{22,24,35} Recently Langer *et al.* were able to show that 0.1 mol% *trans*-[(^tBuP^CN^CP)Fe(H)₂CO] (**1.32**) readily reduced sodium bicarbonate in a THF/H₂O (1:10) solution in the presence of 8.3 bar of hydrogen. Successive optimisation of the reaction conditions

showed that in a 2N sodium hydroxide solution (THF/H₂O = 1:10) with 10 bar H₂/CO₂ mixture (ratio 2:1) TON's of up to 788 with TOF's of $\leq 156 \text{ h}^{-1}$ can be reached. The yields of sodium formate are usually around 40%. To gain some mechanistic understanding of the reaction, stoichiometric reactions were undertaken. **1.32** formed an orange precipitate in a pentane solution in the presence of carbon dioxide. NMR and IR studies suggested that carbon dioxide inserts into one iron hydride bond through direct attack of a hydride giving $[(^t\text{BuP}^{\text{C}}\text{N}^{\text{C}}\text{P})\text{Fe}(\text{H})(\eta^1\text{-OOCH})\text{CO}]$ (**1.33**). The structure was confirmed by X-ray analysis. Dissolution of **1.33** in water showed that the formate ligand can be easily replaced by water to form $[(^t\text{BuP}^{\text{C}}\text{N}^{\text{C}}\text{P})\text{Fe}(\text{H})(\text{H}_2\text{O})\text{CO}]$ (**1.34**). Addition of an excess amount of KOH showed no change of the resulting NMR spectra suggesting that the ligands are not deprotonated. A catalytic cycle was proposed (Figure 1.9), in which carbon dioxide attacks **1.32** forming the formate complex **1.33**. The formate is replaced by an incoming water molecule, which is then followed by coordination of hydrogen to give $[(^t\text{BuP}^{\text{C}}\text{N}^{\text{C}}\text{P})\text{Fe}(\text{H})(\text{H}_2)\text{CO}]$ (**1.35**). An incoming hydroxide activates the hydrogen for heterolytic cleavage. This can either occur externally, giving complex **1.36**, or with involvement of the ligand, forming the dearomatised complex **1.36'**. Elimination of one molecule of water regenerates the starting complex **1.32**.²³

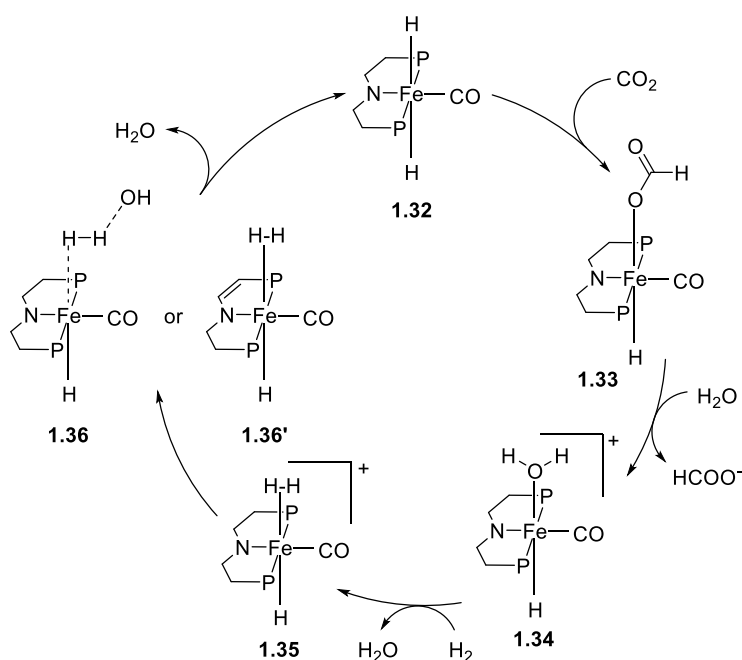


Figure 1.9: Mechanistic proposal for the trapping of CO₂ as formic acid using *trans*-[(^tBuP^CN^CP)Fe(H)₂(CO)] (**1.32**) as a catalyst.

In a THF solution in the presence of trialkylamine bases at 40°C, complex **1.32** showed a high efficiency in the decomposition of formic acid to hydrogen and CO₂. Turnover numbers of up to 100,000 could be reached. **1.32** exhibited a high tolerance towards solvents and the reaction can be performed in good to excellent yields in THF, 1,4-dioxane and DMSO. Even ethanol, acetonitrile and water can be used as solvent, although the reactivity of **1.32** is significantly lower in these cases. The catalytic reaction is tolerant to air. 0.1 mol% of catalyst in a 1,4-dioxane/THF (3:1) mixture with 50 mol% trimethylamine and formic acid were exposed to air. The reaction was complete after three hours. An increase in pressure to 10 bar slightly decreased the TOF to 494 h⁻¹ (compared to 520 h⁻¹ in open-system conditions). These experiments showed that the formic acid decomposition is irreversible under these conditions. Employing **1.33** gave practically the same results. Following the decomposition reaction by NMR also showed the presence of complex **1.33**. This strongly suggested that the hydrido-formate complex **1.33** plays a role in the catalytic cycle.²⁵

1.3 Monoanionic Benzene-Based ^RP^LC^LP Ligand Systems and Their Application in Iron Catalysis

The synthesis and application of ^RP^LC^LP iron complexes is relatively scarce compared to their pyridine counterparts (^RP^LN^LP). One reason for this is that iron has a low tendency to undergo σ -bond metathesis or a two electron oxidative addition, especially in its most stable oxidation states +II and +III. However, these complexes are mostly formed *via* cyclometalation reactions. To promote the iron-carbon bond formation, iron precursors in a low oxidation state or with basic ligands, like alkoxides and alkyl groups, are used.⁴³⁻⁴⁵

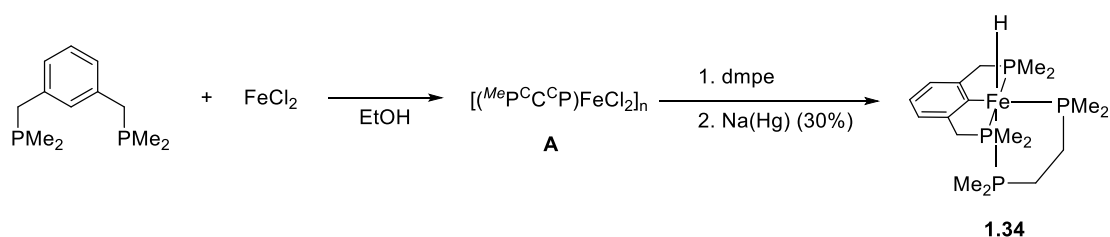


Figure 1.10: Reaction pathway for the formation of $[(\text{MePCCCP})\text{Fe(H)(dmpe)]$ (**1.34**).

Creaser and Kaska described the synthesis of $[(^{\text{Me}}\text{P}^{\text{C}}\text{C}^{\text{P}})\text{Fe}(\text{H})(\text{dmpe})]$ (**1.34**, Figure 1.10). Treating the $^{\text{Me}}\text{P}^{\text{C}}\text{C}^{\text{P}}$ ligand with hydrated ferrous chloride in an ethanolic solution resulted in the precipitation of a white polymeric compound $[(^{\text{Me}}\text{P}^{\text{C}}\text{C}^{\text{P}})\text{FeCl}_2]_n$ (**A**). This polymeric compound readily forms in the presence of dmpe (1,2-bis(dimethylphosphino)ethane) and 30% sodium amalgam **A**. The structure and composition were confirmed by NMR and IR. Apparently the insertion into the C-H bond of the benzene took place when the Fe(II) was reduced to Fe(0). The authors describe that besides **1.34**, some paramagnetic residues could also be observed.⁴⁶

There are yet no examples known to the literature that employ iron $^{\text{R}}\text{P}^{\text{N}}\text{C}^{\text{N}}\text{P}$ complexes. Only a few examples can be found with cobalt,⁴⁷ nickel,⁴⁷⁻⁴⁹ iridium,⁵⁰ and platinum⁴⁹ pincer complexes. The vast majority describe the synthesis of palladium $^{\text{R}}\text{P}^{\text{N}}\text{C}^{\text{N}}\text{P}$ complexes⁵¹ and their application in Heck,⁵²⁻⁵⁶ Suzuki,^{55,57,58} and Sonogashira⁵⁹ coupling reactions.

Bhattacharya *et al.* synthesised $[(^{\text{R}}\text{P}^{\text{O}}\text{C}^{\text{O}}\text{P})\text{FeH}(\text{PMe}_3)_2]$ (**1.35-R**; R = *i*Pr, Ph) in 67% and 69% yield. The reaction proceeds, as above mentioned, *via* cyclometalation of Fe(0)(PMe₃)₄ into the C-H bond of $^{\text{R}}\text{P}^{\text{O}}\text{C}^{\text{O}}\text{P}$ ligand. **1.35-*i*Pr** was then employed in the hydrosilylation reaction of various aryl aldehydes with 1 mol% of catalyst loading using (EtO)₃SiH as a reducing agent. The reaction normally proceeds at 50°C or 65°C in a time range of 1-3.5 hours. The yields obtained were higher than 80%. Aryl ketones were tested under the same reaction conditions and in general they show a lower reactivity. The reaction needed between 4.5 to 48 hours, depending on the substrate. In some cases, it was necessary to raise the temperature needed to 80°C. In order to gain some mechanistic insight, stoichiometric reactions with **1.35-*i*Pr** and benzaldehyde were performed. Benzaldehyde showed no reaction with the iron hydrido complex, which excludes its insertion into the Fe-H bond. Stirring a THF solution of **1.35-*i*Pr** in CO atmosphere for 24 hours at room temperature quantitatively formed $[(^{\text{iPr}}\text{P}^{\text{O}}\text{C}^{\text{O}}\text{P})\text{FeH}(\text{PMe}_3)(\text{CO})]$ (**1.36**) with the CO ligand *trans* to the hydride. This can be expected, since the hydride has a stronger *trans*-effect, which makes the *trans* PMe₃ more labile. Complex **1.36** slowly isomerised to the thermodynamically more stable $[(^{\text{iPr}}\text{P}^{\text{O}}\text{C}^{\text{O}}\text{P})\text{FeH}(\text{PMe}_3)(\text{CO})]$ (**1.36'**) where the CO is positioned *cis* to the hydride, although this reaction took place over 7 days at 60°C. Reaction of deuterium-labelled C₆H₅CDO with Ph₂SiD₂ and **1.35-*i*Pr** (1:1:1) showed the sole formation of Ph₂SiD(OCD₂C₆H₅) and Ph₂Si(OCD₂C₆H₅)₂ in a ratio of 4:1, with no deuterium incorporation into **1.35-*i*Pr**. This experiment excluded the involvement of the hydride in the reaction. Based on these observations Bhattacharya was able to make a mechanistic proposal (Figure 1.11).⁶⁰

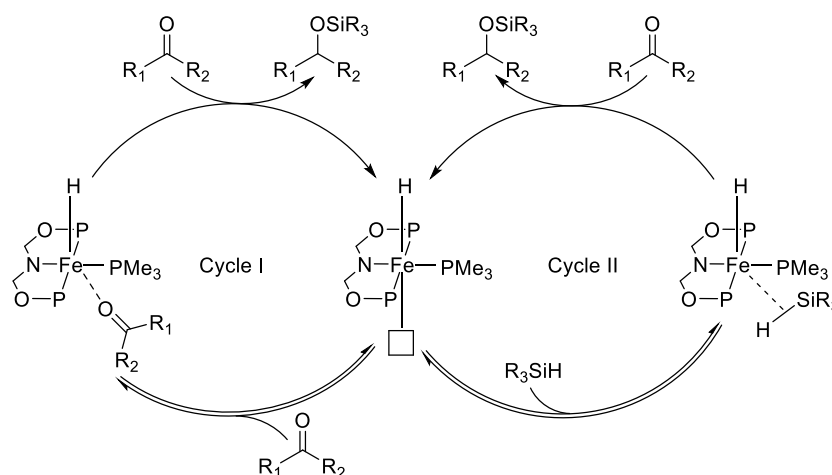


Figure 1.11: Possible pathways of the hydrosilylation reaction of carbonyls using **1.35-*i*Pr** as a catalyst.

The PMe_3 substituent *trans* to the hydride dissociates to give place to a vacant coordination site. The isomerisation where the other PMe_3 ligand moved *trans* to the hydride is too slow to be catalytically relevant. An incoming carbonyl compound can coordinate to the open coordination site either η^1 - or η^2 followed by the reduction of the silane (Figure 1.11; Cycle I). Alternatively, the silane could first couple to the vacant site as a η^2 -silane or as a σ -adduct with a subsequent reduction of the aldehyde (Figure 1.11; Cycle II).⁶⁰ Wang *et al.* recently made a DFT study to confirm either reaction mechanism (Figure 1.11; Cycles I and II). The results obtained favoured cycle I. They found that the coordinated carbonyl isomerised with the coordinated PMe_3 . This isomerisation was followed by an insertion into the Fe-H bond, giving an iron alkoxide complex. The cycle was closed by σ -bond metathesis, yielding the silyl ether and regenerating the iron hydride species.⁶¹ The calculated results were in stark contrast with the experimental findings. The above mentioned experiment using benzaldehyde-*d* and Ph_2SiD_2 showed that the hydride substituent is not involved in the catalytic cycle.⁶⁰

Bhattacharya showed the efficacy of **1.35-*i*Pr** in the hydrogen release reaction of NH_3BH_3 (AB) (Figure 1.12), which is an interesting molecule for chemical storage of H_2 . Mixing **1.35-*i*Pr** with AB in diglyme showed no reaction at room temperature, although heating the solution up to 60°C resulted in an immediate gas formation. After 24 hours, 2.5 equivalents of H_2 per molecule AB were measured. The reactivity of **1.35-*i*Pr** could be increased by replacing the two PMe_3 substituents with PMe_2Ph giving complex $[(^i\text{PrP}^{\text{O}}\text{C}^{\text{O}}\text{P})\text{Fe}(\text{H})(\text{PMe}_2\text{Ph})_2]$ (**1.37**). Complex **1.37** showed an increased activity in the beginning of the reaction, but slowed over the course of the reaction and completely ceased after

12 hours. The colour of the solution became increasingly dark, which could point to degradation of the catalyst. A further attempt was undertaken to increase the electron density of the metal centre, by substituting the benzene ring with a methoxy group *para* to the Fe-C bond (Figure 1.12, complex **1.38**). **1.38** showed a higher activity than **1.35-*i*Pr** and **1.37**. It formed 2.5 equivalents of H₂ per molecule of AB after 16 hours. **1.38** also seemed more stable under catalytic conditions than **1.37**. No colour change was observed.⁶²

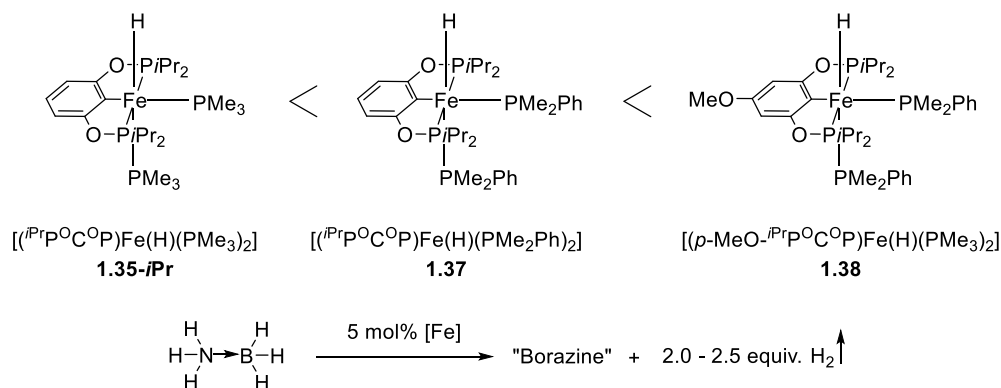


Figure 1.12: Hydrogen liberation reaction from amino boranes. An increase in reactivity from **1.35-*i*Pr** to **1.38** can be observed.

Recently Bhattacharya *et al.* were able to show that [(*i*PrP^OC^OP)FeH(PMe₃)(CO)] (**1.36**) and *cis*-bis carbonyl complex [(*i*PrP^OC^OP)FeH(CO)₂] (**1.39**) readily react with a Brønsted acid, like HBF₄·Et₂O, under hydride abstraction, to give the cationic complexes [(*i*PrP^OC^OP)Fe(PMe₃)(CO)](BF₄) (**1.40**) and *cis*-[(*i*PrP^OC^OP)Fe(CO)₂](BF₄) (**1.41**). The reaction with **1.35-*i*Pr** was not possible due to facile protonation of PMe₃. **1.40** and **1.41** were able to activate hydrogen in the presence of Hünig's base to give back the neutral hydride complexes **1.36** and **1.39**, respectively. (*i*Pr₂EtNH)(BF₄) was formed as a by-product. The catalytic application of both complexes in the hydrogenation of benzaldehyde was unsuccessful. Although both, **1.40** and **1.41**, were active catalysts for the hydrosilylation reactions of benzaldehyde and acetophenone. Interestingly, they showed an increased activity over the corresponding neutral hydride complexes, **1.36** and **1.39**.⁶³

1.4 Pyridine Di(imino) Pincer Systems and Their Application in Iron Catalysis

Iron pyridinediimino (PDI) complexes of the type $[(^{\text{Ar}}\text{N}^{\text{R}}\text{N}^{\text{R}}\text{N})\text{FeX}_2]$ (**1.42-X₂**, Figure 1.13) as described by Brookhart^{64,65} and Gibson^{66,67} have already been successfully studied as catalysts for polymerisation and oligomerisation reactions. These reactions are beyond the scope of this introduction and will not be discussed in this section. The following section will highlight the work that has been done by Chirik and co-workers. Although PDI ligands are seldom referred to as pincer ligands, they can be considered as such due to their meridional coordination around the metal centre.

1.4.1 The Catalytic Activity of Iron Bis(imino)pyridine Pincer Complexes in the Hydrogenation and Hydrosilylation of Unactivated and Functionalised Olefins and Carbonyls

The complexes **1.42-X₂** (X = Cl, Br) were first targeted by Bart and co-workers as potential well-defined iron precursors to synthesise 14-electron Fe(0) complexes of the type $\text{L}_3\text{Fe}(0)$ under mild thermal conditions. PDI pincer ligands proved to be an attractive choice due to their modularity and easy synthesis. Additionally, their relative π -acidity compared to the σ -donating alkyl phosphines (*vide supra*) may also aid in stabilising the electron rich Fe(0) centre.⁶⁸

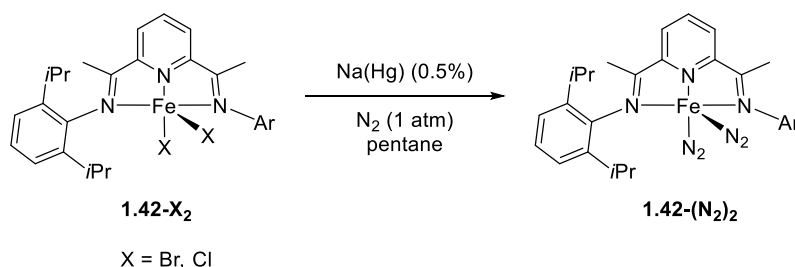


Figure 1.13: Reaction scheme for the formation of $[(^{\text{Ar}}\text{N}^{\text{Me}}\text{N}^{\text{Me}}\text{N})\text{Fe}(\text{N}_2)_2]$ (**1.42-(N₂)₂**; Ar = 2,6-*i*Pr₂-C₆H₃).

1.42-(N₂)₂ can be readily synthesised by reducing **1.42-Br₂** or **1.42-Cl₂** with 0.5% sodium amalgam in pentane and 1 atm of N₂. The compound was characterised by a combination of elemental analysis, IR, electronic spectroscopies and X-ray diffraction as a 5 coordinated compound, with a slightly distorted square pyramidal structure. The PDI ligand occupied three sites of the basal square and the two dinitrogen ligands the apical position. Bart was able to show that upon dissolution in toluene, **1.42-(N₂)₂** lost 1.0 equivalent of N₂ to give **1.42-(N₂)**.

Table 1.1: Hydrogenation of terminal and internal olefins using 0.3 mol% **1.42-(N₂)₂** as catalyst.

Entry	Alkene	Product	Time [min]	TOF [h ⁻¹] ^a
1			12	1814
2			16	1344
3			380	57
4			210	104
5			60	363
6			210	104
7			360	3.3 ^b

^a at 98% conversion. ^b 5.0 mol% **1.42-(N₂)₂** were used.

1.42-(N₂)₂ was then employed in the hydrogenation reaction of various terminal and internal olefins (Table 1.1). The reaction was conducted with 0.3 mol% loading of **1.42-(N₂)₂** at room temperature in a toluene solution, under 4 atm of hydrogen. Terminal alkenes like 1-hexene and styrene could be reduced to the corresponding alkane within several minutes, with TOF's up to 1814 h⁻¹. Internal and geminal olefins, like α -methylstyrene and cyclohexene, could be effectively hydrogenated, although reaction times of 210 min and 380 min were needed for complete conversion. Diolefins, such as 1,5-hexadiene and (*R*)-(+)-limonene, were also hydrogenated within 60 min and 210 min. The hydrogenation of (*R*)-(+)-limonene gave selectively (+)-*p*-menth-1-ene, showing that

this protocol preferentially reduces geminal olefins over tri-alkyl olefins. Preparative hydrogenation can be also carried out in neat alkenes with high activities. For example, applying 4 atm of hydrogen pressure to a 0.04 mol% solution of **1.42-(N₂)₂** in 1-hexane or cyclohexene gave complete conversion after 19 and 26 h, respectively. Internal alkynes were also successfully hydrogenated. The reaction of diphenylacetylene with 0.3 mol% **1.42-(N₂)₂** in benzene-*d*₆ was followed by ¹H-NMR, which showed first the formation of *cis*-stilbene, which was then further reduced to 1,2-diphenylethane. Attempts to hydrogenate terminal alkynes were unsuccessful.⁶⁸ Trovitch *et al.* extended the scope to substituted olefins in order to investigate the tolerance towards functional groups. Primary, secondary and tertiary 3-amino-1-propenes can be readily reduced. Interestingly, the reactivity increased with the substitution degree on the amine. The primary 3-amino-1-propene had a conversion of 20% after 24 hours resulting in a TOF of 3 h⁻¹. 3-(*N*-methylamino)-1-propene showed almost full conversion after 60 minutes with a TOF of 320 h⁻¹. The tertiary 3-(*N,N*-dimethylamino)-1-propene and 4-methyl-1-pentene reached a conversion of 95% after 15 minutes with a TOF of 1270 h⁻¹, which is in a similar range to that of styrene (1311 h⁻¹). The lower activity of the primary and secondary compounds is due to the coordination of the amine to the iron centre. Fluorinated olefins were in general well-tolerated, both *p*-fluoro- and pentafluorostyrene were hydrogenated at a similar rate as styrene. Oxygen-substituted olefins bearing various ether, ester and ketone functionalities were screened, although a higher loading of 5 mol% was needed. The nature and position of the oxygen-containing substituents have an influence on the turnover of the reaction. Ethyl vinyl-, ethyl allyl- and diallyl ethers were hydrogenated at a similar rate to normal hydrocarbons with TOF's higher than 240 and 480 h⁻¹. Carbonyl-substituted alkenes had a drastic impact on the reactivity of **1.42-(N₂)₂**. 5-hexen-2-one only reached 93% conversion at an elevated temperature of 65°C, while (+)-dihydrocarvone showed no conversion after 15 hours at 65°C. Carboxylated olefins showed different hydrogenation activities. Methyl *trans*-cinnamate exhibited similar TOF's as those of 1-phenylpropene. Vinyl- and allyl acetate showed no activity. The geminal olefin diester dimethyl itaconate was also effectively hydrogenated, although the TOF's were low (3.3 h⁻¹). Internal and trisubstituted olefins were also hydrogenated with good to excellent conversions.⁶⁹

The previous success in hydrogenation prompted a further investigation of the reactivity of **1.42-(N₂)₂** in hydrosilylation of olefins. Indeed, 1-hexene readily reacted with either PhSiH₃ or Ph₂SiH₂ in the presence of 0.3 mol% of **1.42-(N₂)₂** over the course of several minutes at room temperature. Both silanes gave the anti-Markovnikov product. The hydrosilylation with PhSiH₃ proceeded faster than with Ph₂SiH₂. Based on these results, the substrate scope was extended to several terminal, geminal and internal olefins (Table 1.2).

Table 1.2: Hydrosilylation of terminal and internal olefins using 0.3 mol% **1.42-(N₂)₂** as catalyst and PhSiH₃ as reducing agent.

Entry	Alkene	Product	Time [min]	TOF [h ⁻¹] ^a
1			60	364
2			90	242
3			4200	0.09 ^b
4			930	23
5			210	104
6			1110	20
7			120	182

^a at >98% conversion. ^b 25% of the internal hydrosilylation product was also obtained.

The results of the hydrosilylation experiments (Table 1.2) show the same trend as in the hydrogenation (Table 1.1). Terminal olefins such as 1-hexene and styrene react fastest, with TOF's of 364 and 242 h⁻¹ (Table 1.2, Entries 1 and 2). Geminal alkenes show a lower reactivity with a TOF of 104 h⁻¹ for α -methylstyrene (Entry 5) and 182 h⁻¹ for (*R*)-(+)-limonene (Entry 7). For the latter, only the geminal double bond was reduced. Internal olefins show the lowest reactivity. In the case of *trans*-2-hexene the terminally-functionalised product is predominant, although 25% of the internal product could be observed. Alkynes could be also reduced. Reacting diphenylacetylene with PhSiH₃ produced the corresponding *cis*-silylstilbene in quantitative yield. A further reaction of the resulting alkene was not observed.⁶⁸

The low and sometimes unpredictable reactivity of **1.42-(N₂)₂** with carboxylated olefins (Table 1.1, Entry 7) can be explained with the oxidative addition reaction of the carbon-oxygen bond of the ester moiety to the metal centre. This reaction forms stable iron complexes that are inactive for

further hydrogenation reactions. This deactivation pathway is competing with the productive hydrogenation and hydrosilylation reactions. Depending on the substrate, the hydrogenation of the double bond can be observed. For example, for substrates such as methyl *trans*-cinnamate, the hydrogenation reaction is faster than the C-O cleavage. Therefore, a conversion to the corresponding methyl 3-phenylpropionate can be observed. For compounds such as vinyl- and allyl acetate, the C-O cleavage reaction is much faster compared to the reduction of the alkene. The reduced alkane cannot be observed.^{69,70}

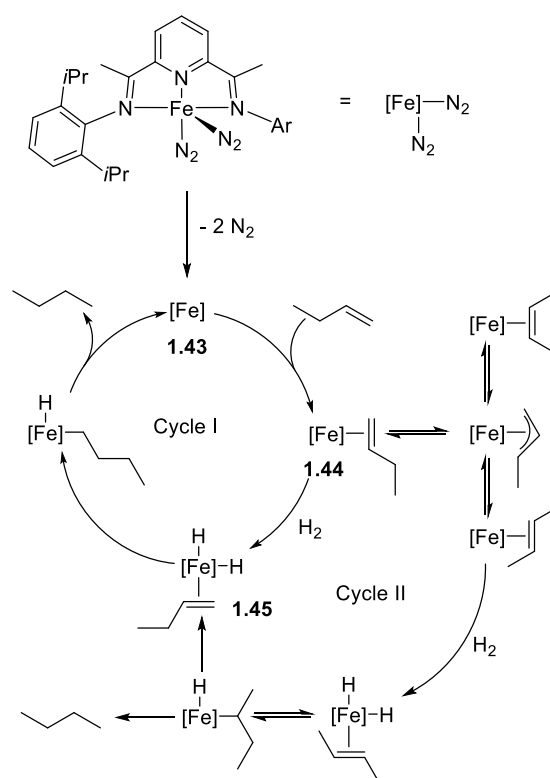


Figure 1.14: Proposed catalytic cycle for the hydrogenation of terminal and internal olefins.

Bart *et al.* could propose a catalytic cycle (Figure 1.14, Cycle I). Loss of the N_2 substituents from $\mathbf{1.42-(N_2)_2}$ (or alternatively $\mathbf{1.42-N_2}$) gave the catalytically-active 14-electron species $[(^{Ar}N^{Me}N^{Me}N)Fe^0]$ ($\mathbf{1.43}$, $Ar = 2,6-iPr_2-C_6H_3$). This step is followed by coordination of an olefin to give $\mathbf{1.44}$. The olefin coordination is preferred over H_2 coordination. The compounds resulting from the reaction of $\mathbf{1.42-(N_2)_2}$ with alkenes and alkynes proved to be more stable than the complexes formed by reaction with hydrogen. The olefin coordination is followed by oxidative addition of hydrogen to intermediate $\mathbf{1.44}$ to give the formal 18-electron iron(II) complex ($\mathbf{1.45}$). Insertion into the Fe-H bond and reductive elimination then give the reduced alkane product and regenerate the starting complex $\mathbf{1.43}$. Isotopic labelling experiments with D_2 revealed that this cycle is accompanied

by “chain walking” of internal olefins (Figure 1.14, Cycle II). This suggests a competing β -hydrogen elimination of the secondary alkyl complex to yield the terminal alkyl dihydride complexes. However, a reverse β -hydrogen elimination of primary alkyl complexes to form internal alkyl complexes does not compete with the catalytic reaction. In the absence of H_2 an isomerisation of olefins was observed. This process probably proceeds *via* allylic C-H bond activation (Figure 1.14, Cycle II). This reaction also did not compete with the hydrogenation reaction, as no isomerised products could be observed.⁶⁸

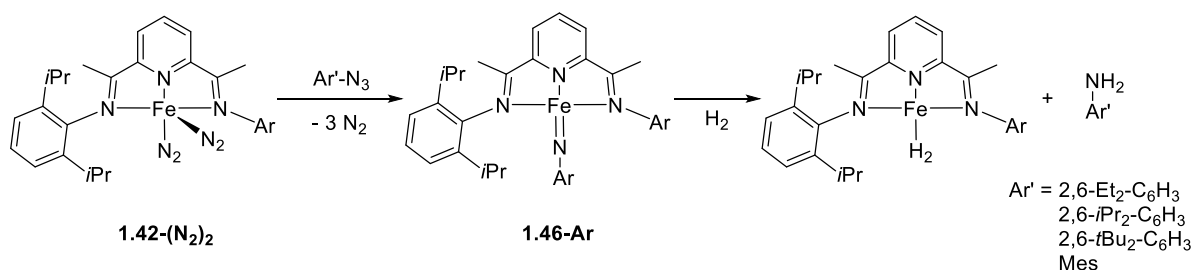


Figure 1.15: Reactivity of aryl azide compounds with **1.42-(N₂)₂** and hydrogen.

1.42-(N₂)₂ reacted with stoichiometric amounts of aryl azides to form iron imide complexes **1.46-Ar** in good yields. Concomitant to the formation, three equivalents of N_2 were observed. The addition of H_2 to a solution of **1.46-Ar** induced resulted in the formation of the free aniline derivative and the iron hydrogen complex **1.42-H₂**. Bart *et al.* were able to show in their previous work that in presence of N_2 the hydrogen easily dissociates from **1.42-H₂** to give back **1.42-N₂**.⁶⁸ This demonstrated that the reaction could also be performed in a catalytic manner. Indeed, a series of azides used to form **1.46-Ar** were hydrogenated at 23°C in the presence of 10 mol% **1.42-(N₂)₂** and 1 atm of H_2 to the corresponding anilines. The reaction rate of the hydrogenation reaction was in direct correlation to the size of the aryl residue. 2,6-*i*Pr₂-C₆H₃ was the fastest reacting, reaching full conversion after 6 hours at 23°C . 2,5-*t*Bu₂-C₆H₃ and 2,6-Et₂-C₆H₃ needed 16 and 96 hours at 65°C . 2,6-Me₂-C₆H₃ showed no conversion after 24 hours at 65°C .⁷¹

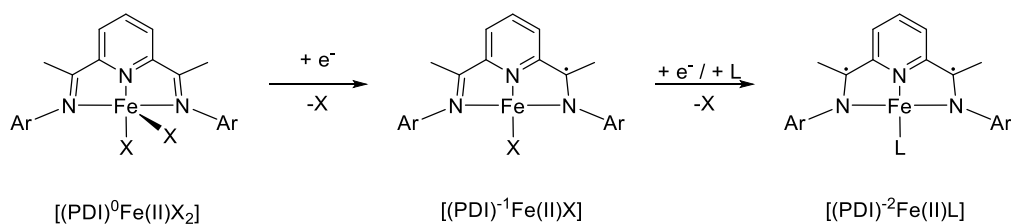


Figure 1.16: Redox-active, not-innocent pyridine bis(imino) pincer ligands.

The electronic structures of **1.42-X₂** had been intensively investigated by Mössbauer spectroscopy, high quality structural analysis and DFT calculations. The results, summarised in Figure 1.16, show that a single electron reduction from **1.42-Cl₂** to **1.42-Cl** results in a formal reduction of the PDI ligand, yielding a monoanionic ligand. The iron centre shows a high spin configuration but is not reduced. Further reduction of **1.42-Cl** in the presence of a weak-field ligand such as N₂ or DMAP (*N,N*-dimethylaminopyridine) resulted in a dianionic PDI ligand and an intermediate spin iron(II) ion.⁷²

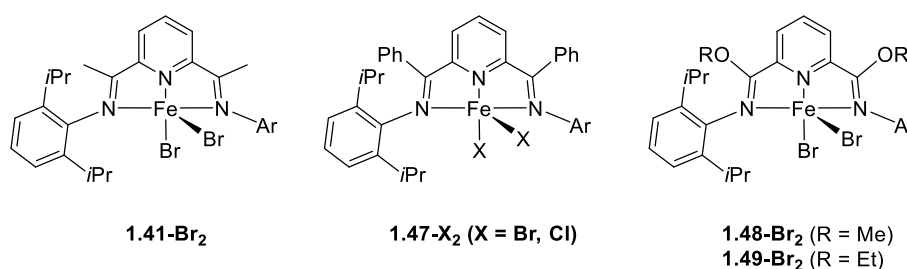


Figure 1.17: Synthesis of phenyl and alkoxy-containing PDI iron pincer complexes, to study the influence of linker substitution on catalytic behaviour.

Given the redox activity of the PDI ligand system, the ligand backbone was modified. The methyl substituent was replaced by phenyl, methyl- and ethoxide substituents (Figure 1.17). These substituents may protect the ligand from unwanted deprotonation reactions and further alter the reactivity of the metal centre. Complexes **1.47-X₂** (X = Cl, Br), **1.48-Br₂** and **1.49-Br₂** were synthesised in analogy to **1.42-Cl₂**. The reduction of **1.47-X₂** (X = Cl, Br) to **1.47-(N₂)₂** with an excess amount of 0.5% sodium amalgam proceeded smoothly, although 4 atm N₂ were needed to prevent unwanted side reactions. The attempted reductions of **1.48-Br₂** and **1.49-Br₂** were unsuccessful. Only the diamagnetic η^6 -arene complexes **1.50** and **1.51** could be isolated (Figure 1.18). These complexes proved catalytically inactive (*vide infra*).

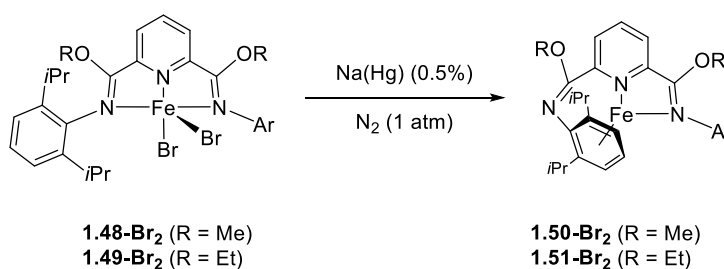
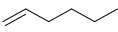
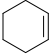
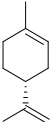


Figure 1.18: Reduction of **1.48-Br₂** and **1.49-Br₂** to give the diamagnetic η^6 -arene complexes **1.50** and **1.51**.

Comparing the N₂ IR stretching bands of **1.42-(N₂)₂** with **1.47-(N₂)₂** showed a shift to higher frequencies. A difference of 13 and 6 cm⁻¹ was observed, suggesting a more electrophilic metal centre in **1.47-(N₂)₂**. Complex **1.47-(N₂)₂** was then employed in the hydrogenation and hydrosilylation of 1-hexene, cyclohexene and (*R*)-(+)-limonene following the standard conditions (Table 1.1 and Table 1.2). The TOF's in Table 1.3 were determined after 98% conversion of 1-hexene and after 60 minutes for cyclohexene and (*R*)-(+)-limonene.

Table 1.3: Hydrogenation and hydrosilylation of 1-hexene, cyclohexene and (*R*)-(+)-limonene using 0.3 mol% of phenylated PDI iron pincer complex **1.47-(N₂)₂**.^a

Entry	Alkene	Hydrogenation TOF (h ⁻¹)		Hydrosilylation TOF (h ⁻¹)	
		1.47-(N₂)₂	1.42-(N₂)₂	1.47-(N₂)₂	1.42-(N₂)₂
1		5300	3300	930	330
2		60	1075	16	20
3		275	1085	37	166

^a 4 atm of hydrogen were used for the hydrogenation; 2.0 equiv. of PhSiH₃ were used for the hydrosilylation.

Comparing the results in Table 1.3 showed that **1.47-(N₂)₂** was more active in the case of 1-hexene (Entry 1). It showed a lower activity for cyclohexene and (*R*)-(+)-limonene (Entries 2 and 3) for both hydrogenation and hydrosilylation reactions. Archer *et al.* were able to show that the reduced activity of **1.47-(N₂)₂** was due to a competing deactivation mechanism. Stability tests at room temperature in benzene-*d*₆ showed the formation of the η⁶-phenyl (**1.52**) and η⁶-aryl complexes (**1.53**) in a ratio of 85:15 (Figure 1.19). Complexes **1.52** and **1.53** could be isolated and characterised by X-ray diffraction, multi nuclear NMR and elemental analysis. Both iron aryl complexes were unreactive towards hydrogenation of olefins.⁷³

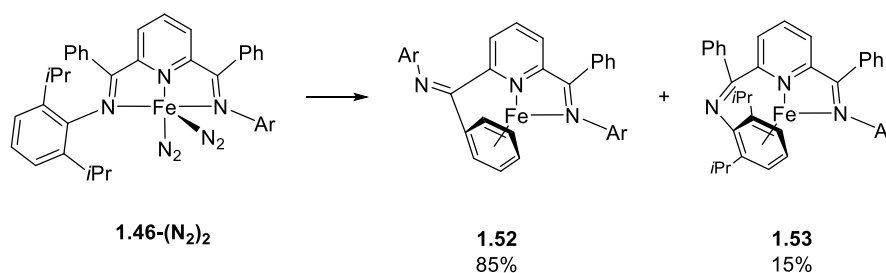


Figure 1.19: Deactivation pathway of **1.47-(N₂)₂** via the formation of catalytically inactive η^6 -aryl complexes.

Russell *et al.* screened the influence of smaller aryl substituents on the bis(imine) side arms. There, methyl and ethyl substituents were chosen to replace the more bulky *i*Pr residues. The synthesis of the corresponding dihalide complexes went smoothly. Further attempts to isolate the reduced PDI iron dinitrogen complexes under standard conditions (excess of 0.5% sodium amalgam in a N₂ atmosphere) were unsuccessful. Upon reduction, only the di-PDI iron complex [(^{Ar}N^{Me}N^{Me}N)₂Fe], was obtained.⁷⁴

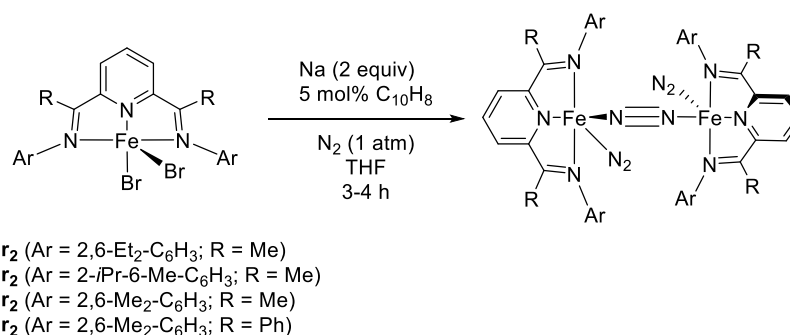
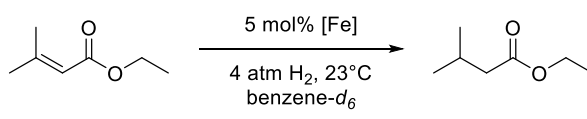


Figure 1.20: Synthesis of dimeric PDI iron(0) nitrogen complexes with smaller aryl substituents.

Unlike the attempted reduction with sodium amalgam, reduction with sodium naphthalenide proved to be successful. [(^{Ar}N^{Me}N^{Me}N)FeBr₂] (**1.54-Br₂**, Ar = 2,6-Et₂-C₆H₃) in the presence of two equivalents of sodium metal and 5 mol% of naphthalene in a THF solution yielded a N₂-containing complex. Spectroscopic and crystallographic analysis revealed a dimeric structure of [(^{Ar}N^{Me}N^{Me}N)FeN₂]₂(η^2 -N₂) (**1.55-(N₂)_{1.5}**, Ar = 2,6-Et₂-C₆H₃). In order to investigate the influence on reactivity, the scope of different aryl substituents was extended (Figure 1.20).⁷⁴ Each of these new complexes were then employed in the catalytic hydrogenation of ethyl-3-methylbut-2-enonate. The reaction was performed with 5 mol% catalyst loading (2.5 mol% of dimer) and 4 atm of hydrogen in benzene-*d*₆ at room temperature (Table 1.4).⁷⁴

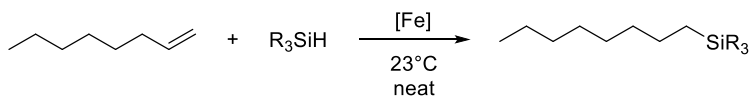
Table 1.4: Results of hydrogenation of ethyl 3,3-dimethylacrylate.



Entry	Complex	Time [h]	Conversion [%]
1	1.42-(N₂)₂	24 (72)	50 (60)
2	1.55-(N₂)_{1.5}	10	>95
3	1.56-(N₂)_{1.5}	5	>95
4	1.57-(N₂)_{1.5}	1.5	>95
5	1.47-(N₂)₂	24	0
6	1.58-(N₂)_{1.5}	24 (72)	21 (45)

The results in Table 1.4 show that the aryl substituents have a significant influence. The 2,6-diisopropyl benzene substituted **1.42-(N₂)₂** showed a conversion of 50% after 24 hours (Entry 1). Leaving the reaction for a longer time increased the yield to a maximum of 60% after 72 hours. The reason for the lower yield is the competing deactivation of the catalyst by the irreversible C-O bond cleavage.^{69,70} The replacement of the isopropyl groups by less bulky ethyl- and methyl substituent yielded a higher reactivity (Entries 2 – 4). The reaction times were reduced to 10 and 1.5 hours. The phenylated derivatives (Entries 5 and 6) showed little to no activity. Analysis of the remaining iron species of the latter reaction showed the formation of a significant amount of PDI iron acetate species. Besides this, η^6 -arene complexes (Figure 1.19) could be observed to a lesser extent. A significant amount of unidentified paramagnetic iron residue was observed. The formation is most likely due to the irreversible C-O bond cleavage reaction.⁷⁰ In the series of PDI iron pincer complexes the 2,6-dimethylbenzene-substituted **1.57-(N₂)_{1.5}** shows the highest activity for the hydrogenation of ester-substituted olefins.⁷⁴

Table 1.5: Reactivity of **1.42-(N₂)₂**, **1.55-(N₂)_{1.5}** and **1.57-(N₂)_{1.5}** as pre-catalysts for the selective, solvent free reduction of 1-octene with various tertiary hydrosilanes.



Entry	Complex	Amount complex [ppm (mol%)]	Silane	Time [min]	Conversion [%] ^a
1	1.42-(N₂)₂	2000 (0.05)	(Me ₃ SiO) ₂ MeSiH	15	>98
2	1.42-(N₂)₂	2000 (0.04)	(EtO) ₃ SiH	15	96
3	1.42-(N₂)₂	2000 (0.03)	Et ₃ SiH	60	trace
4	1.55-(N₂)_{1.5}	2000 (0.03)	(Me ₃ SiO) ₂ MeSiH	15	>98
5	1.55-(N₂)_{1.5}	2000 (0.02)	(EtO) ₃ SiH	15	97
6	1.55-(N₂)_{1.5}	2000 (0.02)	Et ₃ SiH	15	9
7	1.57-(N₂)_{1.5}	200 (0.004)	(Me ₃ SiO) ₂ MeSiH	15	>98
8	1.57-(N₂)_{1.5}	500 (0.007)	(EtO) ₃ SiH	15	97
9	1.57-(N₂)_{1.5}	2000 (0.02)	Et ₃ SiH	45	>98

^a The yields were determined by GC/MS.

Complexes **1.42-(N₂)₂**, **1.55-(N₂)_{1.5}** and **1.57-(N₂)_{1.5}** were also employed in the hydrosilylation reaction of 1-octene with several tertiary silanes (Table 1.5). The reaction was carried out in neat 1-octene. **1.42-(N₂)₂** and **1.55-(N₂)_{1.5}** showed similar reactivity. 2000 ppm of catalyst with (Me₃SiO)₂MeSiH showed, in both cases, a conversion higher than 98% after 15 minutes reaction time. Likewise the reduction with (EtO)₃SiH gave 96% and 97% conversion, respectively, after 15 minutes. The results with Et₃SiH differed slightly. For complex **1.42-(N₂)₂** only trace amounts of 1-(triethylsilyl)octane could be observed after 60 minutes. This corresponds with the findings of Bart *et al.* where **1.42-(N₂)₂** was unreactive towards Et₃SiH and 1-hexene in a toluene solution at room temperature.⁶⁸ The hydrosilylation with **1.55-(N₂)_{1.5}**, however, gave 9% silylated alkane. Consistent with the results obtained for the hydrogenation⁷⁴, the methyl-substituted **1.57-(N₂)_{1.5}** proved to be the most reactive. The hydrosilylation reaction with (Me₃SiO)₂MeSiH (with 200 ppm of **1.57-(N₂)_{1.5}**) gave >98% yield after 15 minutes. Likewise, a mixture of 1-octene with (EtO)₃SiH and 500 ppm **1.57-(N₂)_{1.5}** gave 97% yield. For the reaction with Et₃SiH, 2000 ppm of **1.57-(N₂)_{1.5}** were needed to reach almost full conversion after 45 minutes. All reactions proceeded without formation of side products. Only anti-Markovnikov products were observed. The commonly used Karstedt's catalyst

achieved 80% yield using 1-octene and $(\text{Me}_3\text{SiO})_2\text{MeSiH}$ as a reducing agent (30 ppm of $\text{Pt}_2[(\text{Me}_2\text{SiCH}=\text{CH}_2)_2\text{O}]_3$ in xylene solution at 72°C over 30 minutes). 20% by-products were detected,⁷⁵ while for **1.57-(N₂)_{1.5}**, roughly sevenfold of the normal loading is used (200 ppm) to produce exclusively the terminal silylalkane.⁷⁶

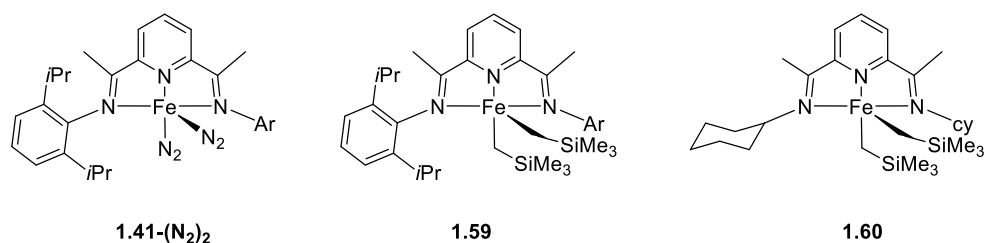
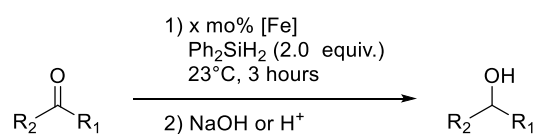
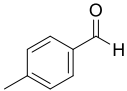
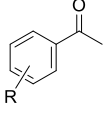
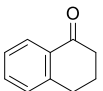
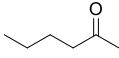
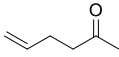


Figure 1.21: Iron PDI pincer complexes as precatalysts for the hydrosilylation of carbonyls.

Extending the scope of hydrosilylation reactions towards the reductions of aldehydes and ketones, **1.42-(N₂)₂** was employed in the catalytic reduction of *p*-tolualdehyde and acetophenone with Ph_2SiH_2 . Both substrates were quantitatively converted in less than one hour with 1 mol% of **1.42-(N₂)₂** at 23°C . Hydrolysis of the silyl ether gave the corresponding alcohol. These results prompted the quest for new iron PDI pre-catalysts. Indeed, the addition of $(\text{py})_2\text{Fe}(\text{CH}_2\text{SiMe}_3)_2$ to a solution of $(^{\text{R}}\text{N}^{\text{Me}}\text{N}^{\text{Me}}\text{N})$ ($\text{R} = \text{cy}, 2,6\text{-iPr}_2\text{-C}_6\text{H}_3$) furnished **1.59** and **1.60** in 63% and 83% yield.^{77,78} **1.59** and **1.60** were then assayed for the catalytic hydrosilylation of aldehydes and ketones at room temperature (Table 1.6). The reaction was performed with two equivalents of Ph_2SiH_2 and 1.0 mol% **1.59** or 0.1 mol% **1.60** in a 0.4 M toluene solution. The results in Table 1.6 show a high reactivity and a broad functional group tolerance.⁷⁸

Table 1.6: Scope of the reduction of functionalised and non-functionalised carbonyls.

**1.59:** $x = 1.0 \text{ mol\%}$ **1.60:** $x = 0.1 \text{ mol\%}$

Entry	Compound	1.59	1.60
1		>99	>99
2	 R = H	>99	>99
3	R = 4- <i>t</i> Bu	>99	>99
4	R = 4-OMe	>99	>99
5	R = 4-CF ₃	>99	>99
6	R = 3,5-(CF ₃) ₂	21	68
7	R = 2,4-(OMe) ₂	57	94
8	R = 4-NMe ₃	27	95
9		27	82
10		>99	58
11		75	54

1.4.2 The Catalytic Activity of Iron Bis(imino)pyridine Pincer Complexes in the $[2\pi+2\pi]$ Cycloaddition and Reductive Cyclisation of Dienes and Enynes.

The metal-catalysed $[2\pi+2\pi]$ cycloaddition is an attractive method to form cyclobutanes from alkenes. Bouwkamp *et al.* showed that addition of 10 mol% of **1.42**-(N₂)₂ successfully induces $[2\pi+2\pi]$ cycloaddition of α,ω -dienes in a benzene-*d*₆ solution at room temperature. The scope of the reaction showed that ester- and amine-containing substrates can be cyclised in excellent yields (Table 1.7). Conversely, *N*-boc-protected and secondary amines showed 24% or no conversion.⁷⁹

Table 1.7: Functional group tolerance in the $[2\pi+2\pi]$ cycloaddition of functionalised α,ω -dienes.

Entry	E	Time [min]	Conversion [%]
1	CH ₂	300	92
2	SiMe ₂	300	0
3	NH	300	0
4	N-Bn	26	90
5	N'-Bu	<5	>95
6	N-Boc	300	24
7	C(COOEt) ₂	141	>95

1,3-butadiene may also undergo intermolecular $[2\pi+2\pi]$ cycloaddition. The exposure of 1,3-butadiene in a benzene-*d*₆ solution to an equimolar amount of ethane gave vinylcyclobutane in >95% yield. For this reaction 5 mol% of **1.42**-(N₂)₂ or **1.57**-(N₂)_{1.5} was used. When 2-methyl-1,3-butadiene was used, the 1,4 addition product, 5-methyl-1,4-hexadiene, was obtained in excellent yields after 16 hours.⁸⁰

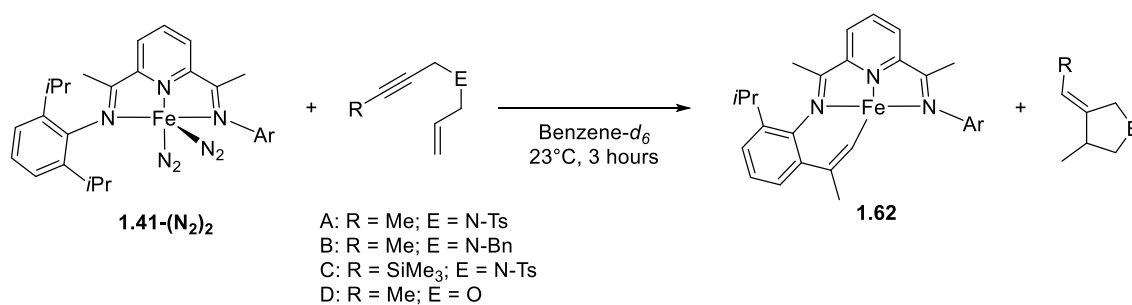
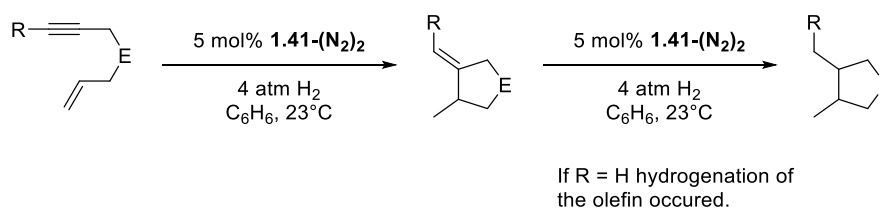


Figure 1.22: Stoichiometric reductive cyclisation reaction of functionalised enyne systems with **1.42-(N₂)₂**.

A stoichiometric reaction of heteroatom-substituted 2-butynyl-allyl compounds and **1.42-(N₂)₂** in benzene-*d*₆ at room temperature yielded the formation of a 3,4-disubstituted heterocycles with only one alkene substituent. The second substituent, which was formerly the olefin, was reduced to an alkane. Hydrolysis of the iron complex and further analysis of the ligand identified the iron complex as an intramolecular olefin complex (**1.62**; Figure 1.22).⁸¹ This stoichiometric cyclisation reaction of the 1,6-enynes was further investigated for catalytic reactivity. Indeed when 4 atm of hydrogen were established in a solution of heteroatom-substituted 1,6-enynes, in the presence of 5 mol% **1.42-(N₂)₂**, the corresponding 5-membered heterocycle was obtained in good to excellent yields (Table 1.8). Both internal and terminal alkynes could be cyclised. In all cases only unsaturated heterocycles were observed. In the cases of terminal alkynes (Entries 1 – 4, 8 and 10) the formed double bond was further hydrogenated. The newly formed methyl groups on the heterocycle showed predominantly *cis* configuration. The products of the cyclisation of the internal alkynes (Entries 5 – 7, 9) were not further reduced due to the reluctance of **1.42-(N₂)₂** to reduce trisubstituted alkenes.^{68,69,81}

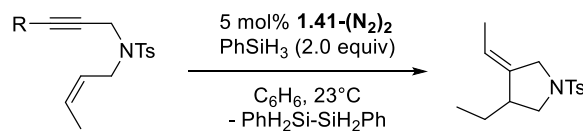
Table 1.8: Hydrogen assisted cyclisation enyne-systems bearing functional groups.



Entry	E	R	Time [min]	Yield ^a [%]	<i>cis/trans</i> (saturated)
1	N- <i>t</i> Bu	H	180	68	99:1
2	N-Ts	H	60	79	75:25
3	N-Bn	H	180	71	99:1
4	N-CH ₂ C ₆ Me ₅	H	180	57 ^b	99:1
5	N-Ts	Me	180	79	n/a
6	N-Bn	Me	180	71	n/a
7	N-Ts	SiMe ₃	540	82	n/a
8	O	H	360	95	61:39
9	O	Me	180	82	n/a
10	C(COOEt) ₂	H	180	74 ^c	79:21

^a Isolated yield. ^b 16% reduced alkyne compound detected. ^c 26% reduced alkyne compound detected.

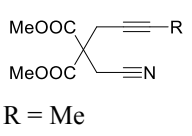
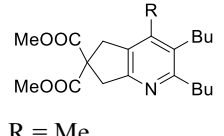
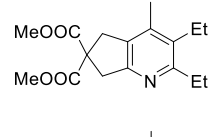
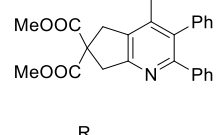
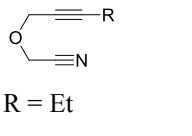
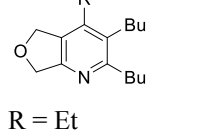
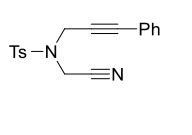
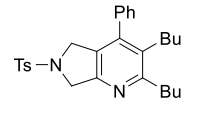
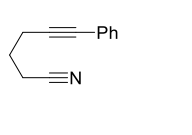
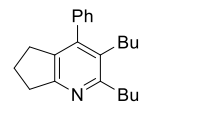
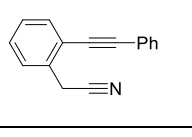
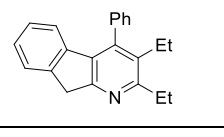
Interestingly, attempts to cyclise *N*-tosylated (*N*-2-butynyl)(*N*-2-butenyl)amine under the previously described reaction conditions (Table 1.8) only gave the hydrogenated acyclic product. Although, when H₂ was replaced by 2 equivalents of PhSiH₃ the reaction reached 95% formation of pyrrolidine compound after three hours (Figure 1.23).⁸¹

Figure 1.23: Reductive cyclisation of *N*-tosylated (*N*-2-butynyl)(*N*-2-butenyl)amine.

Given the efficiency of the cycloaddition reactions, D'Souza *et al.* used an *in situ* formed iron PDI pincer complex to form pyridines from alkyne nitriles with acetylenes. Preliminary optimisation of the reaction showed that the best yields were obtained by using

2,6-(4-OBn-2,6-*i*Pr₂C₆H₂N=CH)₂C₅H₃N (**1.61**) as a ligand (13 mol%) in combination with Fe(OAc)₂ (10 mol%) and Zn (20 mol%) in a DMF solution at 85°C. The scope of the reaction is shown in Table 1.9. Depending on the substituents the yields ranged between 40 and 86%.

Table 1.9: Formation of substituted pyridines using *in situ* formation

Entry	Cyanoalkyne	Alkyne	Time [h]	Product	Yield [%]
1	 R = Me	Bu—C≡C—Bu	2	 R = Me	70
2	R = Et	Bu—C≡C—Bu	26	R = Et	86
3	R = Ph	Bu—C≡C—Bu	5	R = Ph	75
4	R = H	Bu—C≡C—Bu	26	R = H	30
5	R = SiMe ₃	Bu—C≡C—Bu	6	R = SiMe ₃	57
6	R = Me	Et—C≡C—Et	6		71
7	R = Me	Ph—C≡C—Ph	5		54
8	 R = Et	Bu—C≡C—Bu	4	 R = Et	41
9	R = Ph	Bu—C≡C—Bu	4	R = Ph	45
10		Bu—C≡C—Bu	4		41
11		Bu—C≡C—Bu	4		65
12		Et—C≡C—Et	4		64

1.5 Pyridine- and Phenyl Bis(oxazolinyl) Pincer Systems and Their Application in Iron Catalysis

Pyridine-bis(oxazoline) (pybox) ligands in combination with iron salts have been widely used in catalytic reactions. The majority were used with *in situ* formed iron species. The variety of reactions range from cyclisation reactions,⁸²⁻⁸⁵ addition reactions,⁸⁶⁻⁹⁰ kinetic resolution of racemic sulfoxides,⁹¹ and hydrosilylation of aromatic ketones.⁹² The catalytically relevant species are ill-defined and will not be discussed in greater detail below. The groups of Huang and Nomura employed [(pybox-R)FeCl₂] **1.62-R** (R = Me₂, Ph₂, *i*Pr(S)) as co-catalysts in the polymerisation of ethylene gas.⁹³⁻⁹⁵

Redlich and Hossain synthesised a series of [(pybox-R)FeCl₂] (**1.62-R**; R = *i*Pr(S), *t*Bu(S), Ph(S)) complexes and employed them in the formation reaction of aziridines (Figure 1.24). When one equivalent of AgSbF₆ (relative to the amount of catalyst) is used as an activator, **1.62-R** (R = *i*Pr, *t*Bu) produce 47% of the *cis*-aziridine with 45 and 49% ee. The *trans*-isomer, along with β -amino- α,β -unsaturated esters, is formed as a side product.³⁹

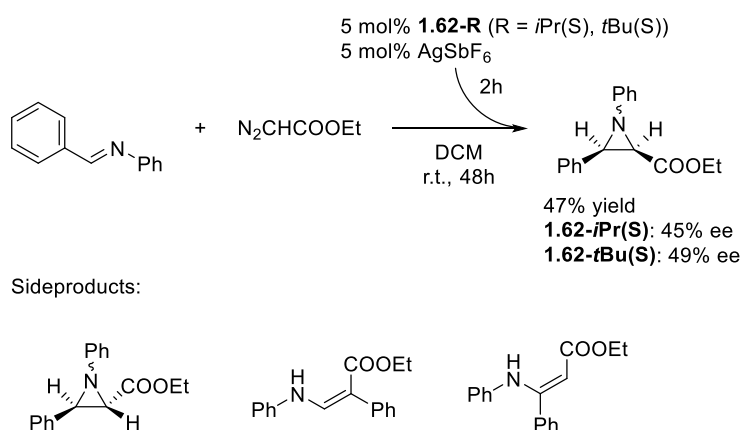
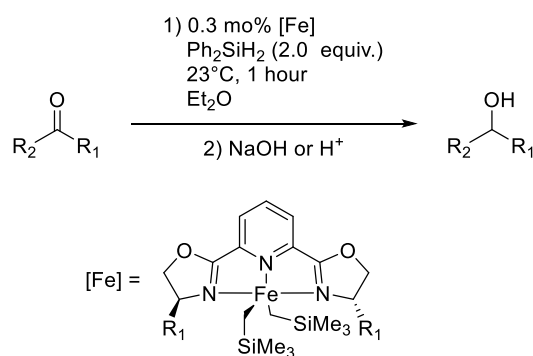


Figure 1.24: Reaction scheme for the formation of aziridine catalysed by pre-activated complexes **1.62-R** (R = *i*Pr(S), *t*Bu(S)).

Table 1.10: Hydrosilylation of functionalised ketones.^a

Entry	Compound	R ₁ = <i>i</i> Pr(S)	<i>i</i> Pr(S) ^b	<i>t</i> Bu(S)	Bn(S)	<i>i</i> Bu(S)
1	 R = H	80 (49)	99 (54)	99 (30)	99 (18)	99 (8)
2	R = 4- <i>t</i> Bu	99 (23)	99 (13)	99 (25)	99 (25)	99 (11)
3	R = 4-OMe	99 (5)	55 (25)	99 (3)	99 (29)	97 (5)
4	R = 4-CF ₃	99 (20)	99 (20)	99 (12)	99 (21)	99 (12)
5	R = 3,5-(CF ₃) ₂	99 (6)	99 (6)	72 (12)	99 (6)	99 (4)
6	R = 2,4-(OMe) ₂	99 (32)	99 (32)	99 (50)	99 (32)	99 (22)
7	R = 2,4,6-Me ₃	<1	1 (30)	2 (5)	4 (44)	2 (26)
8	R = 2,6-Me ₂ -4- <i>t</i> Bu	<1	<1	1 (30)	<1	<1
9		99 (30)	99 (41)	60 (2)	93 (22)	25 (7)
10		58 (10)	99 (11)	99 (25)	46 (17)	46 (17)

^a Conversion [%] (ee [%]) ^b The catalyst was activated by addition of 0.95 equivalents of B(C₆F₅)₃.

Tondreau *et al.* investigated the enantioselective hydrosilylation of ketones. Analogous to **1.42-(N₂)₂**, **1.62-*i*Pr** was stirred with an excess amount of sodium amalgam in toluene under 1 atm of N₂.⁶⁸ Only a catalytically inactive bis-chelate, [(pybox-*i*Pr(S))₂Fe], could be isolated. Other reduction methods with sodium naphthalenide and magnesium, as used in the synthesis of complexes **1.55-(N₂)_{1.5}** – **1.57-(N₂)_{1.5}**,⁷⁴ furnished the same results. Previous examples showed that **1.59** and **1.60-(CH₂SiMe₃)₂** are efficient pre-catalysts for the hydrosilylation of ketones and aldehydes.⁷⁸ Therefore [(pybox-R)Fe(CH₂SiMe₃)₂] (**1.63-R**; R = *i*Pr(S), *t*Bu(S), indane(1 R,2 S), Bn(S), *i*Bu(S))

was synthesised as a potential pre-catalyst. Both methods, ligand displacement of $(\text{py})_2\text{Fe}(\text{CH}_2\text{SiMe}_3)_2$ with pybox-R and alkylation of **1.62-R** with $\text{LiCH}_2\text{SiMe}_3$, gave **1.63-R** in good yields. The hydrosilylation results in Table 1.10 show that **1.63-R** usually catalyses this reaction with high yields and has a broad functional group tolerance. The substrates with more sterically demanding substituents (2,4,6-trimethylacetophenone and 2,6-dimethyl-4-*t*Bu-acetophenone) show almost no conversion. The ee's in all cases were low. In order to increase the reactivity of the hydrosilylation the reaction was also conducted in the presence of an electrophilic, neutral boron, $\text{B}(\text{C}_6\text{F}_5)_3$ (0.95 equivalents to the substrate). Only modest improvements of the ee were observed (Table 1.10).⁹⁶

Hosokawa described the synthesis of chiral and achiral iron complexes consisting of a phenyl-bis(oxazoline) (phebox) ligand. The complex formation proceeds *via* oxidative addition of $\text{Fe}_2(\text{CO})_9$ to the (phebox-R)Br (R = Me₂, *i*Pr) in a toluene solution at 50°C in 52% and 69% yield (Figure 1.25). An analogous reaction with $\text{Fe}_3(\text{CO})_{12}$ and phebox-Me₂ gave 5% yield. The reaction with $\text{Fe}(\text{CO})_5$ showed no conversion. The structure was confirmed by NMR, IR and X-ray diffraction.⁹⁷

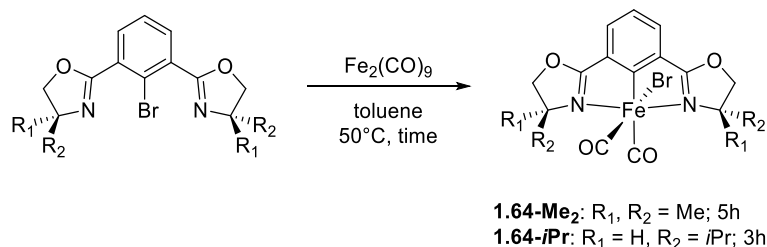


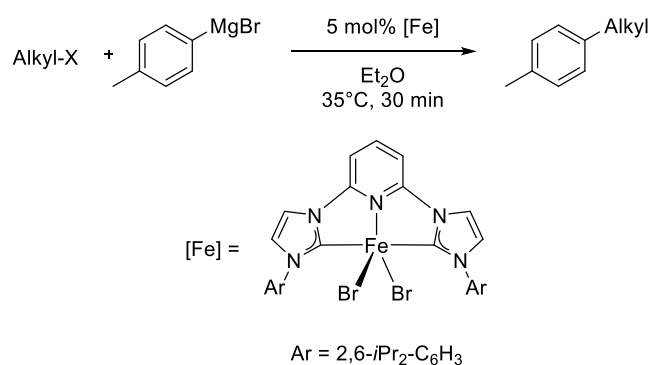
Figure 1.25: Reaction scheme for the complexation of $[(\text{phebox-R})\text{FeBr}(\text{CO})_2]$ (**1.64-R**; R = Me₂, *i*Pr).

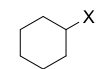
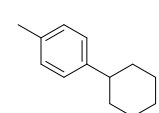
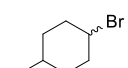
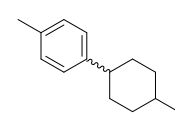
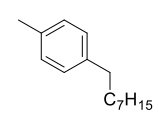
1.64-*i*Pr was then employed in the hydrosilylation reaction of aromatic ketones. The reduction of 4-acetylbiphenyl in the presence of 2 mol% **1.64-*i*Pr** and 2 mol% of Na(acac) in hexane at 50°C gave 99% 1-(4-biphenyl)ethanol with 66% selectivity for the *R*-enantiomer. 1.5 equivalents of $(\text{EtO})_2\text{MeSiH}$ were used as a reducing agent. The reduction of 2-acetylanthracene and 2-acetylnaphthalene gave the secondary alcohol in 49 and 53% ee. In contrast, 1-acetyl-4-methoxybenzene and 1-acetyl-4-methylbenzene gave lower enantioselectivities (21 – 38%).⁹⁷

1.6 Pyridine Bis(*N*-Heterocyclic Carbene) Pincer Systems and Their Application in Iron Catalysis

Bedford and co-workers were able to show that the iron pyridyl bis(carbene) pincer complex, **1.65-Br₂**, is an excellent catalyst for the Kumada cross coupling of secondary and primary alkyl halides with *p*-tolyl Grignard reagents (Table 1.11). The reaction was conducted in refluxing diethylether for 30 minutes. 5 mol% of **1.65-Br₂** were used. While chlorocyclohexane (Table 1.11, Entry 1) showed no conversion, bromocyclohexane and 4-bromo-1-methylcyclohexane could be coupled with 94 and 89% yield (Table 1.11, Entries 2 and 3). The latter showed a *cis:trans* ratio of the of 31:69. The primary alkyl halide 1-bromooctane was coupled with 71% yield.⁹⁸

Table 1.11: Coupling of 4-tolylmagnesium bromide with primary and secondary alkyl halides catalysed by iron pyridyl bis(carbene) pincer complex **1.65-Br₂**.



Entry	Substrate	Product	Yield [%]
1	 X = Br		94
2	X = Cl		-
3			89 ^a
4	Br-CH ₂ -C ₇ H ₁₅		71

^a *Trans:cis* = 69:31

Yu *et al.* synthesised the iron(0) complex **1.65-(N₂)₂** and employed it in the hydrogenation reaction of ethyl 3-methyl-2-butenate, which gave complete conversion after 1 hour. 5 mol% **1.65-(N₂)₂** under 4 atm of hydrogen was used at room temperature. The positive results prompted extension of the scope of possible iron complexes to those with less sterically demanding aryl substituents. Russell *et al.* showed previously that by replacing [(^{Ar}N^{Me}N^{Me}N)Fe(N₂)₂] (**1.42-(N₂)₂**; Ar = 2,6-*i*Pr₂-C₆H₃) with the less sterically demanding [(^{Ar}N^{Me}N^{Me}N)Fe(N₂)₂](μ-N₂) (**1.57-(N₂)_{1.5}**; Ar = 2,6-Me₂-C₆H₃), the catalytic activity can be increased (Table 1.4).⁷⁴ Similarly, the reduction of [(^{Me}CNC)FeBr₂] (**1.66-Br₂**; ^{Me}CNC = 2,6-(2,6-Me₂-C₆H₃-imidazol-2-ylidene)₂-C₅H₃N) or [(^{Mes}CNC)FeBr₂] (**1.67-Br₂**; ^{Mes}CNC = 2,6-(2,4,6-Me₃-C₆H₂-imidazol-2-ylidene)₂-C₅H₃N) with two equivalents of sodium and 5 mol% of naphthalene under a N₂ atmosphere gave [(^{Me}CNC)Fe(N₂)₂] **1.66-(N₂)₂** or [(^{Mes}CNC)Fe(N₂)₂] **1.67-(N₂)₂**.^{74,99} Solid state and solution IR measurements showed that **1.66-(N₂)₂** coexisted as monomeric and dimeric structures.

Table 1.12: Catalytic hydrogenation of tri and tetra substituted alkenes with PDI and CNC (carbene) iron dinitrogen complexes.

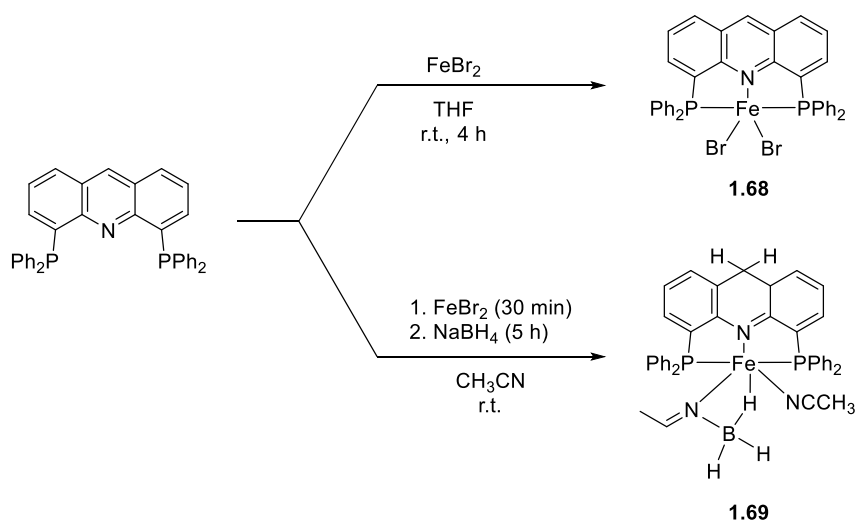
Entry	Compound	1.42-(N₂)₂	1.57-(N₂)_{1.5}	1.65-(N₂)₂	1.66-(N₂)₂	1.67-(N₂)₂
1		65 (24 h)	>95 (1 h)	>95 (1h)	35 (1 h)	35 (1 h)
2		12 (24 h)	4 (24 h)	89 (12 h)	>95 (1 h)	>95 (1 h)
3		32 (24 h)	15 (24 h)	>95 (15 h)	>95 (1 h)	>95 (1 h)
4		0 (24 h)	2 (24 h)	20 (24 h)	>95 (12 h)	>95 (1 h)
5		3 (48 h)	<1 (48 h)	4 (48 h)	68 (48 h) ^a	60 (48 h) ^a
6		0 (24 h)	0 (24 h)	0 (24 h)	0 (24 h)	0 (24 h)

^a *cis:trans* = 3:1.

Complexes **1.65-(N₂)₂** - **1.67-(N₂)₂** were then employed in the hydrogenation of various internal alkenes under standard conditions (5 mol% [Fe], 4 atm H₂, room temperature). The results were compared to their structurally analogous PDI iron pincer complexes, **1.42-(N₂)₂** and **1.57-(N₂)_{1.5}** (Table 1.12). The hydrogenation of ethyl 3-methyl-2-butenate, using **1.66-(N₂)₂** or **1.67-(N₂)₂** as a catalyst, showed a lower conversions. Only 35% were observed. This is due to the competing deactivation pathway which was already described for the iron PDI pincer complexes.⁷⁰ The substrate scope was then extended to a series of functionalised, hindered olefins. In general, the CNC iron pincer complexes, **1.65-(N₂)₂** - **1.67-(N₂)₂**, show a higher reactivity compared to the PDI iron pincer complexes, **1.42-(N₂)₂** and **1.57-(N₂)_{1.5}**. Full conversion was observed in the reduction of methyl-(*E*)-stilbene, 2-methyl-2-butene and 1-methylcyclohexene with **1.66-(N₂)₂** or **1.67-(N₂)₂** as a catalyst (Table 1.12, Entries 2 – 4). **1.65-(N₂)₂** showed lower reactivities. Methyl-(*E*)-stilbene and 2-methyl-2-butene were fully converted after 24 and 15 hours (Entries 2 and 3). 1-Methylcyclohexene gave 20% yield after 24 hours (Entry 4). The tetrasubstituted 2,3-dimethyl-2-butene was not reduced. Although **1.66-(N₂)₂** and **1.67-(N₂)₂** could reduce 2,3-dimethyl-1*H*-indene after 48 hours with 68 and 60% yield respectively, in both cases a *cis:trans* ratio of 3:1 was observed.⁹⁹

1.7 *N,N*-Diphenylamino-Based Pincer Systems and Their Application in Iron Catalysis

Srimani *et al.* prepared the new iron pincer complexes [(^{Ac}PNP)FeBr₂] (**1.68**) and [(^{HAc}PNP)Fe(CH₃CN)(μ²-CH₃CHNBH₃)] (**1.69**) (^{Ac}PNP = 4,5-bis(diphenylphospino)acridine, ^{HAc}PNP = 4,5-bis(diphenylphospino)-9*H*-acridine-10-ide). The reaction of ^{Ac}PNP with FeBr₂ in THF at room temperature gave **1.68** in 87% yield. The solid state structure revealed a distorted square pyramidal structure. Mixing ^{Ac}PNP with FeBr₂ in acetonitrile in the presence of two equivalents of NaBH₄ gave **1.69** in 81% yield. The crystal structure showed the iron centre bound in an octahedral configuration. Interestingly, one nitrile ligand inserted into the metal hydride bond. Further, the hydride reduced the electrophilic carbon atom in the 9 position of the acridine (Figure 1.26).

Figure 1.26: Reaction scheme for the synthesis of **1.68** and **1.69**.

1.68 and **1.69** were probed for their catalytic utility in the hydrosilylation of internal alkynes. A THF solution of diphenylacetylene with 0.6 mol% of catalyst was heated to 90°C under 4 atm of hydrogen. Although **1.69** quantitatively converted the diphenylacetylene to the *E*-stilbene, **1.68** showed no catalytic activity, even after the addition of 12 mol% of KO^tBu . No *Z* isomers were observed. Reducing the temperature to 50 and 25°C lowered the yield and the *E*:*Z* selectivity to 61% (66:34) and 29% (45:55), respectively. Toluene, ethanol and methanol at 90°C reduced the reactivity and selectivity of the catalyst. A solution with *Z*-stilbene and 0.6 mol% **1.69** at 90°C in the absence of hydrogen isomerised to *E*-stilbene. The scope and utility of **1.69** in hydrogenation reactions were then further investigated (Table 1.13).¹⁰⁰ **1.69** shows in general a good reactivity. The yields obtained range between 85 to 100% in favour of the *E*-isomer. 1,2-(*p*-Nitrophenyl)phenylacetylene showed no reaction. 1,2-Bis(tributylstannyl)acetylene gave a mixture of reaction products which could not be further identified. **1.69** has a high functional group tolerance: ether, ester, ketone, halide and nitrile substituents remained intact during the reduction. Even the terminal alkyne, phenylacetylene, could be reduced to styrene with 99% yield.¹⁰⁰

Table 1.13: Hydrogenation of internal alkynes to the corresponding stilbene compounds catalysed by **1.69**.

$$R_1-C\equiv C-R_2 \xrightarrow[H_2, THF]{1.69} R_1-CH=CH-R_2 + R_1-CH=CH-R_2$$

Entry	Alkyne	1.69 [mol%]	Time [h]	Pressure [bar]	Yield [%]	<i>E:Z</i>
1		0.6	12	4	99	100:0
	R = H					
2	R = OMe	0.6	36	4	99	99:1
3	R = COCH ₃	2	65	4	99	64:36
4	R = COOEt	2.2	22	4	89 (11) ^a	99:1
5	R = CN	4	72	10	94	99:1
6	R = NO ₂	2	48	10	NR ^b	-
7	R = Cl	2.2	23	10	87 (13) ^a	99:1
8		2.5	70	10	99	99:1
9		2.2	70	10	90	90:10
10		2	27	10	94 (6) ^a	95:5
11		4	21	4	98 (2) ^a	100:0
12		2	48	4	70 (30)	61:39
13		1.7	17	4	76 (24)	99:1
14		1	30	4	85	100:0
15		2	40	4	n/a ^c	-
16		0.6	11	4	99	-

^a The yield in parantheses is the corresponding alkane product [%]. ^b No reaction. ^c Complicated mixture of products.

Table 1.14: Asymmetric epoxidation of *trans*-stilbene using iodosobenzene as oxidant

1.70

1.71

Ar = 2,6-*i*Pr₂-C₆H₃
SIPrAgCl

Entry	Complex	Additive	Time [min]	Yield [%]	ee [%]
1	1.70	None	30	35	83
2	1.70	None	60	Trace	n/a
3	1.70	SIPrAgCl	60	55	88
4	1.71	SIPrAgCl	60	Trace	n/a

Niwa and Nakada developed a carbazole-based tridentate bis(oxazoline) ligand (CarBox-R) that displayed porphyrin-like properties in the iron catalysed epoxidation reaction of (*E*)-olefins. In the presence of 4 mol% NaBARF, [(CarBox-Ph)FeCl₂] (**1.70**, 1 mol%) catalysed the epoxidation of *trans*-stilbene using iodosobenzene as oxidising reagent (Table 1.14). The reaction gave 35% yield with an ee of 83%. In the absence of NaBARF no reaction was observed. When SIPrAgCl (SIPr = *N,N'*-bis(2,6-*i*Pr₂-C₆H₃)-4,5-dihydroimidazol-2-ylidene) was used as an additive the yield and ee could be increased to 55% and 88%. The reaction with the structurally similar [(bopa-Ph)FeCl₂] (**1.71**; *vide infra*) gave no yield. The investigation of the substrate scope showed the broad utility of this reaction.¹⁰¹ Various substituted *trans*-stilbenes and cinnamyl alcohol derivatives gave the corresponding (*S,S*) epoxides in excellent enantioselectivities, although substrates with electron-rich aromatic substituents showed moderate selectivity.¹⁰¹

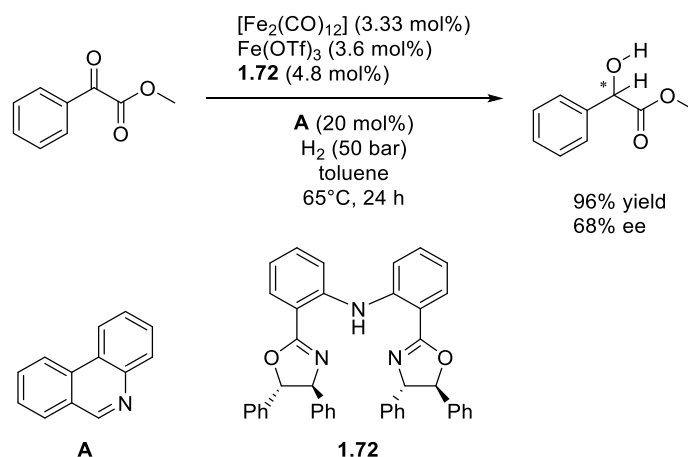


Figure 1.27: Biomimetic reduction of methyl α -keto-2-phenylacetate using bopa-(4*S*,5*S*)Ph₂ as chiral auxiliary.

Lu *et al.* conducted the iron-catalysed biomimetic reduction of methyl 2-oxo-2-phenylacetate in the presence of (bopa-(4*S*,5*S*)Ph₂) (**1.72**) ligands. They reached a yield of 96% with an ee of 68% (Figure 1.27).¹⁰²

In seminal hydrosilylation studies, the group of Nishiyama investigated the influence of various bi- and tridentate nitrogen donor ligands (e.g. bipyridine, tmeda, pybox-Me₂, ^{Mes}PDI) in the reduction of substituted acetophenones catalysed by Fe(OAc)₂. They showed that 5 mol% Fe(OAc)₂ with 10 mol% tmeda is an efficient catalyst. The carbonyl compounds were reduced to the corresponding alcohols in 50 – 95% yield. In order to extend the scope towards enantioselective hydrosilylation reactions bopa-R (R = *i*Pr(*S*), *t*Bu(*S*)) proved to be an efficient catalyst for the reduction of 4-acetylbiphenyl. 57 and 79% of predominantly *R* enantiomer were obtained.⁹² In subsequent work Inagaki and co-workers investigated the reactivity of [(bopa-R)FeX₂] (**1.73-X**₂; X = Cl, OAc, R = (C₆H₅)₂CH, *i*Pr, *t*Bu, Ph, Bn). The outcome of this work will be discussed in detail in Chapter 4.^{103,104}

1.8 Concluding Remarks and Outlook

In conclusion we were able to show that iron pincer complexes were broadly used in the hydrosilylation and hydrogenation reactions of olefins, acetylenes and carbonyls. They show a high

reactivity and selectivity. In some cases they compete even with state-of-the-art precious metal catalysts.⁷⁵ The groups of Milstein and Guan showed potential applications for the storage and liberation of hydrogen.^{23,25,62} Besides this, the applications in other fields especially C-C bond formation reactions are rare.

Herein we describe the application of $[\text{Fe}(\text{bopa-R})\text{Cl}_2]$ as potential pre-catalyst for the Kumada cross coupling reaction of primary and secondary alkyl halides with aryl Grignard reagents. Some catalytic relevant species were isolated and characterised. Their catalytic relevance was then probed. Subsequent experiments with radical-probe substrates, kinetic measurements and DFT calculations established a catalytic cycle in which an “iron-aryl-ate” complex activates the alkyl halides *via* a bimetallic oxidative addition pathway. In a further study it was shown that some of the previously isolated intermediates were also present in the enantioselective hydrosilylation reaction reported by the group of Nishiyama.^{92,103,104} Their catalytic relevance was shown and a preliminary mechanism could be proposed.

1.9 References

- (1) Appl, M. In *Ullmann's Encyclopedia of Industrial Chemistry*; Wiley-VCH Verlag GmbH & Co. KGaA: 2000.
- (2) Benito-Garagorri, D.; Lagoja, I.; Veiros, L. F.; Kirchner, K. A. *Dalton Trans.* **2011**, 40, 4778.
- (3) Bolm, C.; Legros, J.; Le Paih, J.; Zani, L. *Chem. Rev.* **2004**, 104, 6217.
- (4) Plietker, B. *Iron Complexes in Organic Chemistry*; Wiley-VCH Verlag GmbH & Co. KGaA, 2008.
- (5) Plietker, B. *Iron Catalysis - Fundamentals and Applications*; Springer Berlin Heidelberg, 2011.
- (6) Van Koten, G. In *Organometallic Pincer Chemistry*; Van Koten, G., Milstein, D., Eds.; Springer: Berlin Heidelberg, 2013; Vol. 40.
- (7) Benito-Garagorri, D.; Kirchner, K. A. *Acc. Chem. Res.* **2008**, 41, 201.
- (8) Dahlhoff, W. V.; Nelson, S. M. *J. Am. Chem. Soc.* **1971**, 2184.
- (9) Moulton, C. J.; Shaw, B. L. *Dalton Trans.* **1976**, 1020.
- (10) Van Koten, G. *Pure Appl. Chem.* **1989**, 61, 1681
- (11) Rybtchinski, B.; Milstein, D. *Angew. Chem. Int. Ed.* **1999**, 38, 870.
- (12) Jensen, C. M. *Chem. Comm.* **1999**, 2443.
- (13) Albrecht, M.; van Koten, G. *Angew. Chem. Int. Ed.* **2001**, 40, 3750.
- (14) Vigalok, A.; Milstein, D. *Acc. Chem. Res.* **2001**, 34, 798.
- (15) van der Boom, M. E.; Milstein, D. *Chem. Rev.* **2003**, 103, 1759.
- (16) Milstein, D. *Pure Appl. Chem.* **2003**, 75, 445.
- (17) Singleton, J. T. *Tetrahedron* **2003**, 59, 1837.
- (18) Giannoccaro, P.; Vasapollo, G.; Nobile, C. F.; Sacco, A. *Inorg. Chim. Acta* **1982**, 61, 69.
- (19) Zhang, J.; Gandelman, M.; Herrman, D.; Leituss, G.; Shimon, L. J. W.; Ben-David, Y.; Milstein, D. *Inorg. Chim. Acta* **2006**, 359, 1955.
- (20) Trovitch, R. J.; Lobkovsky, E.; Chirik, P. J. *Inorg. Chem.* **2006**, 45, 7252.

- (21) Pelczar, E. M.; Emge, T. J.; Krogh-Jespersen, K.; Goldman, A. S. *Organometallics* **2008**, *27*, 5759.
- (22) Langer, R.; Leitus, G.; Ben-David, Y.; Milstein, D. *Angew. Chem. Int. Ed.* **2011**, *50*, 2120.
- (23) Langer, R.; Diskin-Posner, Y.; Leitus, G.; Shimon, L. J. W.; Ben-David, Y.; Milstein, D. *Angew. Chem. Int. Ed.* **2011**, *50*, 9948.
- (24) Langer, R.; Iron, M. A.; Konstantinovski, L.; Diskin-Posner, Y.; Leitus, G.; Ben-David, Y.; Milstein, D. *Chem. Eur. J.* **2012**, *18*, 7196.
- (25) Zell, T.; Butschke, B.; Ben-David, Y.; Milstein, D. *Chem. Eur. J.* **2013**, *19*, 8068.
- (26) Zell, T.; Ben-David, Y.; Milstein, D. *Angew. Chem. Int. Ed.* **2014**, *53*, 4685.
- (27) Zell, T.; Ben-David, Y.; Milstein, D. *Catal. Sci. Technol.* **2015**, *5*, 822.
- (28) Benito-Garagorri, D.; Becker, E.; Wiedermann, J.; Lackner, W.; Pollak, M.; Mereiter, K.; Kisala, J.; Kirchner, K. A. *Organometallics* **2006**, *25*, 1900.
- (29) Benito-Garagorri, D.; Wiedermann, J.; Pollak, M.; Mereiter, K.; Kirchner, K. A. *Organometallics* **2007**, *26*, 217.
- (30) Benito-Garagorri, D.; Alves, L. G.; Puchberger, M.; Mereiter, K.; Veiros, L. F.; Calhorda, M. J.; Carvalho, M. D.; Ferreira, L. P.; Godinho, M.; Kirchner, K. A. *Organometallics* **2009**, *28*, 6902.
- (31) Benito-Garagorri, D.; Alves, L. G.; Veiros, L. F.; Standfest-Hauser, C. M.; Tanaka, S.; Mereiter, K.; Kirchner, K. A. *Organometallics* **2010**, *29*, 4932.
- (32) Bichler, B.; Holzhaecker, C.; Stoger, B.; Puchberger, M.; Veiros, L. F.; Kirchner, K. A. *Organometallics* **2013**, *32*, 4114.
- (33) Bichler, B.; Glatz, M.; Stoger, B.; Mereiter, K.; Veiros, L. F.; Kirchner, K. A. *Dalton Trans.* **2014**, *43*, 14517.
- (34) Glatz, M.; Bichler, B.; Mastalir, M.; Stoger, B.; Weil, M.; Mereiter, K.; Pittenauer, E.; Allmaier, G.; Veiros, L. F.; Kirchner, K. A. *Dalton Trans.* **2015**, *44*, 281.
- (35) Gorgas, N.; Stöger, B.; Veiros, L. F.; Pittenauer, E.; Allmaier, G.; Kirchner, K. A. *Organometallics* **2014**, *33*, 6905.
- (36) DeRieux, W. S.; Wong, A.; Schrodi, Y. *J. Organomet. Chem.* **2014**, *772*, 60.
- (37) Holmquist, C. R.; Roskamp, E. J. *J. Org. Chem.* **1989**, *54*, 3258.

-
- (38) Mahmood, S. J.; Hossain, M. M. *J. Org. Chem.* **1998**, *63*, 3333.
- (39) Redlich, M.; Mahmood, S. J.; Mayer, M. F.; Hossain, M. M. *Synth. Comm.* **2000**, *30*, 1401.
- (40) Dudley, M. E.; Morshed, M. M.; Brennan, C. L.; Islam, M. S.; Ahmad, M. S.; Atuu, M. R.; Branstetter, B.; Hossain, M. M. *J. Org. Chem.* **2004**, *69*, 7599.
- (41) Alves, L. G.; Dazinger, G.; Veiros, L. F.; Kirchner, K. A. *Eur. J. Inorg. Chem.* **2010**, 3160.
- (42) Bauer, G.; Kirchner, K. A. *Angew. Chem. Int. Ed.* **2011**, *50*, 5798.
- (43) Albrecht, M. *Chem. Rev.* **2010**, *110*, 576.
- (44) Bhattacharya, P.; Guan, H. R. *Comment. Inorg. Chem.* **2011**, *32*, 88.
- (45) Kulkarni, A. A.; Daugulis, O. *Synthesis-Stuttgart* **2009**, *2009*, 4087.
- (46) Creaser, C. S.; Kaska, W. C. *Inorg. Chim. Acta* **1978**, *30*, L325.
- (47) Murugesan, S.; Stoger, B.; Carvalho, M. D.; Ferreira, L. P.; Pittenauer, E.; Allmaier, G.; Veiros, L. F.; Kirchner, K. A. *Organometallics* **2014**, *33*, 6132.
- (48) Sun, Y. Q.; Li, X. Y.; Sun, H. J. *Inorg. Chim. Acta* **2014**, *415*, 95.
- (49) Benito-Garagorri, D.; Bocokic, V.; Mereiter, K.; Kirchner, K. A. *Organometallics* **2006**, *25*, 3817.
- (50) Baroudi, A.; El-Hellani, A.; Bengali, A. A.; Goldman, A. S.; Hasanayn, F. *Inorg. Chem.* **2014**, *53*, 12348.
- (51) Ozerov, O. V.; Guo, C. Y.; Foxman, B. M. *J. Organomet. Chem.* **2006**, *691*, 4802.
- (52) Feng, J.; Cai, C. *J. Fluorine Chem.* **2013**, *146*, 6.
- (53) Nammalwar, B.; Bunce, R. A.; Berlin, K. D.; Bourne, C. R.; Bourne, P. C.; Barrow, E. W.; Barrow, W. W. *Org. Prep. Proced. Int.* **2013**, *45*, 66.
- (54) Blacque, O.; Frech, C. M. *Chem. Eur. J.* **2010**, *16*, 1521.
- (55) Bolliger, J. L.; Frech, C. M. *Chimia* **2009**, *63*, 23.
- (56) Bolliger, J. L.; Blacque, O.; Frech, C. M. *Chem. Eur. J.* **2008**, *14*, 7969.
- (57) Bolliger, J. L.; Frech, C. M. *Adv. Synth. Catal.* **2010**, *352*, 1075.
- (58) Bolliger, J. L.; Blacque, O.; Frech, C. M. *Angew. Chem. Int. Ed.* **2007**, *46*, 6514.
- (59) Bolliger, J. L.; Frech, C. M. *Adv. Synth. Catal.* **2009**, *351*, 891.
-

- (60) Bhattacharya, P.; Krause, J. A.; Guan, H. R. *Organometallics* **2011**, *30*, 4720.
- (61) Wang, W.; Gu, P.; Wang, Y.; Wei, H. *Organometallics* **2014**, *33*, 847.
- (62) Bhattacharya, P.; Krause, J. A.; Guan, H. R. *J. Am. Chem. Soc.* **2014**, *136*, 11153.
- (63) Bhattacharya, P.; Krause, J. A.; Guan, H. R. *Organometallics* **2014**, *33*, 6113.
- (64) Small, B. L.; Brookhart, M.; Bennett, A. M. A. *J. Am. Chem. Soc.* **1998**, *120*, 4049.
- (65) Small, B. L.; Brookhart, M. *J. Am. Chem. Soc.* **1998**, *120*, 7143.
- (66) Britovsek, G. J. P.; Gibson, V. C.; Kimberley, B. S.; Maddox, P. J.; McTavish, S. J.; Solan, G. A.; White, A. J. P.; Williams, D. J. *Chem. Comm.* **1998**, 849.
- (67) Britovsek, G. J. P.; Bruce, M.; Gibson, V. C.; Kimberley, B. S.; Maddox, P. J.; Mastroianni, S.; McTavish, S. J.; Redshaw, C.; Solan, G. A.; Stromberg, S.; White, A. J. P.; Williams, D. J. *J. Am. Chem. Soc.* **1999**, *121*, 8728.
- (68) Bart, S. C.; Lobkovsky, E.; Chirik, P. J. *J. Am. Chem. Soc.* **2004**, *126*, 13794.
- (69) Trovitch, R. J.; Lobkovsky, E.; Bill, E.; Chirik, P. J. *Organometallics* **2008**, *27*, 1470.
- (70) Trovitch, R. J.; Lobkovsky, E.; Bouwkamp, M. W.; Chirik, P. J. *Organometallics* **2008**, *27*, 6264.
- (71) Bart, S. C.; Lobkovsky, E.; Bill, E.; Chirik, P. J. *J. Am. Chem. Soc.* **2006**, *128*, 5302.
- (72) Bart, S. C.; Chlopek, K.; Bill, E.; Bouwkamp, M. W.; Lobkovsky, E.; Neese, F.; Wieghardt, K.; Chirik, P. J. *J. Am. Chem. Soc.* **2006**, *128*, 13901.
- (73) Archer, A. M.; Bouwkamp, M. W.; Cortez, M.-P.; Lobkovsky, E.; Chirik, P. J. *Organometallics* **2006**, *25*, 4269.
- (74) Russell, S. K.; Darmon, J. M.; Lobkovsky, E.; Chirik, P. J. *Inorg. Chem.* **2010**, *49*, 2782.
- (75) Marko, I. E.; Sterin, S.; Buisine, O.; Mignani, G.; Branlard, P.; Tinant, B.; Declercq, J. P. *Science* **2002**, *298*, 204.
- (76) Tondreau, A. M.; Atienza, C. C.; Weller, K. J.; Nye, S. A.; Lewis, K. M.; Delis, J. G.; Chirik, P. J. *Science* **2012**, *335*, 567.
- (77) Fernández, I.; Trovitch, R. J.; Lobkovsky, E.; Chirik, P. J. *Organometallics* **2008**, *27*, 109.
- (78) Tondreau, A. M.; Lobkovsky, E.; Chirik, P. J. *Org. Lett.* **2008**, *10*, 2789.

-
- (79) Bouwkamp, M. W.; Bowman, A. C.; Lobkovsky, E.; Chirik, P. J. *J. Am. Chem. Soc.* **2006**, *128*, 13340.
- (80) Russell, S. K.; Lobkovsky, E.; Chirik, P. J. *J. Am. Chem. Soc.* **2011**, *133*, 8858.
- (81) Sylvester, K. T.; Chirik, P. J. *J. Am. Chem. Soc.* **2009**, *131*, 8772.
- (82) Lu, D. F.; Zhu, C. L.; Jia, Z. X.; Xu, H. *J. Am. Chem. Soc.* **2014**, *136*, 13186.
- (83) Usuda, H.; Kuramochi, A.; Kanai, M.; Shibasaki, M. *Org. Lett.* **2004**, *6*, 4387.
- (84) Kawatsura, M.; Kajita, K.; Hayase, S.; Itoh, T. *Synlett* **2010**, *2010*, 1243.
- (85) Nakanishi, M.; Salit, A. F.; Bolm, C. *Adv. Synth. Catal.* **2008**, *350*, 1835.
- (86) Sharma, A.; Hartwig, J. F. *Nature* **2015**, *517*, 600.
- (87) Jankowska, J.; Paradowska, J.; Rakiel, B.; Mlynarski, J. *J. Org. Chem.* **2007**, *72*, 2228.
- (88) Jankowska, J.; Paradowska, J.; Mlynarski, J. *Tetrahedron Lett.* **2006**, *47*, 5281.
- (89) Kawatsura, M.; Komatsu, Y.; Yamamoto, M.; Hayase, S.; Itoh, T. *Tetrahedron* **2008**, *64*, 3488.
- (90) Kawatsura, M.; Komatsu, Y.; Yamamoto, M.; Hayase, S.; Itoh, T. *Tetrahedron Lett.* **2007**, *48*, 6480.
- (91) Wang, J.; Frings, M.; Bolm, C. *Chem. Eur. J.* **2014**, *20*, 966.
- (92) Nishiyama, H.; Furuta, A. *Chem. Comm.* **2007**, 760.
- (93) Chen, T.; Yang, L. M.; Gong, D. R.; Huang, K. W. *Inorg. Chim. Acta* **2014**, *423*, 320.
- (94) Imanishi, Y.; Nomura, K. *J. Polym. Sci. Pol. Chem.* **2000**, *38*, 4613.
- (95) Nomura, K.; Sidokmai, W.; Imanishi, Y. *B. Chem. Soc. Jpn.* **2000**, *73*, 599.
- (96) Tondreau, A. M.; Darmon, J. M.; Wile, B. M.; Floyd, S. K.; Lobkovsky, E.; Chirik, P. J. *Organometallics* **2009**, *28*, 3928.
- (97) Hosokawa, S.; Ito, J.; Nishiyama, H. *Organometallics* **2010**, *29*, 5773.
- (98) Bedford, R. B.; Betham, M.; Bruce, D. W.; Danopoulos, A. A.; Frost, R. M.; Hird, M. *J. Org. Chem.* **2006**, *71*, 1104.
- (99) Yu, R. P.; Darmon, J. M.; Hoyt, J. M.; Margulieux, G. W.; Turner, Z. R.; Chirik, P. J. *ACS Catal.* **2012**, *2*, 1760.
-

- (100) Srimani, D.; Diskin-Posner, Y.; Ben-David, Y.; Milstein, D. *Angew. Chem. Int. Ed.* **2013**, *52*, 14131.
- (101) Niwa, T.; Nakada, M. *J. Am. Chem. Soc.* **2012**, *134*, 13538.
- (102) Lu, L.-Q.; Li, Y.; Junge, K.; Beller, M. *Angew. Chem. Int. Ed.* **2013**, *52*, 8382.
- (103) Inagaki, T.; Phong, L. T.; Furuta, A.; Ito, J.; Nishiyama, H. *Chem. Eur. J.* **2010**, *16*, 3090.
- (104) Inagaki, T.; Ito, A.; Ito, J.; Nishiyama, H. *Angew. Chem. Int. Ed.* **2010**, *49*, 9384.

Chapter 2

Cross Coupling of Non-Activated Primary and Secondary Alkyl Halides with Aryl Grignard Reagents Catalysed by Chiral Iron Pincer Complexes

Reprinted with permission from “Bauer, G., Cheung, C. W., Hu, X. L. (2015). Cross coupling of Nonactivated Primary and Secondary Alkyl Halides with Aryl Grignard Reagents Catalyzed by Chiral Iron Pincer Complexes. *Synthesis*. doi: 10.1055/s-0034-1380136”. Copyright © 2015 Georg Thieme Verlag KG Stuttgart – New York.

2.1 Introduction

In 2004 Nakamura *et al.* reported the iron-catalysed Kumada cross coupling of secondary alkyl halides with aryl Grignard reagents.¹ Simple FeCl₃ salts in the presence of tetramethylethylenediamine (tmeda) in THF at -78°C to 0°C were utilised to generate alkylarene products in 45–99% yields; the reactions required a slow addition of Grignard reagents and tmeda. Hayashi *et al.* were able to couple primary and secondary alkyl halides with aryl Grignard reagents in the presence of Fe(acac)₃ in refluxing Et₂O. The yields were slightly lower than in Nakamura's case, yet a slow addition of Grignard reagents was not necessary.² By slightly modifying the reaction conditions of Nakamura's system, Bedford *et al.* was able to expand the Fe-catalysis. By pre-coordination of FeCl₃ with various amine, phosphine, phosphite, arsine and carbene ligands, they were able to reduce the amount of ligands used from excess to stoichiometric amount (with respect to the catalyst).^{3,4} Bedford *et al.* also showed that well-defined Fe(III) salen complexes are active towards the Kumada coupling of alkyl halides with aryl Grignard reagents without additives.⁵ In these salen systems the colour turns black upon addition of Grignard reagents, suggesting the formation of Fe nanoparticles. In a further study pre-formed and *in situ* generated nanoparticles proved to be equally active.⁶ Fürstner *et al.* applied an [Fe(C₂H₄)₄][Li(tmeda)]₂ in the cross coupling of various primary and secondary alkyl halides.⁷ The reaction was carried out at -20°C in a THF solution. This reaction shows a remarkable chemoselectivity in presence of various functional groups. Following these pioneering studies, many reports of Fe-catalysed alkyl-aryl Kumada coupling appeared. However, to the best of our knowledge, there was no precedent for Fe-catalysed enantioselective alkyl-aryl coupling.

To achieve enantioselective cross coupling, a strong and modular chiral ligand framework is required. This is challenging for Fe as previous studies suggested that Fe complexes may decompose during cross coupling to give Fe nanoparticles, which were the catalytic active species.^{9, 10} We chose the tridentate bisoxazolinyphenylamido (bopa) pincer ligand for Fe, since the chelating pincer ligand should stabilise Fe ion in different oxidation states and prevent the formation of Fe nanoparticles. Furthermore, the ligand system is modular and modification of the chiral oxazoline units can be easily made. Herein we report that these Fe-bopa complexes are indeed very active catalysts for the coupling of both secondary and primary alkyl halides with phenyl Grignard reagents at ambient temperature (Figure 2.1). In contrast to most previous

reports, the coupling proceeds smoothly without any additives. Furthermore the chelating bopa ligand remains on the Fe centre during catalysis. The synthetic utility of this catalyst system is demonstrated by the coupling of a large number of functionalised substrates. We also describe preliminary attempts towards enantioselective alkyl-aryl coupling using these chiral complexes.

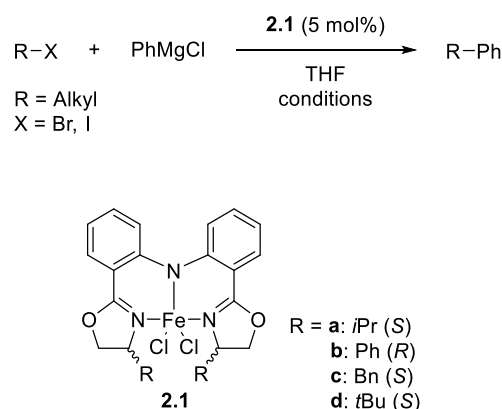


Figure 2.1: General reaction scheme.

2.2 Optimisation of the Reaction Conditions

We commenced our investigations on the cross coupling of 2-iodo-1-phenylbutane with phenyl-magnesium chloride in THF using DMA (dimethylacetamide) as additive at room temperature (r.t.) in the presence of 5 mol% Fe catalyst (Table 2.1). All complexes (**2.1-a** – **2.1-c**) showed similar activity, giving yields of about 50%. **2.1-c** was taken for further screening because it was the best catalyst among the three. **2.1-d** was not included in the screening as it was introduced only in a later stage of this work.

Table 2.1: Optimisation of reaction conditions.^a

Reaction scheme: 2-iodo-1-phenylbutane + PhMgCl $\xrightarrow[\text{THF, temp., 15 min}]{\text{2.1 (5 mol\% additive)}}$ 2-phenylbutane

Entry	Cat., Additive (mol%)	Temp [°C]	Yield ^b (%)	ee (%)
1	2.1-a, DMA (16)	r.t.	47	n/a
2	2.1-b, DMA (16)	r.t.	53	n/a
3	2.1-c, DMA (16)	r.t.	56	n/a
4	2.1-c, DMA (5)	r.t.	57	7
5	2.1-c, tmeda (5)	r.t.	60	7
6	2.1-c, O-tmeda (5) ^c	r.t.	50	6
7	2.1-c, NMP (5)	r.t.	47	10
8	2.1-c, —	r.t.	69	5
9	2.1-c, —	0	78	7
10	2.1-c, —	-20	89	10
11	2.1-c, —	-40	95	10
12	2.1-c, — ^d	r.t.	28	3

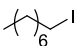
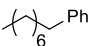
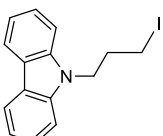
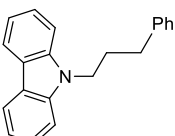
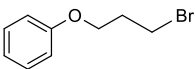
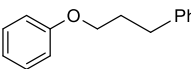
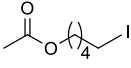
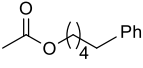
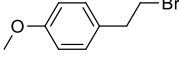
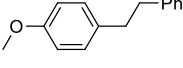
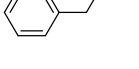
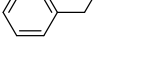
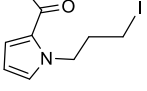
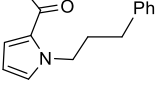
^a Conditions: 2-iodo-1-phenylbutane (0.5 mmol), PhMgCl (0.55 mmol), catalyst (5 mol%), dodecane in THF (4.0 mL). ^b Yields were determined by GC (dodecane as internal standard; 100% conversion.). ^c Bis[2-(N,N-dimethylamino)ethyl]ether. ^d Diethyl ether was used as a solvent.

The effect of additive was next investigated. The amount of DMA was lowered from 16 mol% (Table 2.1, Entries 1 – 3) to 5 mol% (1.0 equivalent to the catalyst, Table 2.1, Entry 4) and the yield remained the same. Changing to different additives such as tmeda, O-tmeda and NMP (Table 2.1, Entries 5 – 7) did not significantly change the yields. To our surprise, a higher yield (69%) was obtained without any additive (Table 2.1, Entry 8). Lowering the temperature (Table 2.1, Entries 9-11) further increased the yield; at -40°C, the yield was 95%. Changing the solvent from THF to diethyl ether (Table 2.1, Entry 12) lowered the yield to 28% at room temperature. Under all conditions, the ee's were similarly low. Although the highest yield was obtained at -40°C, we decided to investigate the scope of the coupling at room temperature for the convenience of experiments.

2.3 Scope of Kumada Cross Coupling of Primary and Secondary Alkyl Halides with Phenyl Grignard Reagents

The optimised coupling conditions at room temperature were applied for the coupling of various primary alkyl halides (Table 2.2, Entries 1 - 7) as well as cyclic and acyclic secondary alkyl halides (Table 2.2, Entries 8 – 14). Both alkyl iodides and bromides reacted smoothly to give the corresponding products in generally high to excellent yields.

Table 2.2: Cross coupling reaction of alkyl halides with phenyl Grignard.

Entry	Halide	Product	Yield ^a (%)
1			92 ^{b,c} 82 ^c
2			83
3			68
4			83
5			98
6			57
7			57 (25) ^d

8			95 ^{b,c} (X=I) 88 ^c (X=I) 93 ^c (X=Br)
9			90
10			75
11			92 ^e
12			71 ^f
13			88
14			65
15			83
16			53 ^g
17			85

^a isolated yields at 100% conversion ^b reaction at -40°C. ^c use of **2.1-b** as a catalyst. ^d 25% starting material was recovered. ^e Mixture of diastereoisomers: 66:34 (d.r. for RX = 91:9).

^f Mixture of diastereoisomers: 52:48 (d.r. for RX = 81:19). ^g Mixture of stereoisomers: 81:19 (d.r. for RX = 100:0)

The protocol tolerates a range of functional groups, including ethers (Entries 3, 5 and 9), carbamates (Entry 14), N-heterocycles (Entries 2 and 7), Boc-protected piperidine (Entry 13) and tetrahydropyran (Entries 10 – 11). Base-sensitive ester (Entries 4 and 12) and ketone (Entry 7) containing compounds were coupled with a high chemoselectivity despite the use of a Grignard reagent. Natural product-derived compounds, including 3-iodocholestene, cholesteryl-6-iodohexanoate and menthyl-6-iodohexanoate (Table 2.2, Entries 15 – 17), were also coupled in moderate to good yields.

2.4 Screening for Applicability in the Enantioselective Kumada Cross coupling of Secondary Alkyl Halides with Aryl Grignard Reagents

Having demonstrated the catalytic efficiency of this Fe-pincer system, we proceeded to study the enantioselective C-C coupling reactions. We chose three different substrates (Table 2.3) and performed the reaction at the previously optimised conditions using the chiral Fe(III) pre-catalysts (**2.1-a** – **2.1-d**). These three phenyl alkyl halides were chosen because previous reports have shown that the phenyl group can be an effective directing group in Ni-catalysed enantioselective alkyl-alkyl coupling.⁸⁻¹⁰ Additionally, the two enantiomers of the products could be readily separated by chiral HPLC. When the phenyl group is at the β -position of the alkyl iodide, nearly no enantioselectivity was obtained for all four Fe catalysts (Table 2.3, Entries 1-4). More encouraging results were obtained for substrates with a phenyl group at the α -position of the alkyl halide. The *tert*-butyl substituted bopa ligand gave the highest enantiomeric excess (ee), in the range of 15-20%. Although only low ee's were obtained in these experiments, the results demonstrate that a bopa-based ligand system is capable of inducing enantioselectivity. They also confirm the homogenous nature of the iron catalysis.

Table 2.3: Determining of ee in the cross coupling of alkyl iodides with phenyl Grignard in presence of 5% **2.1a** – **2.1-d**.

Entry	Substrate	Product	Cat.	Yield ^a (%)	ee (%)
1			2.1-a	83	0
2			2.1-b	>95	1
3			2.1-c	73	1
4			2.1-d	77	3
5			2.1-a	84	7
6			2.1-b	92	3
7			2.1-c	94	5
8			2.1-d	>95	19
9			2.1-a	88	8
10			2.1-b	86	13
11			2.1-c	86	8
12			2.1-d	71	16

^a Yields were determined by GC (dodecane as internal standard; conversion 100%).

To conclude we have found an Fe-complex system that allows the coupling of non-activated and functionalised alkyl halides with phenyl Grignard reagents. The coupling is rapid and tolerates a wide range of different functional groups. Naturally derived compounds could be coupled in high chemoselectivity. Enantioselectivity, albeit low, is demonstrated.

2.5 Measures to Improve the Existing Enantioselectivities

The enantiomeric excess can be influenced by a range of different factors: temperature, solvents and additives, the steric bulkiness generated by the ligand system and the directing groups used in the substrate.¹¹⁻¹³ We explained above that the optimised reaction conditions – in terms of yield and conversion – were already found (Table 2.1). They do not have a grave impact on the asymmetric induction. Therefore a further fine-tuning of the solvent system was not undertaken. The focus was put on improving the ee by varying the substituents on the alkyl electrophiles and altering the scaffold of the bopa ligand system.

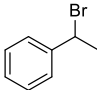
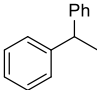
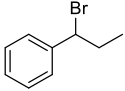
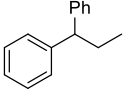
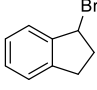
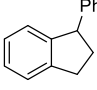
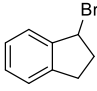
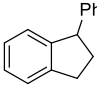
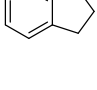
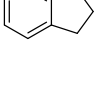
2.5.1 Influence of Secondary Benzylic Bromides on the Asymmetric Induction

The results of Table 2.3 showed that the ee was highest when the phenyl substituent was close to the coupling centre. Therefore we tried to couple secondary benzylic bromides. This class of substrates also shows to be interesting since up to now there is no iron based protocol that successfully couple them. The literature merely reports the coupling of primary benzylic halides.¹⁴⁻²⁰

Table 2.4: Coupling results of the cross coupling of secondary benzylic bromides with phenyl Grignard reagents.^a

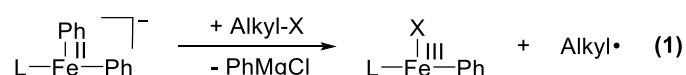
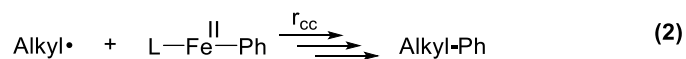
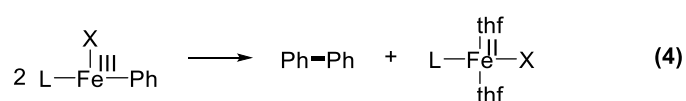
$$\text{R-Br} + \text{PhMgCl} \xrightarrow[\text{-40}^\circ\text{C, 15 min}]{\text{2.1-b (5 mol\%)}} \text{R-Ph}$$

R = Alkyl

Entry	Substrate	Solvent	Additive (mL)	Product	Yield (%) ^b
1		THF	-		trace
2		THF	-		trace
3		THF	-		1 - ^c trace ^d
4		THF	tmeda (0.1 mL)		1
5		THF	O-tmeda (0.1 mL)		trace
6		THF	NMP (0.1 mL)		trace
7		THF	DMA (0.1 mL)		1
8		THF	PPh ₃ (45 mg)		1
9		Toluene	-		2
10		Et ₂ O	-		4
11		DCM	-		5

^a Conditions: benzyl bromide (0.25 mmol), PhMgCl (0.30 mmol), catalyst (5 mol%), dodecane in THF (2.0 mL). ^b Yields were determined by GC/MS (dodecane as internal standard; conversion 100%). ^c 4-Methoxyphenyl Grignard was used. ^d 4-Fluorophenyl Grignard was used.

The results in Table 2.4 show that the cross coupling yields are in general low. The main products were biaryl – yielding from the homo-coupling between two Grignard reagents – and dialkyl compounds – namely 2,3-diphenylbutane, 3,4-diphenylhexane and 1,1'-diindane. The homo-coupling products of the alkyl electrophiles further showed no diastereomeric excess.

Oxidative Addition:Cross-Coupling:Homo-Coupling / Self Termination:

$$k_{\text{st}} \gg k_{\text{cc}}$$

Figure 2.2: Mechanistic rationale explaining the coupling reaction of secondary benzylic bromides.

To discuss the reason behind the low cross coupling yields one has to look into the mechanism of the reaction. The catalytic cycle will be discussed in detail in Chapter 3. However, this mechanism shows that the oxidative addition of the alkyl halide to the metal complex proceed *via* the formation of a free alkyl radical and an oxidised iron halide species (Figure 2.2, Equation 1). Generally speaking, in the case of the cross coupling reaction of unactivated alkyl radicals (Table 2.2), this alkyl radical recombines with an aryl containing iron species to give – upon reductive elimination – the desired coupling product (Figure 2.2, Equation 2). Apparently, in the case of the secondary benzylic radicals, the reaction rate (r_{st}) to undergo a self-termination reaction with each other is much higher than reaction rate (r_{cc}) to recombine with an iron aryl species (Figure 2.2, Equation 3).^{21,22} The non-existing diastereomeric access additionally points out that the coupling between the two benzylic radicals proceeds in solution away from the iron centre. This homo-coupling yields an increased concentration of the iron(III) aryl halide species. This species itself reductively eliminates the aryl residue by forming biphenyl in a bimolecular process (Figure 2.2, Equation 4). Henceforth the predominant formation of homo-coupling products can be observed. Secondary benzylic halides appear not to be a suitable substrate class for the iron-bopa complex system.

2.5.2 Structural Modification on the Ligand System

The structural information that was collected throughout the work, revealed the versatile and flexible nature of the bopa-ligand. It shows amongst others a 6-coordinated octahedral structure (Figure 3.3), a 5-coordinated trigonal-bipyramidal²³ and distorted square pyramidal structure (Figure 4.5) and a 4-coordinated tetrahedral structure (Figures 3.4 – 3.5). This flexible nature may be the reason for the low asymmetric induction during catalysis. To solve this problem we decided on altering the scaffold of the bopa ligand. The ligand can be divided into two sectors, the oxazoline moiety (Figure 2.3, yellow sector) and the diphenylamino backbone (Figure 2.3, blue sector).

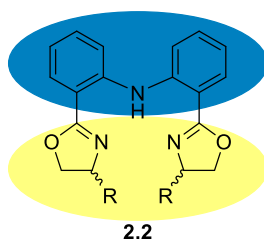


Figure 2.3: Structure of bopa-R (2.2).

2.5.2.1 Ligand Modification on the Oxazoline Moiety

In Table 2.3 we showed already that the ee can be increased by using more bulky substituents as chiral residues in the α -position to the imine functionality. The best results were with complex **2.1-d** (R=*t*Bu) which reached ee's up to 20%. Inagaki *et al.* had the best results in the asymmetric hydrosilylation of acetophenone derivatives using diphenylmethyl as chiral residue.^{23,24} Due to the exorbitant high price of S-2-amino-3,3-diphenyl-1-propanol (L diphenylalaninol) we did not consider it as a viable option.

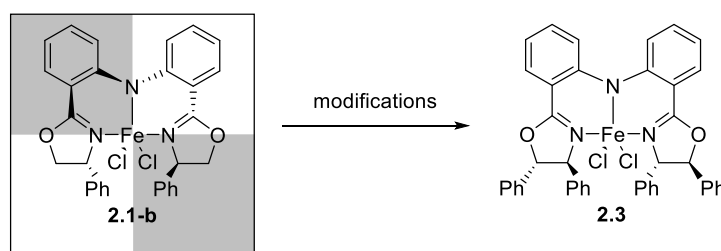


Figure 2.4: Quadrant diagram of **2.1-b** and proposal for modifications on the oxazoline moiety.

The catalyst **2.1-b** shows an open axis with little steric hindrance (Figure 2.4, white quadrants) around the metal centre. Possibly due to this open space the incoming substrate has no preference from which direction it approaches the catalyst, hence the low enantioselectivities. By putting a second substituent in α - position to the oxygen, which is *threo* to the already existing phenyl residue, one might block the front side of the complex. Therefore the substrate would have to approach the complex from the back side which should induce a higher selectivity.

Table 2.5: Results of the cross coupling reaction using complex **2.3** as catalyst.

$$\text{R-X} + \text{4-MeOC}_6\text{H}_4\text{MgCl} \xrightarrow[\text{-40}^\circ\text{C, 15 min}]{\text{2.3 (5 mol\%)}, \text{THF}} \text{4-MeOC}_6\text{H}_4\text{R}$$

Entry	Substrate	Product	Yield ^a (%)	ee (%)
1			85	2
2			85	8

^a Yields were determined by GC (dodecane as internal standard; conversion 100%).

By putting a second phenyl substituent *threo* to the existing phenyl group did not show any improvements of the results. Due to repeated negative results we abandoned the idea of increasing the ee by modifications on the oxazoline moiety.

2.5.2.2 Ligand Modification on the Diphenylamino Backbone

The bopa ligand has a high rotational freedom around the amine bridge (Figure 2.5). By putting substituents in the 5-position of the phenyl rings one can decrease or eliminate the rotation around the amine. We therefore designed three complexes based on: (1) carbazole (Figure 2.5, complex **2.4**), exhibiting a flat structure, (2) 10,11-dihydro-5H-dibenz[b,f]azepine (Figure 2.5, complex **2.5**), which shows a strongly restricted rotation and (3) 5,5'-dimethyl substituted bopa ligand (Figure 2.5, complex **2.6**); the two methyl substituents prevent the two phenyl groups of flipping in the plane.

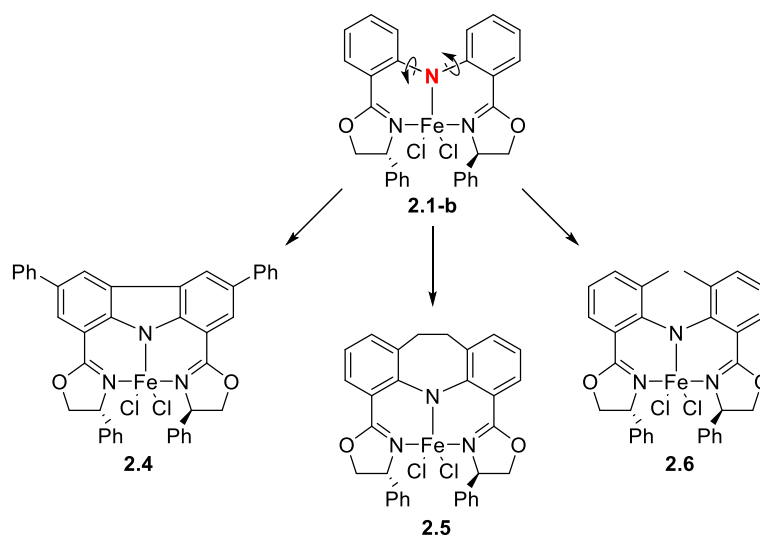


Figure 2.5: Modifications of the diphenylamino backbone to minimise the rotation around the amine bridge (red).

Complex **2.4** was already synthesised by Niwa *et al.* as a non-heme iron(III) complex which shows porphyrin-like properties. It was employed in the asymmetric epoxidation of *trans*-alkenes.²⁵ The ligand of complex **2.5** was synthesised in a 9 step synthesis from 10,11-dihydro-5H-dibenz[b,f]azepine (Figure 2.6).

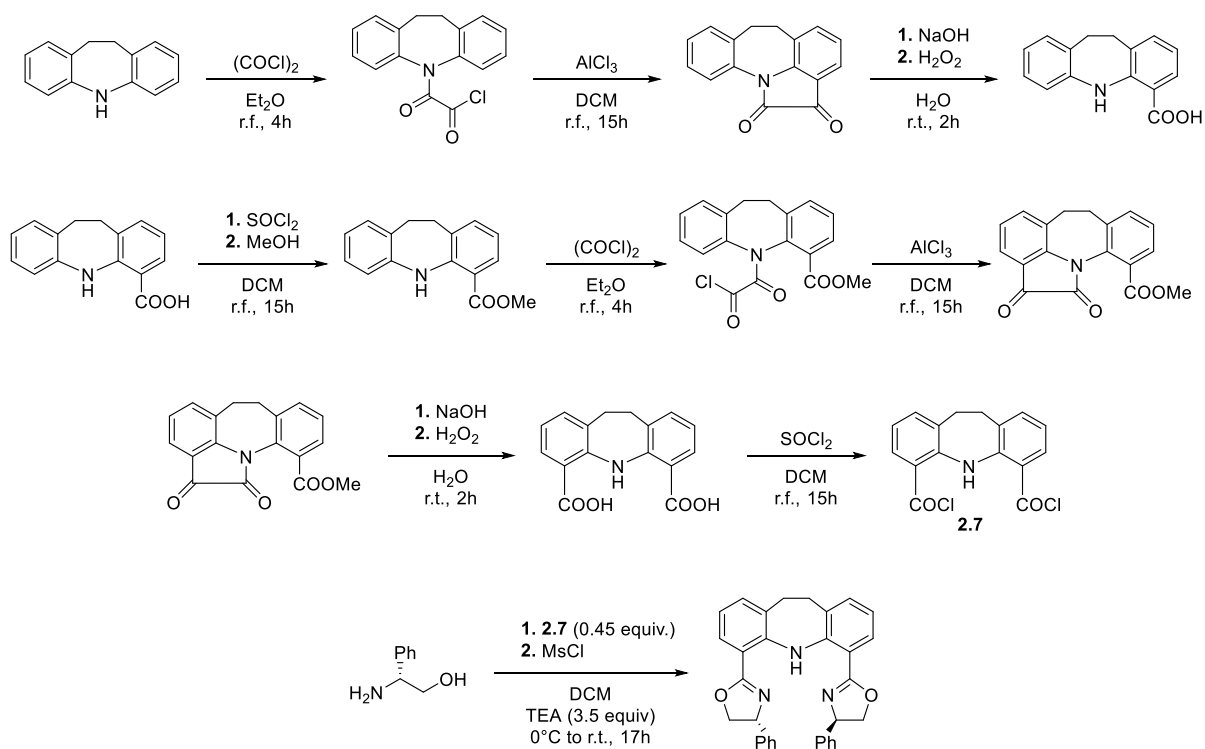


Figure 2.6: Synthetic pathway for the synthesis of 4,6-di((R)-4-phenyl-4,5-dihydrooxazol-2-yl)-10,11-dihydro-5H-dibenz[b,f]azepine.

The synthesis gave the desired ligand in a very low yield (1%). Further complexation with FeCl_2 to the desired complex by following the standard procedure^{23,26} gave a brownish powder (in contrast to a dark green complex). Additionally, complex **2.5** could be confirmed neither by MS nor by elemental analysis. Therefore this compound was not taken into consideration for further screening.

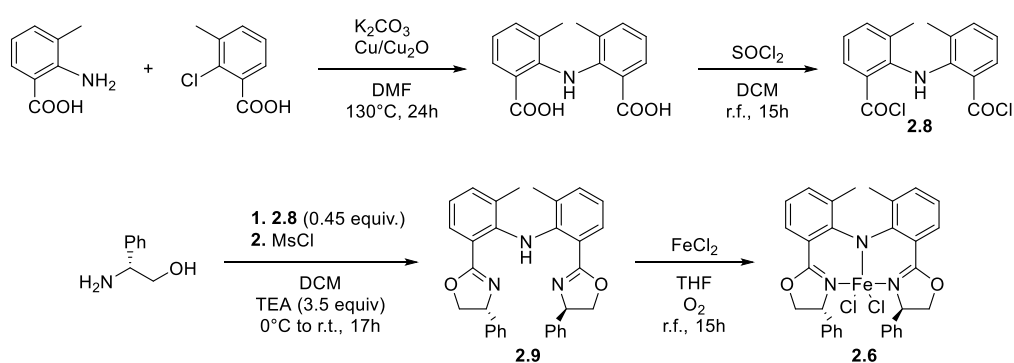


Figure 2.7: Synthetic pathway for the synthesis of bis(2-methyl-6-((R)-4-phenyl-4,5-dihydrooxazol-2-yl)phenyl)amine.

Complex **2.6** was synthesised in analogy to complex **2.1** by using 2-amino-3-methylbenzoic acid and 2-chloro-3-methylbenzoic acid as starting materials (Figure 2.7) to form the 2,2'-imino-bis-3-methylbenzoic acid.²⁷ The synthesis of the ligand was finalised by forming the acid chloride (**2.8**), which was then further condensed to R(-)-phenylglycinol to give the ligand **2.9**. The overall yield was 7%. The NMR spectrum of the ligand (Figure 2.8) shows two sets of signals, which points to the existence of two diastereomers.

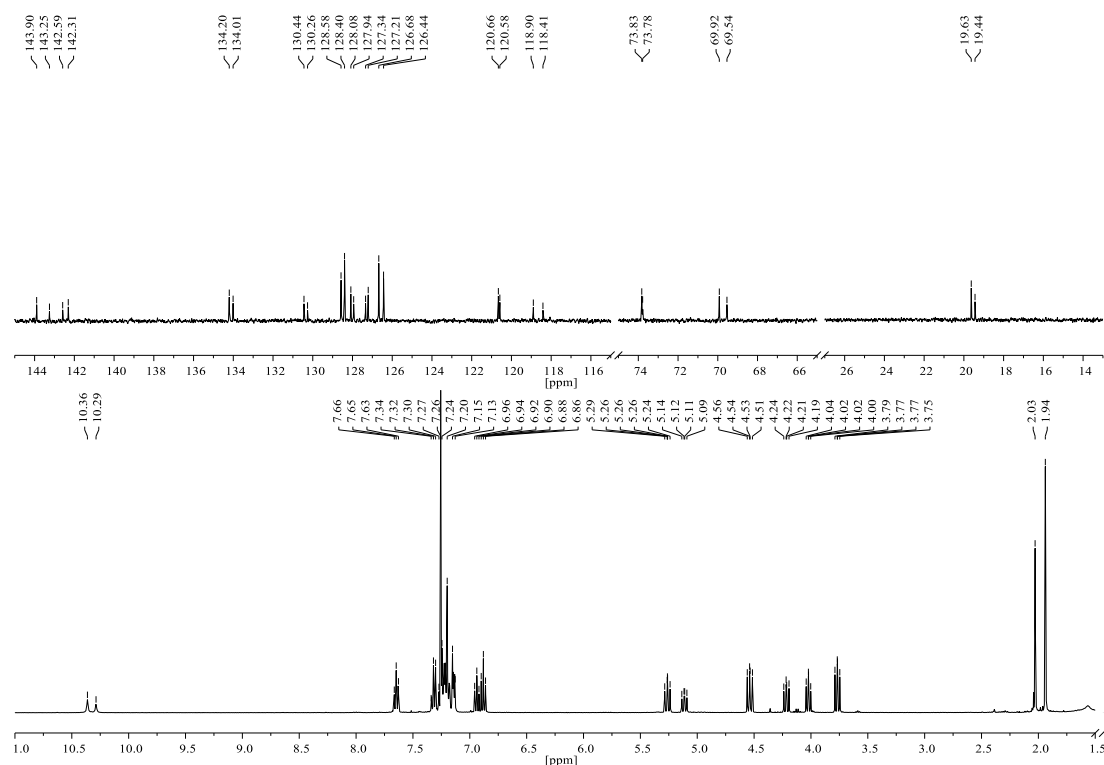


Figure 2.8: Mixture of stereoisomers of bis(2-methyl-6-((R)-4-phenyl-4,5-dihydrooxazol-2-yl)phenyl)amine.

The two methyl substituents ortho to the amine bridge prevent the two phenyl groups of the ligand backbone from flipping the plane and therefore cause a chiral axis (Figure 2.9). The R-S_a-R and the R-R_a-R isomer could not be separated and were further ligated to FeCl₂ to give complex **2.6** as a mixture of both isomers.^{23,26} Therefore **2.6** was employed as diastereomeric mixture in the cross coupling reaction.

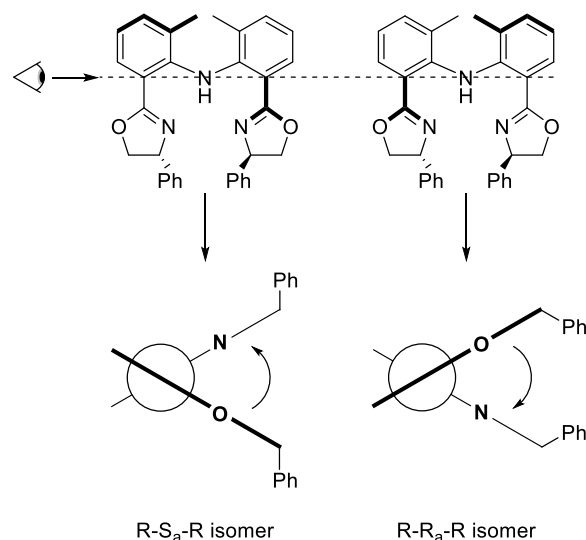


Figure 2.9: Rotational chirality of bis(2-methyl-6-((R)-4-phenyl-4,5-dihydrooxazol-2-yl)phenyl)amine.

Complexes **2.4** and **2.6** were then employed in the Kumada cross coupling reaction using the previously optimised reaction conditions (Table 2.1).

Table 2.6: Results of the cross coupling using complex **2.4** and **2.6** as a catalyst.

Entry	Substrate	Product	Cat.	Yield ^a (%)	ee ^b (%)
1			2.4	47	2
3			2.6	50	6
5			2.4	52	2
7			2.6	71	11

^a Yields were determined by GC (dodecane as internal standard; conversion 100%).

The results in Table 2.6 show that the modifications on the ligand system show no improvement of the enantioselectivities. We therefore abandoned the enantioselective cross coupling of secondary alkyl halides using iron bopa complexes as catalyst and turned our interest to investigate the mechanism involved in the cross coupling.

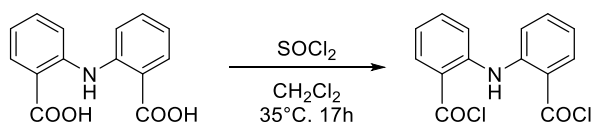
2.6 Experimental

All manipulations were carried out under an inert N₂ atmosphere using standard Schlenk or glove box techniques. The solvents were purified and dried using a two column solid-state purification system (Innovative Technology, NJ, USA). They were transferred to the glove box in a Strauss-flask without exposure to air. The solvents were stored over molecular sieves (3 Å). Deuterated chloroform was purchased from Armar Chemicals and was degassed and stored over dried and activated molecular sieves (3 Å). (S)-2-amino-3,3-dimethyl-1-butanol (L-*tert*-leucinol) was purchased from TCI, (1R,2S)-(-)-2-amino-1,2-diphenylethanol was purchased from Alfa Aesar. The following chemicals were synthesised: 2,2'-iminodibenzoic acid,²⁷ (S)-(+)-2-amino-3-methyl-1-butanol (L-valinol),²⁸ R-(-)-phenylglycinol,²⁸ L(-)-2-amino-3-phenyl-1-propanol (L-phenylalaninol),²⁸ 2,2'-iminodibenzoyl chloride,²⁹ bopa-R (R = *i*Pr, Ph, Bn, *t*Bu),²⁹ [Fe(bopa-R)Cl₂] (R = *i*Pr, Ph, Bn, *t*Bu),^{23,29} 1,8-bis((R)-4-phenyl-4,5-dihydrooxazol-2-yl)-3,6-diphenyl carbazole,³⁰ 4,6-di((R)-4-phenyl-4,5-dihydrooxazol-2-yl)-10,11-dihydro-5H-dibenz[b,f]azepine,^{26,31} bis(2-methyl-6-((R)-4-phenyl-4,5-dihydrooxazol-2-yl)phenyl) amine.^{26,27} All known primary and secondary halides were either commercially available or prepared according to the literature procedures.^{32,33}

The Grignard reagents were titrated prior to every use following the literature procedure.³⁴

2.6.1 Ligand Syntheses

2.6.1.1 Synthesis of 2,2'-Iminodibenzoyl Chloride



2,2'-Iminodibenzoic acid (21.0 g, 1.0 equiv.) was suspended in 100 mL CH₂Cl₂ and thionyl chloride (18.0 mL, 3.0 equiv.) was added. The suspension was heated to reflux overnight. The formed yellow solid was filtered off and washed twice with 20 mL cold CH₂Cl₂. The filtrate was carefully extracted with water to quench the reaction. The organic phase was dried over Na₂SO₄ and evaporated to dryness. The crude product (from the filtrate) was recrystallized from CH₂Cl₂ and hexane. The obtained solids were combined.

Yield: 21.8 g (91%), bright yellow solid

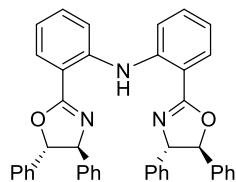
¹H NMR (400 MHz, Chloroform-*d*): δ 10.36 (s, 1H), 8.27 (d, *J*=8.5 Hz, 2H), 7.54 - 7.49 (m, 4H), 7.07 (ddd, *J*=7.1, 2.4 Hz, 2H).

¹³C NMR (101 MHz, Chloroform-*d*) δ 168.45, 144.04, 135.91, 135.72, 121.71, 121.04, 118.73.

Elemental analysis calculated (%) for C₁₄H₉Cl₂NO₂: C 57.17, H 3.08, N 4.76; found: C 57.05, H 3.04, N 4.60

Melting Point: 163 – 165°C

2.6.1.2 Synthesis of Bis(2-((4*S*,5*S*)-4,5-diphenyl-4,5-dihydrooxazol-2-yl)phenyl)amine



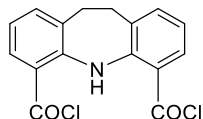
(1*R*,2*S*)-(-)-2-Amino-1,2-diphenylethanol (0.5 g, 2.3 mmol, 2.0 equiv) were dissolved in DCM (50 mL) and TEA (1.1 mL, 8.2 mmol, 7.0 equiv., freshly distilled from KOH) were added. The solution was cooled to 0°C and 2,2'-Iminodibenzoyl chloride (345 mg, 1.2 mmol, 1.0 equiv.) were added slowly in small portions. The reaction was allowed to heat to room temperature and stirred for another 2 hours (the conversion was checked by TLC). The reaction was again cooled to 0°C and MsCl (0.2 mL, 2.5 mmol, 2.1 equiv) was added drop wise. The reaction was again allowed to heat to room temperature and stirred for another 2 hours. The reaction was quenched by addition of saturated aqueous bicarbonate solution (50 mL). The phases were separated and the organic phase was washed with water (50 mL), brine (50 mL) and dried over Na₂SO₄. The solvent was evaporated to give the crude product (688 mg, 96%) which was purified by flash column chromatography (10% EtOAc in hexanes).

Yield: 628 mg (89%), yellowish white solid

¹H NMR (400 MHz, Chloroform-*d*) δ 11.27 (s, 1H), 7.96 (dt, *J* = 7.9, 1.4 Hz, 2H), 7.64 – 7.56 (m, 2H), 7.38 (ddd, *J* = 8.6, 7.3, 1.7 Hz, 2H), 7.29 (dd, *J* = 4.8, 1.9 Hz, 6H), 7.16 (td, *J* = 6.5, 5.1, 3.0 Hz, 10H), 7.07 – 7.02 (m, 4H), 6.97 (td, *J* = 7.5, 1.2 Hz, 2H), 5.09 (d, *J* = 7.6 Hz, 2H), 4.92 (d, *J* = 7.5 Hz, 2H).

¹³C NMR (101 MHz, Chloroform-*d*) δ 163.32, 143.49, 142.08, 140.45, 131.59, 130.66, 128.67, 128.47, 128.15, 127.25, 126.42, 125.76, 119.94, 118.48, 115.84, 87.72, 78.73.

2.6.1.3 Synthesis of 10,11-Dihydro-5H-dibenz[b,f]azepine-4,6-dicarbonyl Chloride (2.7)

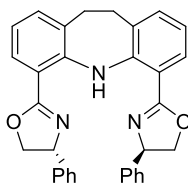


4,6-dicarboxy-10,11-dihydro-5H-dibenz[b,f]azepine³¹ (1.16 g, 4.1 mmol, 1.0 equiv.) was suspended in DCM (40 mL) and thionyl chloride (0.9 mL, 12.3 mmol, 3.0 equiv.) was added. The suspension was heated to reflux for 48 hours. The reaction was cooled to 0°C and the formed solid was filtered off. The remaining solution was quickly extracted with water (20 mL) to destroy the excess amount of thionyl chloride. The organic phase was dried over Na₂SO₄ and the solvent was evaporated. The two solids were combined.

Yield: 1.26 g (96 %), yellow solid

¹H NMR (400 MHz, Chloroform-*d*) δ 11.24 (s, 1H), 8.19 (d, *J* = 8.3 Hz, 2H), 7.31 (d, *J* = 8.5 Hz, 2H), 6.93 (t, *J* = 7.8 Hz, 2H), 3.15 (s, 4H).

2.6.1.4 Synthesis of 4,6-Di((*R*)-4-phenyl-4,5-dihydrooxazol-2-yl)-10,11-dihydro-5H-dibenz[b,f]azepine



R-Phenyglycinol (1.1 g, 8.0 mmol, 2.2 equiv.) was dissolved in 100 mL of dry DCM and TEA (3.6 mL, 26.0 mmol, 7.0 equiv., freshly distilled from KOH) were added. The solution was cooled to 0°C and 10,11-dihydro-5H-dibenz[b,f]azepine-4,6-dicarbonyl chloride (1.18 g, 3.7 mmol, 1.0 equiv.) was added slowly in little portions. The mixture was allowed to heat to room temperature and stirred for 2 hours (conversion checked by TLC). When the reaction was complete, the solution was cooled to 0°C and MsCl (0.6 mL, 7.8 mmol, 2.2 equiv.) were added

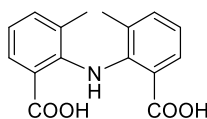
drop wise. The solution was again heated to room temperature and stirred as long as the reaction was complete. The reaction was quenched by adding saturated aqueous NaHCO_3 . The two phases were separated and the aqueous phase was re-extracted with DCM (2x50 mL). The combined organic phases were dried over Na_2SO_4 , the solvent was evaporated and the crude ligand was purified by flash column chromatography (15% EtOAc in hexanes).

Yield: 245 mg (14%), orange solid

^1H NMR (400 MHz, $\text{DMSO-}d_6$) δ 11.46 (s, 1H), 7.60 (dd, $J = 7.8, 1.8$ Hz, 2H), 7.41 – 7.20 (m, 12H), 6.83 (t, $J = 7.6$ Hz, 2H), 5.29 (dd, $J = 10.1, 8.5$ Hz, 2H), 4.41 (dd, $J = 10.1, 8.3$ Hz, 2H), 3.96 (t, $J = 8.4$ Hz, 2H), 3.19 – 3.01 (m, 4H).

^{13}C NMR (101 MHz, DMSO) δ 164.04, 142.76, 142.01, 133.46, 131.65, 128.92, 128.82, 127.76, 126.90, 118.74, 115.00, 73.58, 70.04, 36.18.

2.6.1.5 Synthesis of 2,2'-Imino-bis-3-methylbenzoic Acid

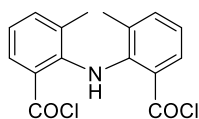


The synthesis is based on the synthesis of 2,2'-imino-bisbenzoic acid.²⁷

A mixture of 2-chloro-3-methylbenzoic acid (3.0 g, 18.0 mmol, 1.0 equiv.) and 2-amino-3-methylbenzoic acid (3.3 g, 22.0 mmol, 1.2 equiv.), anhydrous potassium carbonate (5.47 g, 40.0 mmol, 2.2 equiv.), Cu powder (0.112 g, 1.8 mmol, 0.1 equiv.) and Cu_2O (0.126 g, 0.88 mmol, 5 mol%) in 10 mL of anhydrous DMF was heated to 130°C for 24h. The DMF was then evaporated under reduced pressure, water (50 mL) was added and the solution was filtered to remove solid particles. The mixture was acidified with a 1M aqueous HCl solution until it reached pH 4, thus leading to the formation of a green precipitate. The desired compound was filtered off and purified over a short column of silica using ethyl acetate as eluent. It was finally dried under vacuum.

Yield: 1.84 g (37 %)

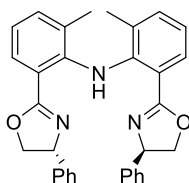
^1H NMR (400 MHz, $\text{DMSO-}d_6$) δ 9.75 (s, 1H), 7.63 (d, $J = 6.6$ Hz, 2H), 7.26 (d, $J = 6.8$ Hz, 2H), 6.93 (t, $J = 6.8$ Hz, 2H), 1.71 (s, 6H).

2.6.1.6 Synthesis of 2,2'-Imino-bis(3-methylbenzoyl Chloride) (**2.8**)

2,2'-imino-bis(3-methylbenzoic acid) (1.84 g, 6.5 mmol, 1.0 equiv.) was suspended in 60 mL of DCM and thionyl chloride (1.4 mL, 20.0 mmol, 3.0 equiv.) was added. The solution was heated and stirred for 48 hours. The solution was extracted with water to destroy the excess amount of thionyl chloride. The organic phase was dried over Na_2SO_4 and the solvent was evaporated.

Yield: 1.53 g (74 %), orange-brown oil

^1H NMR (400 MHz, Chloroform- d) δ 9.03 (s, 1H), 8.05 (d, J = 8.1 Hz, 2H), 7.38 (d, J = 7.4 Hz, 2H), 7.07 (t, J = 7.8 Hz, 2H), 1.84 (s, 6H).

2.6.1.7 Synthesis of Bis(2-methyl-6-((R)-4-phenyl-4,5-dihydro-oxazol-2-yl)phenyl) Amine (**2.9**)

R-(-)-phenylglycinol (1.44 g, 10.5 mmol, 2.2 equiv.) was dissolved in 150 mL of dry DCM and TEA (4.65 mL, 33.3 mmol, 7.0 equiv., freshly distilled from KOH) were added. The solution was cooled to 0°C and 2,2'-imino-bis(3-methylbenzoyl chloride) (1.53 g, 4.7 mmol, 1.0 equiv.) was added slowly in little portions. The mixture was allowed to heat to room temperature and stirred for 2 hours. When the reaction was complete, the solution was cooled to 0°C and MsCl (0.77 mL, 10.0 mmol, 2.1 equiv.) was added drop wise. The solution was again heated to room temperature and stirred for 2 hours. Saturated aqueous NaHCO_3 was added to quench the reaction. The two phases were separated and the aqueous phase was re-extracted (DCM 2x 50 mL). The combined organic phases were dried over Na_2SO_4 , the solvent

was evaporated and the crude ligand was purified by flash column chromatography (15% EtOAc in hexanes).

Yield: 0.584 g (25 %), yellow solid

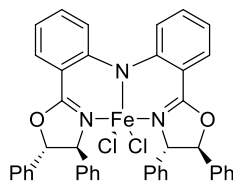
¹H NMR (400 MHz, Chloroform-*d*) Isomer A: δ 10.36 (s, 1H), 7.65 (t, $J = 7.3$ Hz, 2H), 7.40 – 7.10 (m, 12H), 6.88 (t, $J = 7.6$ Hz, 2H), 5.32 – 5.21 (m, 2H), 4.54 (dd, $J = 10.0, 8.2$ Hz, 2H), 3.77 (dd, $J = 8.9, 8.2$ Hz, 2H), 1.94 (s, 6H). Isomer B: δ 10.29 (s, 1H), 7.65 (t, $J = 7.3$ Hz, 2H), 7.40 – 7.09 (m, 12H), 6.94 (t, $J = 7.6$ Hz, 2H), 5.11 (dd, $J = 10.1, 7.7$ Hz, 2H), 4.22 (dd, $J = 10.1, 8.2$ Hz, 2H), 4.02 (t, $J = 8.5$ Hz, 2H), 2.03 (s, 6H).

¹³C NMR (101 MHz, Chloroform-*d*) Isomers A + B: δ 165.48, 143.92, 143.28, 142.61, 142.33, 134.23, 134.04, 130.47, 130.29, 128.60, 128.43, 128.11, 127.97, 127.37, 127.23, 126.70, 126.46, 120.68, 120.61, 118.92, 118.44, 73.85, 73.81, 69.95, 69.56, 19.65, 19.46.

2.6.2 Complex Syntheses

2.6.2.1 General Procedure

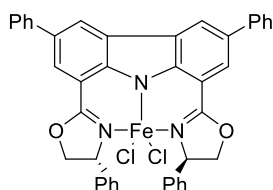
The ligand (1.0 equiv.) and FeCl₂ (1.0 equiv.) were dissolved in THF. The mixture was brought to reflux for 17 hours. The solvent was evaporated and the crude solid was dissolved in DCM and filtered over a pad of celite. The complex solution was concentrated and the complex was precipitated by addition of hexane. The precipitate was filtered off and dried *in vacuo*.

2.6.2.2 Complex **2.3**

Yield: 94%, dark green powder

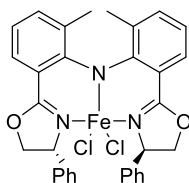
Elemental analysis calculated (%) for $C_{42}H_{32}FeCl_2N_3O_2$: C 68.40, H 4.37, N 5.70; found: C 68.25, H 4.41, N 5.53

MS (APCI): m/z $[M - Cl]^+$ calc. for $C_{42}H_{32}ClFeN_3O_2^+$: 701.1532; found: 701.1529

2.6.2.3 Complex **2.4**²⁵

Yield: 64%, dark green powder

MS (MALDI): m/z $[M - Cl]^+$ calc. for $C_{42}H_{30}ClFeN_3O_2^+$: 699.1376; found: 699.1377

2.6.2.4 Complex **2.6**

Yield: 88%, dark green powder

Elemental analysis calculated (%) for $C_{32}H_{28}FeCl_2N_3O_2$: C 62.66, H 4.60, N 6.85; found: C 62.42, H 4.73, N 6.61

MS (MALDI): m/z $[M - Cl]^+$ calc. for $C_{32}H_{28}ClFeN_3O_2^+$: 577.1219; found: 577.1223

2.6.3 Substrate Syntheses

2.6.3.1 General Procedures for the Preparation of Primary Alkyl Iodides (Table 2.2, Entries 15 and 17).

A 250 mL conical flask equipped with a Teflon-coated magnetic stirrer was charged with 6-bromohexanoic acid (1.0 equiv), natural product alcohol (1.1 equiv), N,N'-dicyclohexylcarbodiimide (DCC, 1.0 equiv), 4-dimethylaminopyridine (2 mol %) and dichloromethane (DCM, 100 mL). The reaction mixture was stirred at room temperature overnight. The reaction mixture was then filtered and the filtrate was washed with HCl solution (~1 M (aq), ~100 mL). The organic fraction was dried *in vacuo* to give a crude alkyl bromide which was introduced into a 250 mL round-bottom flask equipped with a Teflon-coated magnetic stirrer, followed by the addition of NaI (5 equiv), acetone (50 mL) and water (5 mL). The reaction mixture was then heated at 60°C until all alkyl bromide was consumed as determined by GC analysis. After cooling to room temperature, the reaction mixture was concentrated *in vacuo*, washed with CH₂Cl₂ (50 mL) and water (100 mL). The aqueous solution was further washed with CH₂Cl₂ (2 x 50 mL). The combined organic fractions were concentrated *in vacuo* and the residue was purified by flash chromatography with silica gel using a mixture of hexanes and EtOAc as an eluent to afford the alkyl iodide.

2-Isopropyl-4-methylcyclohexyl 6-iodohexanoate (Table 2.2, entry 15).

Following the general procedure, 6-bromohexanoic acid (2.54 g, 13 mmol), (+/-)-menthol (2.24 g, 14.3 mmol), DCC (2.68 g, 13 mmol), 4-dimethylaminopyridine (32 mg, 0.20 mmol) and NaI (9.74 g, 65 mmol) were used to prepare the title product.

Yield: 2.43 g, 49%, yellow liquid

¹H NMR (400 MHz, Chloroform-*d*): δ 4.64-4.58 (m, 1 H), 3.11 (t, $J = 7.0$ Hz, 2 H), 2.23 (t, $J = 7.5$ Hz, 2 H), 1.94-1.88 (m, 1 H), 1.84-1.74 (ovrlp, 3 H), 1.63-1.54 (ovrlp, 4 H), 1.47-1.33 (ovrlp, 4 H), 1.04-0.78 (ovrlp, 9 H), 0.69 (d, $J = 6.8$ Hz, 3 H).

¹³C NMR (100 MHz, Chloroform-*d*): δ 172.7, 73.8, 46.9, 40.9, 34.3, 34.2, 33.1, 31.3, 29.9, 26.2, 23.9, 23.3, 22.0, 20.7, 16.3, 6.4.

(3S,8S,9S,10R,13R,14S,17R)-10,13-dimethyl-17-((R)-6-methylheptan-2-yl)-2,3,4,7,8,9,10,11,12,13,14,15,16,17-tetradecahydro-1H-cyclopenta[a]phenanthren-3-yl 6-iodohexanoate (Table 2.2, entry 17).

Following the general procedure, 6-bromohexanoic acid (1.95 g, 10 mmol), cholesterol (4.25 g, 11 mmol), DCC (2.06 g, 10 mmol), 4-dimethylaminopyridine (24 mg, 0.20 mmol) and NaI (7.50 g, 50 mmol) were used to prepare the title product.

Yield: 4.28 g, 70%, white powder

¹H NMR (400 MHz, Chloroform-*d*): δ 5.37 (d, $J = 4.7$ Hz, 1 H), 4.66-4.57 (m, 1 H), 3.19 (t, $J = 7.0$ Hz, 2 H), 2.32-2.27 (ovrlp, 4 H), 2.04-1.93 (ovrlp, 2 H), 1.90-1.81 (ovrlp, 5 H), 1.68-1.24 (m, 16 H), 1.19-0.94 (ovrlp, 12 H), 0.91 (d, $J = 6.5$ Hz, 3 H), 0.87-0.85 (ovrlp, 6 H), 0.68 (s, 3 H).

¹³C NMR (100 MHz, Chloroform-*d*): δ 172.9, 139.7, 122.7, 74.0, 56.8, 56.2, 50.1, 42.4, 39.8, 39.6, 38.3, 37.1, 36.7, 36.3, 35.9, 34.5, 33.2, 32.01, 31.95, 30.0, 28.3, 28.1, 27.9, 24.4, 24.1, 23.9, 23.0, 22.7, 21.1, 19.4, 18.8, 12.0, 6.7.

2.6.4 Cross Coupling Reactions and Results

2.6.4.1 General Procedure for Screening (Table 2.1 and Table 2.3 – 2.6).

Alkyl halide (0.5 mmol) and dodecane (60 μ L as internal standard) were dissolved in 3.0 mL THF and 1.0 mL of [Fe(bopa-R)Cl₂] (**1a-d**) stock solution (25 mM) was added. The solution was brought to the corresponding temperature and 0.3 mL PhMgCl (1.85 M in THF) or 0.6 mL (*p*-MeO)PhMgCl (1.00 M in THF) was added over a time period of 5 min. The reaction mixture stirred for another 10 minutes and was quenched with water. The solution was acidified with HCl (1M) and extracted with 3 x 20 mL of CH₂Cl₂. The crude extract was dried over Na₂SO₄ and analysed by GC. The solvent was then further evaporated and the product was purified for HPLC measurement by LC on silica (0 to 1% ethyl acetate in hexanes).

2.6.4.2 General Procedure for Substrate Scope (Table 2.2).

Alkyl halide (*Method A*: 0.5 mmol, *Method B*: 0.25 mmol) was dissolved in 3.0 (**A**)/1.5 (**B**) mL THF and 1.0 (**A**)/0.5 (**B**) mL [Fe(bopa-*t*Bu)Cl₂] (**1d**) stock solution (25mM) was added. Afterwards 0.5 (**A**)/ 0.25 (**B**) mL PhMgCl (1.00 M) was added over a time period of 15 min. the solution stirred for another 45 min. *Method A*: The reaction was then quenched with water, acidified with HCl (1N) and extracted with 3 x 20 mL CH₂Cl₂. The crude extract was dried over Na₂SO₄ and further purified by LC on silica. *Method B*: The reaction was quenched by adding 0.5 mL of ethanol. The reaction mixture was transferred on a preparative TLC plate and then further separated.

2.6.4.3 Results

1-Phenyloctane (Table 2.2, Entry 1).

Method A:

Yield (r.t.): 78 mg (82%); at -40°C: 87 mg (92%), Colourless liquid

The ¹H NMR spectrum obtained is in accordance with the literature.³⁵

¹H NMR (400 MHz, Chloroform-*d*) δ = 7.32 – 7.28 (m, 2H), 7.23 – 7.17 (m, 3H), 2.63 (t, J = 7.8 Hz, 2H), 1.64 (quint, J = 6.0 Hz, 2H), 1.39 – 1.29 (m, 10H), 0.91 (t, J = 6.9, 3H).

9-(3-Phenylpropyl)-9H-carbazole (Table 2.2, Entry 2).

Method A:

Yield: 118 mg (83%), white solid, mp: 110 – 112°C

The ¹H NMR spectrum obtained is in accordance with the literature.³²

¹H NMR (400 MHz, Chloroform-*d*) δ 8.10 (d, J = 7.7 Hz, 2H), 7.63 – 7.38 (m, 3H), 7.38 – 7.11 (m, 10H), 4.33 (t, J = 7.3 Hz, 2H), 2.72 (t, J = 7.7 Hz, 2H), 2.23 (quint, J = 7.5 Hz, 2H).

(3-Phenoxypropyl)benzene (Table 2.2, Entry 3).

Method B:

Yield: 36 mg (68%), yellow oil

The ¹H NMR spectrum obtained is in accordance with the literature.³²

¹H NMR (400 MHz, Chloroform-*d*) δ 7.37 – 7.12 (m, 7H), 6.95 – 6.85 (m, Hz, 3H), 3.97 (t, J = 6.1 Hz, 2H), 2.82 (t, J = 7.5 Hz, 2H), 2.13 (quint, J = 6.9 Hz, 2H).

5-Phenylpentylacetate (Table 2.2, Entry 4).

Method A:

Yield: 86 mg (83%), yellow oil

The ^1H NMR spectrum obtained is in accordance with the literature.³⁶

^1H NMR (400 MHz, Chloroform-*d*) δ 7.35 – 7.24 (m, 2H), 7.15 – 7.21 (m, 3H), 4.05 (t, $J = 6.7$ Hz, 2H), 2.62 (t, $J = 7.7$ Hz, 2H), 2.03 (s, 3H), 1.45 (quint, $J = 7.5$ Hz, 4H), 1.40 (quint, $J = 7.6$ Hz, 2H).

1-Methoxy-4-(2-phenethyl)benzene (Table 2.2, Entry 5).

Method A:

Yield: 104 mg (98%), white solid, mp: 58 – 60°C

The ^1H NMR spectrum obtained is in accordance with the literature.³⁷

^1H NMR (400 MHz, Chloroform-*d*) δ 7.30 – 7.26 (m, 2H), 7.22 – 7.15 (m, 3H), 7.11 – 7.06 (m, 2H), 6.85 – 6.78 (m, 2H), 3.79 (s, 3H), 2.92 – 2.82 (m, 4H).

1,2-Diphenylethane (Table 2.2, Entry 6).

Method A:

Yield: 52 mg (57%), colourless oil

The ^1H NMR spectrum obtained is in accordance with the literature.³⁸

^1H NMR (400 MHz, Chloroform-*d*) δ 7.35 – 7.29 (m, 4H), 7.27 – 7.19 (m, 6H), 2.95 (s, 4H).

1-(1-(3-Phenylpropyl)-1H-pyrrol-2-yl)ethanone (Table 2.2, Entry 7).

Method B:

Yield: 32 mg (57%), yellow oil

The ^1H NMR spectrum obtained is in accordance with the literature.³⁸ ^1H NMR (400 MHz, Chloroform-*d*) δ 7.33 – 7.28 (m, 2H), 7.24 – 7.16 (m, 3H), 6.99 (dd, J = 4.1, 1.7 Hz, 1H), 6.85 (dd, J = 2.4, 1.8 Hz, 1H), 6.15 (dd, J = 4.1, 2.5 Hz, 1H), 4.36 (t, J = 7.2 Hz, 2H), 2.69 – 2.61 (t, J = 7.8 Hz, 2H), 2.46 (s, 3H), 2.10 (quint, J = 7.5 Hz, 2H).**1,3-Diphenylbutane (Table 2.2, Entries 8).**

Method A:

Yield: r.t. (X=Br): 98 mg (93%); r.t. (X=I): 86 mg (88%); at -40°C (X=I): 100 mg (95%), colourless oil

The ^1H NMR spectrum obtained is in accordance with the literature.³⁹ ^1H NMR (400 MHz, Chloroform-*d*) δ 7.42 – 7.13 (m, 10H), 2.75 (hex, J = 7.1 Hz, 1H), 2.61 – 2.47 (m, 2H), 2.02 – 1.86 (m, 2H), 1.31 (d, J = 7.0 Hz, 3H).**1-Methoxy-4-(2-phenylpropyl)benzene (Table 2.2; Entry 9).**

Method A:

Yield: 102 mg (90%), colourless oil

The ^1H NMR spectrum obtained is in accordance with the literature.³⁹ ^1H NMR (400 MHz, Chloroform-*d*) δ 7.34 – 7.23 (m, 2H), 7.23 – 7.11 (m, 3H), 6.98 (d, J = 8.7 Hz, 2H), 6.77 (d, J = 8.7 Hz, 2H), 3.77 (s, 3H), 3.01 – 2.83 (m, 2H), 2.71 (dd, J = 13.3, 8.1 Hz, 1H), 1.23 (d, J = 6.8 Hz, 3H).

4-Phenyltetrahydro-2H-pyran (Table 2.2, Entry 10).

Method A:

Yield: 61 mg (75%), white solid, mp: 42 – 44°C

The ¹H NMR spectrum obtained is in accordance with the literature.⁴⁰

¹H NMR (400 MHz, Chloroform-*d*) δ 7.40 – 7.20 (m, 5H), 4.15 – 4.07 (m, 2H), 3.56 (td, *J* = 11.5, 2.7 Hz, 2H), 2.78 (tt, *J* = 11.5, 4.4 Hz, 1H), 1.94 – 1.75 (m, 4H).

2-(4-Fluorophenyl)-4-phenyltetrahydro-2H-pyran (Table 2.2, Entry 11).

Method A:

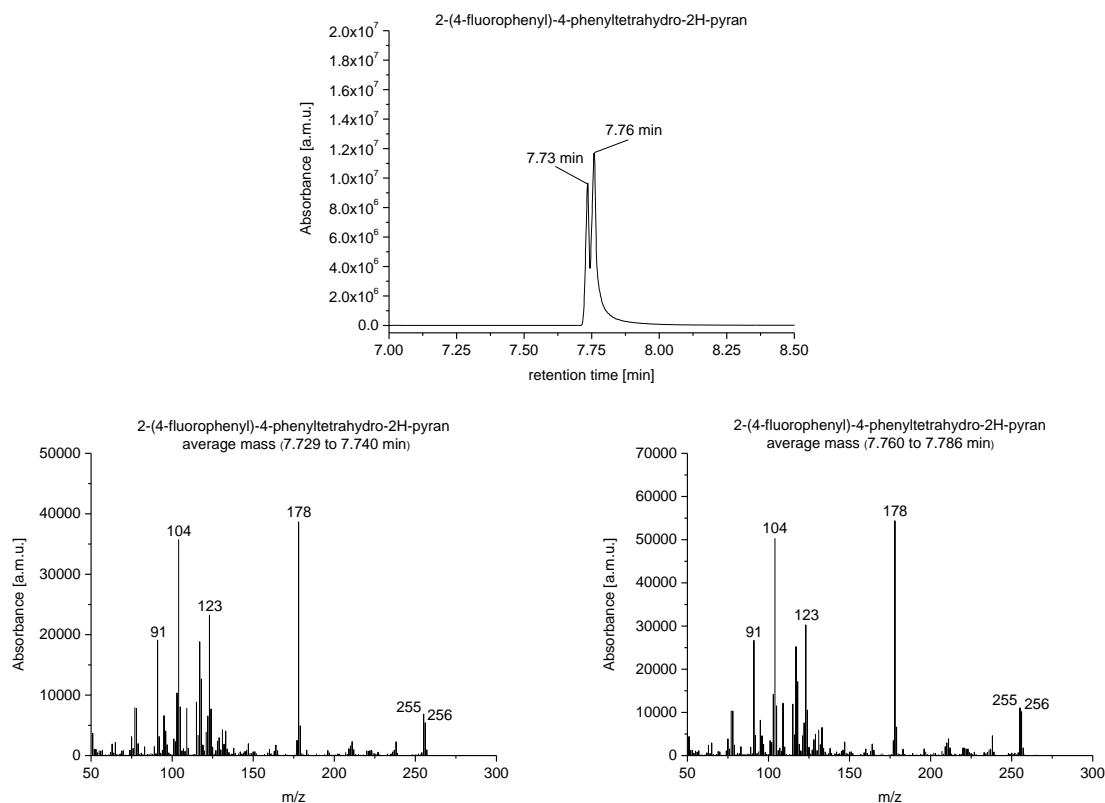
Yield: 118 mg (92%), yellow oil

The ¹H NMR spectrum obtained is in accordance with the literature.⁴¹

Mixture of stereoisomers:

¹H NMR (400 MHz, Chloroform-*d*) δ 7.42 – 7.31 (m, 14H), 7.27 – 7.14 (m, 11H), 7.11 – 6.95 (m, 7H), 4.91 (t, *J* = 5.0 Hz, 1H), 4.47 (dd, *J* = 11.2, 2.0 Hz, 2H), 4.34 – 4.25 (m, 2H), 3.89 – 3.71 (m, 5H), 3.11 – 3.02 (m, 1H), 2.96 (ddd, *J* = 16.0, 10.2, 3.9 Hz, 2H), 2.39 – 2.23 (m, 3H), 2.06 – 2.02 (m, 2H), 1.97 – 1.81 (m, 5H), 1.80 – 1.67 (m, 2H), 1.28 – 1.20 (m, 2H).

¹³C NMR (101 MHz, Chloroform-*d*) δ 128.59, 128.57, 128.09 (d, *J* = 8.0 Hz), 127.48 (d, *J* = 8.0 Hz), 127.15, 126.73, 126.45, 126.23, 115.30 (d, *J* = 21.2 Hz), 115.13 (d, *J* = 21.3 Hz), 79.29, 73.45, 68.71, 62.81, 42.07, 41.52, 35.93, 35.46, 33.26, 32.12.



Ethyl 3-phenylcyclohexanecarboxylate (Table 2.2, Entry 12).

Method A:

Yield: 82 mg (71%), colourless oil

Mixture of stereoisomers:

^1H NMR (400 MHz, Chloroform-*d*) δ 7.43 – 7.12 (m, 5H), 4.34 – 4.03 (m, 2H), 2.85 – 1.40 (m, 10H), 1.38 – 1.23 (m, 3H).

^{13}C NMR (101 MHz, Chloroform-*d*) δ 175.72, 175.12, 146.90, 146.65, 128.40, 128.33, 126.86, 126.80, 126.15, 125.94, 60.21, 60.19, 43.86, 43.67, 39.90, 39.75, 36.45, 34.86, 33.49, 33.26, 28.57, 27.20, 25.87, 23.02, 14.34, 14.24.

HRMS (APCI): m/z $[\text{M} + \text{H}]^+$ calcd for $\text{C}_{15}\text{H}_{21}\text{O}_2^+$: 233.1542; found: 233.1544

***tert*-Butyl 4-phenylpiperidine-1-carboxylate (Table 2.2, Entry 13).**

Method A:

Yield: 115 mg (88%), yellow oil

The ¹H NMR spectrum obtained is in accordance with the literature.³⁸

¹H NMR (400 MHz, Chloroform-*d*) δ 7.30 (m, 2H), 7.25 – 7.16 (m, 3H), 4.24 (dd, *J* = 9.6, 8.0 Hz, 2H), 2.80 (t, *J* = 12.1 Hz, 2H), 2.64 (tt, *J* = 12.1, 3.5 Hz, 1H), 1.82 (m, 2H), 1.64 (m, 2H), 1.48 (s, 9H).

Benzyl 3-phenylazetidine-1-carboxylate (Table 2.2, Entry 14).

Method A:

Yield: 87 mg (65%), yellow oil

¹H NMR (400 MHz, Chloroform-*d*) δ 7.45 – 7.26 (m, 10H), 5.15 (d, *J* = 13.9 Hz, 2H), 4.44 (t, *J* = 8.8 Hz, 2H), 4.10 (dd, *J* = 8.8, 6.1 Hz, 2H), 3.82 (ddt, *J* = 12.3, 8.8, 6.1 Hz, 1H).

¹³C NMR (101 MHz, Chloroform-*d*) δ 142.17, 137.01, 129.09, 128.79, 128.35, 128.30, 127.41, 127.03, 66.99, 34.24, 0.31.

HRMS (ESI): *m/z* [M + Na]⁺ calc. for C₁₇H₁₇NO₂Na⁺: 290.1157; found: 290.1170

Menthyl (6-phenylhexan)oate (Table 2.2, Entry 15).

Method B:

Yield: 66 mg (83%), colourless oil

¹H NMR (400 MHz, Chloroform-*d*) δ 7.43 – 7.05 (m, 5H), 4.67 (td, *J* = 10.9, 4.3 Hz, 1H), 2.72 – 2.50 (m, 2H), 2.28 (t, *J* = 7.5 Hz, 2H), 2.03 – 1.81 (m, 2H), 1.67 – 1.24 (m, 10H), 0.86 (ddd, *J* = 56.1, 27.3, 7.2 Hz, 12H)

¹³C NMR (101 MHz, Chloroform-*d*) δ 173.37, 142.55, 128.39, 128.28, 125.68, 73.93, 47.03, 40.96, 35.80, 34.67, 34.29, 31.39, 31.14, 28.79, 26.27, 25.01, 23.42, 22.06, 20.79, 16.31.

HRMS (APCI): *m/z* [M + Na]⁺ calc.. for C₂₂H₃₄O₂Na: 353.2457; found: 353.2447

3-Phenylcholest-5-ene (Table 2.2, Entry 16).

Method B:

Yield: 59 mg (53%), white solid, mp: 126 – 129°C

The ¹H NMR spectrum obtained is in accordance with the literature.⁴²

¹H NMR (400 MHz, Chloroform-*d*) δ 7.40 – 7.12 (m, 5H), 5.45 (s, 0.2H), 5.35 (d, *J* = 4.7 Hz, 0.8H), 2.52 – 2.52 (m, 2H), 2.06 – 1.94 (m, 3H), 1.87 – 1.70 (m, 4H), 1.61 – 1.34 (m, 12H), 1.17 – 1.00 (m, 14H), 0.94 – 0.90 (m, 3H), 0.87 (dd, *J* = 6.5, 1.7 Hz, 6H), 0.69 (d, *J* = 8.6 Hz, 3H).

HRMS (APCI): *m/z* [M + H]⁺ calc.. for C₃₃H₅₁: 447.3985; found:447.3988**3-Cholest-5-eneyl (6-phenylhexan)oate (Table 2.2, Entry 17).**

Method B:

Yield: 119 mg (85%), yellow oil

¹H NMR (400 MHz, Chloroform-*d*) δ 7.32 – 7.20 (m, 2H), 7.11 – 7.18 (m, 3H), 5.30 (m, 1H), 4.64 – 4.57 (dt, *J* = 15.5, 7.5 Hz, 1H), 2.60 (t, *J* = 7.6 Hz, 2H), 2.27 (dd, *J* = 15.1, 7.7 Hz, 4H), 2.02 – 1.95 (t, *J* = 15.7 Hz, 2H), 1.89 – 1.78 (m, 3H), 1.69 – 1.43 (m, 12H), 1.39 – 1.25 (m, 8H), 1.17 – 1.06 (m, 6H), 1.01 (s, 3H), 0.92 (d, *J* = 6.1 Hz, 3H), 0.89 – 0.82 (m, 6H), 0.66 (s, 4H).

¹³C NMR (101 MHz, Chloroform-*d*) 173.25, 142.60, 139.77, 128.48, 128.36, 125.75, 122.70, 73.81, 56.79, 56.24, 50.12, 42.42, 39.84, 39.64, 38.26, 37.11, 36.70, 36.30, 35.92, 35.85, 34.71, 32.02, 31.97, 31.22, 28.82, 28.36, 28.14, 27.91, 25.03, 24.41, 23.96, 22.96, 22.70, 21.15, 19.45, 18.84, 11.98.

HRMS (ESI): *m/z* [M + Na]⁺ calc. for C₃₉H₆₀O₂K⁺: 599.4230; found: 599.4226

2.7 References

- (1) Nakamura, M.; Matsuo, K.; Ito, S.; Nakamura, E. *J. Am. Chem. Soc.* **2004**, *126*, 3686.
- (2) Nagano, T.; Hayashi, T. *Org. Lett.* **2004**, *6*, 1297.
- (3) Bedford, R. B.; Bruce, D. W.; Frost, R. M.; Hird, M. *Chem. Comm.* **2005**, 4161.
- (4) Bedford, R. B.; Betham, M.; Bruce, D. W.; Danopoulos, A. A.; Frost, R. M.; Hird, M. *J. Org. Chem.* **2005**, *71*, 1104.
- (5) Bedford, R. B.; Bruce, D. W.; Frost, R. M.; Goodby, J. W.; Hird, M. *Chem. Comm.* **2004**, 2822.
- (6) Bedford, R. B.; Betham, M.; Bruce, D. W.; Davis, S. A.; Frost, R. M.; Hird, M. *Chem. Comm.* **2006**, 1398.
- (7) Martin, R.; Fürstner, A. *Angew. Chem. Int. Ed.* **2004**, *43*, 3955.
- (8) Saito, B.; Fu, G. C. *J. Am. Chem. Soc.* **2008**, *130*, 6694.
- (9) Binder, J. T.; Cordier, C. J.; Fu, G. C. *J. Am. Chem. Soc.* **2012**, *134*, 17003.
- (10) Arp, F. O.; Fu, G. C. *J. Am. Chem. Soc.* **2005**, *127*, 10482.
- (11) Walsh, P. J.; Kozlowski, M. C. *Fundamentals of asymmetric catalysis*; University Science Books: Sausalito, Calif., 2009.
- (12) Rousseau, G.; Breit, B. *Angew. Chem. Int. Ed.* **2011**, *50*, 2450.
- (13) Hoveyda, A. H.; Evans, D. A.; Fu, G. C. *Chem. Rev.* **1993**, *93*, 1307.
- (14) Bedford, R. B.; Brenner, P. B.; Carter, E.; Carvell, T. W.; Cogswell, P. M.; Gallagher, T.; Harvey, J. N.; Murphy, D. M.; Neeve, E. C.; Nunn, J.; Pye, D. R. *Chem. Eur. J.* **2014**, *20*, 7935.
- (15) Bedford, R. B.; Brenner, P. B.; Carter, E.; Clifton, J.; Cogswell, P. M.; Gower, N. J.; Haddow, M. F.; Harvey, J. N.; Kehl, J. A.; Murphy, D. M.; Neeve, E. C.; Neidig, M. L.; Nunn, J.; Snyder, B. E. R.; Taylor, J. *Organometallics* **2014**, *33*, 5767.
- (16) Chard, E. F.; Dawe, L. N.; Kozak, C. M. *J. Organomet. Chem.* **2013**, *737*, 32.
- (17) Kawamura, S.; Nakamura, M. *Chem. Lett.* **2013**, *42*, 183.
- (18) Hasan, K.; Dawe, L. N.; Kozak, C. M. *Eur. J. Inorg. Chem.* **2011**, *2011*, 4610.

- (19) Bedford, R. B.; Huwe, M.; Wilkinson, M. C. *Chem. Comm.* **2009**, 600.
- (20) Fürstner, A.; Martin, R.; Krause, H.; Seidel, G.; Goddard, R.; Lehmann, C. W. *J. Am. Chem. Soc.* **2008**, *130*, 8773.
- (21) Fischer, H. *Chem. Rev.* **2001**, *101*, 3581.
- (22) Studer, A. *Chem. Eur. J.* **2001**, *7*, 1159.
- (23) Inagaki, T.; Phong, L. T.; Furuta, A.; Ito, J.-i.; Nishiyama, H. *Chem. Eur. J.* **2010**, *16*, 3090.
- (24) Inagaki, T.; Ito, A.; Ito, J.-i.; Nishiyama, H. *Angew. Chem.* **2010**, *122*, 9574.
- (25) Niwa, T.; Nakada, M. *J. Am. Chem. Soc.* **2012**, *134*, 13538.
- (26) Lu, S.-F.; Du, D.-M.; Zhang, S.-W.; Xu, J. *Tetrahedron: Asymm.* **2004**, *15*, 3433.
- (27) Paul, A.; Ladame, S. *Org. Lett.* **2009**, *11*, 4894.
- (28) McKennon, M. J.; Meyers, A. I.; Drauz, K.; Schwarm, M. *J. Org. Chem.* **1993**, *58*, 3568.
- (29) See the Experimental for further information.
- (30) Inoue, M.; Suzuki, T.; Nakada, M. *J. Am. Chem. Soc.* **2003**, *125*, 1140.
- (31) Hess, B. A.; Boekelheide, V. *J. Am. Chem. Soc.* **1969**, *91*, 1672.
- (32) Di Franco, T.; Boutin, N.; Hu, X. L. *Synthesis-Stuttgart* **2013**, *45*, 2949.
- (33) Cheung, C. W.; Ren, P.; Hu, X. *Org. Lett.* **2014**, *16*, 2566.
- (34) Love, B. E.; Jones, E. G. *J. Org. Chem.* **1999**, *64*, 3755.
- (35) Matsubara, K.; Ishibashi, T.; Koga, Y. *Org. Lett.* **2009**, *11*, 1765.
- (36) Lee, J.-Y.; Fu, G. C. *J. Am. Chem. Soc.* **2003**, *125*, 5616.
- (37) Dreher, S. D.; Lim, S.-E.; Sandrock, D. L.; Molander, G. A. *J. Org. Chem.* **2009**, *74*, 3626.
- (38) Vechorkin, O.; Proust, V.; Hu, X. L. *J. Am. Chem. Soc.* **2009**, *131*, 9756.
- (39) Denmark, S. E.; Cresswell, A. J. *J. Org. Chem.* **2013**, *78*, 12593.
- (40) Aikawa, H.; Tago, S.; Umetsu, K.; Haginiwa, N.; Asao, N. *Tetrahedron Lett.* **2009**, *65*, 1774.
- (41) Reddy, U. C.; Bondalapati, S.; Saikia, A. K. *J. Org. Chem.* **2009**, *74*, 2605.
- (42) Li, L. J.; Lu, B.; Li, T. S.; Li, J. T. *Synth. Comm.* **1998**, *28*, 1439.

Chapter 3

Iron Pincer Complexes as Catalysts and Intermediates in Alkyl-Aryl Kumada Coupling Reactions

Reprinted with permission from “Bauer, G., Wodrich, M. D., Scopelliti, R., Hu, X. L. (2015). Iron Pincer Complexes as Catalysts and Intermediates in Alkyl–Aryl Kumada Coupling Reactions. *Organometallics*, 34(1), 289-298”. Copyright © 2015 American Chemical Society.

3.1 Introduction

Iron-catalysed cross coupling of alkyl halides with aryl Grignard reagents is one of the most attractive methods for alkyl-aryl coupling for a number of reasons: (1) Iron is inexpensive, abundant and non-toxic. (2) The iron-catalysed alkyl-aryl Kumada coupling generally has a high yield, a short reaction time (within several hours) and a high functional group tolerance. (3) The use of alkyl electrophiles as the alkylating reagent allows the coupling of functionalised alkyl groups.¹⁻⁵ Whereas significant progress has been made in the development of new catalysts, reaction conditions and scope,⁶⁻¹⁴ the mechanism of this and related iron-catalysed coupling reactions of alkyl halides is now only being unveiled. Fürstner and co-workers showed that Fe-"ate" complexes in which the formal oxidation states of Fe range from -2 to +2 might be catalytically active;^{8,15} treatment of FeCl₃ with a large excess amount of aryl Grignard reagents could lead to Fe(0)-"ate" species.⁸ They also showed that a formal Fe(-2) complex, [(Li(tmeda))₂Fe(C₂H₄)₄] was a highly active and selective catalyst for alkyl-aryl Kumada coupling.⁶ The low-valent iron-"ate" species would be difficult to generate in most *in situ* catalyst systems where reduction of the initial Fe(III) salt to Fe(0) or below by a Grignard reagent without β -hydrogen is difficult.

Nagashima and co-workers observed the formation of (tmeda)Fe(mesityl)₂ and (tmeda)Fe(mesityl)Br (tmeda = tetramethylethylenediamine) from the coupling between 1-bromooctane with mesitylMgBr under conditions similar to the FeCl₃-tmeda protocol originally developed by Nakamura and co-workers.⁷ They proposed a catalytic cycle where a tmeda-chelated Fe(II) was the active species.¹⁶ However, Bedford and co-workers showed that the actual active species in that reaction was the homoleptic "ate" complex [Fe(mesityl)₃]⁻. Tmeda seemed to trap intermediates in the off-cycle of the catalysis and suppressed side reactions.¹⁷ They also isolated defined Fe(I) phosphine complexes that were competent pre-catalysts in related Fe-catalysed alkyl-aryl Negishi coupling,^{18,19} while Cárdenas and co-workers obtained a EPR-based evidence for the involvement of Fe(I) carbene species in alkyl-alkyl Kumada coupling.²⁰

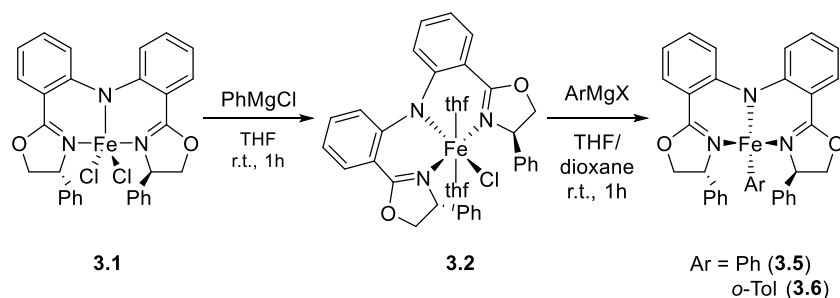
A challenge in the mechanistic study of iron-catalysed alkyl-aryl Kumada coupling is the coordinative lability of ligands on Fe, especially when the latter undergoes oxidation and spin

state changes. It is reported that tmeda dissociates from the Fe(II) centre during alkyl-aryl Kumada coupling,¹⁷ and even a bidentate phosphine ligand can fall off from an Fe ion during alkyl-aryl Negishi coupling.¹⁹ Therefore, extrapolation of active iron species from complexes isolated from the catalysis mixture or defined pre-catalysts might be error-prone without considering ligand dissociation. A strong chelating ligand can alleviate this complication. Herein we employ a bisoxazolinyphenylamido (bopa) pincer ligand to support the catalytically active Fe centre. The rigid tridentate chelate allows for the isolation and characterisation of several intermediate species whose catalytic roles are then probed. Subsequent experiments using radical-probe substrates, kinetic measurements and DFT computations then establish a catalytic cycle in which an Fe(II)-aryl-“ate” complex activates alkyl halide *via* a bimetallic oxidative addition pathway.

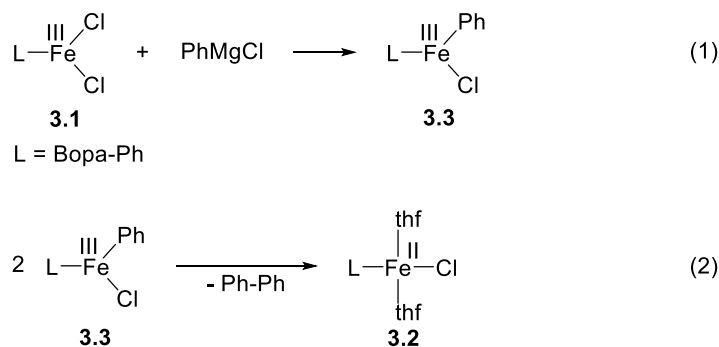
3.2 Results

3.2.1 Synthesis, Characterisation and Reactivity of Catalysts and Intermediates

The Fe(III) complex [Fe(bopa-Ph)Cl₂] (**3.1**, Figure 3.1) was previously applied for iron-catalysed hydrosilylation reactions.^{21,22} We showed in Chapter 2 that the pincer bopa ligand is suitable for the use in iron-catalysed cross coupling reactions. The bis(aryl)amido pincer backbone gives both structural rigidity and chemical stability; the two oxazoliny donors can accommodate both Fe(III) and Fe(II) and perhaps, for a short time, Fe(I) due to possible π -back bonding.

Figure 3.1: Synthesis of complexes **3.2**, **3.5** and **3.6**.

Complex **3.1** served as the entry point of our mechanistic study. The transformation of **3.1** by an aryl Grignard reagent was then examined. Addition of one equivalent of PhMgCl to a THF solution of **3.1** at room temperature produced [Fe(bopa-Ph)Cl(THF)₂] (**3.2**) (Figure 3.1). Concomitant to the reduction of **3.1** to **3.2**, 0.5 equivalents of biphenyl were formed, indicating that the phenyl anion in PhMgCl was the electron donor in this process. A possible pathway for the reduction is that the PhMgCl replaces one chloride of the [Fe(bopa-Ph)Cl₂] (**3.1**) with a phenyl substituent to form [Fe(bopa-Ph)PhCl] (**3.3**) (Figure 3.2, Equation 1). This species further reductively eliminates the phenyl group by forming biphenyl in a bimolecular process (Figure 3.2, Equation 2). This hypothesis is in accordance with the previously observed formation of biphenyl in the coupling of secondary benzylic bromines (Chapter 2.5.1).

Figure 3.2: Possible reduction pathway from [Fe(bopa-Ph)Cl₂] (**3.1**) to [Fe(bopa-Ph)Cl(THF)₂] (**3.2**).

Complex **3.2** could be independently synthesised by first lithiating the pincer ligand followed by a metathesis reaction with FeCl₂(THF)_{1.5}. The crystal structure of **3.2** (Figure 3.3) shows an Fe(II) centre in an octahedral coordination geometry, with the pincer bopa ligand adapting the expected meridional configuration. The complex has a solution magnetic moment of 5.11 μ_B,²³ consistent with an Fe(II) complex in a high-spin state.

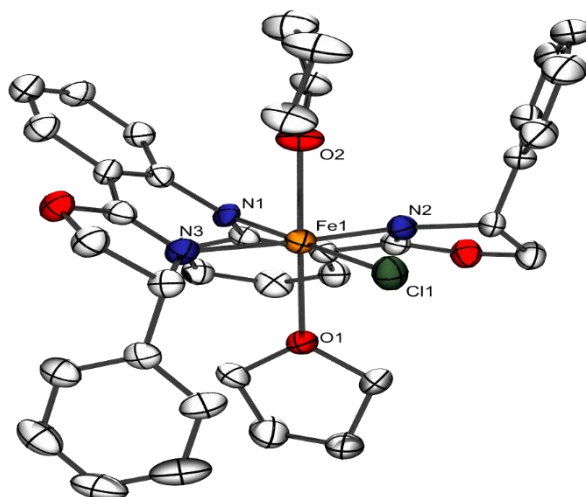


Figure 3.3: The molecular structure of complex **3.2**. Hydrogen atoms are omitted for clarity. The thermal ellipsoids are displayed at a 50% probability. Selected bond lengths (Å) and angles (deg): Fe(1)-N(1): 2.114(2); Fe(1)-N(2): 2.1256(16); Fe(1)-O(2): 2.2906(15); Fe(1)-Cl(1): 2.4152(9); N(1)-Fe(1)-N(2): 85.41(5); N(2)-Fe(1)-N(2): 170.81(9); N(1)-Fe(1)-O(2): 91.03(5); N(2)-Fe(1)-O(2): 86.32(7); N(1)-Fe(1)-Cl(1): 180.00(6); N(2)-Fe(1)-Cl(1): 94.59(5).

When complex **3.2** is dissolved in a less polar solvent, like Et₂O or toluene, it loses both THF substituents to give [Fe(bopa-Ph)Cl] (**3.4**). The crystal structure (Figure 3.4) shows the metal centre in a tetrahedral configuration. **3.4** has an effective magnetic moment of 5.06 μ_B ,²³ consistent with a high-spin Fe(II) complex. This process is fully reversible. Dissolving complex **3.4** in THF gives again complex **3.2**.

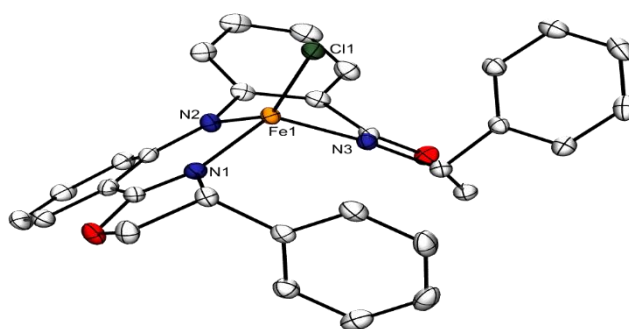


Figure 3.4: The molecular structure of complex **3.4**. Hydrogen atoms are omitted for clarity. The thermal ellipsoids are displayed at a 50% probability. Selected bond lengths (Å) and angles (deg): Fe(1)-N(1) 2.0125(15); Fe(1)-N(2) 2.0167(16); Fe(1)-N(3) 2.0748(16); Fe(1)-Cl(1) 2.2553(6); N(1)-Fe(1)-N(2) 89.88(6); N(1)-Fe(1)-N(3) 124.35(6); N(2)-Fe(1)-N(3) 89.68(6); N(1)-Fe(1)-Cl(1) 106.89(5); N(2)-Fe(1)-Cl(1) 143.62(5); N(3)-Fe(1)-Cl(1) 105.62(5)

Complex **3.2** is unreactive towards (3-iodobutyl)benzene, suggesting that **3.2** needs to be further transformed during catalysis. Indeed, further addition of PhMgCl to a solution of **3.2** shows an immediate reaction. This reaction produced no more biphenyl, suggesting that the Fe-centre is not further reduced. The reactions of **3.2** with ArMgCl (Ar = Ph, o-Tol) gave [Fe(bopa-Ph)-Ar] (**3.5**, Ar = Ph; **3.6**, Ar = o-Tol). Crystals of **3.6** were obtained in a THF/dioxane mixture and its structure was determined to reveal the 4-coordinate nature of the complex in the solid state (Figure 3.5). The Fe ion is in a tetrahedral geometry. While the crystal structure of **3.5** could not be obtained, its composition was confirmed by elemental analysis. Complexes **3.5** and **3.6** have a solution magnetic moment of 5.00 and 4.76 μ_B , respectively,²³ consistent with a high-spin Fe(II) centre in both complexes.

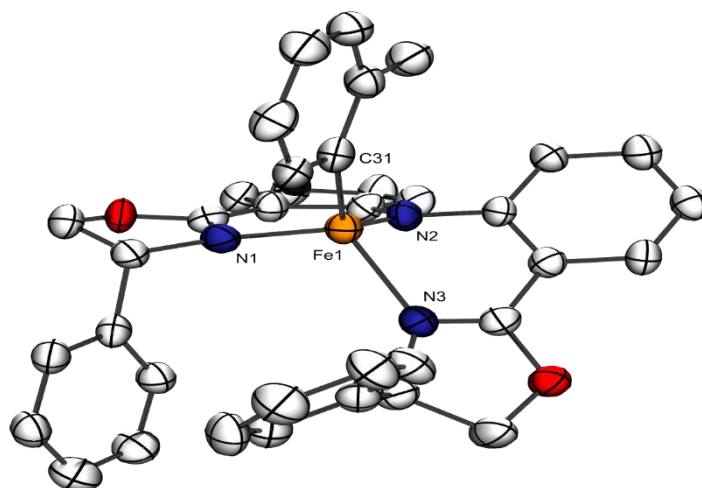


Figure 3.5: The molecular structure of complex **3.6**. Hydrogen atoms and a co-crystallised 1,4-dioxane molecule are omitted for clarity. The thermal ellipsoids are displayed at a 50% probability. Selected bond lengths (\AA) and angles (deg): Fe(1)-N(2): 2.032(4); Fe(1)-N(1): 2.033(4); Fe(1)-C(31): 2.053(5); Fe(1)-N(3): 2.083(4); N(2)-Fe(1)-N(1): 90.25(15); N(2)-Fe(1)-C(31): 127.37(18); N(1)-Fe(1)-C(31): 110.88(16); N(2)-Fe(1)-N(3): 87.65(15); N(1)-Fe(1)-N(3): 114.31(15); C(31)-Fe(1)-N(3): 121.52(18).

Complex **3.5** shows a similar behaviour as complex **3.2**. Measuring a solution of **3.5** in THF- d_8 by NMR shows the formation of a new set of signals, which are perfectly congruent with the NMR signals of complex **3.2** (Figure 3.6). These peaks can be explained by coordinating two solvent molecules to complex **3.5** forming the octahedral analogue, [Fe(bopa-Ph)Ph(THF)₂] (**3.7**). Coincidentally the chlorine and phenyl substituents have a similar influence on the magnetic susceptibility of **3.5** and **3.2** (5.00 and 5.11 μ_B). Therefore the shifts of the NMR signals are in the same range. The shift of signals obtained for complex **3.5**

in toluene- d_8 do not overlap to the signals obtained in THF- d_8 . This is due to the different solvents used. In contrast to reaction of complex **3.2** to **3.3** in THF, which is converted quantitatively, complex **3.5** forms an equilibrium with **3.7** in THF, which can be explained by the presence of both species in the NMR spectrum (Figure 3.6, spectrum 2).

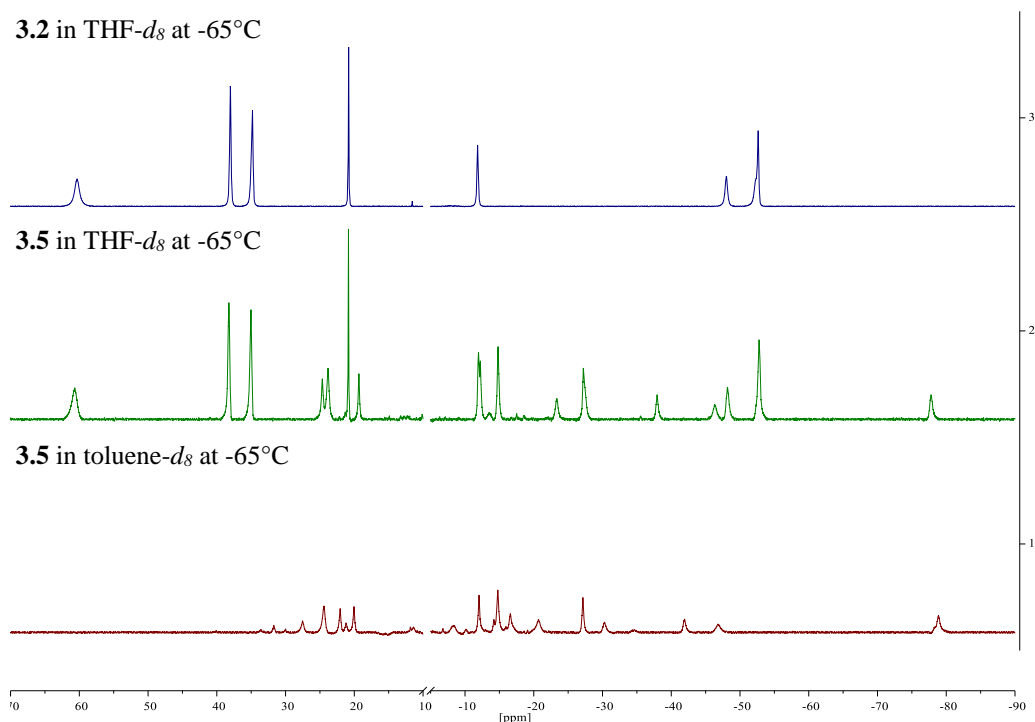


Figure 3.6: Comparison of **3.2** in THF- d_8 (spectrum 1), **3.5** in THF- d_8 (spectrum 2) and **3.5** in toluene- d_8 (spectrum 3); confirmation of the formation of the new species **3.7**. All spectra were measured at -65°C .

In the presence of one equivalent PhMgCl, **3.5** decomposed with a half-life of about 10 minutes at room temperature. The colour of the solution changed from deep red to a turbid brown and NMR spectrum of the solution suggested the formation of a Mg-bopa-Ph adduct; biphenyl was not observed.²³ However, this decomposition is too slow to be catalytically relevant, except at the end of the catalysis where the iron complex was demetallated to form a presumable Mg-bopa species (Figure 3.7).

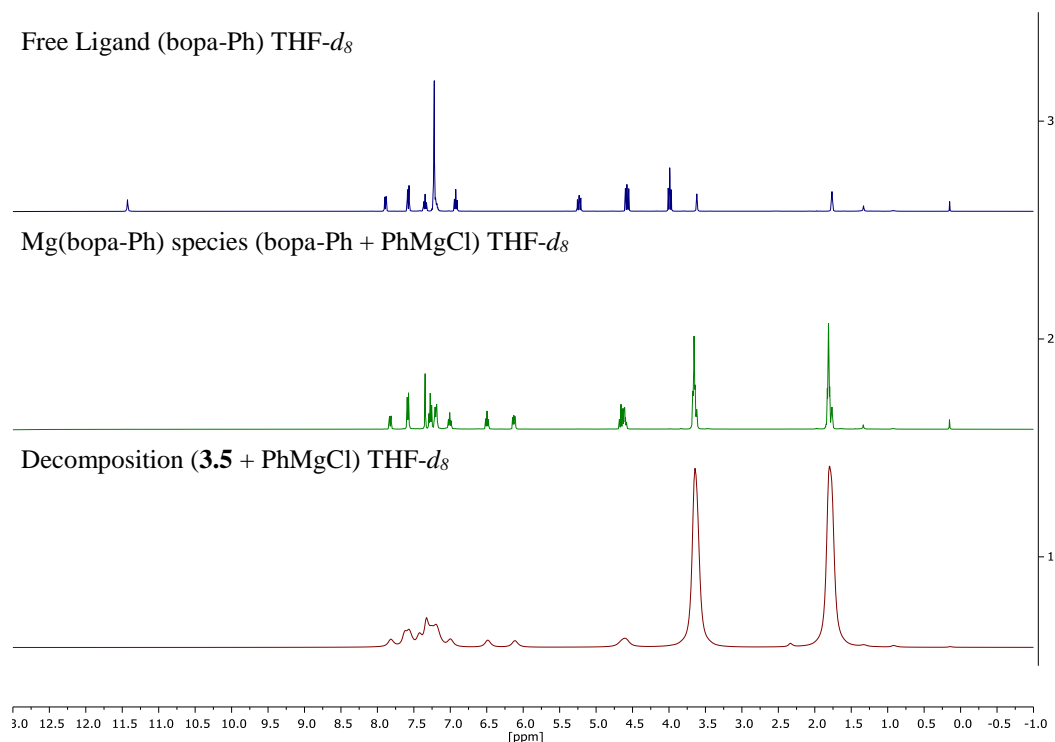
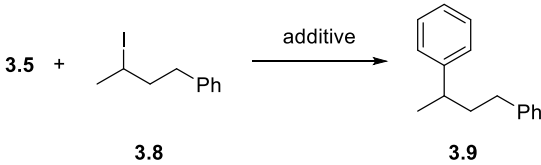


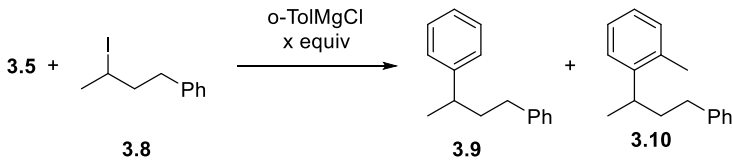
Figure 3.7: Comparison of the spectra of the free bopa-Ph, Mg(bopa-Ph) and the mixture of **3.5** with one equivalent PhMgCl.

To analyse the reactivity and the catalytic relevance of complex **3.5**, this complex was reacted with 20 equivalents (3-iodobutyl)benzene (**3.8**) at -40°C in a THF solution to the C-C coupled product 1,3-diphenylbutane (**3.9**) (Table 3.1). However, the reaction was slow compared to the catalysis, as forty minutes (Entry 1, Table 3.1) were needed for 50% conversion ($t_{1/2}$), whereas the catalysis generally completed within several minutes. The difference in reaction rates suggests that **3.5** is not the active species to activate alkyl halides in the catalytic reaction. In the presence of PhMgCl and PhLi, the reaction of **3.5** with **3.8** was greatly accelerated. The $t_{1/2}$ was less than 15 sec (Entries 2 and 3, Table 3.1), which was comparable to the rate of the catalytic coupling reaction. This result suggests that **3.5** reacted with PhMgCl to form either an associated species, $[\text{Fe}(\text{bopa-Ph})\text{Ph}](\text{PhMgCl})$, or an “ate”-complex, $[\text{Fe}(\text{bopa-Ph})\text{Ph}_2]^-$, as the catalytic active species.

Table 3.1: Influence of Additive on the Reaction of Complex **3.5** with **3.8**.


Entry	Additive	$t_{1/2}$
1	none	40 min
2	PhMgCl	< 15 sec
3	PhLi	< 15 sec

To probe whether an associated species or an “ate”-complex is involved, two cross-over experiments were performed. First, the reaction of **3.5** with **3.8** in the presence of *o*-TolMgCl was examined in THF at room temperature (Table 3.2). Both 1,3-diphenylbutane (**3.9**) and 3-(2-methylphenyl)-1-phenylbutane (**3.10**) were produced. When the ratio of **3.5** to *o*-TolMgCl was increased, the ratio of **3.9** to **3.10** also increased in a similar manner (Table 3.2). Second, the reactions of complex **3.6** with **3.8** in the presence of PhMgCl were conducted.²³ The reactions yielded coupling products containing both Ph and *o*-Tol groups. These results are more consistent with an active species being the “ate” complex, $[\text{Fe}(\text{bopa-Ph})\text{Ar}_2]^-$ (**3.11**), where the two aryl groups behave similarly in catalysis.

Table 3.2: Influence of *o*-TolMgCl on the Reaction of Complex **3.5** with **3.8**.


Entry	Equiv. <i>o</i> -TolMgCl	Ratio 3.5 / <i>o</i> -TolMgCl	Yield (%) 3.9 / 3.10 (conversion of 3.8)	Ratio 3.9 / 3.10
1	1.0	1.0	37 / 45 (92)	0.8
2	0.8	1.3	32 / 33 (73)	1.0
3	0.6	1.7	33 / 30 (71)	1.1
4	0.4	2.5	33 / 19 (60)	1.7

3.2.2 Mechanism of the Cross coupling Reaction

After the transmetallation step from **3.2** to **3.5** and the activation step from **3.5** to **3.11** were examined, the oxidative addition of alkyl halide was probed. The results of the radical clock experiments indicate that the oxidative addition produces alkyl radicals (Figure 3.8). For example, the coupling of enantiomerically enriched 3-bromo-1-phenylbutane (**3.12**) led to the racemic product (**3.9**) while coupling of (bromomethyl)cyclopropane (**3.13**) gave almost exclusively ring-opened product (**3.14-L**).

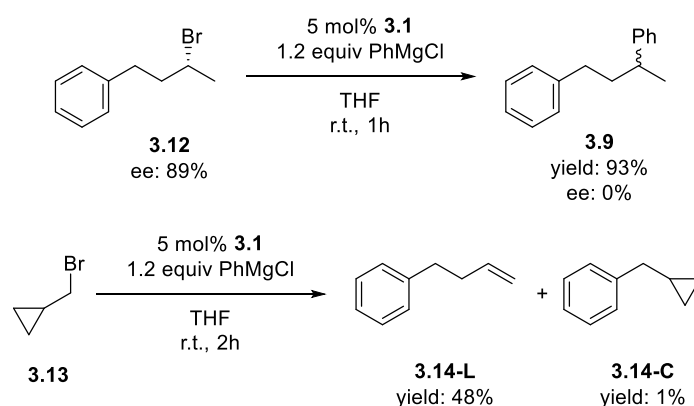


Figure 3.8: Evidence for a radical pathway in the activation of alkyl halide.

We propose that the first step of oxidative addition is a single electron transfer between an iron(II) bis(aryl)-ate species, represented here by **3.11** and an alkyl halide to give an Fe(III) halide complex (**3.3**) and an alkyl radical (Figure 3.9). The alkyl radical then may engage in one of the three possible pathways to give the coupling product: cage-rebound, escape-rebound, or bimetallic oxidative addition.²⁴ In the cage-rebound pathway (Pathway A, Figure 3.9), the alkyl radical stays in the solvent cage and recombines with **3.3** to give a [Fe(IV)(Ph)(Alkyl)(X)] (**3.15**, X = halide), which, upon reductive elimination, gives the coupling product and regenerates complex **3.2**, or its analogue (**3.2-X**). In the escape-rebound pathway (Pathway B, Figure 3.9), the alkyl radical first leaves the solvent cage and then re-enters it to combine with **3.3** to give complex **3.15**. Reductive elimination from **3.15** then yields the coupling product. In the bimetallic oxidative addition pathway (Pathway C, Figure 3.9), the alkyl radical leaves the solvent cage and combines with another molecule of Fe(II) phenyl complex **3.5** to form a [Fe(III)(Ph)(Alkyl)] complex (**3.16**). Reductive elimination from **3.16** gives the coupling product and an Fe(I) complex (**3.17**), which reacts with the Fe(III) complex **3.3** to give Fe(II)

complexes **3.2** and **3.5**. In our considerations we neglect the possibility that C-C coupling occurs *via* attack of free radical on an Fe-aryl species; Norbby and co-workers reported a competitive Hammett study that ruled out radicals in the coupling step.²⁵

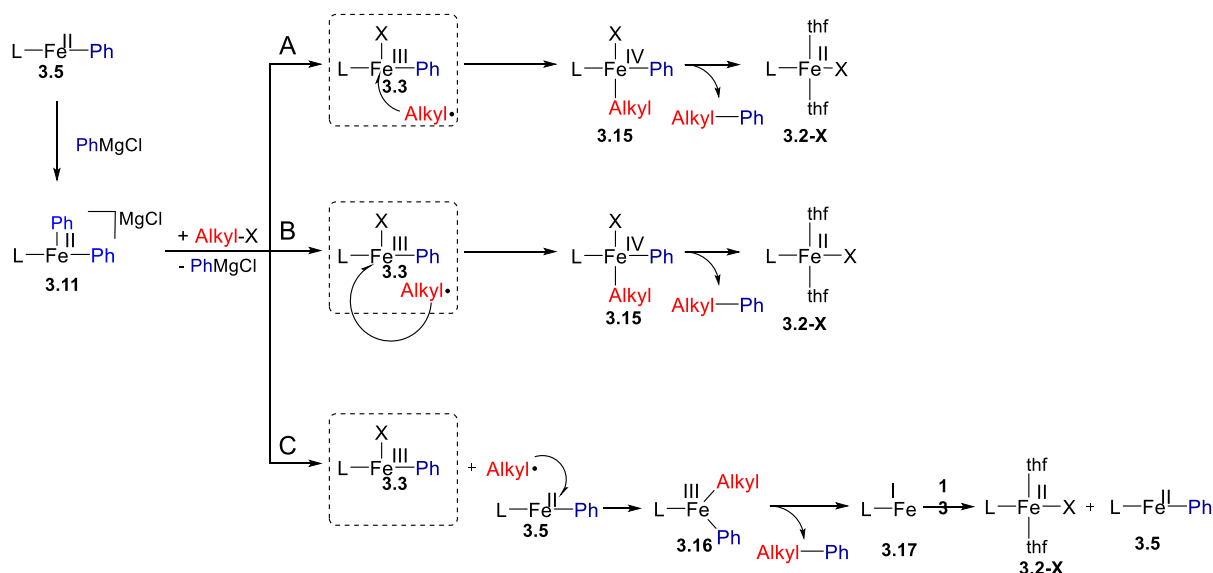


Figure 3.9: Three possible pathways for the oxidative addition of alkyl halide and the consequent reductive elimination.

The reaction outcomes of the coupling of radical-probe substrates can be used to distinguish the cage-rebound pathway from the escape-rebound and bimetallic oxidative addition pathways.^{24,26-29} In the current case, the coupling of 1-bromo-5-hexene (**3.18**) with PhMgCl in the presence of **3.1** was employed for this purpose (Figure 3.10). Activation of **3.18** first gives the alkyl radical (**3.19**) that can combine with an Fe-Ph species to give the linear coupling product **3.20**. Radical **3.19** can also undergo an intramolecular ring-closing rearrangement ($k_2 \approx 10^5 \text{ s}^{-1}$) to give a cyclised radical **3.19'**.³⁰ Combination of **3.19'** with an Fe-Ph intermediate then gives the cyclised coupling product **3.21**. The ratio of **3.20** and **3.21** is a function of r_1 and r_2 . For all scenarios $r_2 = k_2[\mathbf{3.19}]$. However, r_1 depends upon the reaction pathway. In the cage-rebound pathway, the recombination is considered an intramolecular reaction and is 0th order on the iron catalyst. Hence, $r_1 = k_1[\mathbf{3.19}]$ and r_1/r_2 is independent of the concentration of the iron catalyst. It follows that the ratio of **3.20/3.21** is independent of catalyst loading. On the other hand, in the bimetallic oxidative addition and escape-rebound pathways, the combination of an alkyl radical with an iron ion is an intermolecular reaction and is 1st order on the catalyst. Therefore, $r_1 = k_1[\text{cat}][\mathbf{3.19}]$ and the ratio of **3.20/3.21** is dependent on catalyst loading.

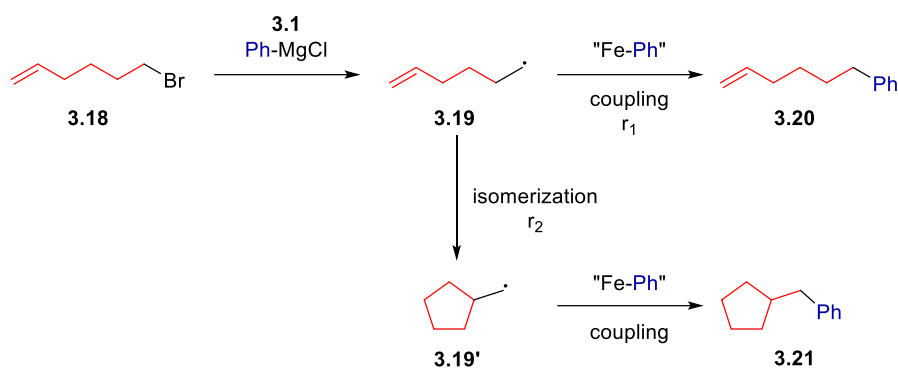


Figure 3.10: Coupling of a radical-clock substrate to differentiate the pathways for oxidative addition and C-C bond formation.

Figure 3.11 shows that the ratio of **3.20/3.21** is linearly dependent on the loading of catalyst (**3.1**) in the coupling of **3.18** with PhMgCl. This result eliminates the cage-rebound pathway. It is, however, consistent with either an escape-rebound or a bimetallic oxidative addition mechanism.

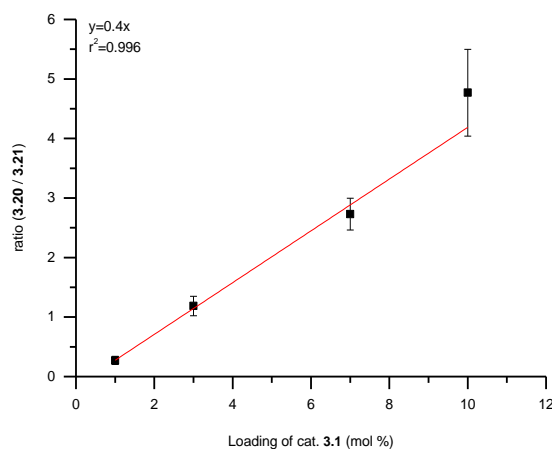


Figure 3.11: Ratio of **3.20/3.21** in the coupling of **3.18** with PhMgCl as a function of catalyst loading. The results are averaged over 2 independent runs.

To probe the feasibility of the bimetallic oxidative addition, the reaction of **3.5** with an *in situ* formed alkyl radical was examined (Figure 3.12). If the mechanism is operating, the combination of **3.5** with an alkyl radical will lead to an alkyl-aryl coupling product as predicted by Path C in Figure 3.9. In the experiment a phenylpropyl radical was generated by the photolysis of *tert*-butyl 4-phenylbutaneperoxoate (**3.22**).³¹ In the presence of one equivalent of **3.5**, 1,3-diphenylpropane was formed in a 27% yield (relative to **3.5**). The formation of the alkyl-aryl coupled product in this process, indicates that the bimetallic oxidative addition pathway

proposed in Figure 3.9 is probable, although it is not a proof. As the Fe(III) halide complex **3.3** cannot be isolated due to its tendency to reductively eliminate biphenyl, an analogous reactivity test, to probe for the escape rebound mechanism, cannot be conducted.

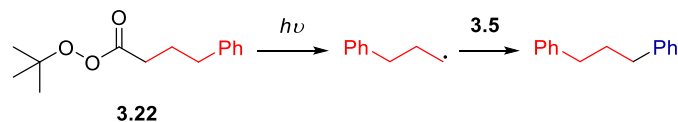


Figure 3.12: Reaction of **3.5** with an *in situ* generated alkyl radical.

To elucidate additional mechanistic details we employed density functional theory computations at the PBE0^{32,33}-dDsC³⁴⁻³⁷/TZ2P//M06^{38,39}/def2-SVP level to determine the reaction free energy profiles in implicit THF solvent (using the COSMO-RS⁴⁰ solvation model) of the bimetallic oxidative addition and escape-rebound pathways.²³ Owing to the extremely flat nature of the full catalyst potential energy surface (PES) our computations employed a model of the Fe catalyst in which some methyl groups replaced some phenyl groups as chiral residues. In the model, the aryl nucleophile is represented using a tolyl moiety (**3.6**) while the isopropyl radical (*i*Pr) represents the alkyl group.

Figure 3.13 illustrates the bimetallic oxidative addition pathway. Beginning from the reactant complex (**3.6** + *i*Pr), the isopropyl radical first associates with the Fe(II) centre by overcoming a small transition state barrier, TS_{3.6,3.16} (+6.3 kcal/mol), thereby forming a Fe(III) species characterised by a high-spin sextet, **3.16**_{Sextet}, in which both the aryl and alkyl groups are bound to the iron centre. Initial computations on the sextet PES revealed the reductive elimination step leading to final product formation to be energetically inaccessible (e.g., > 60 kcal/mol at the M06/def2-SVP level). As a result, we examined the possibility that the final product forming steps occur on the PES of the intermediate spin quartet state rather than sextet PES, as the energies of **3.16**_{Sextet} and **3.16**_{Quartet} lie within 4 kcal/mol (+6.6 kcal/mol at the M06/def2-SVP level). Indeed, a minimum energy crossing point (MECP) between the high (sextet) and intermediate (quartet) spin states was located ~11 kcal/mol above **3.16**_{Sextet} and ~4 kcal/mol above **3.16**_{Quartet} (Figure 3.14). Proceeding along the reaction coordinate, **3.16**_{Quartet} adopts a more stable conformer, **3.16'**_{Quartet}, in which the carbon atoms of the aryl and alkyl groups that ultimately form the new C-C bond are in closer proximity (3.060 Å vs 2.707 Å). From **3.16'**_{Quartet} reductive elimination forms the final product (**3.17**). The highest point on the

bimetallic oxidative addition PES corresponds to the reductive elimination TS located 10.8 kcal/mol above the reactant complex.

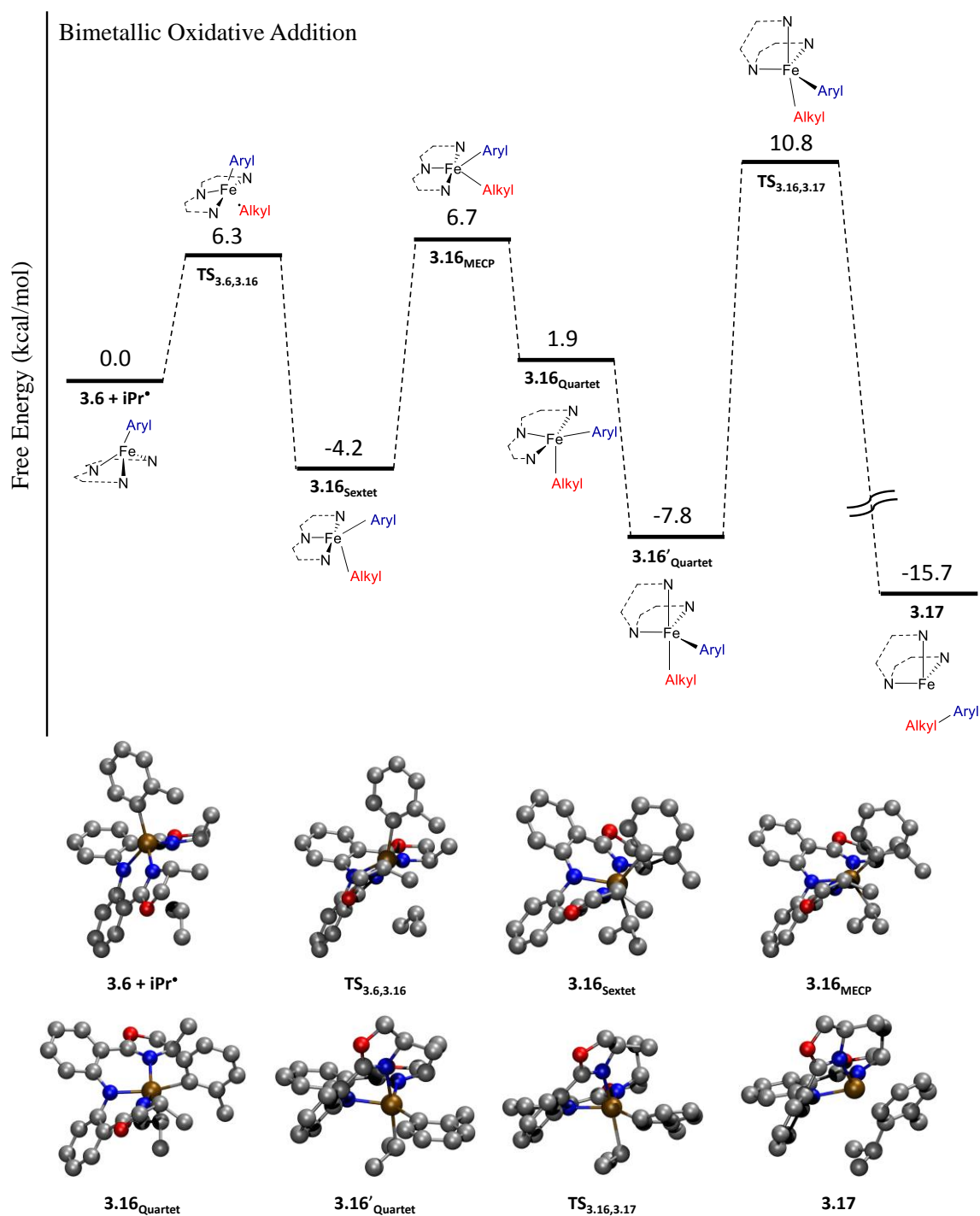


Figure 3.13: Reaction free energy profile and relevant structures for the bimetallic oxidative addition pathway computed at the unrestricted PBE0-dDsC/TZ2P//M06/def2-SVP level (including THF implicit solvation using the COSMO-RS model).

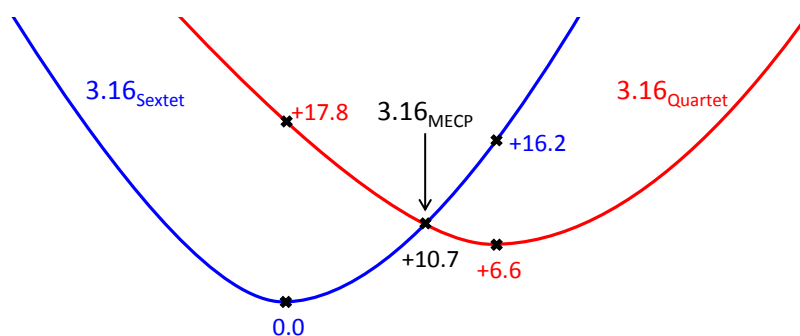


Figure 3.14: Relative electronic energies (at the M06/def2-SVP level) of the sextet (blue), quartet (red) and minimum energy crossing point (MECP, black) of 15. Values in kcal/mol.

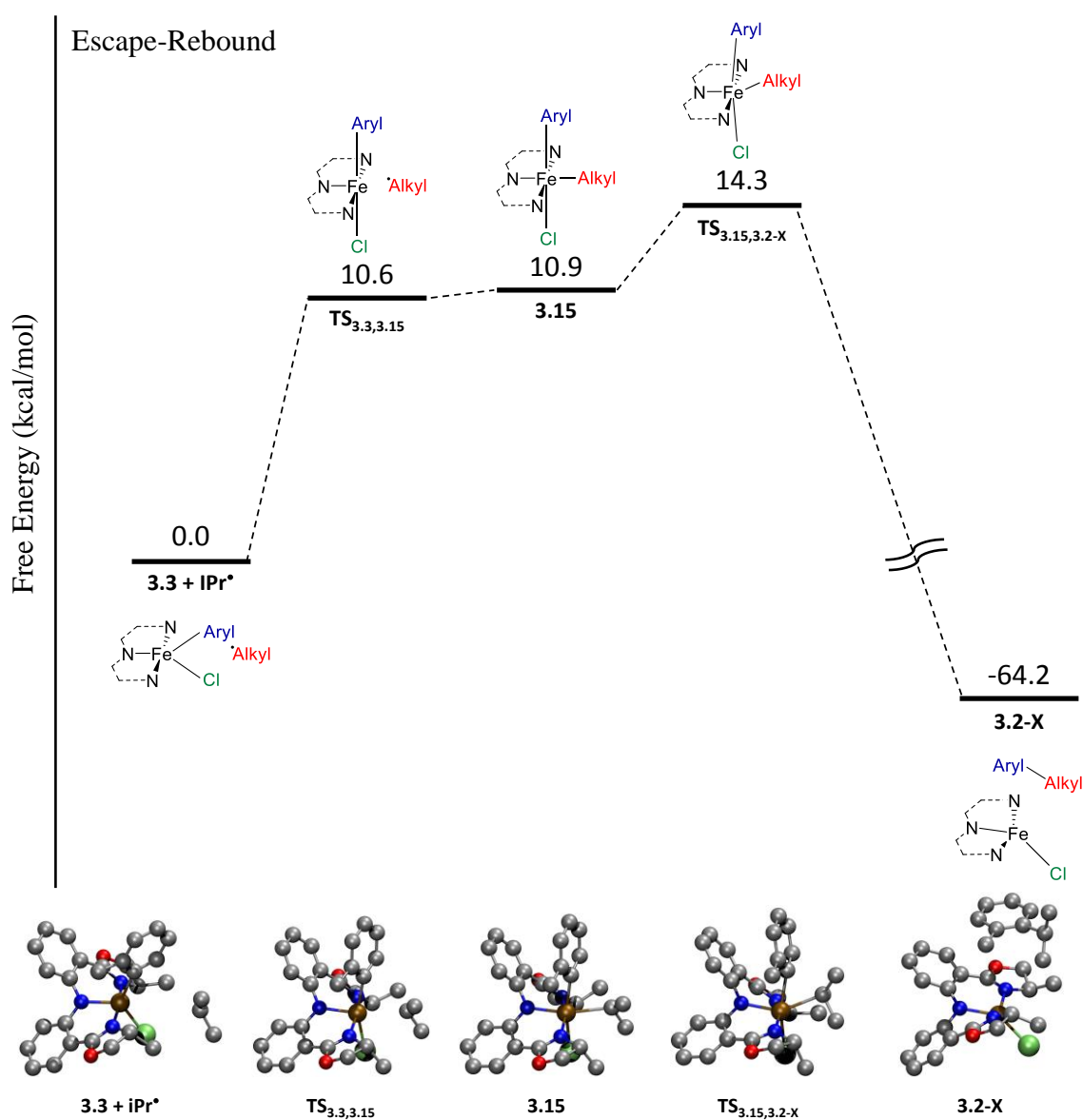


Figure 3.15: Reaction free energy profile and relevant structures for the escape-rebound pathway computed at the unrestricted PBE0-dDsC/TZ2P//M06/def2-SVP level (including THF implicit solvation using the COSMO-RS model).

The escape-rebound pathway represents a second possible mechanism for forming the cross-coupled product. Moving from the high-spin quintet Fe(III) reactant complex (**3.3**+*iPr*[•]) to the TS corresponding to association of the alkyl radical requires 10.6 kcal/mol of energy (Figure 3.15). The Fe(IV) intermediate **3.15** in which both the alkyl, aryl and halogen groups are bound is roughly isoenergetic with **TS**_{3.3,3.15} (**TS**_{3.3,3.15}→**3.15** -0.65 kcal/mol at the M06/def2-SVP level). Product formation *via* reductive elimination requires an addition 3.4 kcal/mol of energy to overcome the TS barrier (**3.15**→**TS**_{3.15,3.2-x}). Given that the highest point on this pathway lies higher in energy than proceeding through the bimetallic oxidative addition route (14.3 vs. 10.8 kcal/mol); the DFT computations indicate that bimetallic oxidative addition is the favoured mechanistic pathway.

3.2.3 Kinetics

The kinetics of the Fe-catalysed alkyl-aryl coupling was determined using complex **3.2** as the catalyst. Complex **3.1** was not suitable for the kinetic studies since the reduction from **3.1** to **3.2** is too slow at -84°C and leads to an induction period. The use of complex **3.2** is justified because **3.1** and **3.2** have the same efficiency for the reactions shown in Figure 2.1. The coupling reaction rates between (3-iodobutyl)benzene (**3.8**) and PhMgCl (5 mol% **3.2** as catalyst) were measured using the initial rate approximation.²³ Figure 3.16 (A) and (B) show the dependence of the reaction rate on the concentration of PhMgCl and catalyst, respectively. The data could be approximately fitted with a 1st order in Grignard reagent and 2nd order in catalyst. Only a small and random change in the reaction rate was observed when the concentration of the substrate (**3.8**) was varied (Figure 3.16C). This result suggested that the reaction is 0th order in alkyl iodide. To further confirm this, the reaction profile of a given catalytic run was evaluated by the integrated rate law (in the range of up to 77% conversion). The conversion of the substrate could be fit with a 1st order decay.²³ Assuming a constant concentration of catalyst, the result agrees with a 1st order in Grignard and 0th order in substrate.

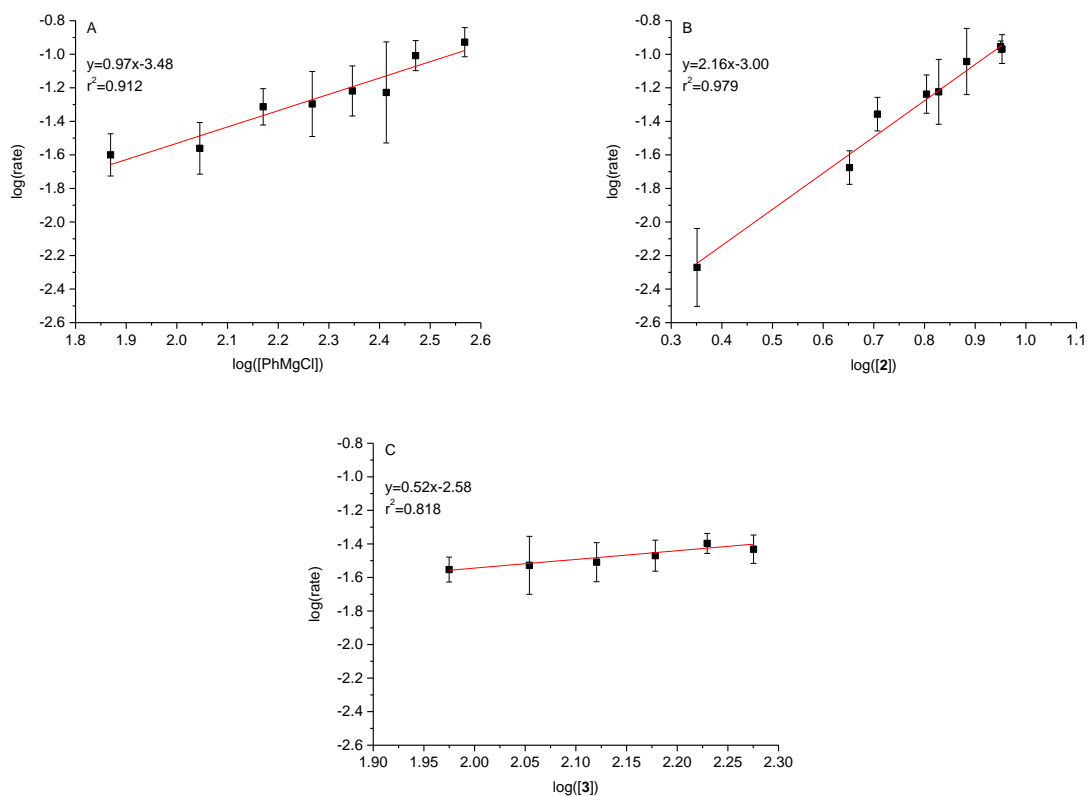


Figure 3.16: The influence of $c(\text{PhMgCl})$ (A), $c(\mathbf{3.2})$ (B) and $c(\mathbf{3.8})$ (C) in the initial rates of the coupling of **3.8** with PhMgCl. The slope of the log rate vs. log reagent is the approximate rate order.²³

The coupling of **3.8** and PhMgCl was also monitored by UV-Vis spectroscopy. Although the spectral change might be consistent with the resting state of the catalyst being the Fe(II) phenyl complex **3.5**, the definitive assignment is difficult due to overlap of absorption bands (Figure 3.17).

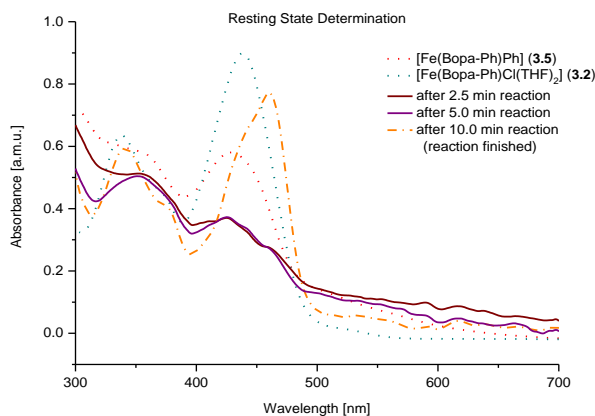


Figure 3.17: Absorption spectra of reaction mixture during a catalytic coupling of (3-iodobutyl)benzene with PhMgCl using **3.1** as catalyst.

To confirm **3.5** as resting state the coupling reaction was followed by NMR at -65°C . The resulting spectra showed two species. The signals from the $[\text{Fe}(\text{bopa-Ph})\text{Ph}]$ (**3.5**) can be clearly assigned (Figure 3.18, spectrum (1), annotation “A”). Comparing the remaining peaks of spectrum (1) with the peaks for complex **3.7** (Figure 3.18, spectrum (2), annotation “B”) one can see a 3-4 ppm upfield shift. This shift is due to some interaction of **3.7** with other compounds in the reaction mixture, e.g. Grignard. Further details are discussed below.

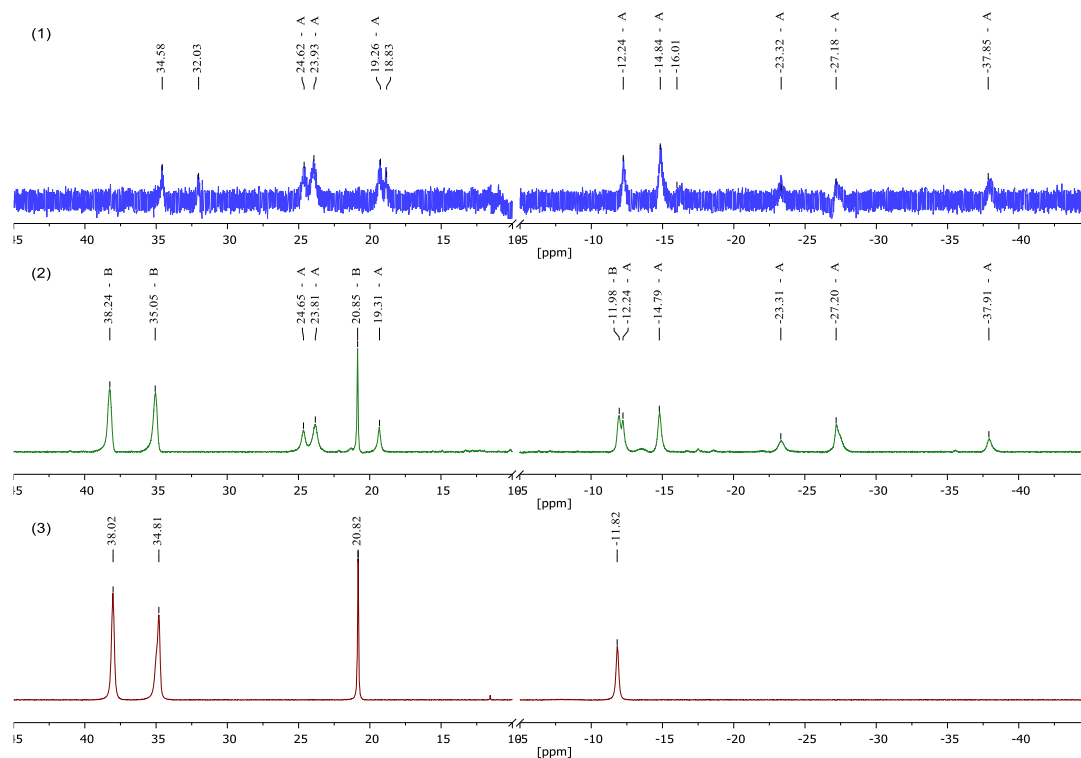


Figure 3.18: Determination of the resting state with ^1H -spectroscopy. Spectrum (1): Reaction mixture.²³ (2) **3.5** in $\text{THF-}d_8$. (3): **3.2** in $\text{THF-}d_8$. Peak annotation: A = Complex **3.5**; B = Complex **3.7**.

3.3 Discussion

Based on the results described in the previous section, a catalytic cycle can be proposed (Figure 3.19). The Fe(III) pre-catalyst, $[\text{Fe}(\text{bopa-Ph})\text{Cl}_2]$ (**3.1**), is first reduced by PhMgCl to form the Fe(II) catalyst, $[\text{Fe}(\text{bopa-Ph})\text{Cl}(\text{THF})_2]$ (**3.2**). Transmetalation of complex **3.2** with PhMgCl gives $[\text{Fe}(\text{bopa-Ph})\text{Ph}]$ (**3.5**), which is in an equilibrium with a yet unknown species.

This equilibrium is proposed as the resting state of the catalyst. Species **3.5** is activated by another molecule of PhMgCl to give an “ate” complex $[\text{Fe}(\text{bopa-Ph})(\text{Ph})_2]^-$ (**3.11**). Fürstner and co-workers showed that FeCl_3 reacted with an excess of MeLi to give an analogous Fe(II)-ate complex $[(\text{Me}_4\text{Fe})(\text{MeLi})](\text{Li}^*\text{Et}_2\text{O})_2$, which is capable of methylation of vinyl and acyl electrophiles.¹⁵ While the exact structure and composition remain unclear, the two Ph groups in complex **3.11** appear equivalent in reactivity. Species **3.11** reacts much faster than **3.5** with alkyl halide; therefore, it is the relevant active species for oxidative addition. Reaction of **3.11** with alkyl halide gives an alkyl radical and an Fe(III) complex, $[\text{Fe}(\text{bopa-Ph})(\text{Ph})(\text{X})]$ (**3.3**, X = halide). The alkyl radical escapes the solvent cage and recombines with another molecule of a Fe(II) aryl complex, i.e. **3.5** (it could be **3.11** as well), to give $[\text{Fe}(\text{bopa-Ph})(\text{Ph})(\text{Alkyl})]$ (**3.16**). Reductive elimination from **3.16** gives the alkyl-aryl coupled product and an Fe(I) species $[\text{Fe}(\text{bopa-Ph})]$ (**3.17**). Species **3.17** should be unstable and quickly react with the unstable Fe(III) complex **3.3**, to give the two Fe(II) complexes **3.2** and **3.5** which can re-enter the catalytic cycle.

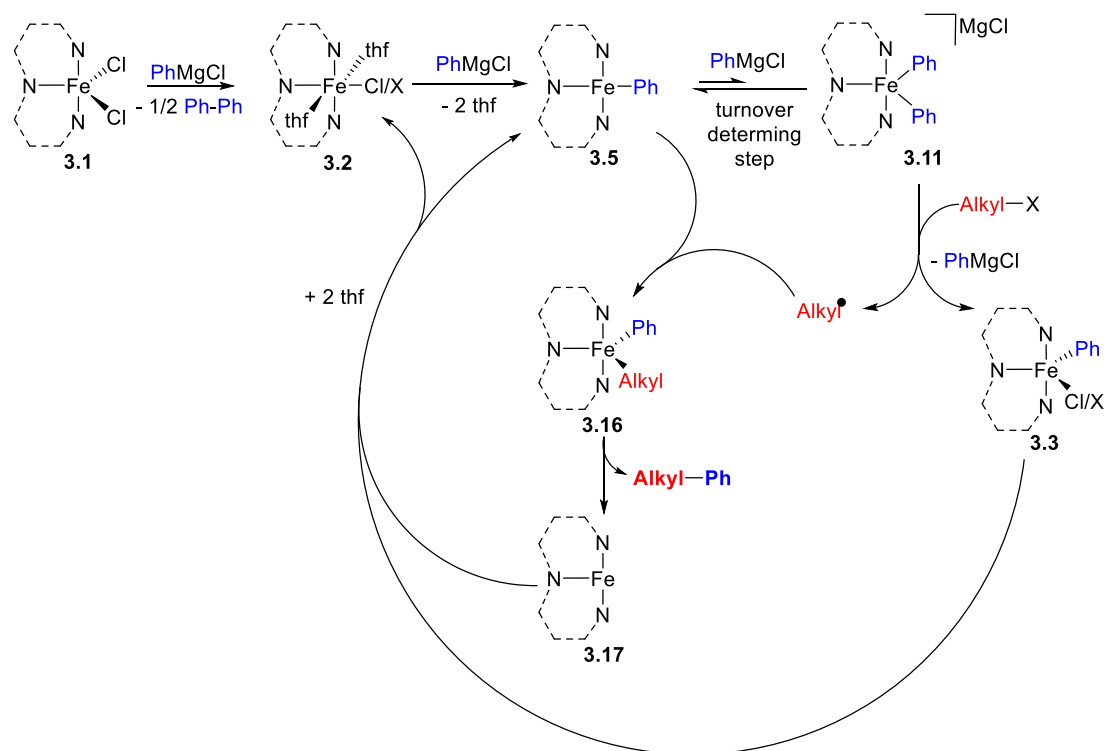


Figure 3.19: A proposed catalytic cycle for the coupling of alkyl halide with PhMgCl. The X ligand in species **3.2** and **3.3** is identical to the X group in alkyl-X. The pincer bopa-Ph is simplified for clarity.

Several deviations from this catalytic cycle might be proposed. For example, the alkyl radical might combine with species **3.11** rather than **3.5** to an Fe(III) species analogous to **3.16**. This variation does not significantly alter the overall catalytic cycle. On the other hand, species **3.17** might react with alkyl halide to generate an alkyl radical and the Fe(II) species **3.2**, which would result in a different catalytic cycle where the transformation of **3.5** to **3.11** serves only as the initiation step. However, this possibility is incompatible with **3.5** being the resting state and the catalysis being 1st order in Grignard reagent. Furthermore, it is inconsistent with the reaction profile of the catalysis, which shows no change of kinetic behaviour over the course of the reaction.

The kinetics of the catalysis, i.e. 2nd order in catalyst, 1st order in Grignard and 0th order in alkyl iodide, indicates that transmetalation, but not oxidative addition, is the turnover determining step. The 2nd order in catalyst suggests that the transformation of **3.5** to **3.11** goes through a bimetallic intermediate; a possibility is shown in Figure 3.20. This hypothesis would explain the NMR resting state measurements (Figure 3.18). The undefined signals in spectrum (1) could represent the dimeric species **3.23** (Figure 3.20), which is in equilibrium with **3.5**. Dimeric Fe(II) μ -aryl complexes such as $[\text{Fe}_2(\text{mesityl})_4]$ (**3.24**, Figure 3.21),^{41,42} $[\text{Fe}_2(2,4,6\text{-}i\text{Pr}_3\text{-C}_6\text{H}_2)_4]$ (**3.25**),⁴² and $[\{\text{Ar}^*\text{Fe}(\mu\text{-Ph})\}_2]$ (**3.26**, $\text{Ar}^* = 2,6\text{-Ph}_2\text{-C}_6\text{H}_3$)⁴³ have previously been reported. Furthermore, $[\text{Fe}_2(\text{mesityl})_4]$ reacts with mesitylMgBr to form the tris(mesityl)ferrate (**3.27**), which could activate the alkyl halide.¹⁷

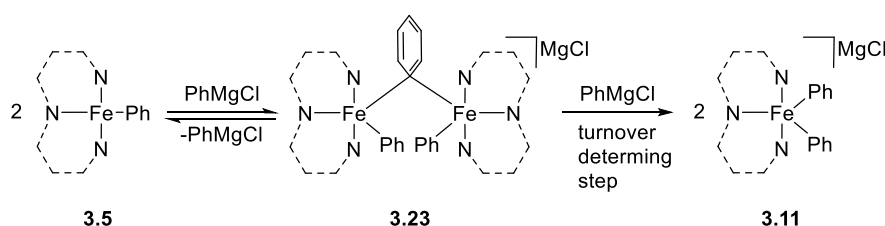


Figure 3.20: A hypothetical mechanism for the transformation of **3.5** to **3.11**.

The mechanism described here might be compared with those recently proposed for Fe-catalysed, tmeda-assisted alkyl-aryl Kumada coupling.¹⁷ When a bulky aryl Grignard reagent such as mesitylMgBr is used, homoleptic $[\text{Fe}(\text{mesityl})_3]$ is the catalyst and tmeda does not serve as a ligand. If less bulky aryl Grignard reagents are used, then the true catalyst is unknown, although there is EPR evidence for an Fe(I) species in the reaction mixture. In the present system, ligated Fe(II) complexes are genuine catalysts for the coupling. This is due to the strong

chelating ability of the tridentate pincer ligand bopa, which in turn facilitates the mechanistic study. As in the Fe-tmeda system for the coupling of less bulky Grignard reagent, Fe(I) species (**3.17**) is involved; but this Fe(I) species is an unstable intermediate rather than a resting species in the former. Stable Fe(I) species have been shown as catalysts in Fe-catalysed alkyl-aryl Negishi coupling^{18,19} and alkyl-alkyl Kumada coupling.²⁰ These Fe(I) species are supported by soft, neutral donors such as phosphine and N-heterocyclic carbene ligands, which match well with the low-valent Fe(I) centre. On the contrary, the nitrogen-based anionic bopa ligand renders the Fe(I) centre highly reactive so that species **3.17** cannot be observed or isolated.

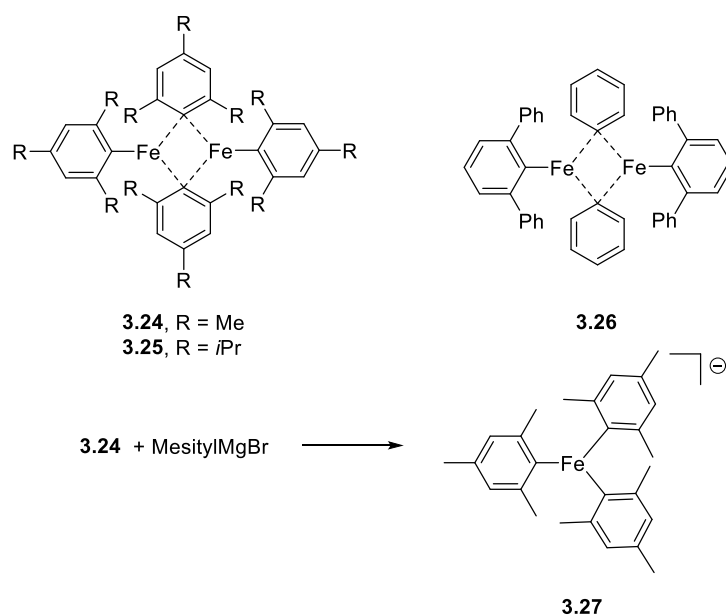


Figure 3.21: Structure and reactivity of some Fe(II) μ -aryl complexes.

The mechanism of this Fe catalysis might also be compared with that of alkyl-alkyl Kumada coupling catalysed by the nickel pincer complex, Nickamine.²⁴ There are a number of similarities. In both systems, transmetalation precedes oxidative addition and the oxidative addition follows a bimetallic radical pathway. Furthermore, stable organometallic intermediates (Fe(II) Ar or Ni(II) alkyl) both need to be activated by one molecule of Grignard reagent to activate alkyl halide. It is tempting to consider these as common features in Kumada coupling reactions catalysed by ligated 1st row transition metals, although more systems should be investigated. The Fe and Ni systems exhibit significant differences as well. There is a remarkable and surprising change of coordination geometries of the Fe intermediates in the solid-state. The Fe(III) halide pre-catalyst is 5-coordinate, the Fe(II) halide catalyst is 6-coordinate with two solvent ligands and the Fe(II) aryl catalyst is tetrahedral 4-coordinate. It

is however not excluded that in the solution the Fe(II) species will additionally bind the solvent molecules (e.g., THF) in an octahedral geometry. In contrast, the Ni catalysts remain Ni(II) and square-planar. An additional difference is the reactivity of the active species $[\text{Fe}(\text{bopa-Ph})(\text{Ph})_2]\text{MgCl}$ and $[\text{Ni}(\text{N}_2\text{N})(\text{Alkyl})](\text{AlkylMgCl})$. In the former, the two phenyl groups are coupled in similar probability with alkyl halide and can be treated as a genuine "ate" complex. In the latter, the original alkyl group is coupled preferentially with alkyl halide, so the second molecule of AlkylMgCl is only weakly associated.

3.4 Concluding Remarks

By using a strongly chelating pincer ligand bopa, we are able to prepare and isolate ligated Fe complexes, which are genuine catalysts and intermediates in Fe-catalysed alkyl-aryl Kumada coupling reactions. The easily accessible Fe(III) dichloride pre-catalyst is first reduced by the Grignard reagent to form the Fe(II) halide catalyst, which is transmetallated to form the Fe(II) aryl catalyst. The structural elucidation of the Fe catalysts reveals remarkable geometric changes of the Fe species. Although the Fe(II) aryl catalyst activates alkyl halide to form the alkyl-aryl coupling product, this reaction is too slow to be catalytically relevant. Instead, the Fe(II) aryl catalyst is further transmetallated to form an Fe(II) bis(aryl) "ate" complex that is the true active species for oxidative addition of alkyl halides. This oxidative addition proceeds *via* a bimetallic and radical pathway in which two Fe(II) aryl species provide one-electron each. The kinetics of the coupling of an alkyl iodide with PhMgCl is measured, showing a 2nd order in catalyst, 1st in Grignard reagent and 0th order in alkyl iodide. The turnover determining step is transmetallation of Fe(II) aryl catalyst to form the active "ate" complex; this reaction seems to proceed *via* a bimetallic intermediate. The mechanisms of Fe-catalysed coupling reactions are likely ligand-dependent and the particular mechanism described here is only confirmed for the Fe-bopa pincer system. However, this comprehensive mechanistic study using well-defined Fe pincer catalysts should provide significant new insights in the general understanding of Fe-catalysed coupling reactions of alkyl halides.

3.5 Experimental

3.5.1 Chemical and Reagents

All manipulations were carried out under an inert N₂ atmosphere using standard Schlenk or glove box techniques. The solvents were purified and dried using a two column solid-state purification system (Innovative Technology, NJ, USA). They were transferred to the glove box in a Strauss-flask without exposure to air. The solvents were stored over molecular sieves (3 Å). Deuterated solvents were purchased from Cambridge Isotope Laboratories, Inc. and were degassed and stored over dried and activated molecular sieves (3 Å). All other chemicals were purchased from commercial sources and were degassed by standard freeze-pump-thaw procedures prior to use. The following chemicals were synthesised: 2,2'-iminodibenzoic acid,⁴⁴ R-(-)-phenylglycinol,⁴⁵ 2,2'-iminodibenzoyl chloride, bopa-Ph, (bopa-Ph)Li,⁴⁶ [Fe(bopa-Ph)Cl₂] (**3.1**),⁴⁷ [Fe(bopa-Ph)Cl(THF)₂] (**3.2**), [Fe(bopa-Ph)Cl] (**3.4**), [Fe(bopa-Ph)Ar] (**3.5** Ar = Ph; **3.6** Ar = o-Tol), R-(3-bromobutyl)benzene,⁴⁸ *tert*-butyl-4-phenylbutaneperoxoate.³¹ The Grignard reagents were titrated prior to every use following the literature procedure.⁴⁹

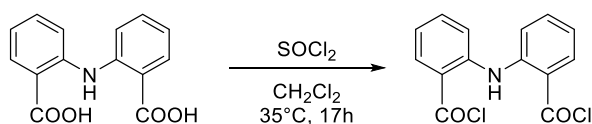
3.5.2 Physical Methods

NMR spectra were recorded on a Bruker Avance 400. ¹H NMR chemical shifts were referenced to residual solvent peak as determined relative to TMS ($\delta = 0$ ppm). GC measurements were conducted on a Perkin-Elmer Clarus 400 GC equipped with a FI-detector. GC-MS measurements were conducted on a Perkin-Elmer Clarus 600 GC equipped with Clarus 600T MS and a FI-detector. Photochemical experiments were performed in a Rayonet Photochemical Reactor, using Rayonet Photochemical Reactor Lamps of 2537 Å for homogenic irradiation of the samples. The internal temperature was maintained within a

40-60 °C range with the aid of an integrated mechanical ventilation system. UV-Vis-absorption spectra were recorded with a Hellma Excalibur UV-Vis fiber optic probe connected to a Varian 50 Bio UV-Vis spectrometer.

3.5.3 Syntheses

3.5.3.1 Synthesis of 2,2'-Iminodibenzoyl Chloride



2,2'-Iminodibenzoic acid (21.0 g, 1,0 equiv.) was suspended in 100 mL DCM and thionyl chloride (18.0 mL, 3.0 equiv.) was added. The suspension was heated to reflux overnight. The formed yellow solid was filtered off and washed twice with 20 mL cold DCM. The filtrate was carefully extracted with water (2x50 mL) to quench the reaction. The organic phase was dried over Na₂SO₄ and evaporated to dryness. The crude product (from the filtrate) was recrystallised from DCM and hexane. The obtained solids were combined.

Yield: 21.8 g (91%), bright yellow solid

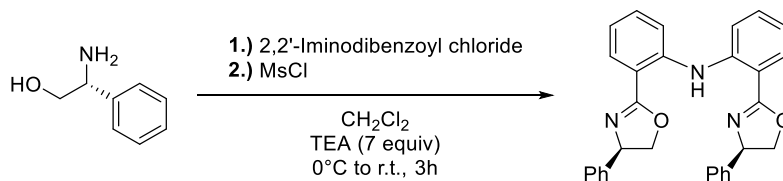
¹H NMR (400 MHz, Chloroform-*d*): δ 10.36 (s, 1H), 8.27 (d, *J*=8.5 Hz, 2H), 7.54 - 7.49 (m, 4H), 7.07 (ddd, *J*=7.1, 2.4 Hz, 2H).

¹³C NMR (101 MHz, Chloroform-*d*) δ 168.45, 144.04, 135.91, 135.72, 121.71, 121.04, 118.73.

Elemental analysis calculated (%) for C₁₄H₉Cl₂NO₂: C 57.17, H 3.08, N 4.76; found: C 57.05, H 3.04, N 4.60

Melting Point: 163 – 165°C

3.5.3.2 Synthesis of bopa-Ph



The procedure is based on the literature synthesis by Lu S.-F. *et al.*⁵⁰

R-(-)-Phenylglycinol (4.1 g, 2.0 equiv) was dissolved in 150 mL DCM and triethylamine (14.5 mL, 7.0 equiv; freshly distilled from KOH) was added. The solution was cooled to 0°C and 2,2'-iminodibenzoyl chloride (4.4 g, 1.0 equiv) was added slowly in small portions. After addition the cooling bath was removed and the solution stirred for 1h at room temperature (r.t.). The conversion was checked by TLC. The solution was cooled again to 0°C and methanesulfonyl chloride (MsCl) was slowly added. The reaction mixture was warmed to r.t. and stirred for 2h. The conversion was checked by TLC.

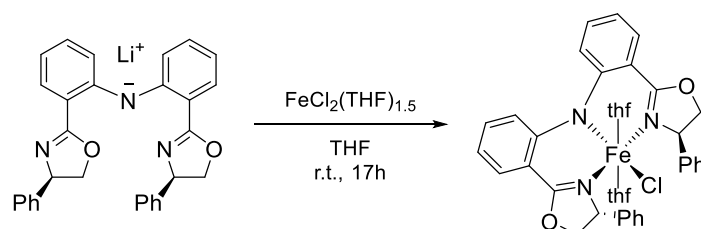
The reaction mixture was quenched with water (50 mL) and the organic phase was extracted with water (2x50 mL), saturated sodium bicarbonate solution (50 mL) and dried over Na₂SO₄. The crude product (99%) was purified by column chromatography (EtOAc:Hexane: 1:9).

Yield: 4.9 g (71%), yellowish white solid

¹H NMR (400 MHz, Chloroform-*d*): δ 11.10 (s, 1H), 7.91 (dd, *J* = 7.9, 1.6 Hz, 2H), 7.60 – 7.53 (m, 2H), 7.40 – 7.32 (m, 2H), 7.28 – 7.13 (m, 10H), 7.00 – 6.91 (m, 2H), 5.20 (dd, *J* = 10.0, 8.2 Hz, 2H), 4.50 (dd, *J* = 10.1, 8.3 Hz, 2H), 4.02 (t, *J* = 8.2 Hz, 2H).

¹³C NMR (101 MHz, Chloroform-*d*): δ 164.31, 143.28, 142.74, 131.64, 130.74, 128.64, 127.42, 126.81, 119.99, 118.26, 115.89, 73.86, 70.16.

3.5.3.3 Synthesis of [Fe(bopa-Ph)Cl(THF)₂] (3.2)



(bopa-Ph)Li (2.0 g, 1.1 equiv) was dissolved in 10 mL THF and FeCl₂(THF)_{1.5} (930 mg, 1.0 equiv) was added. The solution was stirred overnight. The solvent was evaporated and the complex was redissolved in toluene and filtered over celite. The filtrate was concentrated and precipitated with pentane. The formed solid was filtered off and recrystallised from THF/pentane giving red octahedral crystals.

The crystals for the x-ray analysis were obtained by diffusing pentane into a THF solution of **3.2**.

Yield: 2.6 g (93%), red octahedral crystals

Elemental analysis calculated (%) for C₃₈H₄₀ClFeN₃O₂: C 65.76, H 5.81, N 6.05; found: C 65.34, H 5.78, N 6.04

3.5.3.4 Synthesis of [Fe(bopa-Ph)Cl] (3.4)

Method A:

(bopa-Ph)Li (2.0 g, 1.1 equiv) was dissolved in 10 mL THF and FeCl₂(THF)_{1.5} (930 mg, 1.0 equiv) was added. The solution was stirred overnight. The solvent was evaporated and the complex was redissolved in toluene and filtered over celite. The filtrate was concentrated and precipitated with pentane, filtered and dried *in vacuo*.

The crystals for the x-ray analysis were obtained by evaporating a toluene/pentane solution of **3.4** into heptane.

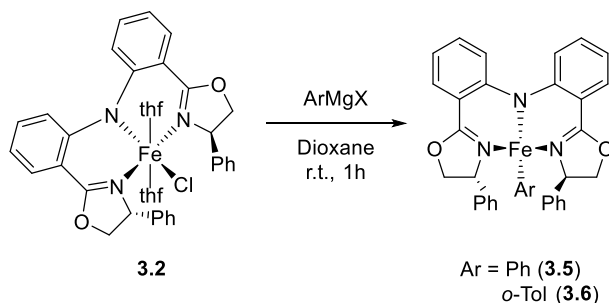
Yield: 2.26 g (96%), orange powder

Method B:

[Fe(bopa-Ph)Cl(THF)₂] (500 mg) was suspended in Et₂O and stirred for 72 hours. The complex slowly dissolves and immediately precipitates. The product was filtered off and dried *in vacuo*.

Yield: 267 mg (63%), orange powder

Elemental analysis calculated (%) for C₃₀H₂₄ClFeN₃O₂: C 65.53, H 4.40, N 7.64; found: C 65.44, H 4.49, N 7.58

3.5.3.5 Synthesis of [Fe(bopa-Ph)Ar] (3.5 and 3.6)**Method A:**

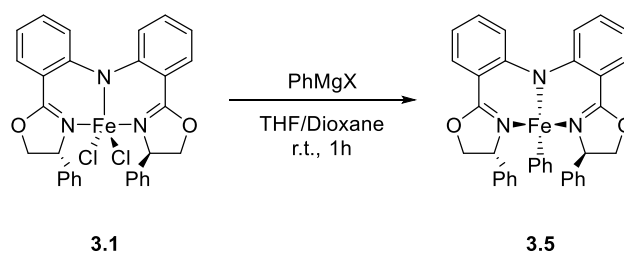
3.2 (1.0 equiv) was dissolved in 5 mL of dioxane and aryl Grignard (1.0 equiv) was added dropwise at r.t. The reaction was stirred for 30 min. The stirring was stopped to precipitate the formed Mg-salts. The supernatant was slowly filtered over a pad of celite. The solvent was removed and the residue was redissolved in a minimum amount of toluene and filtered again slowly over a pad of celite. The resulting solution was precipitated by adding pentane. The formed precipitate was filtered off and washed with pentane.

Crystals of **3.6** were obtained by overlaying a solution of **5** in THF/Dioxane (1:1) with pentane.

Crystals of **3.5** were tried to be obtained in the same manner. But the formed solids show no diffraction pattern. Further attempts with different solvents and solvent systems were also not successful. Therefore we considered an analogous structure as of complex **3.6** which was confirmed by elemental analysis.

Yield: **3.5**: 75%, **3.6**: 86%

Method B:



3.1 (798 mg, 1.0 equiv) was dissolved in 50 mL THF and 10 mL dioxane were added (the addition of dioxane is crucial to precipitate the formed MgCl_2 ; otherwise part of the complex start to decompose). 1.40 mL PhMgCl (1.83 M solution in THF, 1.9 equiv) were added dropwise over an hour. The formed solids were filtered off over a pad of celite and the solution was concentrated to about 20 mL and then precipitated by adding pentane. The formed solid was filtered off and redissolved in a minimum amount of benzene, filtered over celite and precipitated by adding pentane. The solid was filtered off and thoroughly washed with pentane.

Yield: 43%

Elemental analysis calculated (%) for $\text{C}_{36}\text{H}_{29}\text{FeN}_3\text{O}_2$ (**3.5**) + 0.5 Dioxane: C 71.81, H 5.23, N 6.61;
found: C 71.54, H 5.55, N 6.42

Elemental analysis calculated (%) for $\text{C}_{37}\text{H}_{31}\text{FeN}_3\text{O}_2$ (**3.6**) + 1.5 dioxane: C 69.97, H 5.87, N 5.69;
found: C 69.26, H 5.75, N 5.66

3.5.4 $T_{1/2}$ – Measurements

Stock solutions with (3-iodobutyl)benzene (0.250M, **Sol.A**) and naphthalene as an internal standard, [Fe(bopa-Ph)Ph] (6.44mM, **Sol.B**), PhMgCl in THF (12.5mM, **Sol.C**) and PhLi in *n*Bu₂O (12.5mM; stock solution in THF, **Sol.D**).

Standard experiment:

1.0 mL of **Sol.B** was put in a vial and cooled to -40°C under stirring. 0.5 mL of **Sol.A** was added and 50 μ L samples were taken after 0.5, 1, 2, 4, 8, 12, 16, 30, 60 minutes and immediately quenched with 100 μ L 2-propanol. The yield was determined by GC (a FI-Detector was used for quantification).

Experiment with additives:

1.0 mL of **Sol.B** was put in a vial and cooled to -40°C and 0.5 mL of **Sol.A** was added. Immediately after 0.5 mL of either **Sol.C**, or **Sol.D**, was added. 50 μ L samples were taken after 15, 30, 45 and 60 seconds and immediately quenched with 100 μ L 2-propanol. The yield was determined by GC (a FI-Detector was used for quantification).

3.5.5 Magnetic Bulk Susceptibility Measurements (Evan's method)

The sample is weight into a J.Young-NMR tube and dissolved in a – preferably – non-coordinating solvent. TMS was added as an internal standard (homogeneous phase). Afterwards a capillary with exactly the same solvent and standard was inserted into the NMR tube (heterogeneous phase). Meanwhile the NMR probe was heated to around 25°C (the exact temperature was measured and noted) and the sample was inserted. After about 5 minutes (when

the temperature was constant) a spectrum was measured. The susceptibility is calculated by the following formula:

$$\mu_{eff} = 2.828 \sqrt{\frac{\Delta_x T}{4\pi c S 10^3}} \quad (\text{Eq. 1})$$

μ_{eff}	Effective magnetic moment [μ_B]
Δ_x	Bulk magnetic susceptibility shifts [ppm]
T	Temperature [K]
c	Concentration [$\text{mol} \cdot \text{L}^{-1}$]
S	Spherical factor (1/3 for a cylindrical shaped sphere parallel to the magnetic field)

The number of unpaired electrons can be approximated by spin-only formula, which is direct proportional to the magnetic moment (μ_{eff}):

$$\mu_{eff} = \sqrt{n(n+2)} \quad (\text{Eq. 2})$$

n	number of unpaired electrons
---	------------------------------

3.5.5.1 [Fe(bopa-Ph)Cl₂] (**3.1**)

m(3.1)	12.3 mg
m(Benzene- <i>d</i> ₆)	488.4 mg
Standard	TMS
T [K]	297.65
Δ_x [ppm]	0.43
μ_{eff}	5.61 μ_B

3.5.5.2 [Fe(bopa-Ph)Cl(THF)₂] (**3.2**)

m(3.2)	4.8 mg
m(THF- <i>d</i> ₈)	487.0 mg
Standard	TMS
T [K]	308.95
Δ _x [ppm]	0.62
μ _{eff}	5.11 μ _B

3.5.5.3 [Fe(bopa-Ph)Cl] (**3.4**)

m(3.2)	42.8 mg
m(Benzene- <i>d</i> ₆)	479.7 mg
Standard	TMS
T [K]	297.76
Δ _x [ppm]	5.5
μ _{eff}	5.06 μ _B

3.5.5.4 [Fe(bopa-Ph)Ph] (**3.5**)

m(3.5)	7.0 mg
m(Benzene- <i>d</i> ₆)	420.1 mg
Standard	TMS
T [K]	299.55
Δ _x [ppm]	1.17
μ _{eff}	5.00 μ _B

3.5.5.5 [Fe(bopa-Ph)o-Tol] (**3.6**)

m(3.6)	32.6 mg
m(Benzene- <i>d</i> ₆)	519.8 mg
Standard	TMS
T [K]	302.15
Δ _x [ppm]	3.88
μ _{eff}	4.76 μ _B

3.5.6 Reaction of 3.5 in Presence of PhMgCl

3.5.6.1 Decomposition Experiment

15.3 mg (25.9 μmol) of **3.5** was dissolved in 0.5 mmol THF- d_8 and 14 μL (26.0 μmol , 1.0 equiv.) PhMgCl in THF (1.86 M) and a drop of TMS were added *via* a Hamilton syringe. The sample was transferred to an NMR tube and the spectra were measured in regular intervals. During the measurement one could see that the log signal was strongly shifting. One representative spectrum is shown in Figure 3.7 (spectrum 1).

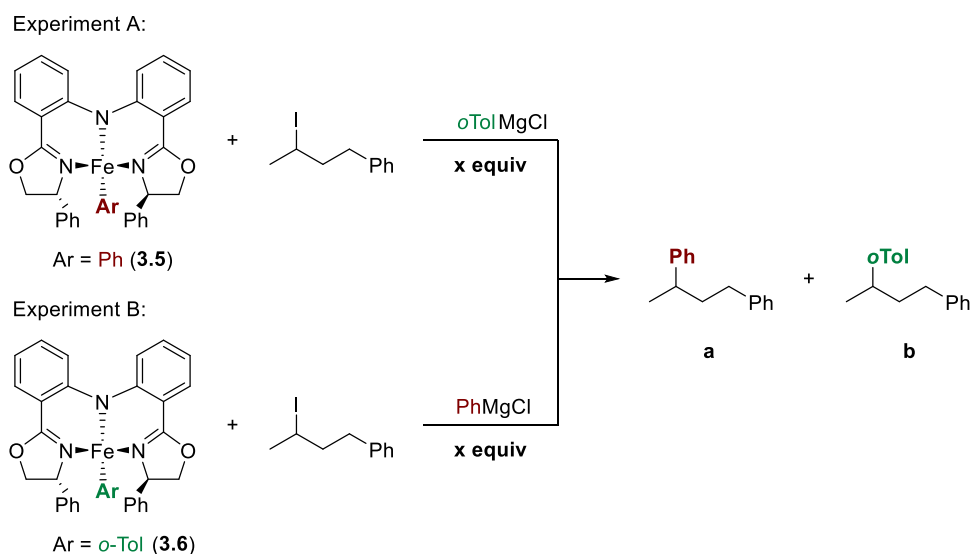
3.5.6.2 *In situ* formation of Mg-(bopa)-Ph species

9.3 mg (20.2 μmol) of bopa-Ph was dissolved in 0.5 mL THF- d_8 and its ^1H -NMR was recorded. Then 20 μL (37.2 μmol , 1.8 equiv.) of PhMgCl in THF (1.86 M) were added. The solution turned immediately fluorescent yellow. A ^1H -NMR spectrum was recorded (Figure 3.7).

3.5.7 Cross-Over Experiments

General remarks:

Two experiments were conducted (see scheme below).



Before the following standard solutions were prepared:

Sol.A: (3-Iodobutyl)benzene (11.9 mg, 47.5 μmol) and naphthalene (4.6 mg, 35.9 μmol) as an internal standard were dissolved in 5.0 mL THF

Sol.B: [Fe(bopa-Ph)Ph] (15.0 mg, 25.4 μmol) were dissolved in 5.0 mL THF

Sol.C: o-TolMgCl in THF (0.68 M, 0.33 mL) were dissolved in 25.0 mL THF

Sol.D: [Fe(bopa-Ph) o-Tol] (15.6 mg, 25.8 μmol) were dissolved in 5.0 mL THF

Sol.E: PhMgCl in THF (1.86 M, 0.12 mL) were dissolved in 25.0 mL THF

The solutions were mixed as followed (Table 3.3):

Table 3.3: Sample composition of the results corresponding to Figure S2 (left graph).

Experiment A				Experiment B		
	Sol.A	Sol.B	Sol.C	Sol.A	Sol.D	Sol.E
A	0.5 mL	1.0 mL	0.5 mL	0.5 mL	1.0 mL	0.5 mL
B	0.5 mL	1.0 mL	0.4 mL	0.5 mL	1.0 mL	0.4 mL
C	0.5 mL	1.0 mL	0.3 mL	0.5 mL	1.0 mL	0.3 mL
D	0.5 mL	1.0 mL	0.2 mL	0.5 mL	1.0 mL	0.2 mL

The complex stock solution (**Sol.B** or **Sol.D**) were put in a vial and **Sol.A** was added. Immediately after the Grignard stock solution (**Sol.C** or **Sol.E**) was added. And the reaction was allowed to stir for an additional 30 min at room temperature. The reaction was quenched by adding 100 μ L of ethanol. The coupling products were determined by GC/MS using a FI-detector for quantification.

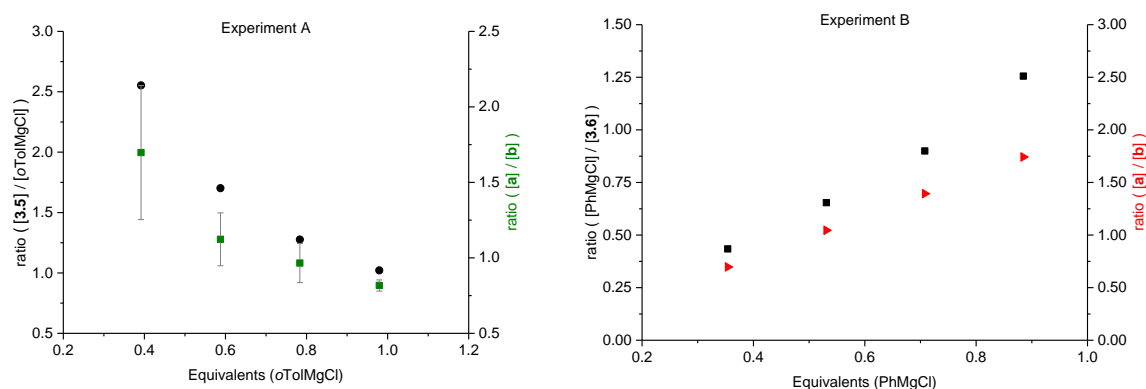


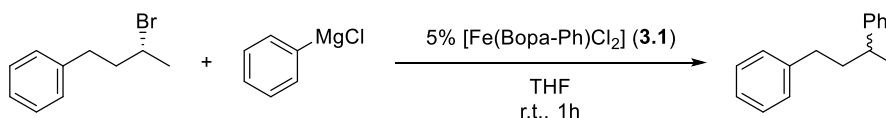
Figure 3.22: Left Graph: Experiment A was repeated twice with **3.5** and o-TolMgCl in order to prove the reproducibility. It shows the Ph/o-Tol ratio of the starting materials (black dots) in comparison to Ph/o-Tol ratio of the products (green rectangles); this graph corresponds to Table 3.2 – see above. Right Graph: Experiment B was only conducted once. It shows the Ph/o-Tol ratio of both starting material (black rectangles) and product (red triangle).

3.5.8 Radical trap experiments

General procedure:

The bromoalkane (0.25 mmol) and **3.1** (12.5 μ mol) were weighed into a vial and dissolved in THF (2.0 mL). PhMgCl in THF (0.30 mmol) were added dropwise over a time period of 5 minutes at room temperature. After addition the solution stirred for another 10 minutes. The solution was quenched with water and further acidified with HCl (1M) and extracted with 3 x 20 mL of DCM. The combined organic phases were dried over Na₂SO₄ and the solvent was evaporated to dryness.

3.5.8.1 Results Racemization Experiment



The sample was purified before the HPLC run by preparative TLC (solvent: hexane).

Yield (isolated): 48.9 mg (93%)

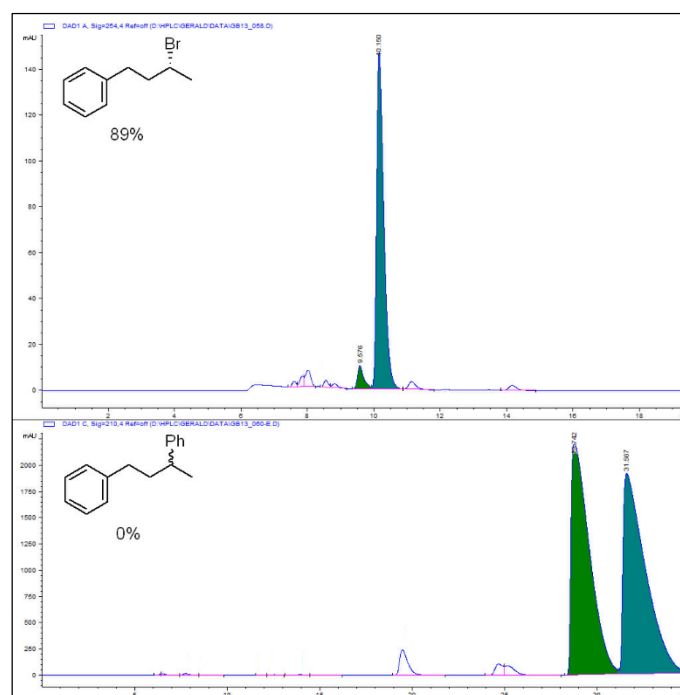


Figure 3.23: HPLC spectra of R-(3-bromobutyl)benzene and 1,3-diphenylbutane to show the racemisation during the cross coupling reaction.

3.5.8.2 Results Ring Opening Experiment

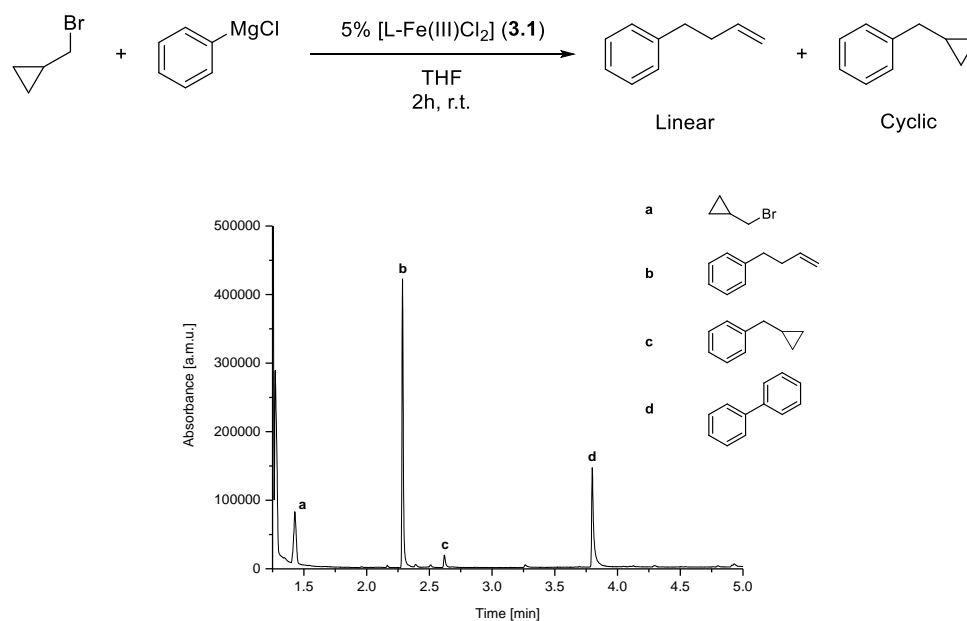
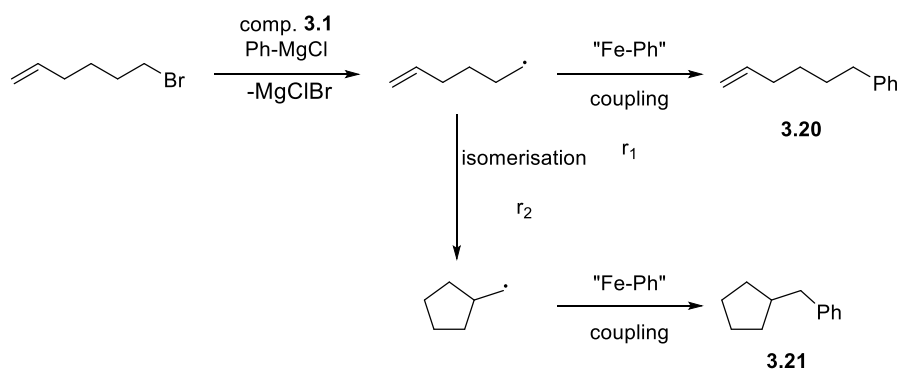


Figure 3.24: GC spectrum of the products formed during the cross coupling of (bromomethyl)cyclopropane with PhMgCl.

It was attempted to isolate the product from the crude mixture by preparative TLC (mobile phase: hexanes). But it was co-isolated with the byproducts. The coupling product (**b**) was thus identified by $^1\text{H-NMR}$ spectroscopy by comparing with the commercially available 4-phenyl-1-butene (Figure 3.38). **Ring closing experiment**



General remark:

In one experiment 4 samples were prepared with variable catalyst loadings. The reaction and work-up procedure is described in the above section "General Procedure" (reaction was performed at room temperature overnight). Two consecutive experiments were performed. Beforehand two standard solutions were prepared:

Sol.A: $[\text{Fe}(\text{bopa-Ph})\text{Cl}_2]$ (73.2 mg, 125.1 μmol) were dissolved in 5.0 mL THF ($c = 25.0\text{mM}$)

Sol.B: 6-Bromo-1-hexene (408.6 mg, 2.51 mmol) and dodecane as an internal standard (218.5 mg, 1.28 mmol) were dissolved in 10.0 mL THF ($c = 251\text{ mM}$)

The solutions were mixed according to Table 3.4:

Table 3.4: Sample composition of a single experiment.

Sample	V (Sol.A)	V (THF)	V (Sol.B)	Catalyst loading [%]
A	1.0 mL	0.0 mL	1.0 mL	10%
B	0.7 mL	0.3 mL	1.0 mL	7%
C	0.3 mL	0.7 mL	1.0 mL	3%
D	0.1 mL	0.9 mL	1.0 mL	1%

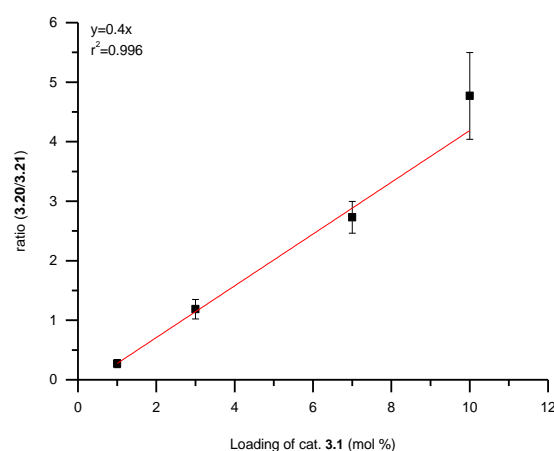


Figure 3.25: Dependence of the ratio of compounds **3.20/3.21** relative to the catalyst loading.

Identification:

The formed products were separated and identified by GC/MS. The yields were determined using naphthalene as an internal standard and a FI-detector for quantification. Further on, the crude mixture was purified by column chromatography (gradient 1% ethyl acetate to 3% in hexanes). The linear products (**b**, **c**) were isolated (sample consisted of biphenyl impurities) and identified by $^1\text{H-NMR}$ and compared to the literature.⁵¹

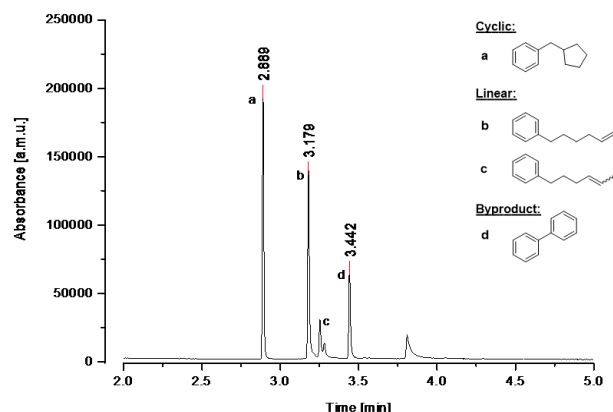


Figure 3.26: GC spectrum of the products formed during the cross coupling of 6-bromo-1-hexene with PhMgCl.

NMR is shown in Figure 3.39.

^1H NMR (400 MHz, Chloroform-*d*) δ 7.35 – 7.23 (m, 5H), 5.92 – 5.82 (m, 1H), 5.08 – 4.99 (m, 2H), 2.67 (t, $J = 7.6$ Hz, 2H), 2.15 – 2.11 (m, 2H), 1.76 – 1.64 (m, 2H), 1.52 – 1.46 (m, 2H).

3.5.9 Attempt to prove the feasibility of the bimolecular oxidative addition mechanism:

3.5.9.1 Reaction of [Fe(bopa-Ph)Ph] (**3.5**) with *tert*-butyl-4-phenylbutaneperoxoate under UV-irradiation

A solution with [Fe(bopa-Ph)Ph] (6.44mM, 1.0 mL) and dodecane as an internal standard was put in a J. Young-NMR tube and *tert*-butyl-4-phenylbutaneperoxoate (5.6mg; 23.7 μmol) was added. The sample was put in a Rayonet Photochemical reactor for 1.5h. The reaction mixture was quenched with methanol and the coupling products were checked by GC/MS using dodecane as an internal standard (a FI-detector was used for quantification). The 1,3-diphenylpropane was independently synthesised from 1-bromo-3-phenylpropane using the

standard coupling protocol (see chapter 2.3, Table 1.2). The product was confirmed by GC/MS and $^1\text{H-NMR}$ (Figure 3.40 - Figure 3.42). The other peaks shown in Figure 3.27 were found in the blank reaction and therefore not taken under consideration. The yields for the phenyl containing products which is derived from $[\text{Fe}(\text{bopa-Ph})\text{Ph}]$ were calculated to be 20% for compound (a) and 27% for compound (b) (Figure 3.27).

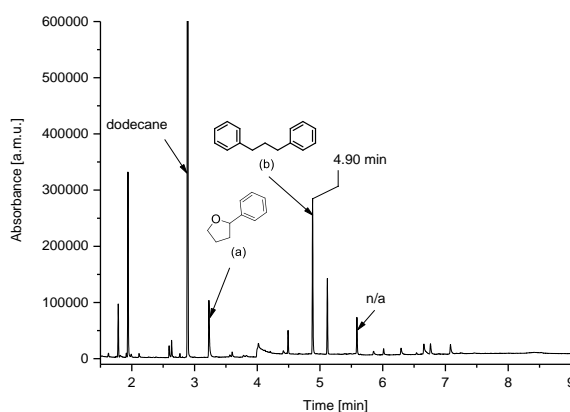


Figure 3.27: GC spectrum of the products formed during the UV irradiation of **3.5** in presence of *tert*-butyl-4-phenylbutaneperoxoate. The other peaks came from the background reaction (Figure 3.43) and were not further taken under consideration.

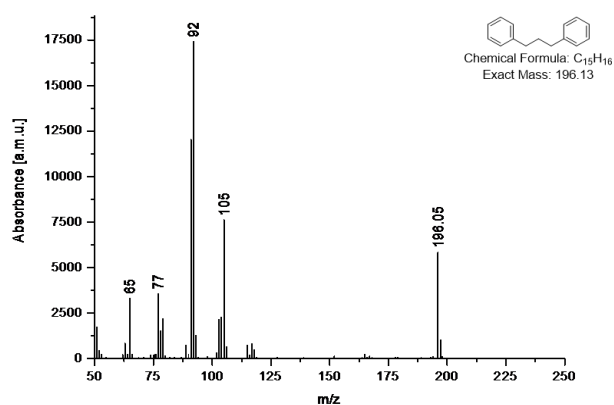


Figure 3.28: Averaged MS-spectrum taken from the crude GC spectrum between 4.88 – 4.89 min retention time.

3.5.9.2 Reaction of PhMgCl with *tert*-butyl-4-phenylbutaneperoxoate under UV-irradiation

A J. Young-NMR tube was charged with 1.0 mL THF and PhMgCl in THF (20 μ L, 1.90 M, 38.0 μ mol) and *tert*-butyl-4-phenylbutaneperoxoate (6.8 mg, 28.8 μ mol) were added. The sample was put in a Rayonet Photochemical reactor and irradiated for 1.5h. The reaction mixture was put in a GC vial and analysed by GC/MS. No starting material could be found meaning that all the *tert*-butyl-4-phenylbutaneperoxoate was reacted. The resulting spectrum (Figure 3.29) shows no formation of 1,3-diphenylpropane (coupling product of the phenylpropyl radical with PhMgCl).

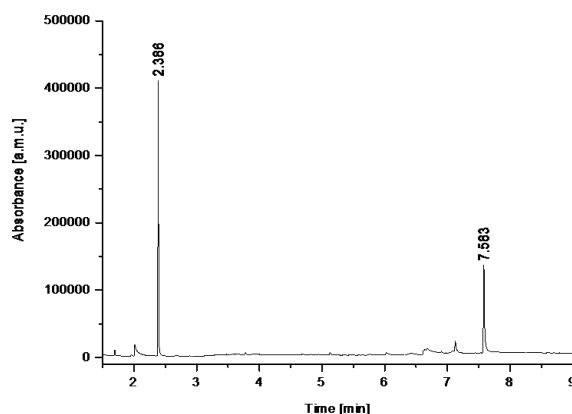


Figure 3.29 GC spectrum of the products of blank reaction of PhMgCl and *tert*-butyl-4-phenylbutaneperoxoate under UV irradiation. Neither of the formed products were observed in the reaction of *tert*-butyl-4-phenylbutaneperoxoate with **3.5**.

3.5.9.3 Reaction of [Fe(bopa-Ph)Ph] (**3.5**) under UV-irradiation

A J. Young-NMR tube was charged with 0.5 mL THF-*d*₈ and [Fe(bopa-Ph)Ph] (1.9 mg, 3.2 μ mol) was added. The NMR tube was placed in the NMR spectrometer and a ¹H-NMR spectrum was recorded. Afterwards the sample was put in a Rayonet Photochemical reactor and irradiated for 1.5h. After the irradiation the sample was measured again. The NMR showed that no complex decomposed during the irradiation (Figure 3.31).

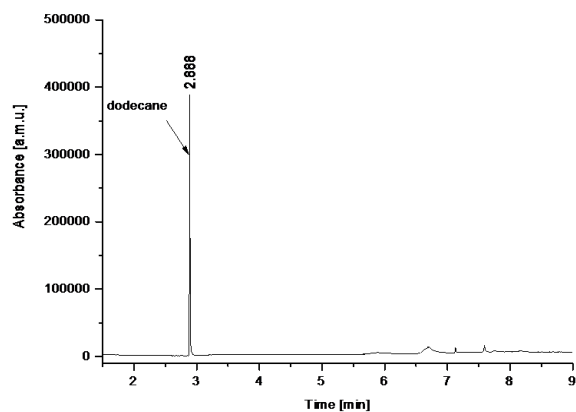


Figure 3.30: GC spectrum of the products of blank reaction of **3.5** in THF under UV irradiation.

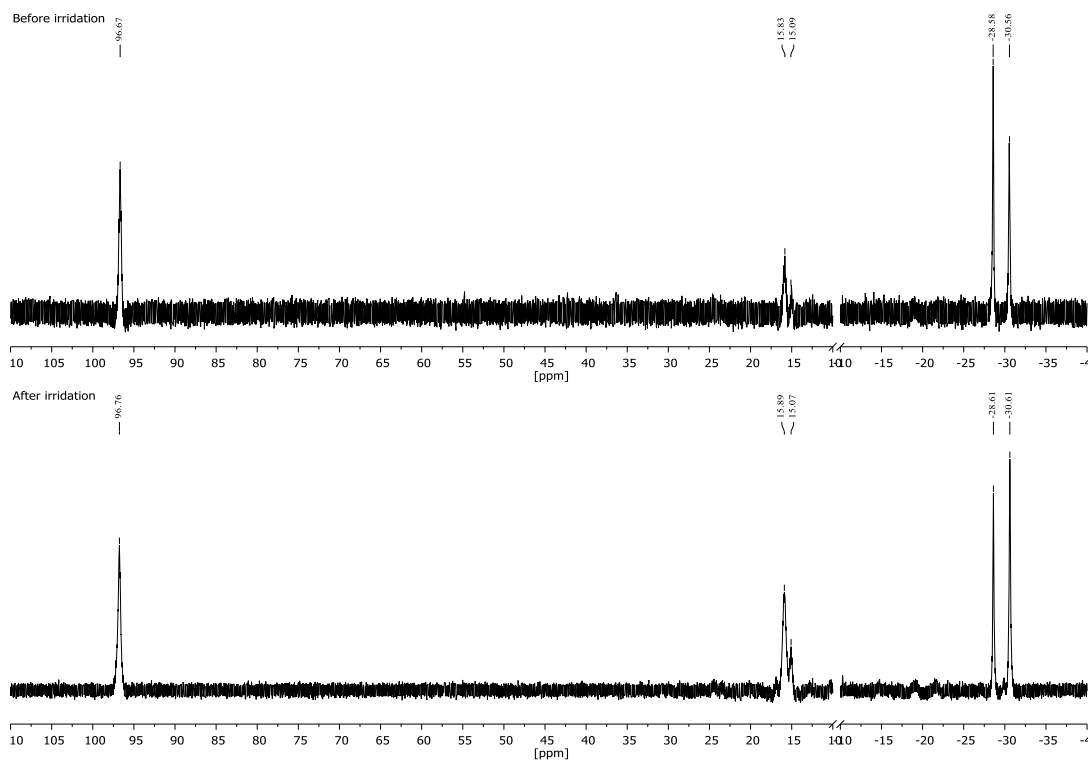


Figure 3.31: NMR spectra of [Fe(bopa-Ph)Ph] (**3.5**) before and after the irradiation with UV light (out of clarity reasons the residue solvent signals in the range from -10 - 10 ppm were omitted).

3.5.9.4 Reaction of *tert*-butyl-4-phenylbutaneperoxoate under UV-irradiation

A J. Young-NMR tube was charged with 1.0 mL THF and *tert*-butyl-4-phenylbutaneperoxoate (12.2 mg, 51.6 μmol) was added. The sample was put in a Rayonet Photochemical reactor and irradiated for 1.5h. The reaction mixture was put in a GC vial and analysed by GC/MS. No starting material could be found meaning that all the *tert*-butyl-4-phenylbutaneperoxoate reacted. The resulting spectrum (Figure 3.32) shows the formed products.

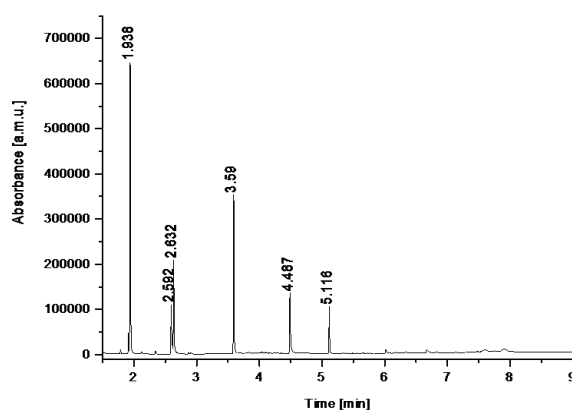


Figure 3.32: GC spectrum of the products of blank test of *tert*-butyl-4-phenylbutaneperoxoate in THF under UV irradiation.

3.5.10 Kinetic studies:

General considerations:

The reaction rate v can be calculated as followed:

$$v = k[\text{Complex}]^a[\text{Alkyl}]^b[\text{PhMgCl}]^c \quad (\text{Eq. 3})$$

If the concentration of one reaction partner is varied while the other one are kept constant, one can simplify equation 3 to:

$$v = k_{eff}[X]^n \quad (\text{Eq. 4})$$

This assumption can be drawn in the first few per cent of the formed product ($\leq 10\%$). Since the other reactants are in large excess than the formed product, they can be considered as constant. Further logarithmic calculus gives a linear dependence of rate and concentration:

$$\ln(v) = \ln(k_{eff}) + n * \ln([X]) \quad (\text{Eq. 5})$$

The reaction rate n can then be determined by plotting $\ln(v)$ versus $\ln([X])$. The slope then gives the order n of the reaction.

General remarks:

In the first screening reactions to find the ideal concentration and temperature range, it was noticed that the reaction rate of the reduction from $[\text{Fe}(\text{bopa-Ph})\text{Cl}_2]$ to $[\text{Fe}(\text{bopa-Ph})\text{Cl}(\text{THF})_2]$ drastically reduces at lower temperatures. Since there was no noticeable reaction at -84°C (melting point of ethyl acetate) we decided to perform the kinetic measurements with $[\text{Fe}(\text{bopa-Ph})\text{Cl}(\text{THF})_2]$.

3.5.10.1 Dependence on PhMgCl

General remarks:

In one experiment 8 reaction solutions were prepared with variable Grignard concentrations. The reactions were performed in a consecutive order to maintain the same reaction and sampling conditions. For each reaction 10 GC samples were prepared. To achieve a constant reaction temperature a slurry of melting ethyl acetate (m.p. = -84°C) was prepared before the experiment. The example given below depicts one single experiment. In order to determine the order of the reaction the mean value of at least three independent experiments was taken.

Before the experiment three stock solutions were prepared:

Sol.A: 1.0 mL of PhMgCl in THF (1.85 M) were diluted to 5.0 mL THF solution ($c = 0.37\text{ M}$).

Sol.B: (3-Iodobutyl)benzene (289.6 mg, 1.11 mmol) and naphthalene (60.3 mg, 0.47 mmol) as an internal standard were diluted to 9.0 mL THF solution ($c = 0.124\text{ M}$).

Sol.C: $[\text{Fe}(\text{bopa-Ph})\text{Cl}(\text{THF})_2]$ (43.8 mg, 63.1 μmol) were dissolved in 5.0 mL THF ($c = 12.6\text{ mM}$).

Inside the glove box screw vials with a stirring bar were filled with 0.2, 0.3, 0.4, 0.5, 0.6, 0.7, 0.8 and 1.0 mL of **Sol.A**, then 1.0 mL of **Sol.B** was added. The vials were filled up with THF to a total volume of 2.0 mL. The vials were closed with a rubber septum. 0.5 mL of **Sol.C** was put in 1.0 mL insulin syringes (the tip of the needle was put in a rubber stopper to minimise the exposure to air). The vials were taken out of the glove box and attached to the Schlenk line by piercing a needle through the septum. The following procedure was done consecutively with every reaction vial: The vial was put in the ethyl acetate slurry and stirred for about 5 minutes (to be sure that the temperature is constant). Then the rubber septum was removed from the vial (while maintaining the nitrogen flow). **Sol.C** was added at once. An aliquot of 100 μL was taken in regular intervals (depending on the concentration of Grignard reagent and hence its reaction rate) and immediately pipetted in a GC vial containing 50 μL acetonitrile. The GC vials were then filled with diethyl ether and analysed by GC (a FI-detector was used for quantification).

The yields of the 1,3-diphenylbutane were determined in respect to naphthalene as an internal standard. Figure 3.33 shows the results (yield versus time) of a single experiment. In order to determine the reaction rate, the data points (up to 10% yield) were fitted linear. The reaction rates were then logarithmised, averaged and then plotted versus the logarithm of the PhMgCl concentration (Graph A, Figure 3.16).

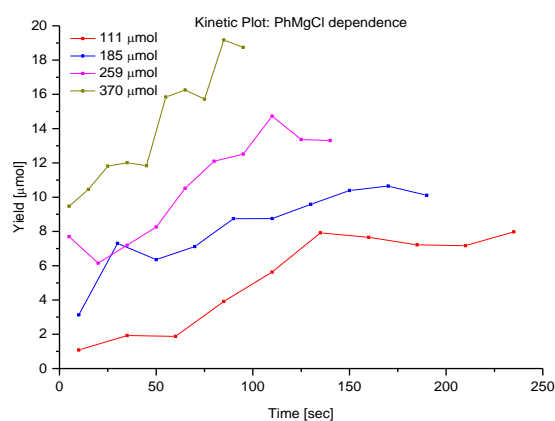
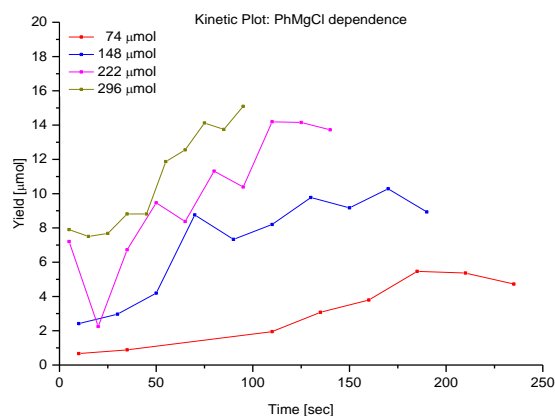


Figure 3.33: Reaction profile of single experiments under variable concentrations of PhMgCl.

3.5.10.2 Dependence on $[\text{Fe}(\text{bopa-Ph})\text{Cl}(\text{THF})_2]$ (3.2)

General remarks:

The results depicted in Graph B (Figure 3.16) consist of two sets of experiments with each 4 reactions. The first set covers a catalyst loading of 4.0, 5.0, 6.0 and 7.0% and the second set covers a catalyst loading of 1.8, 3.6, 5.4, 7.2%. In each set different solutions with variable complex concentrations were prepared. The reactions were performed in a consecutive order to maintain the same reaction and sampling conditions. For each reaction 10 GC samples were prepared. To achieve a constant reaction temperature a slurry of melting ethyl acetate (m.p. = -84°C) was prepared before the experiment. The example given below depicts one

single experiment. In order to determine the order of the reaction the mean value of three independent experiments (in each set) was taken.

Before the experiment three stock solutions were prepared:

Sol.A: [Fe(bopa-Ph)Cl(THF)₂] (38.9 mg, 56.0 μmol) were dissolved in 5.0 mL THF (c = 11.2 mM).

Sol.B: (3-Iodobutyl)benzene (290.9 mg, 1.12 mmol) and naphthalene (75.6 mg, 0.59 mmol) as an internal standard were diluted to 9.0 mL THF solution (c = 0.124 M).

Sol.C: 0.95 mL of PhMgCl in THF (1.85 M) were diluted to 7.0 mL THF solution (c = 0.25 M).

Inside the glove box screw vials with a stirring bar were filled with 0.2, 0.4, 0.6 and 0.8 mL of **Sol.A**, then 1.0 mL of **Sol.B** was added. The vials were filled up with THF to a total volume of 2.0 mL. The vials were closed with a rubber septum. 0.5 mL of **Sol.C** was put in 1.0 mL insulin syringes (the tip of the needle was put in a rubber stopper to minimise the exposure to air). The vials were taken out of the glove box and attached to the Schlenk line by piercing a needle through the septum. The following procedure was done consecutively with every reaction vial: The vial was put in the ethyl acetate slurry and stirred for about 5 minutes (to be sure that the temperature is constant). Then the rubber septum was removed from the vial (while maintaining the nitrogen flow). **Sol.C** was added at once. An aliquot of 100 μL was taken in regular intervals (depending on the complex concentration and hence its reaction rate) and immediately pipetted in a GC vial containing 50 μL acetonitrile. The GC vials were then filled with diethyl ether and analysed by GC (a FI-detector was used for quantification).

The yields of the 1,3-diphenylbutane were determined using naphthalene as an internal standard. Figure 3.34 shows the results (yield versus time) of a single experiment. In order to determine the reaction rate, the data points (up to 10% yield) were fitted linear. The reaction rates were then logarithmised, averaged and then plotted versus the logarithm of [Fe(bopa-Ph)Cl(THF)₂] concentration (Graph B, Figure 3.16).

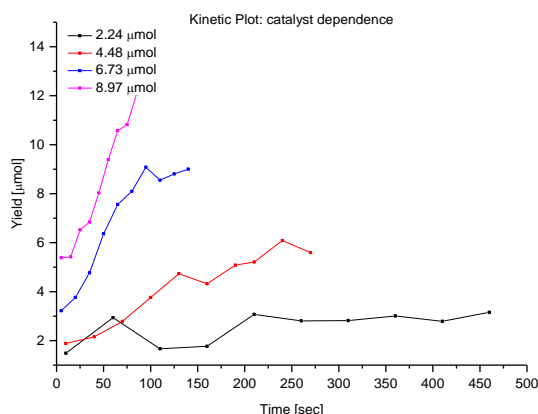


Figure 3.34: Reaction profile of a single experiment under variable concentrations of **3.2**.

3.5.10.3 Dependence on (3-iodobutyl)benzene

General remarks:

In one experiment 6 reaction solutions were prepared with variable substrate concentrations. The reactions were performed in a consecutive order to maintain the same reaction and sampling conditions. For each reaction 10 GC samples were prepared. To achieve a constant reaction temperature a slurry of melting ethyl acetate (m.p. = -84°C) was prepared before the experiment. The example given below depicts one single experiment. In order to determine the order of the reaction the mean value of at eight independent experiments was taken.

Before the experiment three stock solutions were prepared:

Sol.A: (3-Iodobutyl)benzene (244.2 mg, 0.94 mmol) and naphthalene (62.7 mg, 0.49 mmol) as an internal standard were diluted to 5.0 mL THF solution ($c = 0.188\text{ M}$).

Sol.B: $[\text{Fe}(\text{bopa-Ph})\text{Cl}(\text{THF})_2]$ (30.7 mg, 44.2 μmol) were dissolved in 7.0 mL THF ($c = 6.3\text{ mM}$).

Sol.C: 0.54 mL of PhMgCl in THF (1.85 M) were diluted to 4.0 mL THF solution ($c = 0.25$ M).

Inside the glove box screw vials with a stirring bar were filled with 0.5, 0.6, 0.7, 0.8, 0.9 and 1.0 mL of **Sol.A**, then 1.0 mL of **Sol.B** was added. The vials were filled up with THF to a total volume of 2.5 mL. The vials were closed with a rubber septum. 0.5 mL of **Sol.C** was filled in 1.0 mL syringes (the tip of the needle was put in a rubber stopper to minimise the exposure to air). The vials were taken out of the glove box and attached to the Schlenk line by piercing a needle through the septum. The following procedure was done consecutively with every reaction vial: The vial was put in the previously prepared ethyl acetate slurry and stirred for about 5 minutes (to be sure that the temperature is constant). Then the rubber septum was removed from the vial (while maintaining the nitrogen flow). **Sol.C** was added at once. An aliquot of 100 μL was taken every 20 seconds and immediately pipetted in a GC vial containing 50 μL acetonitrile. The GC vials were then filled with diethyl ether and analysed by GC (a FI-detector was used for quantification).

The yields of the 1,3-diphenylbutane were determined in respect to naphthalene as an internal standard. Figure 3.35 shows the results (yield versus time) of a single experiment. In order to determine the reaction rate, the data points (up to 10% yield) were fitted linear. The reaction rates were then logarithmised, averaged and then plotted versus the logarithm of (3-iodobutyl)benzene concentration (Graph C, Figure 3.16).

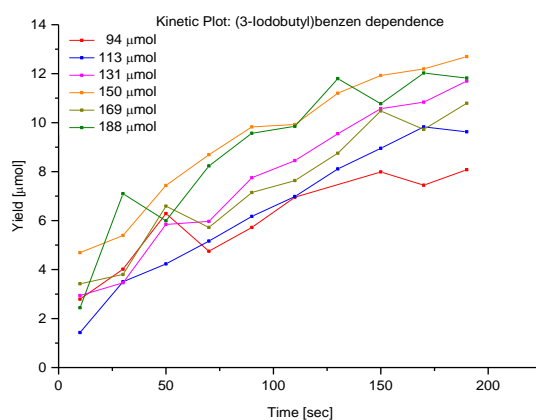


Figure 3.35: Reaction profile of a single experiment under variable concentrations of (3-iodobutyl)benzene.

3.5.10.4 Confirmation of the 0th-order by integrated rate law

General considerations:

The reaction rate v can be calculated as followed (with the previously shown 2nd order for catalyst loading and 1st order for Grignard loading):

$$v = \frac{d[Alkyl]}{dt} = -k[Complex]^2[PhMgCl]^1[Alkyl]^n \quad (\text{Eq. 6})$$

In a reaction where $A + B \rightarrow C$ without any side reaction the $[A] = [B]$ at any time of the reaction. Furthermore, the concentration of the catalyst stays constant throughout the reaction. Hence equation 6 can be simplified to:

$$\begin{aligned} \frac{d[Alkyl]}{dt} &= -k_{eff} * [Alkyl]^1 * [Alkyl]^n \\ &= -k_{eff} * [Alkyl]^{(1+n)} \end{aligned} \quad (\text{Eq. 7})$$

With:

$$k_{eff} = k * [Complex]^2 \quad (\text{Eq. 8})$$

Therefore:

$$\int_{[Alkyl]_0}^{[Alkyl]} \frac{1}{[Alkyl]^{(1+n)}} d[Alkyl] = -k_{eff} \int_{t_0}^t dt \quad (\text{Eq. 9})$$

In case:

$$n = 0: \quad \ln\left(\frac{[Alkyl]}{[Alkyl]_0}\right) = -k_{eff} * t \quad (\text{Eq. 10})$$

$$n = 1: \quad \frac{[Alkyl]_0 - [Alkyl]}{[Alkyl][Alkyl]_0} = k_{eff} * t \quad (\text{Eq. 11})$$

$$n = 2: \quad \frac{[Alkyl]_0^2 - [Alkyl]^2}{2 * ([Alkyl][Alkyl]_0)^2} = k_{eff} * t \quad (\text{Eq. 12})$$

General remarks:

In one experiment two reaction solutions were prepared. The reactions were performed in a consecutive order to maintain the same reaction and sampling conditions. For each reaction 10 GC samples were prepared. To achieve a constant reaction temperature a slurry of melting m-xylene (m.p. = -48°C) was prepared before the experiment.

Before the experiment three stock solutions were prepared:

Sol.A: (3-Iodobutyl)benzene (132.9 mg, 0.51 mmol) and naphthalene (41.9 mg, 0.33 mmol) as an internal standard were diluted to 5.0 mL THF solution (c = 0.102 M).

Sol.B: [Fe(bopa-Ph)Cl(THF)₂] (21.6 mg, 31.1 μmol) were dissolved in 5.0 mL THF (c = 6.2 mM).

Sol.C: 0.54 mL of PhMgCl in THF (1.85 M) were diluted to 4.0 mL THF solution (c = 0.25 M).

Inside the glove box screw vials with a stirring bar were filled with 1.0 mL of **Sol.A** and then 1.0 mL of **Sol.B** was added. The vials were closed with a rubber septum. 0.5 mL of **Sol.C** was put in 1.0 mL insulin syringes (the tip of the needle was put in a rubber stopper to minimise the exposure to air). The vials were taken out of the glove box and attached to the Schlenk line by piercing a needle through the septum. The following procedure was done consecutively with every reaction vial: The vial was put in the previously prepared m-xylene slurry and stirred for

about 5 minutes (to be sure that the temperature is constant). Then the rubber septum was removed from the vial (while maintaining the nitrogen flow). **Sol.C** was added at once. An aliquot of 100 μL was taken every 45 seconds and immediately pipetted in a GC vial containing 50 μL acetonitrile. The GC vials were then filled with diethyl ether and analysed by GC (a FI-detector was used for quantification).

The graphs in Figure 3.36 show the 3 scenarios described above in Eq. 10 - 12.

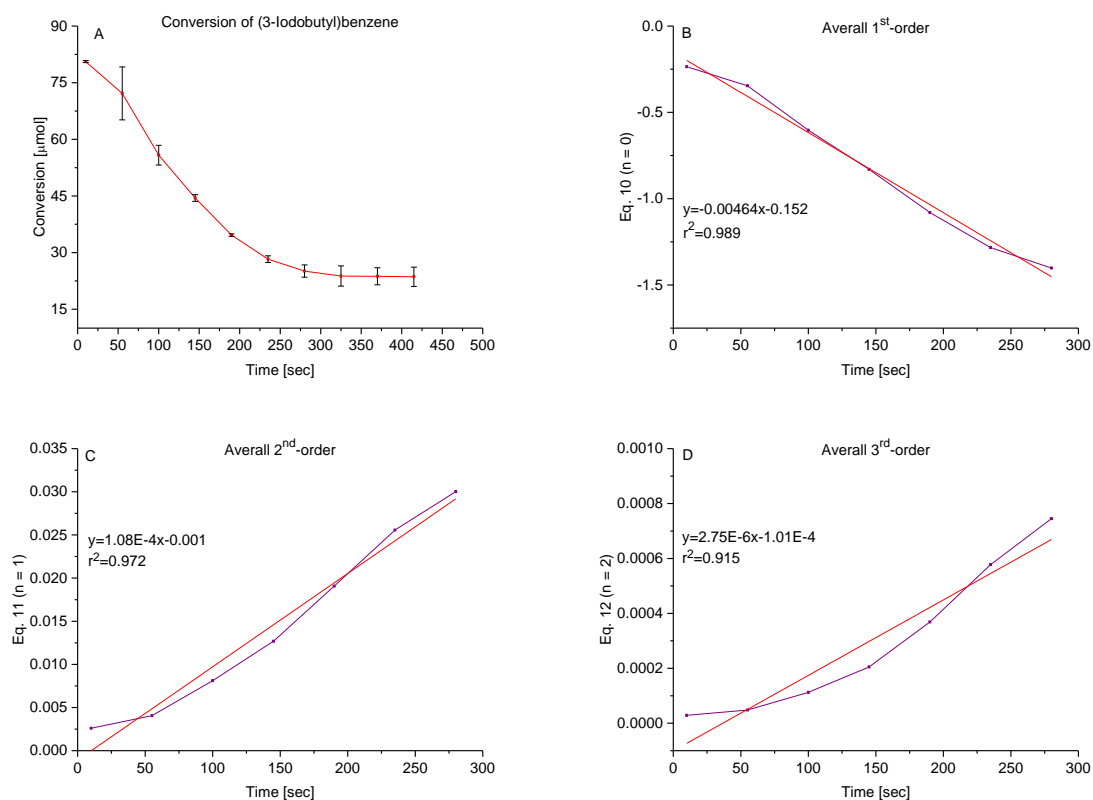


Figure 3.36: Results of the integrated rate law method. Graph A shows the conversion of (3-iodobutyl)benzene over the time. Graphs B – D show the results of Eq. 10 – 12. The last 3 data points at (325, 370 and 415 seconds) were not included in the calculations.

3.5.11 Determination of the Resting State

3.5.11.1 UV-VIS Method

Before the experiment two stock solutions were prepared:

Sol.A: (3-Iodobutyl)benzene (388.1 mg, 1.49 mmol) and [Fe(bopa-Ph)Cl₂] (44.0 mg, 75.2 μmol) were diluted to 5.0 mL THF solution.

Sol.B: 0.97 mL of PhMgCl in THF (1.85 M) was diluted to 5.0 mL THF solution.

Sol.A and **Sol.B** were found to be too concentrated; therefore they were diluted 1:10.

Inside the glove box 28 mL were put in a 50 mL round bottom flask and cooled to -40°C. Then the UV-Probe was tipped in. After 15 minutes 1.0 mL **Sol.A** was added and the measurement was started. Then **Sol.B** was added and a UV-Vis spectrum was measured every 30 seconds for 10 minutes. The reaction was repeated 2 times.

If the reaction was monitored at room temperature, the immediate spectrum of the reaction mixture was identical to that observed after 10 min at -40°C. No intermediate spectrum was observed.

3.5.11.2 NMR Method

Inside the glove box [Fe(bopa-Ph)Cl₂] (2.2 mg, 3.8 μmol, 0.05 equiv) and (3-iodobutyl)benzene (19.6 mg, 75.3 μmol, 1.0 equiv) were weighed in a J.Young-NMR tube and dissolved in 0.5 mL d₈-THF. The solution was cooled to -65°C and 0.050 mL PhMgCl (1.83M in THF, 1.2 equiv) were added. The NMR tube was immediately inserted into the

already tempered NMR and measured. The quality of the spectra is getting increasingly worse, since solid Mg-salts are precipitating in the reaction.

3.5.12 Crystal Structures

3.5.13 [Fe(bopa-Ph)Cl₂] (**3.1**): CCDC number 1004323

Empirical formula	C ₃₀ H ₂₄ Cl ₂ FeN ₃ O ₂
Formula weight	585.27
Temperature	140(2) K
Wavelength	0.71073 Å
Crystal system	Orthorhombic
Space group	P2 ₁ 2 ₁ 2 ₁
Unit cell dimensions	a = 9.829(4) Å α = 90°. b = 13.481(3) Å β = 90°. c = 19.904(7) Å γ = 90°.
Volume	2637.4(15) Å ³
Z	4
Density (calculated)	1.474 Mg/m ³
Absorption coefficient	0.808 mm ⁻¹
F(000)	1204
Crystal size	0.38 x 0.26 x 0.19 mm ³
Theta range for data collection	2.31 to 25.53°.
Index ranges	-11 ≤ h ≤ 11, -16 ≤ k ≤ 16, -22 ≤ l ≤ 22
Reflections collected	4714
Independent reflections	4714 [R _{int} = 0.0000]
Completeness to theta = 25.00°	96.1 %
Absorption correction	None
Refinement method	Full-matrix least-squares on F ²
Data / restraints / parameters	4714 / 0 / 344
Goodness-of-fit on F ²	1.038
Final R indices [I > 2σ(I)]	R1 = 0.0670, wR2 = 0.1592
R indices (all data)	R1 = 0.0880, wR2 = 0.1747
Absolute structure parameter	0.04(3)
Largest diff. peak and hole	0.911 and -0.975 e.Å ⁻³

3.5.14 [Fe(bopa-Ph)Cl(THF)₂] (**3.2**): CCDC number 1004324

Empirical formula	C ₃₈ H ₄₀ ClFeN ₃ O ₄	
Formula weight	694.03	
Temperature	293(2) K	
Wavelength	1.54178 Å	
Crystal system	Tetragonal	
Space group	P4 ₃ 2 ₁ 2	
Unit cell dimensions	a = 16.2274(2) Å	α = 90°.
	b = 16.2274(2) Å	β = 90°.
	c = 13.1625(3) Å	γ = 90°.
Volume	3468.71(11) Å ³	
Z	4	
Density (calculated)	1.329 Mg/m ³	
Absorption coefficient	4.545 mm ⁻¹	
F(000)	1456	
Crystal size	0.28 x 0.25 x 0.19 mm ³	
Theta range for data collection	3.85 to 73.56°.	
Index ranges	-20 ≤ h ≤ 20, -16 ≤ k ≤ 20, -15 ≤ l ≤ 16	
Reflections collected	24779	
Independent reflections	3480 [R _{int} = 0.0408]	
Completeness to theta = 73.56°	99.7 %	
Absorption correction	Semi-empirical from equivalents	
Max. and min. transmission	1.00000 and 0.42332	
Refinement method	Full-matrix least-squares on F ²	
Data / restraints / parameters	3480 / 81 / 242	
Goodness-of-fit on F ²	1.046	
Final R indices [I > 2σ(I)]	R1 = 0.0306, wR2 = 0.0804	
R indices (all data)	R1 = 0.0373, wR2 = 0.0840	
Absolute structure parameter	0.000(4)	
Largest diff. peak and hole	0.229 and -0.295 e.Å ⁻³	

3.5.15 [Fe(bopa-Ph)Cl] (3.4):

Empirical formula	C ₃₀ H ₂₄ ClFeN ₃ O ₂
Formula weight	549.82
Temperature	100(2) K
Wavelength	0.71073 Å
Crystal system	Orthorhombic
Space group	P2 ₁ 2 ₁ 2 ₁
Unit cell dimensions	a = 11.0523(17) Å α = 90°. b = 13.952(2) Å β = 90°. c = 16.3909(16) Å γ = 90°.
Volume	2527.6(6) Å ³
Z	4
Density (calculated)	1445 Mg/m ³
Absorption coefficient	0.736 mm ⁻¹
F(000)	1136
Crystal size	0.43 x 0.39 x 0.32 mm ³
Theta range for data collection	2.22 to 29.99°
Index ranges	-15 ≤ h ≤ 15, -19 ≤ k ≤ 19, -22 ≤ l ≤ 23
Reflections collected	39570
Independent reflections	7337 [R _{int} = 0.0409]
Completeness to theta = 73.56°	99.8 %
Absorption correction	Semi-empirical from equivalents
Max. and min. transmission	0.7460 and 0.5829
Refinement method	Full-matrix least-squares on F ²
Data / restraints / parameters	7337 / 0 / 334
Goodness-of-fit on F ²	1.125
Final R indices [I > 2σ(I)]	R1 = 0.0324, wR2 = 0.0651
R indices (all data)	R1 = 0.0423, wR2 = 0.0700
Absolute structure parameter	0.049(10)
Largest diff. peak and hole	0.331 and -0.292 e.Å ⁻³

3.5.16 [Fe(bopa-Ph)o-Tol] (**3.6**): CCDC number 1004325

Empirical formula	C ₄₁ H ₃₉ FeN ₃ O ₄	
Formula weight	693.60	
Temperature	140(2) K	
Wavelength	0.71073 Å	
Crystal system	Orthorhombic	
Space group	P2 ₁ 2 ₁ 2 ₁	
Unit cell dimensions	a = 10.295(3) Å	α = 90°.
	b = 18.192(4) Å	β = 90°.
	c = 20.799(5) Å	γ = 90°.
Volume	3895.4(17) Å ³	
Z	4	
Density (calculated)	1.183 Mg/m ³	
Absorption coefficient	0.429 mm ⁻¹	
F(000)	1456	
Crystal size	0.41 x 0.36 x 0.21 mm ³	
Theta range for data collection	2.78 to 27.68°.	
Index ranges	-13 ≤ h ≤ 13, -23 ≤ k ≤ 23, -27 ≤ l ≤ 27	
Reflections collected	9032	
Independent reflections	9032 [R _{int} = 0.0000]	
Completeness to theta = 27.68°	99.3 %	
Absorption correction	None	
Refinement method	Full-matrix least-squares on F ²	
Data / restraints / parameters	9032 / 0 / 445	
Goodness-of-fit on F ²	0.941	
Final R indices [I > 2σ(I)]	R1 = 0.0721, wR2 = 0.1602	
R indices (all data)	R1 = 0.1084, wR2 = 0.1797	
Absolute structure parameter	0.03(2)	
Extinction coefficient	0.030(2)	
Largest diff. peak and hole	0.496 and -0.641 e.Å ⁻³	

3.5.17 Computational Details

Geometries of all species were optimised in the gas-phase at the unrestricted M06^{38,39}/def2-SVP level using the “Ultrafine” grid in Gaussian09.⁵² The relative energetics of the various spin states of the Fe complexes **3.6**, **3.3**, **3.15**, **3.16** were confirmed from computations using both the M06 and OPBE^{32,53} functionals (Table 3.5). The latter functional feature OPTZ exchanges, which assists in the accurate reproduction of energies of inorganic complexes with different spin states.⁵⁴⁻⁵⁶ The M06/def2-SVP geometries of relevant compounds were then recomputed as single point energies using a density-dependent dispersion correction³⁴⁻³⁷ appended to the PBE0^{32,33} functional (PBE0-dDsC) with the triple-ζ slater-type

orbital TZ2P basis set in ADF.^{57,58} Solvation corrections (in THF) employed the continuum solvent model for realistic solvents¹⁸ (COSMO-RS), as implemented in ADF. The minimum energy crossing point of **3.16** was located using the “MECP Location Program” of Harvey.⁵⁹ The supplemental file Fe_Coupling_CartesianCoords contains the computed Cartesian coordinates of all of the molecules reported in this study.

Table 3.5: Optimised geometries of relevant complexes in different spin states.

Species	M06/def2-SVP Electronic Energy (hartree)	M06 Relative Energy (kcal/mol)	OPBE/def2-SVP Electronic Energy (hartree)	OPBE Relative Energy (kcal/mol)
3.6 – Singlet	-2621.383964	37.54	-2622.136822	19.30
3.6 – Triplet	-2621.419003	15.55	-2622.155719	7.44
3.6 – Quintet	-2621.443786	0.00	-2622.167577	0.00
3.3 – Doublet	-3081.502578	26.85	-3082.217543	12.14
3.3 – Quartet	-3081.532439	8.11	-3082.234075	1.77
3.3 – Sextet	-3081.545366	0.00	-3082.236894	0.00
3.15 – Singlet	Dissociates	n/a	Dissociates	n/a
3.15 – Triplet	Dissociates	n/a	-3200.534437	11.32
3.15 – Quintet	-3199.824253	0.00	-3200.552481	0.00
3.16 – Doublet	-2739.741886	13.67	-2740.514266	1.16
3.16 – Quartet	-2739.753196	6.57	-2740.512905	2.01
3.16 – Sextet	-2739.763670	0.00	-2740.516107	0.00

Table 3.6: Electronic energies (hartree), free energy corrections (hartree) and solvation corrections (in kcal/mol) for relevant compounds.

Compound	M06/def2-SVP Electronic Energy	M06/def2-SVP Free Energy Correction	PBE0-dDsC/TZ2P Electronic Energy	PBE0-dDSC COMSO-RS Solvation Energy
3.6 + <i>i</i> Pr•	-2739.742173	0.501147	-19.806264	-20.776
TS _{3.6,3.16}	-2739.737126	0.505133	-19.801997	-19.701
3.16 _{Sextet}	-2739.763670	0.508481	-19.824147	-18.343
3.16 _{MECP}	-2739.746587	0.508551	-19.807272	-18.080
3.16 _{Quartet}	-2739.753196	0.511789	-19.818664	-17.771
3.16 _{Quartet}	-2739.760219	0.510125	-19.830210	-19.178
TS _{3.16,3.17}	-2739.739211	0.512545	-19.804448	-18.294
3.17	-2739.802550	0.514368	-19.848242	-18.392
3.3 + <i>i</i> Pr•	-3199.831366	0.503913	-19.972166	-21.329
TS _{3.3,3.15}	-3199.824052	0.511594	-19.963281	-21.128
3.15	-3199.824253	0.512781	-19.964321	-20.899
TS _{3.15,3.2-X}	-3199.819698	0.513414	-19.958890	-21.325
3.2-X	-3199.938674	0.512279	-20.082926	-21.232

Table 3.7: Contributions to reaction free energies (in kcal/mol).

Reaction	M06/def2-SVP Electronic Energy	M06/def2-SVP Free Energy Correction	PBE0-dDsC/TZ2P Electronic Energy	PBE0-dDSC COMSO-RS Solvation Energy
Bimetallic Oxidative Addition				
$3.6+iPr\cdot \rightarrow TS_{3.5,3.16}$	3.16	2.50	2.68	1.08
$TS_{3.6,3.16} \rightarrow 3.16_{Sextet}$	-16.66	2.10	-13.90	1.36
$3.16_{Sextet} \rightarrow 3.16_{MECP}$	10.72	0.04	10.59	0.26
$3.16_{MECP} \rightarrow 3.16_{Quartet}$	-4.15	2.03	-7.15	0.31
$3.16_{Quartet} \rightarrow 3.16'_{Quartet}$	-4.41	-1.04	-7.25	-1.41
$3.16'_{Quartet} \rightarrow TS_{3.16,16}$	13.17	1.52	16.17	0.88
$TS_{3.16,3.17} \rightarrow 3.17_{Quartet}$	-39.75	1.14	-27.48	-0.10
Escape Rebound				
$3.3+iPr\cdot \rightarrow TS_{3.3,3.15}$	4.59	4.82	5.58	0.20
$TS_{3.3,3.15} \rightarrow 3.15$	-0.13	0.74	-0.65	0.23
$3.15 \rightarrow TS_{3.15,3.2-X}$	2.86	0.40	3.41	-0.43
$TS_{3.15,3.2-X} \rightarrow 3.2-X$	-74.66	-0.71	-77.83	0.09

3.6 Appendix

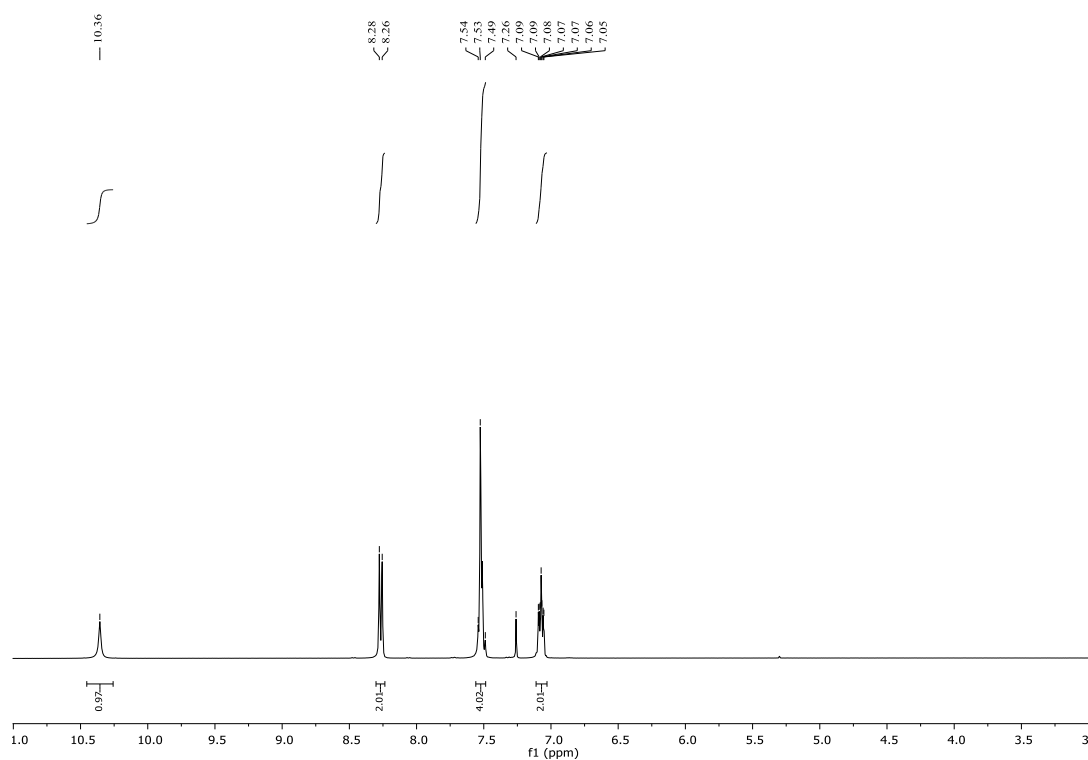


Figure 3.37: ¹H-NMR spectrum of 2,2'-iminodibenzoic acid chloride

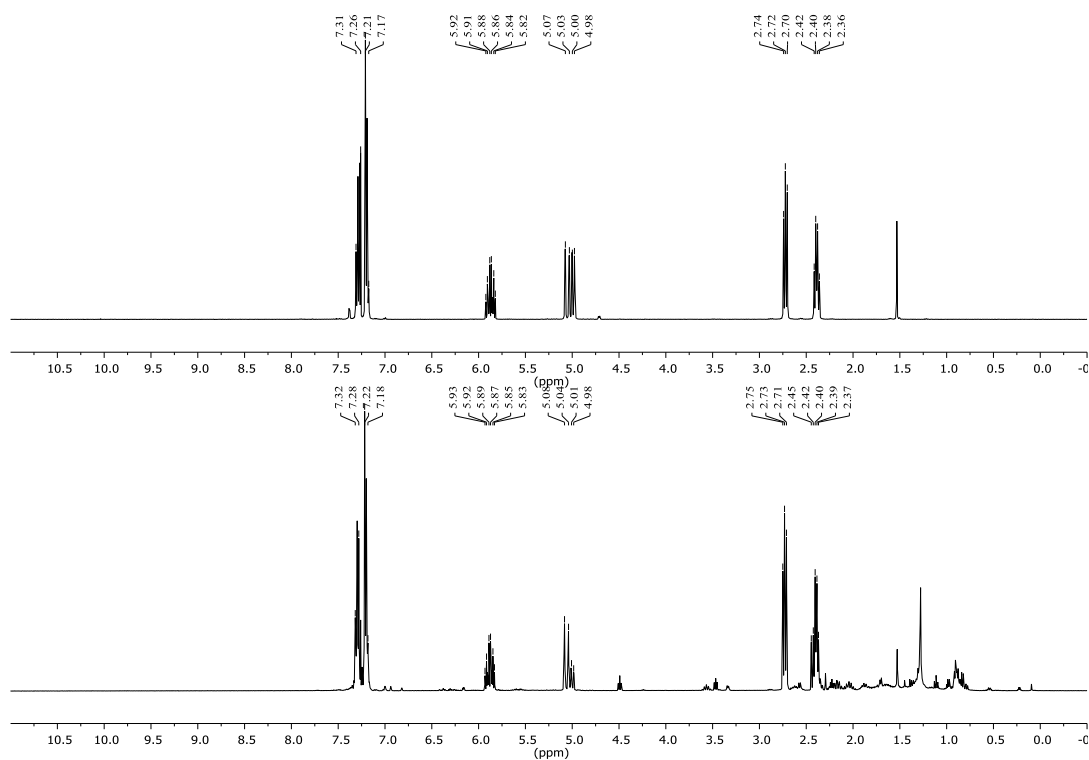


Figure 3.38: Phenylbutene ring opening radical probe.

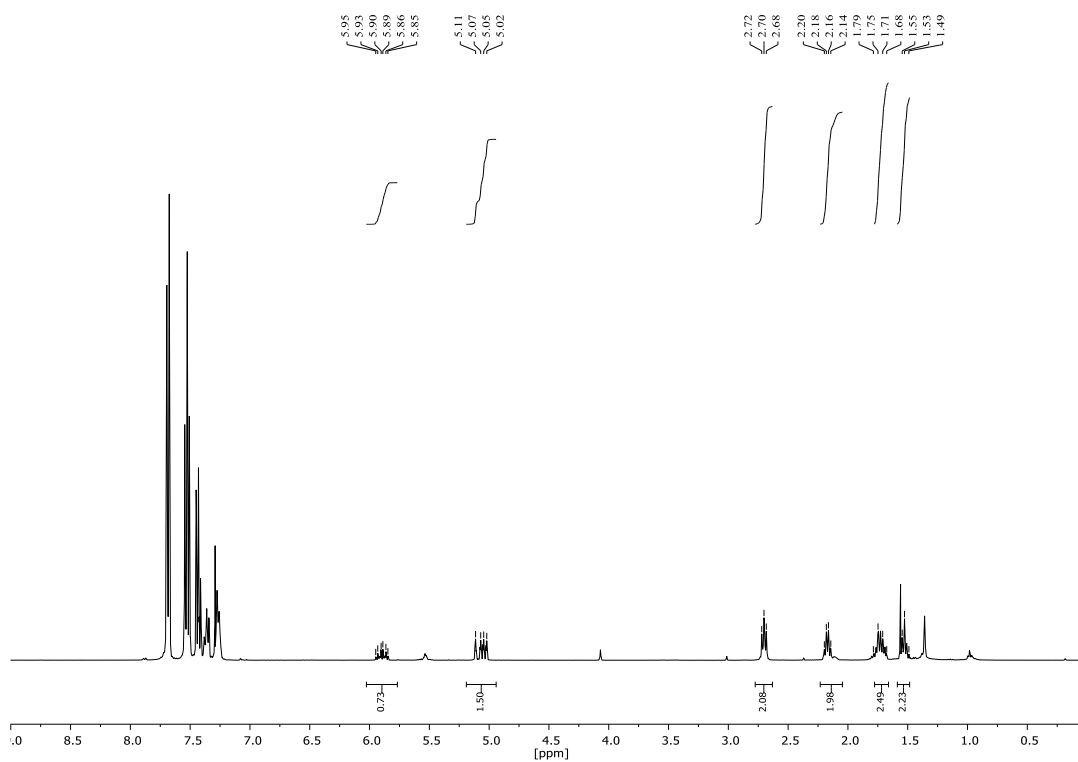


Figure 3.39: $^1\text{H-NMR}$ of 6-Phenyl-1-hexene (with biphenyl impurities).

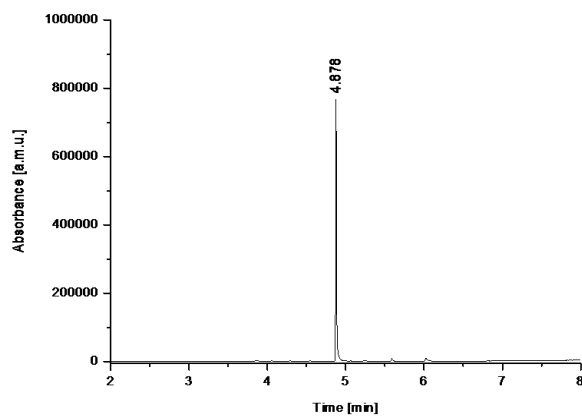


Figure 3.40: GC spectrum of 1,3-diphenylpropane directly synthesised as a reference.

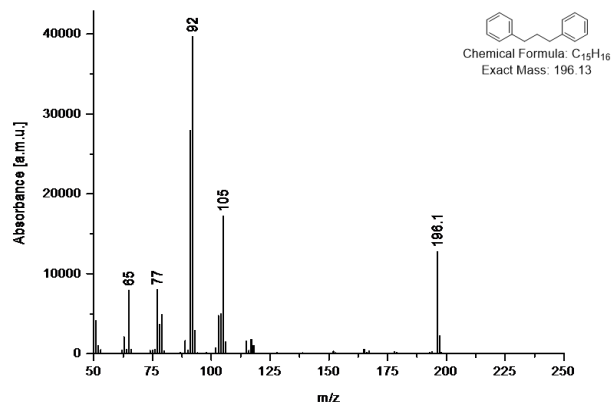


Figure 3.41: Averaged MS-spectrum between 4.87-4.89 min retention time (MS spectrum corresponding to the GC spectrum in Figure 3.40).

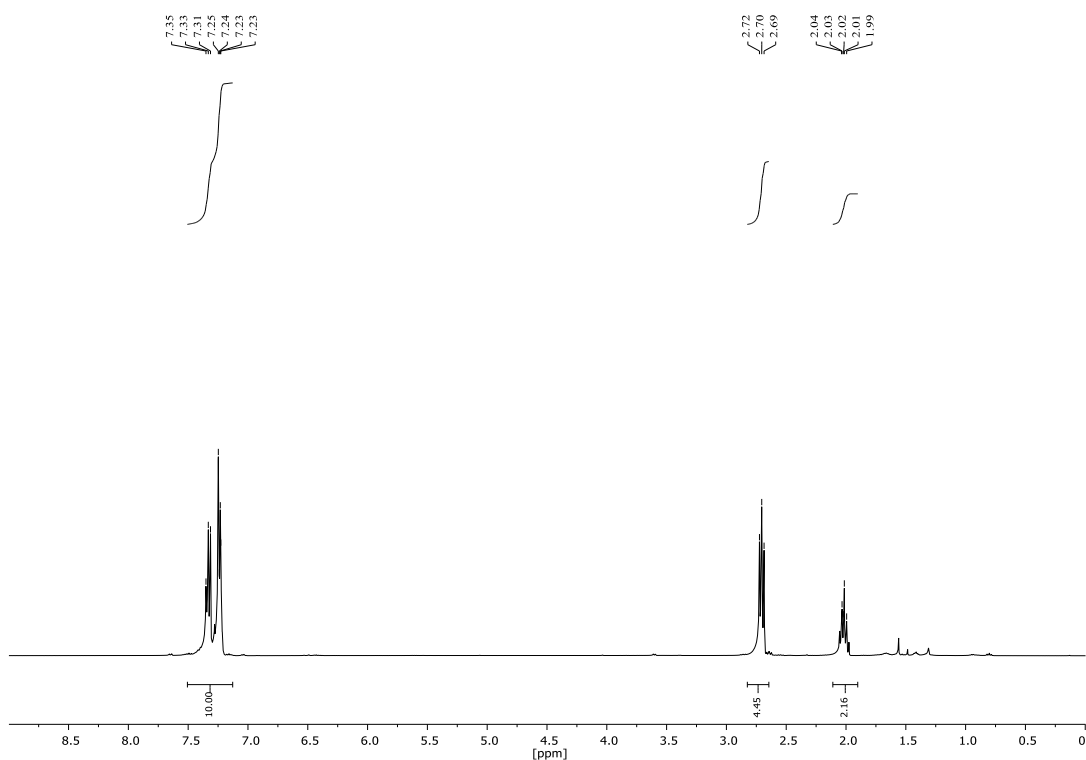


Figure 3.42: $^1\text{H-NMR}$ spectrum of synthesised 1,3-diphenylpropane (corresponding to the GC spectrum in Figure 3.40).

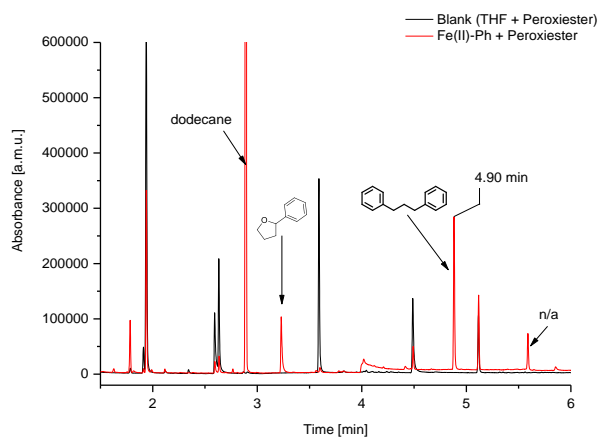


Figure 3.43: Superposition of the reaction of $[\text{Fe}(\text{bopa-Ph})\text{Ph}]$ with *tert*-butyl-4-phenylbutaneperoxate and its blank reaction (*tert*-butyl-4-phenylbutaneperoxate in THF).

3.7 References

- (1) Sherry, B. D.; Fürstner, A. *Acc. Chem. Res.* **2008**, *41*, 1500.
- (2) Rudolph, A.; Lautens, M. *Angew. Chem. Int. Ed.* **2009**, *48*, 2656.
- (3) Fürstner, A.; Martin, R. *Chem. Lett.* **2005**, *34*, 624.
- (4) Leitner, A. In *Iron Catalysis in Organic Chemistry*; Wiley-VCH: Weinheim, 2008, p 147.
- (5) Bolm, C.; Legros, J.; Le Paih, J.; Zani, L. *Chem. Rev.* **2004**, *104*, 6217.
- (6) Martin, R.; Fürstner, A. *Angew Chem Int Edit* **2004**, *43*, 3955.
- (7) Nakamura, M.; Matsuo, K.; Ito, S.; Nakamura, E. *J. Am. Chem. Soc.* **2004**, *126*, 3686.
- (8) Fürstner, A.; Martin, R.; Krause, H.; Seidel, G.; Goddard, R.; Lehmann, C. W. *J. Am. Chem. Soc.* **2008**, *130*, 8773.
- (9) Ghorai, S. K.; Jin, M.; Hatakeyama, T.; Nakamura, M. *Org. Lett.* **2012**, *14*, 1066.
- (10) Nagano, T.; Hayashi, T. *Org. Lett.* **2004**, *6*, 1297.
- (11) Cahiez, G.; Habiak, V.; Duplais, C.; Moyeux, A. *Angew. Chem. Int. Ed.* **2007**, *46*, 4364.
- (12) Czaplik, W. M.; Mayer, M.; Jacobi von Wangelin, A. *Angew. Chem. Int. Ed.* **2009**, *48*, 607.
- (13) Bedford, R. B.; Betham, M.; Bruce, D. W.; Danopoulos, A. A.; Frost, R. M.; Hird, M. *J. Org. Chem.* **2006**, *71*, 1104.
- (14) Bedford, R. B.; Betham, M.; Bruce, D. W.; Davis, S. A.; Frost, R. M.; Hird, M. *Chem. Comm.* **2006**, 1398.
- (15) Fürstner, A.; Krause, H.; Lehmann, C. W. *Angew. Chem. Int. Ed.* **2006**, *45*, 440.
- (16) Noda, D.; Sunada, Y.; Hatakeyama, T.; Nakamura, M.; Nagashima, H. *J. Am. Chem. Soc.* **2009**, *131*, 6078.
- (17) Bedford, R. B.; Brenner, P. B.; Carter, E.; Cogswell, P. M.; Haddow, M. F.; Harvey, J. N.; Murphy, D. M.; Nunn, J.; Woodall, C. H. *Angew. Chem. Int. Ed.* **2014**, *53*, 1804.

- (18) Adams, C. J.; Bedford, R. B.; Carter, E.; Gower, N. J.; Haddow, M. F.; Harvey, J. N.; Huwe, M.; Cartes, M. A.; Mansell, S. M.; Mendoza, C.; Murphy, D. M.; Neeve, E. C.; Nunn, J. *J. Am. Chem. Soc.* **2012**, *134*, 10333.
- (19) Bedford, R. B.; Carter, E.; Cogswell, P. M.; Gower, N. J.; Haddow, M. F.; Harvey, J. N.; Murphy, D. M.; Neeve, E. C.; Nunn, J. *Angew. Chem. Int. Ed.* **2013**, *52*, 1285.
- (20) Guisan-Ceinos, M.; Tato, F.; Bunuel, E.; Calle, P.; Cardenas, D. J. *Chem. Sci.* **2013**, *4*, 1098.
- (21) Inagaki, T.; Ito, A.; Ito, J.; Nishiyama, H. *Angew. Chem. Int. Ed.* **2010**, *49*, 9384.
- (22) Inagaki, T.; Phong, L. T.; Furuta, A.; Ito, J.; Nishiyama, H. *Chem. Eur. J.* **2010**, *16*, 3090.
- (23) See the Experimental for further information.
- (24) Breitenfeld, J.; Ruiz, J.; Wodrich, M. D.; Hu, X. L. *J. Am. Chem. Soc.* **2013**, *135*, 12004.
- (25) Hedstrom, A.; Bollmann, U.; Bravidor, J.; Norrby, P. O. *Chem. Eur. J.* **2011**, *17*, 11991.
- (26) Kinney, R. J.; Jones, W. D.; Bergman, R. G. *J. Am. Chem. Soc.* **1978**, *100*, 635.
- (27) Kinney, R. J.; Jones, W. D.; Bergman, R. G. *J. Am. Chem. Soc.* **1978**, *100*, 7902.
- (28) Biswas, S.; Weix, D. J. *J. Am. Chem. Soc.* **2013**, *135*, 16192.
- (29) Breitenfeld, J.; Wodrich, M. D.; Hu, X. L. *Organometallics* **2014**, doi: 10.1021/om500506y.
- (30) Fossey, J. S.; Lefort, D.; Sorba, J. *Free radicals in organic chemistry*; Wiley, 1995.
- (31) Rueda-Becerril, M.; Chatalova Sazepin, C.; Leung, J. C. T.; Okbinoglu, T.; Kennepohl, P.; Paquin, J.-F.; Sammis, G. M. *J. Am. Chem. Soc.* **2012**, *134*, 4026.
- (32) Perdew, J. P.; Burke, K.; Ernzerhof, M. *Phys. Rev. Lett.* **1996**, *77*, 3865.
- (33) Adamo, C.; Barone, V. *J. Chem. Phys.* **1999**, *110*, 6158.
- (34) Steinmann, S. N.; Corminboeuf, C. *J. Chem. Theory Comput.* **2010**, *6*, 1990.
- (35) Steinmann, S. N.; Corminboeuf, C. *J. Chem. Theory Comput.* **2011**, *7*, 3567.
- (36) Steinmann, S. N.; Corminboeuf, C. *J. Chem. Phys.* **2011**, *134*, 044117.
- (37) Steinmann, S. N.; Corminboeuf, C. *Chimia* **2011**, *65*, 240.
- (38) Zhao, Y.; Truhlar, D. G. *Theor. Chem. Acc.* **2008**, *120*, 215.

- (39) Zhao, Y.; Truhlar, D. G. *Acc. Chem. Res.* **2008**, *41*, 157.
- (40) Klamt, A. *Wiley Interdis. Rev.-Comp. Mol. Sci.* **2011**, *1*, 699.
- (41) Muller, H.; Seidel, W.; Gorls, H. *J. Organomet. Chem.* **1993**, *445*, 133.
- (42) Klose, A.; Solari, E.; Floriani, C.; Chiesivilla, A.; Rizzoli, C.; Re, N. *J. Am. Chem. Soc.* **1994**, *116*, 9123.
- (43) Ni, C. B.; Power, P. P. *Organometallics* **2009**, *28*, 6541.
- (44) Paul, A.; Ladame, S. *Org. Lett.* **2009**, *11*, 4894.
- (45) McKennon, M. J.; Meyers, A. I.; Drauz, K.; Schwarm, M. *J. Org. Chem.* **1993**, *58*, 3568.
- (46) Csok, Z.; Vechorkin, O.; Harkins, S. B.; Scopelliti, R.; Hu, X. L. *J. Am. Chem. Soc.* **2008**, *130*, 8156.
- (47) Inagaki, T.; Phong, L. T.; Furuta, A.; Ito, J.-i.; Nishiyama, H. *Chem. Eur. J.* **2010**, *16*, 3090.
- (48) Crosignani, S.; Nadal, B.; Li, Z.; Linclau, B. *Chem. Comm.* **2003**, 260.
- (49) Love, B. E.; Jones, E. G. *J. Org. Chem.* **1999**, *64*, 3755.
- (50) Lu, S.-F.; Du, D.-M.; Zhang, S.-W.; Xu, J. *Tetrahedron: Asymm.* **2004**, *15*, 3433.
- (51) Gamage, S. A.; Smith, R. A. *J. Tetrahedron* **1990**, *46*, 2111.
- (52) Frisch, M. J.; Trucks, G. W.; Schlegel, H. B.; Scuseria, G. E.; Robb, M. A.; Cheeseman, J. R.; Scalmani, G.; Barone, V.; Mennucci, B.; Petersson, G. A.; Nakatsuji, H.; Caricato, M.; Li, X.; Hratchian, H. P.; Izmaylov, A. F.; Bloino, J.; Zheng, G.; Sonnenberg, J. L.; Hada, M.; Ehara, M.; Toyota, K.; Fukuda, R.; Hasegawa, J.; Ishida, M.; Nakajima, T.; Honda, Y.; Kitao, O.; Nakai, H.; Vreven, T.; Montgomery, J., J. A.; Peralta, J. E.; Ogliaro, F.; Bearpark, M.; Heyd, J. J.; Brothers, E.; Kudin, K. N.; Staroverov, V. N.; Kobayashi, R.; Normand, J.; Raghavachari, K.; Rendell, A.; Burant, J. C.; Iyengar, S. S.; Tomasi, J.; Cossi, M.; Rega, N.; Millam, M. J.; Klene, M.; Knox, J. E.; Cross, J. B.; Bakken, V.; Adamo, C.; Jaramillo, J.; Gomperts, R.; Stratmann, R. E.; Yazyev, O.; Austin, A. J.; Cammi, R.; Pomelli, C.; Ochterski, J. W.; Martin, R. L.; Morokuma, K.; Zakrzewski, V. G.; Voth, G. A.; Salvador, P.; Dannenberg, J. J.; Dapprich, S.; Daniels, A. D.; Farkas, O.; Foresman, J. B.; Ortiz, J. V.; Cioslowski, J.; Fox, D. J.; Gaussian, Inc.: Wallingford, CT, 2009.

- (53) Handy, N. C.; Cohen, A. J. *Mol. Phys.* **2001**, *99*, 403.
- (54) Conradie, J.; Ghosh, A. *J. Phys. Chem. B* **2007**, *111*, 12621.
- (55) Rotzinger, F. P. *J. Chem. Theory Comput.* **2009**, *5*, 1061.
- (56) Curchod, B. F.; Rotzinger, F. P. *Inorg. Chem.* **2011**, *50*, 8728.
- (57) te Velde, G.; Bickelhaupt, F. M.; van Gisbergen, S. J. A.; Fonseca Guerra, C.; Baerends, E. J.; Snijders, J. G.; Ziegler, T. *J. Comput. Chem.* **2001**, *22*, 931.
- (58) Fonseca Guerra, C.; Snijders, J. G.; te Velde, G.; Baerends, E. J. *Theor. Chem. Acc.* **1998**, *99*, 391.
- (59) Harvey, J. N.; Aschi, M.; Schwarz, H.; Koch, W. *Theor. Chem. Acc.* **1998**, *99*, 95.

Chapter 4

Investigation of Active Species in Enantioselective Hydrosilylation of Substituted Acetophenones Catalysed by Bis(oxazolinyldiphenyl)amino Iron(II) Pincer Complexes

4.1 Introduction

While primary and racemic alcohols can be synthesised by standard synthetic routes, synthesis of enantiomerically pure secondary alcohols is often done by enantioselective reduction of prochiral ketones. For this, hydrogenation and transfer hydrogenation reactions are ideal due to their environment friendliness. Owing to the concern of harsh reaction conditions and elevated hydrogen pressures, functional group selectivity, hydrosilylations are developed as an alternative. The silyl ethers that are formed during hydrosilylation are hydrolysed to give the corresponding alcohol.^{1,2} First enantioselective hydrosilylation of carbonyl compounds was published in 1972 by Kumada's group using simple platinum complex with chiral monophosphine as ligand with enantioselectivity below 20%.³

In the last decade the focus for the asymmetric and non-asymmetric reduction of ketones was on iron, copper, titanium and rhodium-based catalysts.² Brunner *et al.* described the first hydrosilylation of acetophenone with diphenylsilane using with Fe(cp)(CO)(L) derived half-sandwich complexes. The reaction proceeded usually under UV irradiation.⁴⁻⁶ More recently Nishiyama *et al.* showed that simple iron(II) acetate in the presence of tmeda, as N-donor ligand, can catalyse the reduction of various ketones to the corresponding silylether. Acidic work-up cleaves the ether leaving back the corresponding alcohol.⁷ The reaction proceeds smoothly in refluxing THF over a time period of 24 hours with yields up to 95%. Efforts were also paid towards enantioselective hydrosilylation by using pybox-Bn and bopa-R (**4.1-R**; **R** = *i*Pr(S), *t*Bu(S)) instead of tmeda. Surprisingly, use of pybox-Bn gave 93% yield and 37% ee. Interestingly, **4.1-*i*Pr(S)** and **4.1-*t*Bu(S)** increased the ee up to 57% and 79%, respectively. The yields for the latter two reactions were slightly lower than with the pybox ligand.⁷ Inagaki *et al.* further screened an extended set of **4.1-R** (**R** = Ph(S), dpm(S) (CH(Ph)₂), *i*Pr(S), *t*Bu(S)) for their scope and limitations with first-row transition metals such as iron, cobalt, nickel and copper. As shown above; iron(II) acetate had remarkably good results with yields from 90 – 99% and ee's up to 73% (Figure 4.1, Equation (2)). The best results were with **4.1-dpm(S)**. Although nickel and copper did not show the expected catalytic results, cobalt(II) acetate in combination with the **4.1-R** ligand was very active for hydrosilylation with yields up to 99% and ee's <94%. Attempts to isolate the active complex by mixing iron(II) acetate with **4.1-R** were unsuccessful. However, they were able to isolate [Fe(bopa-*i*Pr)Cl₂] (**4.2-*i*Pr(S)**) from a refluxing mixture of FeCl₂ and **4.1-*i*Pr(S)** in THF under air (Figure 4.1, Equation (1)). An X-ray

structure confirmed that the ligand and the chlorine substituents take a trigonal-bipyramidal structure around the iron centre with a C_2 symmetry. The two oxazoline substituents position themselves in an apical position. **4.2-*i*Pr(S)** was inactive towards the hydrosilylation of 4-acetylbiphenyl (Figure 4.1, Equation (3)).⁸

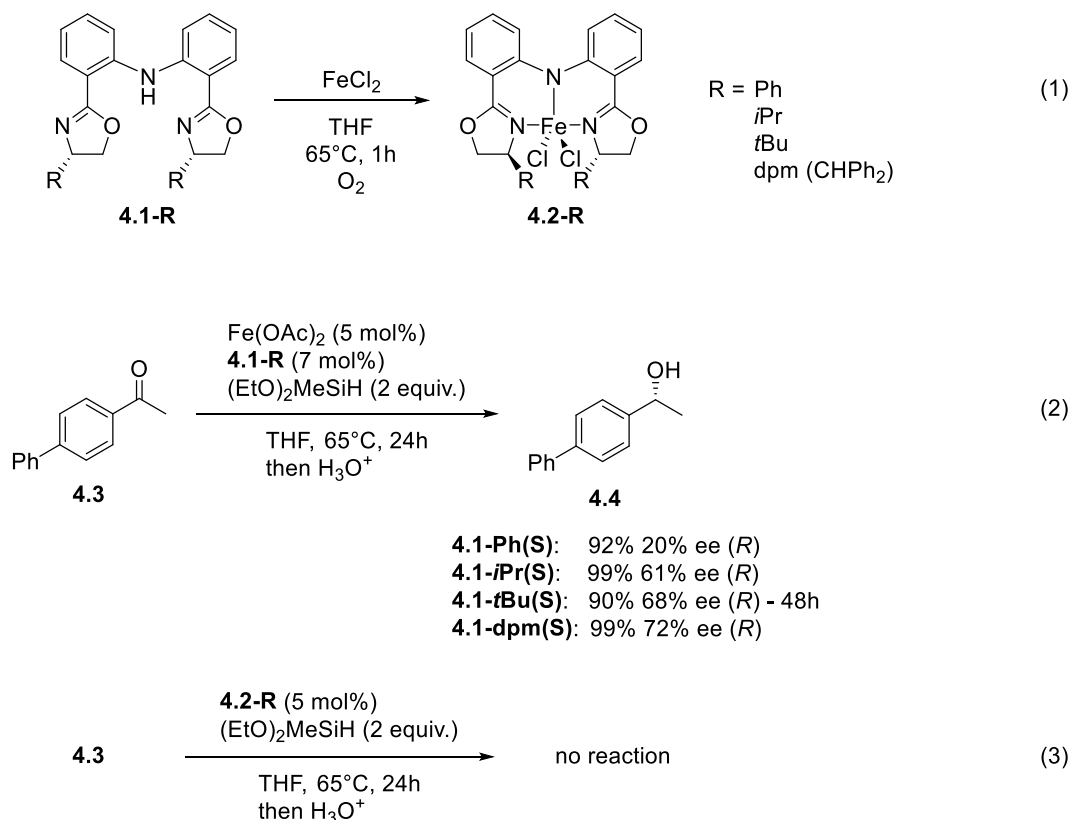


Figure 4.1: Formation of **4.1-R** (equation (1)); Reactivity towards hydrosilylation of 4-acetylbiphenyl (**4.3**) using: Fe(OAc)₂ plus **4.1-R** (equation (2)), **4.2-R** (equation (3)) and **4.2-R** plus additives (equation (4)) as catalyst.⁹

In a further study Inagaki *et al.* were able to show that by adding additives **4.2-R** showed to be catalytically active.⁹ The results are depicted in Table 4.1. The addition of NaOAc and NaO*t*Bu to a solution of **4.3** and **4.2-*i*Pr(S)** (Entries 1 and 2) with a subsequent addition of (EtO)₂MeSiH activated the complex, which gave 97% and 99% yield with 57% and 55% ee with the *R* enantiomer in excess. The addition of copper and manganese did not promote the reduction (Entries 3 and 4), but the addition of magnesium activated complex **4.2-*i*Pr(S)** with 92% yield and 15% (*R*) ee (Entry 5). The addition of zinc, however, lowered the yield to 60% after 24 hours (Entry 6). Leaving the reaction for 48 hours increased the yield to 97% with change in ee (Entry 7). These reactions gave 44% (*S*) and 41% (*S*). This was an interesting finding since the standard reaction conditions (Figure 4.1, Equation (2)) gave predominantly

the R enantiomer. Inagaki *et al.* then probed the involvement of zinc in the reaction. The addition of ligand **4.1-*i*Pr(S)** to a mixture of **4.2-*i*Pr(S)** and zinc inhibited the reaction (Entry 8). ZnEt₂ also activated **4.2-*i*Pr(S)** for hydrosilylation (Entry 9). 33% ee (S) were observed. Addition of ZnCl₂ completely retarded the reaction (Entry 10). Although, ZnCl₂ itself showed to be a potent catalyst yielding 97% racemic product (Entry 11), in combination with **4.1-*i*Pr(S)** it showed no reaction (Entry 12). However, using Zn(OAc)₂ in combination with **4.1-*i*Pr(S)** showed the formation of 96% alcohol with an ee of 21% (R) (Entry 13). Adding zinc to a mixture of Fe(OAc)₂ and **4.1-*i*Pr(S)** (Entry 14) lowered the ee to 23% (R). **4.2-Ph(S)** and **4.2-dpm(S)** could be also successfully activated by adding zinc, giving predominantly the S-enantiomer in an excess of 21% and 65%, respectively.⁹

Table 4.1: Reduction of **4.3** via hydrosilylation using **4.2-R** with various additives.⁹

Entry	Cat., Additive (mol%)	t [h]	Yield [%] (recovered 4.3 [%])	ee [%]
1	4.2-<i>i</i>Pr(S) , NaOAc (9)	24	97	57 (R)
2	4.2-<i>i</i>Pr(S) , NaOtBu (9)	24	99	55 (R)
3	4.2-<i>i</i>Pr(S) , Cu (10)	48	n.r.	–
4	4.2-<i>i</i>Pr(S) , Mn (10)	24	n.r.	–
5	4.2-<i>i</i>Pr(S) , Mg (10)	24	92	15 (R)
6	4.2-<i>i</i>Pr(S) , Zn (6)	24	60 (40)	44 (S)
7	4.2-<i>i</i>Pr(S) , Zn (6)	48	97	41 (S)
8	4.2-<i>i</i>Pr(S) , Zn (6), 4.1-<i>i</i>Pr(S) (7)	48	n.r.	–
9	4.2-<i>i</i>Pr(S) , ZnEt ₂ (5)	24	64 (36)	33 (S)
10	4.2-<i>i</i>Pr(S) , ZnCl ₂ (4.5)	24	n.r.	–
11	–, ZnCl ₂ (5)	24	97	–
12	–, ZnCl ₂ (5), 4.1-<i>i</i>Pr(S) (7)	48	n.r.	–
13	–, Zn(OAc) ₂ (5), 4.1-<i>i</i>Pr(S) (7)	48	96 (3)	21 (R)
14	–, Fe(OAc) ₂ (5), 4.1-<i>i</i>Pr(S) (6), Zn (8)	48	83 (17)	23 (R)
15	4.2-Ph(S) , Zn (6)	48	67 (32)	21 (S)
16	4.2-dpm(S) , Zn (6)	48	98 (2)	65 (S)

The effect of zinc as an additive on the enantioselectivity proved to be interesting for further investigation of the reaction mechanism. Inagaki *et al.* first followed the reduction of **4.2-*i*Pr(S)** with Zn by UV-Vis spectroscopy. The initial green solution changed to yellow upon addition of Zn. The resulting UV-Vis spectra showed the disappearance of a peak at 631 nm. This peak is characteristic for the iron(III) complex. Further a new peak at 432 nm was formed. Magnetic susceptibility measurements showed that the initial Fe(III) high spin complex ($5.9 \mu_B$) was reduced by Zn to an Fe(II) high spin complex ($4.8 \mu_B$). Besides these findings no catalytic relevant species could be isolated and characterised.⁹

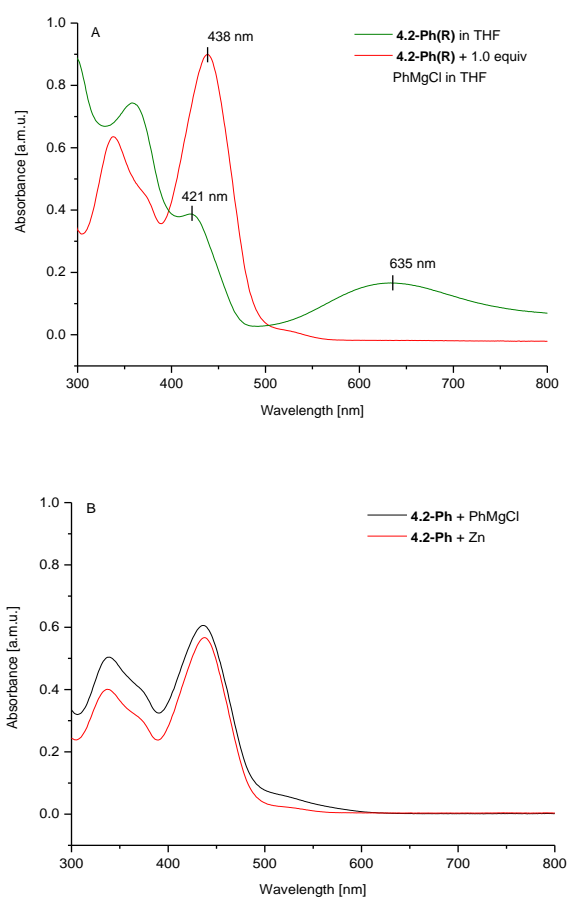


Figure 4.2: Reduction of **4.2-Ph(R)** with either 1.0 equiv. of PhMgCl or an excess of Zn.

In the previous chapter on the mechanistic investigation of the Kumada coupling reaction we were able to show that **4.2-R** got reduced by addition of 1.0 equivalents of aryl Grignard reagent. Interestingly the resulting UV-Vis spectrum from the reduced complex $[\text{Fe}(\text{bopa-Ph})\text{Cl}(\text{THF})_2]$ (**4.5-Ph(R)**) showed similarities to the reduction with zinc. The peak at 635 nm completely disappeared and new peak at 438 nm appeared (Figure 4.2, Graph A).

We therefore believed that zinc reduces $[\text{Fe}(\text{bopa-Ph})\text{Cl}_2]$ to $[\text{Fe}(\text{bopa-Ph})\text{Cl}(\text{THF})_2]$ in a THF solution. To confirm this theory we followed the reduction by UV-Vis and confirmed the outcome with results of the reduction with aryl Grignard reagent (Figure 4.2, Graph B). Indeed, both gave the same results. The formation of **4.5-Ph(R)** was further confirmed by isolating single crystals and elemental analysis. XRD measurement gave the same structure as in Figure 3.3. The confirmation of some key intermediates in hand we decided to further investigate the involved mechanism.

4.2 Acetate Route

4.2.1 Results

To begin this project, we chose the ligands **4.1-Ph(R)** and **4.1-*i*Pr(S)** using 4-acetylbiphenyl (**4.3**) as a model substrate. The catalyst was formed *in situ* by mixing $\text{Fe}(\text{OAc})_2$ and **4.1-R** in refluxing THF for an hour. After addition of 4-acetylbiphenyl (**4.3**) and the $(\text{EtO})_2\text{MeSiH}$ (2.0 equiv.), reaction was kept at 65°C for 24 hours. In both cases 96% 1-biphenylethanol (**4.4**) were obtained with an ee of 27% (S) and 52% (R). These results were in accordance with the previously published results. We then tried to isolate catalytic relevant species in order to have detail mechanistic information.^{8,9}

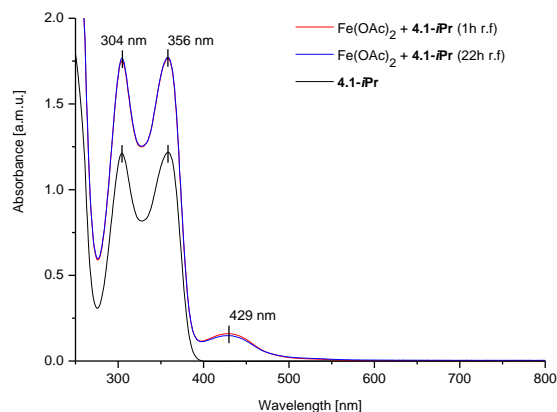


Figure 4.3: Comparison of the free ligand (black line) with *in situ* formed iron species (red line: conversion after 1h; blue line reaction after 22h).

For further investigation, complex formation between **4.1-*iPr*(S)** and $\text{Fe}(\text{OAc})_2$ in refluxing THF was monitored by UV-Vis spectroscopy. After one and 22 hours aliquots of the reaction were measured. Figure 4.3 shows the formation of a new species (peak formation at 429 nm). The concentration of this new species stays the same regardless if the reaction was kept at 65°C for one or 22 hours. The dominating species in the UV-Vis spectrum is still the free ligand (peaks at 304 nm and 356 nm).

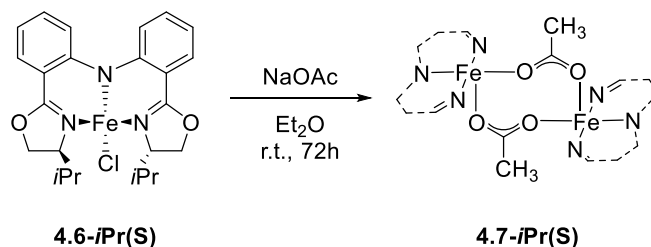


Figure 4.4: Synthesis of complex **4.7-*iPr*(S)**. The bopa-*iPr* ligand of **4.7-*iPr*(S)** has been simplified for clarity reasons.

Since isolation of the complex was not possible, we hypothesised possible structures that can evolve from the reaction of **4.1-*iPr*(S)** with $\text{Fe}(\text{OAc})_2$. Assuming that there is no redox chemistry involved in the complex formation, the final complex should be an iron(II) complex which features structural similarities to complex **4.5-R**, $[\text{Fe}(\text{bopa-R})\text{Cl}(\text{THF})_2]$. Indeed mixing a suspension of complex $[\text{Fe}(\text{bopa-}i\text{Pr})\text{Cl}]$ (**4.6-*iPr*(S)**) with one equivalent of NaOAc in Et_2O at room temperature over three days yielded in a complete dissolution of the complex **4.6-*iPr*(S)** (Figure 4.4). Removal of the solvent afforded $[(\text{Fe}(\text{bopa-}i\text{Pr})\text{OAc})_2]$ (**4.7-*iPr*(S)**) as red powder

in 73% yield. An alternative synthetic pathway could be by first lithiating **4.1-*i*Pr(S)** and further transmetalation with $\text{Fe}(\text{OAc})_2$. **4.7-*i*Pr(S)** was characterised by elemental analysis and X-ray diffraction. The solid-state structure shows a dimeric structure with the acetates as bridging ligands. The iron(II) centre is 5-coordinated and has a distorted square pyramidal structure. The bopa-ligand coordinates in a meridonal configuration around the iron centre.

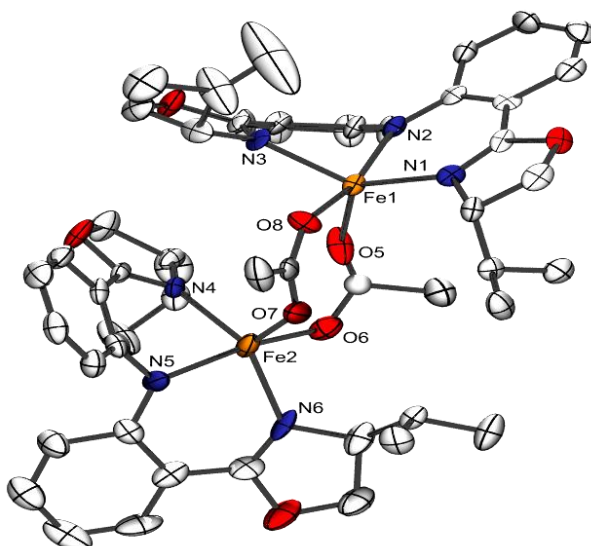
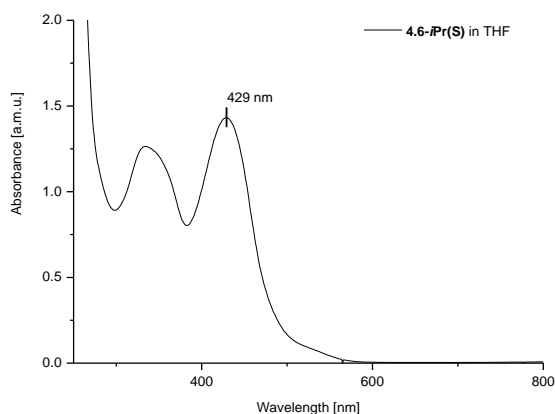
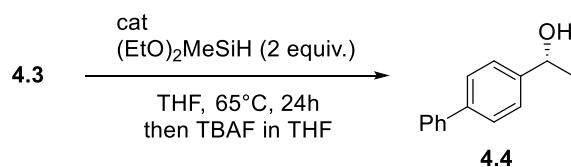


Figure 4.5: The molecular structure of complex **4.7-*i*Pr(S)**. Hydrogen atoms are omitted for clarity. The thermal ellipsoids are displayed at a 50% probability. Selected bond lengths (Å) and angles (deg): Fe(1)-O(8) 1.974(6); Fe(1)-N(2) 2.080(5); Fe(1)-N(1) 2.110(5); Fe(1)-N(3) 2.115(6); Fe(1)-O(5) 2.133(5); Fe(2)-O(6) 2.024(6); Fe(2)-N(4) 2.075(5); Fe(2)-N(6) 2.106(5); Fe(2)-O(7) 2.125(4); Fe(2)-N(5) 2.132(5); O(8)-Fe(1)-N(2) 103.4(2); O(8)-Fe(1)-N(1) 106.8(2); N(2)-Fe(1)-N(1) 84.2(2); O(8)-Fe(1)-N(3) 108.6(2); N(2)-Fe(1)-N(3) 84.1(2); N(1)-Fe(1)-N(3) 144.4(2); O(8)-Fe(1)-O(5) 98.9(2); N(2)-Fe(1)-O(5) 157.2(2); N(1)-Fe(1)-O(5) 94.2(2); N(3)-Fe(1)-O(5) 84.2(2); O(6)-Fe(2)-N(4) 119.9(2); O(6)-Fe(2)-N(6) 105.5(2); N(4)-Fe(2)-N(6) 134.6(2); O(6)-Fe(2)-O(7) 96.2(2); N(4)-Fe(2)-O(7) 90.61(18); N(6)-Fe(2)-O(7) 85.76(19); O(6)-Fe(2)-N(5) 100.8(2); N(4)-Fe(2)-N(5) 86.19(19); N(6)-Fe(2)-N(5) 83.94(19); O(7)-Fe(2)-N(5) 162.01(18)

To compare the newly formed species with the *in situ* formed complex, **4.7-*i*Pr(S)** was dissolved in THF and measured by UV-Vis. Figure 4.6 shows the UV-Vis spectrum of **4.7-*i*Pr(S)**. The peak at 429 nm indicates that the species may be also formed in the reaction of **4.1-*i*Pr(S)** with $\text{Fe}(\text{OAc})_2$. Further relating the concentration of the complex solution with the peak intensity, the conversion of **4.7-*i*Pr(S)** in Figure 4.3 can be estimated to 10%. Due to the overlap of the free ligand to the formed complex it is difficult to tell whether **4.7-*i*Pr(S)** is present or not.

Figure 4.6: UV-Vis spectrum of **4.7-*i*Pr(S)**.

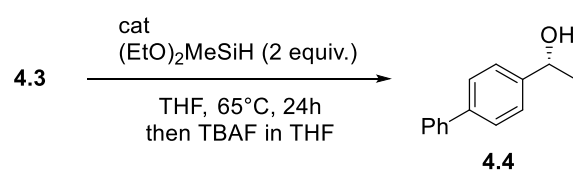
Complex **4.7-*i*Pr(S)** was then employed in reduction of **4.3** with $(\text{EtO})_2\text{MeSiH}$ to compare the reactivity to the previously published results. Additionally, complex **4.7-*i*Pr(S)** was formed *in situ* by mixing **4.5-*i*Pr(S)** with NaOAc.

Table 4.2: Reduction of **4.3** *via* hydrosilylation using **4.2-R** employing pre- and *in situ* formed complex **4.7-*i*Pr(S)**.

Entry	Cat., Additive (mol%)	t [h]	Yield [%]	ee [%]
1	4.7-<i>i</i>Pr(S) (5), –	24	>99	48 (<i>R</i>)
2	4.5-<i>i</i>Pr(S) (5), NaOAc (6)	24	>99	45 (<i>R</i>)
3	$\text{Fe}(\text{OAc})_2$ (5), 4.1-<i>i</i>Pr(S) (10)	24	96	52 (<i>R</i>)

The pre-formed and the *in situ* formed complexes **4.7-*i*Pr(S)** (Table 4.2, Entries 1 and 2) showed similar reactivity as the result obtained following the literature procedure (Table 4.2, Entry 3) which confirms that the reaction proceeds *via* formation of $[(\text{Fe}(\text{bopa-*i*Pr})\text{OAc})_2]$. To compare the reactivity the reaction was further monitored over time.

Table 4.3: Evolution of yield and ee over time.



Entry	Cat., Additive (mol%)	2h ^a	4h ^a	6h ^a	22h ^a	24h ^a
1	4.7-<i>i</i>Pr(S) (5), –	>90 (54 <i>R</i>)	>90 (55 <i>R</i>)	>90 (55 <i>R</i>)	>90 (55 <i>R</i>)	>90 (55 <i>R</i>)
2	4.5-<i>i</i>Pr(S) (5), NaOAc (6)	48 (40 <i>R</i>)	>90 (53 <i>R</i>)	>90 (53 <i>R</i>)	>90 (53 <i>R</i>)	>90 (54 <i>R</i>)
3	Fe(OAc) ₂ (5), 4.1-<i>i</i>Pr(S) (10)	n/a (0)	26 (4 <i>R</i>)	36 (23 <i>R</i>)	90 (53 <i>R</i>)	>90 (53 <i>R</i>)

^a Yield (ee) [%]; the yield and ee were determined by HPLC.

Complex **4.7-*i*Pr(S)** showed high reactivity (Table 4.3, Entry 1) and the reaction is almost completed after two hours. The *in situ* formed complexes (Table 4.3, Entries 2 and 3) showed an induction period, which is related to the slow formation of the complex.

To get some insights about the reactivity, **4.7-*i*Pr(S)** was mixed with (EtO)₂MeSiH. Upon addition a colour shift to a deeper red was observed. Attempts to isolate a reaction product were unsuccessful. We could just isolate complex **4.7-*i*Pr(S)**.

4.2.2 Discussion

Most recently Bleith *et al.* reported the enantioselective hydrosilylation of ketones using (R)-boxmiH-R ligand system (Figure 4.7).¹⁰ The boxmiH-R ligand has structural similarity to the bopa ligand system. The reported yields were >95% with ee's up to 99%.

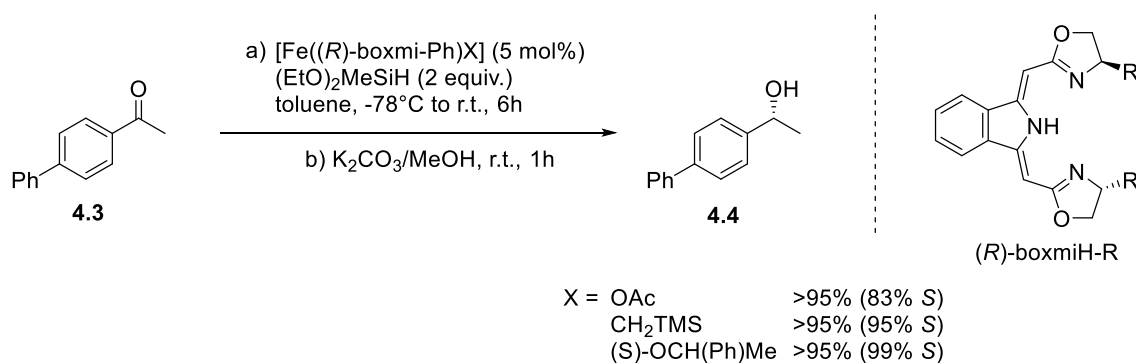


Figure 4.7: Hydrosilylation of 4-acetylbiphenyl employing (*R*)-boxmi-R iron(II) pincer complexes.¹⁰

Based on experimental evidence Bleith *et al.* proposed an inner sphere mechanism. Activation of the pre-catalyst forms an iron-alkoxy species that undergoes σ -bond metathesis with hydrosilane to give the silylether and iron-hydride species. The prochiral ketone immediately coordinates to the hydrido complex and subsequently inserts into the metal hydride bond to reform the iron-alkoxy complex.¹⁰

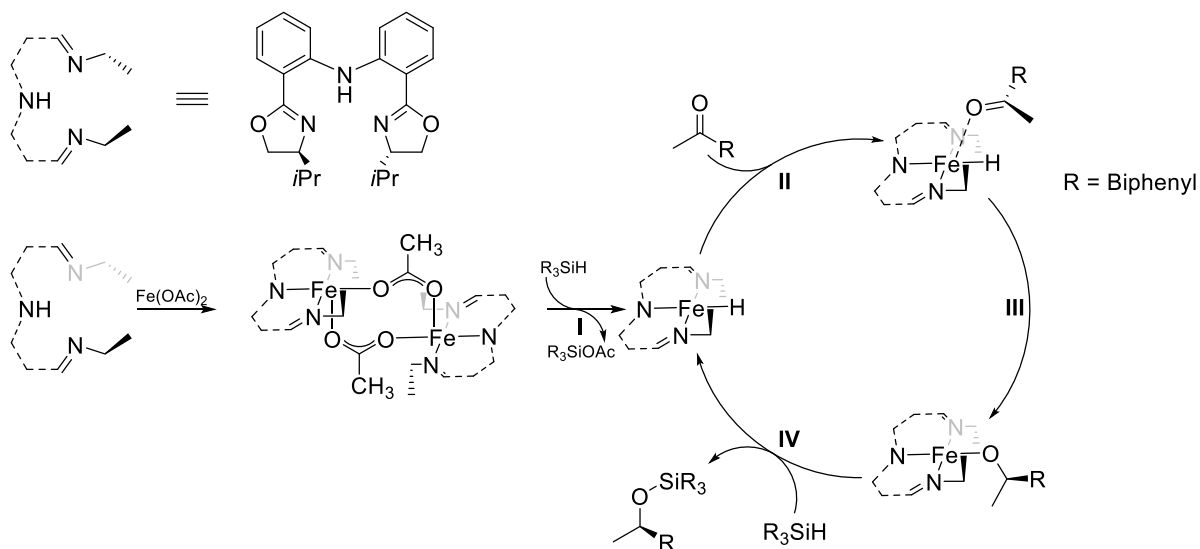


Figure 4.8: Proposal for a catalytic cycle following an inner sphere mechanism.

Given the similarities to the above mentioned system we assume that the catalytic cycle also proceeds *via* an inner sphere route rather than an outer sphere mechanism. Adding $(\text{EtO})_2\text{MeSiH}$ to a THF solution of $[(\text{Fe}(\text{bopa-R})\text{OAc})_2]$ leads to the formation of an iron hydride complex (Figure 4.8, Reaction I).^{11,12} Though, it is uncertain whether this reaction goes *via* oxidative addition to an iron(IV) species, with and subsequent reductive elimination of the

silyl ester, or *via* a σ -bond metathesis. Bleith *et al.* proposed the metathesis pathway due to the fact that iron preferably undergoes SET (or no formal change of the oxidation state) rather than a two electron oxidative addition and reductive elimination.¹⁰ The isolation of the hydride species was not yet successful. To confirm its existence some other experiments should be undertaken: (1) The formation of the iron(II) hydrido complex also produces one equivalent of (diethoxymethylsilyl)acetate which should be traceable by NMR and/or GC. (2) Metal-hydrides normally react with CCl_4 or benzylic chloride to give either chloroform or toluene; the hydride species can be detected by adding one of the two afore mentioned reagents to a THF solution of **4.7-R** and $(\text{EtO})_2\text{MeSiH}$. The hydride formation is then followed by coordinating a ketone to the metal centre (Reaction **II**) which then subsequently inserts into the iron-hydride bond to form an iron(II) alkoxy species (Reaction **III**). Further exchange with another silane gives the desired silyl ether and again the iron hydrido complex (Reaction **IV**).

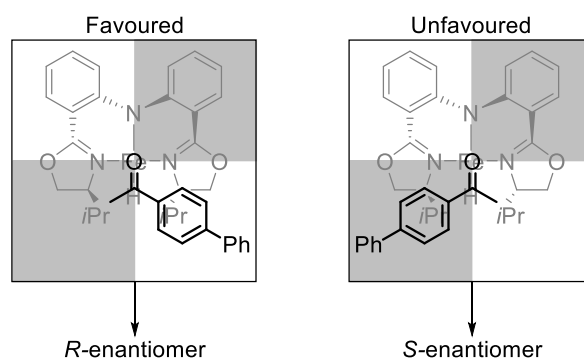


Figure 4.9: Quadrant diagram of the carbonyl coordination. The left diagram shows the scenario that forms the R enantiomer. The right diagram shows the scenario that forms the S-enantiomer.

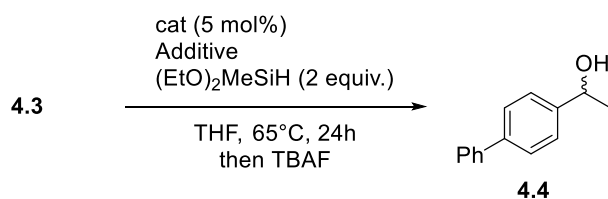
This assumption that the reaction proceeds *via* an inner sphere mechanism is in accordance to the formed enantiomer and the high enantioselectivities of up to 90%.^{8,9} Figure 4.9 shows the sketch of an iron(II) hydride species in a quadrant diagram. Due to steric reasons, the ketone approaches the complex with the bulky residue on the right side (left diagram). Which yields into the preferred formation of the R enantiomer. In the right diagram the more bulky residue of the substrate overlaps with the chiral residue of the ligand, which would be unfavourable. Scenarios where the reduction of the carbonyl take place away from the iron centre, would lead to a lower selectivity.

4.3 Zinc Route

4.3.1 Results

Prior to the coupling reaction $[\text{Fe}(\text{bopa-R})\text{Cl}_2]$ (**4.2-R**) was activated with zinc in refluxing THF solution. The reaction was started by addition of the ketone and $(\text{EtO})_2\text{MeSiH}$. In Chapter 4.1 we already showed that $[\text{Fe}(\text{bopa-R})\text{Cl}_2]$ (**4.2-R**) react with an excess amount of zinc in THF solution at room temperature to give reduced $[\text{Fe}(\text{bopa-R})\text{Cl}(\text{THF})_2]$ (**4.5-R**). Complex **4.5-Ph(R)** was already shown to be the catalytic active species in the Kumada cross coupling reaction of unactivated alkyl-halides with aryl Grignard reagents.¹³ **4.5-*i*Pr(S)** and **4.5-Ph(R)** were then taken to further elucidate a possible mechanism. Out of convenience reasons the tetrahedral analogue – $[\text{Fe}(\text{bopa-R})\text{Cl}]$ (**4.6-R**) – was taken. **4.5-R** is then formed *in situ* when dissolved in THF (compare Chapter 3.2.1 for the reactivity of **4.6-R**). Firstly, we tried to artificially mimic the reaction conditions which are present during the cross coupling reaction.⁹ Therefore, **4.5-*i*Pr(S)** and **4.5-Ph(R)** were used as a catalyst and the influence of various additives was probed. The results were then compared to the results of **4.2-*i*Pr(S)** and **4.2-Ph(R)** reduced *in situ* with zinc metal.

In general, we were not yet able to reproduce the results published by Inagaki *et al.*⁹ In the hydrosilylation reaction of **4.3** (4-acetylbiphenyl) using **4.2-Ph(S)** and **4.2-*i*Pr(S)** 67% yield with 21% (S) ee and 97% yield with 41% (S) ee were achieved (compare Table 4.1, Entries 7 and 15). **4.2-Ph(R)** in combination with zinc and activated zinc (Table 4.4, Entries 1 and 2) gave higher yields and the ee's were in the same range (87% with 19% (R) ee and 85% with 26% (R) ee). For complex **4.2-*i*Pr(S)** (Table 4.4, Entries 5 and 6) the results seemed more arbitrary and random. In the case of unactivated zinc (Entry 5) 58% alcohol were produced with 30% (S) ee. For the reaction with activated zinc (Entry 6) 75% of product were obtained with an ee of 12% (S). The yields and ee's of both reactions were below the previously published results. More interesting were the results using **4.6-R** as a catalyst. Both the phenyl and *iso*-propyl complex yielded racemic mixtures (Entries 3 and 7). This shows that complex **4.6-R** itself is not the catalytic relevant species. Zinc has to be involved in the reaction.

Table 4.4: Reduction of **4.3** via hydrosilylation probing the influence of zinc derivatives as additives.

Entry	Cat., Additive (mol%)	t [h]	Yield [%] ^a	ee [%]
1	4.2-Ph(R) , Zn (6)	48	87	19 (<i>R</i>)
2	4.2-Ph(R) , Zn ^b (6)	48	85	26 (<i>R</i>)
3	4.6-Ph(R) , –	48	42	1 (<i>R</i>)
4	4.6-Ph(R) , ZnCl ₂ (5)	48	42	1 (<i>R</i>)
5	4.2-<i>i</i>Pr(S) , Zn (6)	48	58	30 (<i>S</i>)
6	4.2-<i>i</i>Pr(S) , Zn ^b (6)	48	75	12 (<i>S</i>)
7	4.6-<i>i</i>Pr(S) , –	48	89	2 (<i>R</i>)
8	4.6-<i>i</i>Pr(S) , ZnCl ₂ (5)	48	20	4 (<i>S</i>)
9	4.6-<i>i</i>Pr(S) , ZnCl ₂ (2.5)	48	31	2 (<i>S</i>)
10	4.6-<i>i</i>Pr(S) , ZnCl ₂ (2.5), Zn (5)	48	48	5 (<i>S</i>)
11	4.2-<i>i</i>Pr(S) , Zn (12)	48	38	1 (<i>S</i>)
12	4.2-<i>i</i>Pr(S) , Zn (18)	48	25	5 (<i>S</i>)
13	ZnCl ₂ , 4.1-<i>i</i>Pr(S) (6)	48	24	5 (<i>S</i>)
14	ZnCl ₂ , (bopa- <i>i</i> Pr(S)) ⁻ Li ⁺ (6)	48	91	22 (<i>R</i>)
15	[Zn(bopa- <i>i</i> Pr(S))Cl], –	48	8	13 (<i>S</i>)

^a Isolated yields. ^b Zinc powder was activated with HCl prior to use following the literature procedure.¹⁴

Adding 5 or 2.5 mol% ZnCl₂ to the reaction (Entries 4, 8 and 9) does not show significant influence on the ee. In the reaction with **4.6-*i*Pr(S)** the reaction was even retarded, which resulted in a lower yield. Addition of zinc and ZnCl₂ to the reaction lowered the yield and had no influence on the ee (Entry 10). Although more interesting phenomenon was observed in the reactions involving zinc metal. The iron complex in the reaction mixture usually shows an orange/red colour. In all these reactions a black metallic precipitate was observed that stuck to the magnetic stirring bar. Zinc metal is diamagnetic. Therefore the ferro-magnetic precipitate is metallic iron. Some of the reactions also turned bright yellow. Exposure to air of these yellow solutions showed no colour change. Normally, all the iron (II) intermediates immediately turned green upon exposure to air. Hence the yellow complex is a bopa-Zn species. All this evidence showed that the excess zinc metal replaced the iron in bopa-complex. Further the influence of zinc and zinc derivatives on the reaction was tested. The addition of the double and triple excess

amount of zinc (relative to the catalyst) to a solution of **4.2-*i*Pr(S)** reduced the yields to 38% and 25%; the ee's were 1% (S) and 5% (S) (Entries 11 and 12). In both cases the solution turned bright yellow after 10 – 22 hours, in the case of 6% zinc loading the solution stayed orange. In contrast to the literature values, the reaction of ZnCl₂ with **4.1-*i*Pr(S)** gave 24% yield with 5% (S) ee (Entry 13). Mixing the lithium salt of bopa-*i*Pr(S) (**4.1-*i*Pr(S)**) with ZnCl₂ gave 91% yield with an enantiomeric excess of 22% (R) (Entry 14). Pre-forming and isolating the [Zn(bopa-*i*Pr(S))Cl] complex and employing in the reduction reaction just gave 8% yield with 13% excess of the S-enantiomer (Entry 15). Further reactions are yet to be undertaken.

4.3.2 Discussion

The results in the above section are inconsistent with the published values. It is therefore not possible for a mechanistic proposal. Although a few observations have been made. Interestingly, employing **4.6-R** in the hydrosilylation reaction gave exclusively a racemic product. This suggests that the addition of the hydrosilane to a THF solution of **4.6-R** yields a different species than the previously suggested iron(II) hydrido complex (compare Figure 4.8). In the original protocol 6 mol% (equals 1.2 equiv. in respect to the catalyst) of zinc were added to the reaction. For the reduction from **4.2-R** to **4.5-R** 0.5 equivalents are needed. That leaves an excess of 0.7 equivalents of zinc. Above we were able to show that the zinc metal slowly exchanges with the iron. This means that within the first 24 hours of the reaction both species, [Fe(bopa-R)Cl(THF)₂] and [Zn(bopa-R)Cl], are forming in a ratio of three to seven. Additionally to these complexes ZnCl₂, Zn and Fe are present in the cause of the reaction. Some of these species were already proven catalytically active. It is therefore difficult to make a proposal about the mechanism involved in the reaction.

4.4 Concluding Remarks

In summary we were able to show that $[(\text{Fe}(\text{bopa-R})\text{OAc})_2]$ (**4.7-R**) is formed *in situ*, when bopa-R is mixed with $\text{Fe}(\text{OAc})_2$. The slow complex formation during the hydrosilylation resulted in an induction period of several hours. If complex **4.7-R** is directly employed the reaction time can be reduced to about two hours. The formation of the *R* enantiomer from **4.7-*i*Pr(S)** is consistent with an inner sphere reaction pathway, including the formulation of an iron-hydride species (Figure 4.8). Although further experiments need to be undertaken to confirm this theory. For the reactions involving zinc we were able to show that the reaction proceeds *via* a different intermediate complexes. A plausible mechanism could not be proposed due to a lack and inconsistencies in the experimental data.

4.5 Experimental

4.5.1 Chemicals and Reagents

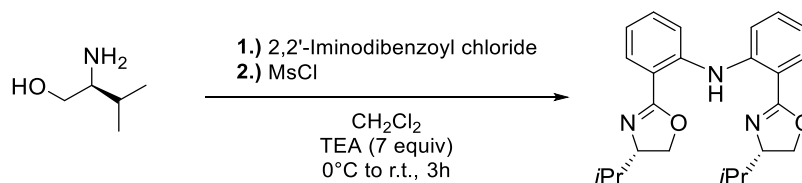
All manipulations were carried out under an inert N_2 atmosphere using standard Schlenk or glove box techniques. The solvents were purified and dried using a two column solid-state purification system (Innovative Technology, NJ, USA). They were transferred to the glove box in a Strauss-flask without exposure to air. The solvents were stored over molecular sieves (3 Å). Deuterated solvents were purchased from Cambridge Isotope Laboratories, Inc., or Armar Chemicals, GmbH and were degassed and stored over dried and activated molecular sieves (3 Å). All other chemicals were purchased from commercial sources and were degassed by standard freeze-pump-thaw procedures prior to use. The following chemicals were synthesised: 2,2'-iminodibenzoic acid,¹⁵ *R*-(-)-phenylglycinol,¹⁶ 2,2'-iminodibenzoyl chloride (Chapter 3.5.3.1), bopa-R (**4.1-Ph(R)**, **4.1-*i*Pr(S)**); see Chapter 3.4.3.2), (bopa-*i*Pr)Li,¹⁷ $[\text{Fe}(\text{bopa-R})\text{Cl}_2]$ (**4.2-Ph(R)**, **4.2-*i*Pr(S)**),⁸ $[\text{Fe}(\text{bopa-*i*Pr})\text{Cl}]$ (**4.5-*i*Pr(S)**), see Chapter 3.5.3.4), $[(\text{Fe}(\text{bopa-*i*Pr})\text{OAc})_2]$ (**4.7-*i*Pr(S)**), $[\text{Zn}(\text{bopa-R})\text{Cl}]$.

4.5.2 Physical methods

NMR spectra were recorded on a Bruker Avance 400. ^1H NMR chemical shifts were referenced to residual solvent peak as determined relative to TMS ($\delta = 0$ ppm). GC measurements were conducted on a Perkin-Elmer Clarus 400 GC equipped with a FI-detector. UV-Vis-absorption spectra were recorded with a Hellma Excalibur UV-Vis fiber optic probe connected to a Varian 50 Bio UV-Vis spectrometer. The enantiomeric excess was determined by HPLC using Chiralpak AD-H[®] as stationary and *i*PrOH/hexanes (5/95; 0.8 mL flow rate) as mobile phase.

4.5.3 Syntheses

4.5.3.1 Synthesis of bopa-*i*Pr (**4.1-*i*Pr(S)**)

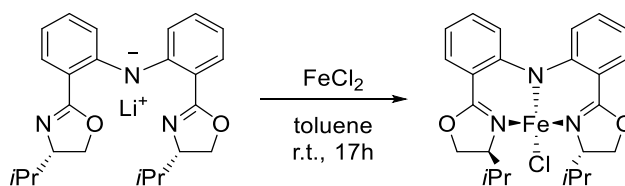


For experimental details see Chapter 3.4.3.2.

2,2'- Iminodibenzoyl chloride (1.0 equiv, 12.8 mmol, 3.8 g), L-2-Amino-3-methylbutanol (L-Valinol; 2.1 equiv., 26.2 mmol, 2.7 g), triethylamine (7.0 equiv, 88.0 mmol, 12.2 mL), Mesylchloride (2.2 equiv, 28.3 mmol, 2.2 mL).

Yield: 4.8 g (95%), yellowish, white solid

^1H NMR (400 MHz, Chloroform-*d*) δ 10.77 (s, 1H), 7.83 (d, $J = 7.9$ Hz, 2H), 7.43 (d, $J = 8.3$ Hz, 2H), 7.34–7.24 (m, 4H), 6.91 (t, $J = 7.5$ Hz, 2H), 4.35 (t, $J = 8.5$ Hz, 2H), 4.10 (dd, $J = 9.2$, 6.7 Hz, 2H), 4.03 (t, $J = 7.9$ Hz, 2H), 1.82 (q, $J = 6.6$ Hz, 2H), 1.03 (d, $J = 6.7$ Hz, 8H), 0.93 (d, $J = 6.7$ Hz, 8H).

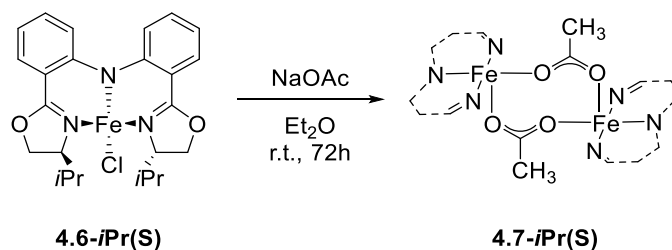
4.5.3.2 Synthesis of [Fe(bopa-*i*Pr)Cl] (**4.5-*i*Pr(S)**)

For experimental details see Chapter 3.5.3.4.

bopa-*i*Pr-Li salt (1.0 equiv, 1.33 mmol, 528 mg), FeCl₂ (1.0 equiv, 1.33 mmol, 168 mg).

Yield: 538 mg (84%), orange powder.

Elemental analysis calculated (%) for C₂₄H₂₈ClFeN₃O₂: C 59.83, H 5.86, N 8.72; found: C 60.01, H 5.94, N 8.45

4.5.3.3 Synthesis of [(Fe(bopa-*i*Pr)OAc)₂] (**4.7-*i*Pr(S)**)

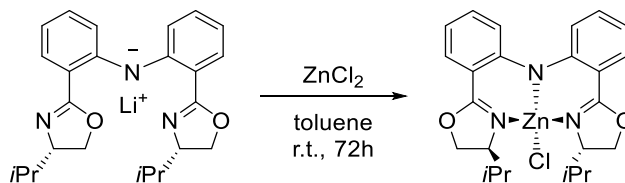
[Fe(bopa-*i*Pr)Cl] (**4.5-*i*Pr(S)**), 1.0 equiv., 0.31 mmol, 150 mg) were suspended in Et₂O and NaOAc (1.0 equiv, 0.31 mmol, 26 mg) were added. The mixture stirred for 72 hours at room temperature. A white precipitate was filtered off over celite, the solution was concentrated *in vacuo* and precipitated by addition of pentane.

Crystals for X-ray analysis were obtained by redissolving **4.7-*i*Pr(S)** in Et₂O and slowly diffusing the solvent into heptane.

Yield: 114 mg (73%), red crystalline solid.

Elemental analysis calculated (%) for C₅₂H₆₂Fe₂N₆O₈: C 61.79, H 6.18, N 8.31; found: C 62.00, H 6.31, N 8.05

4.5.3.4 Synthesis of [Zn(bopa-R)Cl]



bopa-*i*Pr-Li salt (1.0 equiv, 1.50 mmol, 596 mg) and ZnCl₂ (1.0 equiv, 1.50 mmol, 204 mg) were dissolved in toluene (10.0 mL). The reaction mixture stirred for 72 hours at room temperature. The solution was then filtered over celite, concentrated and precipitated by addition of pentane.

Yield: 597 mg (81%), bright yellow powder.

Elemental analysis calculated (%) for C₂₄H₂₈ZnClN₃O₂ (+30% toluene impurities): C 60.40, H 5.90, N 8.10; found: C 60.81 H 6.03, N 8.50

¹H NMR (400 MHz, Chloroform-*d*) δ 7.78 (dd, *J* = 8.1, 1.7 Hz, 2H), 7.36 (d, *J* = 8.6 Hz, 2H), 7.25 (t, *J* = 8.0 Hz, 2H), 6.71 (s, 2H), 4.52 – 4.29 (m, 6H), 2.28 (s, 2H), 1.02 (d, *J* = 7.0 Hz, 6H), 0.95 (d, *J* = 6.8 Hz, 6H).

¹³C NMR (101 MHz, Chloroform-*d*) δ 168.62, 153.78, 133.32, 131.30, 129.16, 128.35, 69.59, 67.84, 31.32, 19.01, 15.64.

4.5.4 Hydrosilylation Reactions

4.5.4.1 General Procedure for the results in Tables 4.2 and 4.4

Inside the glove box, 4-acetylbiphenyl (0.25 mmol, 1.0 equiv.), *catalysyt* (compare Table 4.2 and 4.4 for loading) and *additive* (compare Table 4.2 and 4.4 for loading) were weight into a 30 mL scintillation vial and suspended in 2.0 mL THF. The vial was closed and heated to reflux for one hour. After the silane (0.50 mmol, 2.0 equiv.) was added and the reaction was kept at

65°C for 24 hours. The reaction was cooled to 0°C and quenched by slowly adding TBAF in THF (1M, 0.5 mL), KF (28 mg) and MeOH were added. The crude mixture was separated between H₂O (1x10 mL) and DCM (3x 20 mL) and dried over Na₂SO₄. After evaporation of the solvent the crude product was separated by flash column chromatography (5 – 35% EtOAc in Hexanes). The enantiomeric excess of 1-(biphenyl-4-yl)ethanol was determined by HPLC (Chiralpak AD-H[®], 5% *i*PrOH in hexanes, 0.8 mL flow rate; retention times: 15.99 min, 17.48 min).

4.5.4.2 General Procedure for the results in Tables 4.3

Inside the glove box, 4-acetylbiphenyl (0.25 mmol, 1.0 equiv.), *catalysyst* (compare Table 4.2 and 4.4 for loading), *additive* (compare Table 4.2 and 4.4 for loading) and Naphthalene – as internal standard – were weight into a 30 mL scintillation vial and suspended in 2.0 mL THF. The vial was closed and heated to reflux for one hour. After the silane (0.50 mmol, 2.0 equiv.) was added and the reaction was kept at 65°C for 24 hours. In regular time intervals 100 µL sample were taken and immediately quenched in 100 µL TBAF (1M in THF, plus 5% H₂O). The sample was filtered over a short pad of silica usind Et₂O as solvent. The solvent was evaporated and the residue was redissolved in *i*PrOH /hexanes (5/95). The sample was analysed by HPLC (Chiralpak AD-H[®], 5% *i*PrOH in hexanes, 0.8 mL flow rate; retention times: 15.99 min, 17.48 min). The yield/conversion was determined by comparing the areas of 4-acetylbiphenyl and 1-(biphenyl-4-yl)ethanol (See further details about calibration below).

4.5.4.3 Calibration of the HPLC Signals

General remarks

The samples had previously been calibrated on naphthalene. During the first experiments we realised that the standard and/or sample are not transferred quantitatively into the HPLC vial. Therefore we calibrated the conversion/yield on the ratio between 4-acetylbiphenyl and 1-(biphenyl-4-yl)ethanol. This can be done since the reaction proceeds without side reaction.

Preparations

Sol A: 4-acetylbiphenyl (**4.3**; 25.2 mg, 128.4 μmol) were dissolved in 10.0 mL *i*PrOH/hexanes (5/95).

Sol B: 1-(biphenyl-4-yl)ethanol (**4.4**; 26.7 mg, 134.7 μmol) were dissolved in 10.0 mL *i*PrOH /Hexanes (5/95).

Table 4.5: Composition of the calibration solutions.

Sample	Sol A [mL]	Sol B [mL]	Yield [%] ^a
A	0.1	0.9	90.4
B	0.2	0.8	80.8
C	0.3	0.7	71.0
D	0.4	0.6	61.1
E	0.5	0.5	51.2
F	0.6	0.4	41.2
G	0.7	0.3	31.0
H	0.8	0.2	20.8
I	0.9	0.1	10.4

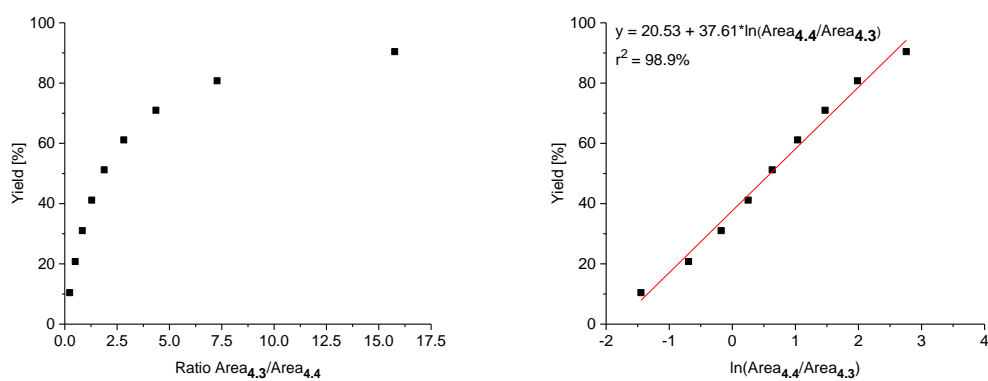


Figure 4.10: Left graph: Raw data received from the ratio of the Areas of educt and product. Right graph: linearised values from left graph.

Discussion

The ratios received from the measurements were logarithmised to linearise them. The right graph (Figure 4.10) shows still a slight sigmoid line shape, but the fitting of 99% is acceptable for this measurement. For the analysis values between $-1.44 < \ln(\text{Area}_{4.4}/\text{Area}_{4.3}) < 2.75$ (equivalent to $10\% < \text{Yield} < 90\%$) were taken. Values outside this range were declared as yields $<10\%$ or $>90\%$, respectively.

4.5.5 Crystal Structure of [(Fe(bopa-*i*Pr)OAc)₂] (4.7-*i*Pr(S)):

Empirical formula	C ₅₂ H ₆₂ ClFe ₂ N ₆ O ₈	
Formula weight	1010.78	
Temperature	100(2) K	
Wavelength	0.71073 Å	
Crystal system	Orthorhombic	
Space group	P2 ₁ 2 ₁ 2 ₁	
Unit cell dimensions	a = 9.9749(12) Å	α = 90°.
	b = 12.3700(9) Å	β = 90°.
	c = 40.162(3) Å	γ = 90°.
Volume	4955.6(8) Å ³	
Z	4	
Density (calculated)	1.355 Mg/m ³	
Absorption coefficient	0.645 mm ⁻¹	
F(000)	2128	
Crystal size	0.43 x 0.18 x 0.14 mm ³	
Theta range for data collection	2.24 to 25.00°.	
Index ranges	-11 ≤ h ≤ 11, -14 ≤ k ≤ 14, -47 ≤ l ≤ 47	
Reflections collected	46914	
Independent reflections	8679 [R _{int} = 0.0869]	
Completeness to theta = 73.56°	99.8 %	
Absorption correction	Semi-empirical from equivalents	
Max. and min. transmission	0.7248 and 0.5929	
Refinement method	Full-matrix least-squares on F ²	
Data / restraints / parameters	8679 / 24 / 612	
Goodness-of-fit on F2	1.105	
Final R indices [I > 2σ(I)]	R1 = 0.0731, wR2 = 0.1446	
R indices (all data)	R1 = 0.0928, wR2 = 0.1555	
Absolute structure parameter	0.13(3)	
Largest diff. peak and hole	01.039 and -1.121 e.Å ⁻³	

4.6 References

- (1) Enthaler, S.; Junge, K.; Beller, M. In *Iron Catalysis in Organic Chemistry*; Plietker, B., Ed.; Wiley-VCH: Weinheim, 2008, p 125.
- (2) Yamamoto, K.; Hayashi, T.; Nishiyama, H. In *Transition Metals for Organic Synthesis*; Beller, M., Bolm, C., Eds.; Wiley-VCH Verlag GmbH: Weinheim, 2004, p 167.
- (3) Yamamoto, K.; Hayashi, T.; Kumada, M. *J. Organomet. Chem.* **1972**, *46*, C65.
- (4) Brunner, H.; Rötzer, M. *J. Organomet. Chem.* **1992**, *425*, 119.
- (5) Brunner, H.; Fisch, K. *J. Organomet. Chem.* **1991**, *412*, C11.
- (6) Brunner, H.; Fisch, K. *Angew. Chem.* **1990**, *102*, 1189.
- (7) Nishiyama, H.; Furuta, A. *Chem. Comm.* **2007**, 760.
- (8) Inagaki, T.; Phong, L. T.; Furuta, A.; Ito, J.-i.; Nishiyama, H. *Chem. Eur. J.* **2010**, *16*, 3090.
- (9) Inagaki, T.; Ito, A.; Ito, J.; Nishiyama, H. *Angew. Chem. Int. Ed.* **2010**, *49*, 9384.
- (10) Bleith, T.; Wadepohl, H.; Gade, L. H. *J. Am. Chem. Soc.* **2015**, *137*, 2456.
- (11) Corey, J. Y. *Chem. Rev.* **2011**, *111*, 863.
- (12) Corey, J. Y.; Braddock-Wilking, J. *Chem. Rev.* **1999**, *99*, 175.
- (13) Bauer, G.; Wodrich, M. D.; Scopelliti, R.; Hu, X. L. *Organometallics* **2015**, *34*, 289.
- (14) Smith, C. R. *Synlett* **2009**, *2009*, 1522.
- (15) Paul, A.; Ladame, S. *Org. Lett.* **2009**, *11*, 4894.
- (16) McKennon, M. J.; Meyers, A. I.; Drauz, K.; Schwarm, M. *J. Org. Chem.* **1993**, *58*, 3568.
- (17) Csok, Z.; Vechorkin, O.; Harkins, S. B.; Scopelliti, R.; Hu, X. L. *J. Am. Chem. Soc.* **2008**, *130*, 8156.

Curriculum Vitae

Gerald Bauer

Laboratory of Inorganic Synthesis and Catalysis (LSCI)
EPFL SB ISIC LSCI (BCH 3201)
CH-1015 Lausanne
Phone: +41 (0)21 693 9877
E-Mail: gerald.bauer@a3.epfl.ch

Research Experience

- Synthesis of well-defined iron bis(phosphino)pyridine and bis(oxazolinyphenyl)amino pincer complexes and their application in hydrogenation, hydrosilylation and C-C bond formation reactions.
- Mechanistic studies related to alkyl-aryl cross coupling and hydrosilylation reactions.

Education

- 06.2011 – current **PhD** - Ecole Polytechnique Fédéral de Lausanne (EPFL)
Supervisor: Prof. Xile HU
Mechanistic investigation and reactivity tests of iron bis(oxazolinyphenyl)amino (NNN) pincer complexes as potential catalysts in cross coupling and hydrosilylation reactions.
- 11.2009 – 12.2010 **MSc** - University of Technology Vienna (TU Wien)
Diploma Thesis under supervision of Prof. Karl A. KIRCHNER and Prof. Kazushi MASHIMA
Synthesis of iron bis(phosphino)pyridine (PNP) pincer complexes and their application in the hydrogenation and transfer-hydrogenation of aromatic ketones.
- 10.2004 – 11.2009 BSc University of Technology Vienna (TU Wien)

Internships and Semesters Abroad

03. – 05.2010 Internship (part of Diploma Thesis); University of **Osaka**, Japan
Supervisor: Prof. Kazushi MASHIMA
01. – 06.2008 Semester Abroad; ICT **Prague**, Czech Republic
09. – 12.2007 Internship; University of **Waterloo**, ON, Canada
Supervisor: Prof. J. Michael CHONG
Study of the ligand effect of palladium catalysed hydrostannation reaction of terminal aryl acetylenes.

Core Skills

- Proficient in organic synthesis in milligram and multi-gram scale
- Proficient in the synthesis under inert atmosphere (Schlenk and glove box techniques)
- Proficient in analytics (GC, HPLC, MS, NMR, IR, UV-Vis)

Teaching Experience

- Mentor for 2 master students during their master thesis and semester project.
- 670 hours of teaching experience as teaching assistant in biochemistry, organic- and inorganic synthesis.

Languages

- **German** (mother tongue)
- **English** (excellent in writing and speaking)
- **French** (fluent)
- Czech (basic knowledge)

Publications:

- **Bauer, G.**; Cheung, C. W.; Hu, X. L.: *Synthesis* 2015 (in press)
“Cross coupling of Nonactivated Primary and Secondary Alkyl Halides with Aryl Grignard Reagents Catalyzed by Chiral Iron Pincer Complexes.”
- **Bauer, G.**; Wodrich, M. D.; Scopelliti, R.; Hu, X. L.: *Organometallics* 2015 **34**, 289
„Iron Pincer Complexes as Catalysts and Intermediates in Alkyl–Aryl Kumada Coupling Reactions.”
- Carnevale, D., Perez Linde, A. J., **Bauer, G.**, Bodenhausen, G.: *Chem. Phys. Lett.* 2013 **580** 172
“Solid-state proton NMR of paramagnetic metal complexes: DANTE spin echoes for selective excitation in inhomogeneously broadened lines.”
- **Bauer, G.**, Kirchner, K. A.: *Angew. Chem. Int. Ed.* 2011 **50**, 5798 / *Angew. Chem.* 2011 **123**, 5918
“Well-Defined Bifunctional Iron Catalysts for the Hydrogenation of Ketones: Iron, the New Ruthenium.“ / “Definierte difunktionelle Eisenkatalysatoren zur Hydrierung von Ketonen – Eisen, das neue Ruthenium.“

Conference Contributions

- SCS-Fall Meeting 2014, Zürich, Switzerland (Poster Contribution)
- SCS-Snow Symposium 2014, Saas-Fee, Switzerland (Poster Contribution)
- Swiss Summer School “Synthesis and Catalysis” 2013, Villars-sur-Ollon, Switzerland (Poster Contribution)
- 20th Conference on Organometallic Chemistry 2013 (EuCOMC XX) St. Andrews, Scotland (Poster Contribution, Oral Presentation)

Scholarships and Grants

- 2011 : GCOE scholarship
- 2010 : Grant for excellent studies (Leistungsstipendium)